Wave Propagation in a Model of the Human Arterial System

9

A dissertation submitted for the degree of

Doctor of Philosophy

of the

University of London

JIUN-JR WANG

Abstract

Wave propagation is an important phenomenon in the cardiovascular system. The method of characteristics, is being used to investigate pressure and flow waves in the arterial system. There are numerous advantages: (1) It can clearly show the reasons for the development of the pressure and velocity waveforms as they propagate and are reflected in the arteries. (2) The contribution of waves originating in a specific organ can be identified. (3) The contribution of the forward and backward waves can easily be separated. (4) Using published physiological data for the human body, the output of the heart can be calculated from experimental data measured in the arteries. (5) The calculation time is much less than either finite difference calculation. The first calculation are made assuming that convection, viscous effect are not important and wavespeed depends only on the wall properties. Under these condition, the problem can be linearized and the formation of waveforms of each section can be determined by the convolution of the input wave with transfer function. Transfer function is determined from the impulse response of the model. The second part of the research is to discuses the importance of nonlinear properties, including convection of the waves and pressure dependant wave speeds.

To My Beloved Parents

Acknowledgements

I would like to express my deep gratitude to Dr. Kim Parker for his excellent supervision, full of patience and knowledge. From him I learned how to look at problems which we never encountered before.

I would like to thank two of my best friends, Christopher Murphy and Ashraf Khir. The knowledgeable Chris helps me and broadens my view in English, physiology and many things. Ashraf is always my best companion in discussing 'waves'. Thanks for their tolerance and patience and our international friendship will last forever. I would like to thank all the members of PFSU for their kind help.

I would like to give my appreciation to all the brothers and sisters in the Church. Isaac Liu, Paul Chai, Linda Ngo and many other brothers and sisters took care of me and made a home for me, that I may be sheltered and grow in life. I am very grateful for each member in brother's house, Lacson, Newman and Edward, for their perfecting and friendship.

Finally, I would like to give my deep thankfulness and respect to my parents and grandparents for their support in all respects. I would like to give thanks to Bao-Yu for her faithful support.

" *If anyone thinks that he knows anything, he has not yet come to know as he ought to know; But if anyone loves God, this one is known by Him*". - *1 Corinthians 8.*

Table of Contents

1. Introduction 1
    1.1 Models of the Human Arterial System-History Review 1
    1.2 Major Features of Waves 4
    1.3 Methods of General Analysis 6
    1.4 Motivation 9

2. Theoretical Analysis 11
    2.1 Introduction 11
    2.2 Governing Equations 12
    2.3 Linearised Treatment 19
    2.4 Reflections 20
        2.4.1 Reflections at Arterial Bifurcations 21
        2.4.2 The Reflection Coefficient as a Function of Geometry 24
        2.4.3 The Variation of the Reflection Coefficient Caused by Pressure Changes 29
        2.4.4 Reflections at the Terminal Arteries 31
    2.5 The Method of Calculation 32
        2.5.1 The Transfer Function of the Arterial System 34
    2.6 Algorithm for Calculating the Transfer Function 36

3. Results and Extension of the Tree of Waves Model 38
    3.1 Introduction 38
    3.2 Waveforms in the Ascending Aorta 39
    3.3 Characteristics of the Pressure and Velocity Waveforms 41
    3.4 The General Features of Wave Transmission in the Systemic Arteries 44
    3.5 The Role of the Heart in Wave Reflection 46
        3.5.1 Aortic Valve Regurgitation-Pathological Waveforms Related to the Reflections of the Aortic Valve 48
    3.6 The Incisura and Diastolic Wave 49
    3.7 The Effect of a Complete Occlusion of the Aorta 56
    3.8 Analyses by the Wave Intensity Method 59
    3.9 Left Ventricular Analysis 61
    3.10 The Influence of Terminal Resistances and the Coronary Circulation on Waveforms in the Ascending Aorta 64

4. Nonlinear Programming 67
4.1 Introduction 67
4.2 Nonlinear Factors 68
4.3 Governing Equations 72
4.4 Mechanism of Wave Transmission in the Arterial System 74
4.4.1 Program Structure 76
4.5 The Effect of Convection 77
4.5.1 Intersections of Waves 79
4.5.2 Algorithm 80
4.5.3 Results and Discussion for the Convection Case 82
4.6 Pressure Dependent Wavespeed 85
4.6.1 Validity of the Assumptions 86
4.6.2 Program of the Pressure Dependent Wavespeed Case 87
4.6.3 The Results for the Pressure Dependent Wavespeed Case 88
4.7 Conclusions 89

5. Conclusions 91

References 97

Tables 112

Figures 119

Appendix 177

1

Introduction

1.1 Models of the Human Arterial System-

Historical Review

William Harve y (1628) was a pioneer of experimental physiology. It was he who first put forward the idea that blood flows in a "continuous circular pathway" around the body. He subsequently proved this experimentally. The most convincing proof lay in calculations which Harvey made about the heart. By estimating the volume of the ventricles during systole and diastole and observing the heart rate, he concluded that much more blood passes through the heart continually than either can be supplied by the ingested food or be contained in the veins. He concluded that blood must flow in a circular pathway around the body.

From that age, topics of circulatory research diverged into several areas. Hales (1733) investigated the cardiac output and concluded that the elasticity of arterial walls was responsible for transforming the discontinuous cardiac outflow into a relatively steady motion of the blood in vessels downstream. He introduced the idea by means of an analogy for explaining the haemodynamics in the human body, comparing the heart and arteries to the apparatus of a fire engine, where the repeated strokes of the water pump were smoothed into an almost continuous stream by an air compression chamber. This model, called the "Windkessel" model in German, has remained a popular model of the arteries up to the present day. Frank (1899), used the isolated frog heart and found that isovolumic contractions with an increase in diastolic cardiac volume developed increased pressure. He

was probably the first one to describe the cardiac pump in terms of the pressure-volume diagram and put Hales' concept into mathematical form. He assumed the quantitative model of the arterial system as an elastic chamber and the microcirculation as a constant resistance, which was determined by Poiseuille's law. The pressure generated by the heart is assumed to be transmitted instantaneously throughout the Windkessel, whereas a finite, though relatively short time is actually required for transmission in the major arteries. Originally proposed for use in the determination of stroke volume, this model has been modified by Warner (1956) and Beneken (1965) and applied to the closed vascular system.

Other lumped parameter linear models of the Windkessel type or a passive electrical analogy, have been proposed by the followers of Frank, which are based on a comparison between equations describing propagation along a transmission line with a simplified equation of motion of the blood and the equation of continuity for fluid flow in a short segment of artery. Landes (1943) proposed modifications to the Windkessel model (**Fig. 1 (a)**) by adding one resistance to represent viscous or one resistance r plus one inductance L which represents the inertial properties of blood (**Fig. 1 (b)**). Westerhof (1969) has extensively studied the r-C-R model (**Fig. 1 (c)**) and concluded that this model gives a better representation of the pressure-flow relation at the aortic root than the Windkessel model, the inductance L does not improve the model. Other simple models with more parameters were proposed by Spencer and Denison (1963) (**Fig. 1 (d)**), Goldwyn and Watt (1967) (**Fig. 1 (e)**) and Dick *et al.* (1968) who used operational amplifiers instead of passive electrical networks in their analogy. Recently the three-element Windkessel has been extensively used in studies of arterial ventricular coupling (Sunagawa *et al.*, 1982; Burkhoff *et al.*, 1988). Those three parameters are the characteristic impedance, the peripheral arterial resistance and the arterial compliance. The equations based on the Windkessel allow a rough estimation of stroke

volume from measured pulse pressure under certain conditions. However, for an accurate description of the detailed behaviour and timing of waveforms within the arterial system, the classic Windkessel fails, since it does not account for wave travel as has been concluded by Frank and others.

The transmission line or impedance method which has been widely used in electrical engineering was introduced by Taylor (1957 a, b) for explaining afterload and wave reflection behaviour in the arterial system. Afterload, defined as the external factors opposing the shortening of muscle fibres, is one of the determinants of myocardial performance in the intact heart (Milnor, 1975; Hunter and Noordergraaf, 1976). In this model the arteries are considered as a single closed end tube and the minimum impedance should occur at a specific frequency in the impedance power spectrum and phase angle diagram, where the incident and reflected waves are exactly in phase. Two popular types of the impedance models are used to represent the arterial system, the single tube model, by assumption of only one effective reflection site (Westerhof *et al.*, 1972; Murgo *et al.*, 1980; Burattini and Di Carlo, 1988) and the T-tube model which contains two effective reflection sites, one in the head and the other in the lower limbs (O'Rourke and Avolio, 1980; Avolio *et al.* 1980; Campbell *et al.*, 1990; Burattini et al., 1991). The waveforms in the systemic and pulmonary beds presented by Taylor's model agree well with experiments, but it fails to explain the waveform transformation of the pressure and velocity wave shapes along the arteries. Also, the quarter wavelength rule (the distance from a node to the closed end terminal is a quarter of a wavelength) is not really a reliable guide *in vivo*. The transmission line calculations are essentially looking for an effective length and apparent or dominant reflection site for the system, the location of which has become the topic of many arguments.

1.2 Major Features of Waves

Knowledge about alter-ations in the contour of the pressure and velocity waveforms is not new. The changes in contour of the arterial pressure pulse with age and in hypertension were discovered as early as the late nineteenth century. The more precise waveform of the systolic and diastolic phase measurement was not seen until the invention of the arterial catheter measuring system (Cournand and Ranges, 1941). Even now at the end of twentieth century, there are still few detailed studies of the transmission of pressure and velocity waves along the human arteries. The most famous experiment about the variation of the waveforms in different locations of the aorta was done on dogs by McDonald (1974). He illustrated the simultaneous change in amplitude and form of the pressure and flow waves at five sites from the ascending aorta to the saphenous artery as shown in **Fig. 2.** Three characteristics of wave behaviour are noted:

(1) The pressure wave exhibits a marked steepening of its wavefront and also an increase in its amplitude with distance from the heart.

(2) The amplitude of the velocity wave diminishes as the wave propagates distally.

(3) The amplitude of the reverse flow decreases and increases subsequently.

Some theoretical investigations (Frank, 1930; Hamilton and Dow, 1939; Wezler and Bolger, 1939; Peterson, 1954) have suggested that the shape of the pressure and flow waveforms in the aorta could be explained by the effects of reflections (Milnor, 1989).

Over the years there has been debate about whether or not the waves originating from the heart would be reflected and, if they are reflected, where the reflection sites are. The principal evidence for reflections is that the flow and pressure waves have different shapes at the input of the system whereas the two shapes should be the same in a reflection free system (Singer, 1969; Kouchoukos *et al.*, 1970; Westerhof *et al.*, 1972). Other phenomena,

such as a strong systolic peak and a prominent inflection point in the pressure waveform in the human ascending aorta, especially in the aged have been described (Murgo *et al.*, 1980). The large pressure jump at the beginning of diastole (incisura) when the aortic valve is closed and flow ceases is also cited to be the evidence of the reflection of waves.

Some evidence of reflections was found in the large variations in waveforms caused by the injection of ethoxamine, a vasoconstrictor, or nitropruside, a vasodilator, in subjects (Gundel *et al.*, 1981; Brin and Yin, 1984, Burattini *et al.*, 1991). However, the identification of reflection sites varies among different authors. Westerhof *et al.* (1972) suggested that reflections should occur at all junctions, Bergel and Milnor (1965) reported that the main reflection would be contributed by the small arteries 0.5-1.0 mm in diameter and Pollack *et al.* (1968) found that arteries 3.5-4 mm in diameter are responsible for the reflection. The aortoiliac bifurcation was suggested as the major reflection site by Hamilton and Dow (1939), the renal artery by Latham *et al.* (1985) and the abdominal aorta by O'Rourke and Taylor (1966) through their studies of aortic impedance. Taylor (1957 a) studied the general features of wave transmission in the arterial system which is simulated by a random branching system. Gosling *et al.* (1971) made a series of measurements on the area ratio of the daughter to parent vessels and concluded that the arterial system should be well matched for forward going waves. Other experiments in the literature claimed that little or no reflections could be found in the arterial system. Peterson and Gerst (1956) induced a wave in the femoral artery of a living dog but no sign of waves was detected at the ascending aorta. Starr and Schild (1957) induced a wave in the aorta and could only detect it in the aortic arch but there was no sign of secondary reflections.

1.3 Methods of General Analysis

The first general analysis of the motion of blood in arteries was developed by Euler as early as 1775. His one-dimensional equations for invisid flow in an elastic tube are still used in the modelling of the arterial systems. A sophisticated analytical solution of wave propagation in an elastic tube was developed by Womersley (1957). He improved Witzig's (1914) equations and assumed that both the pressure gradient and flow are simple harmonic functions. The analysis starts from flow in a rigid tube without friction and then to the elastic and viscoelastic tube. The effect of external constraint by perivascular tissues is included in his simulation. His model shows the strong relation between the frequency and velocity profile, which will be flattened by increased frequency.

Due to the better processing capability of the digital computer, computational fluid dynamics techniques were introduced into the investigation of arterial waves. Computational fluid dynamics has been widely applied in mechanics, aerodynamics and plasma physics and it allows one to deal with the complicated structure of arteries and more realistic conditions, such as the flow field in a bifurcation and through a stenosis (Deshpands *et al.*, 1976; Fukushima *et al.,* 1988; Stergiopolus, 1996). The multi-branched arterial system was simulated by several authors with a one-dimensional fluid dynamics model. Anliker and Rockwell (1971) investigated the pressure and velocity variations with ageing, vasoconstriction or dilation and the possibility of shock formation in the arteries. Schaaf and Abbrecht (1972) used simplified, idealised branches to simulate wave transmission in the systemic arteries. Everett (1973) predicted the spatial variation of the velocity and pressure by specifying the variation of diameter with transmural pressure and wave speed. The branching of the arterial tree was simulated by a distributed outflow and the cardiac ejection rate was prescribed at the root of the aorta in his model. Raines *et al.*

(1974) investigated pulse propagation in the human leg. Rumberger and Nerem (1977) compared their one-dimensional unsteady flow in an elastic tube model with results measured in the horse coronary artery. Gerrard (1982) used the one-dimensional equations of motion to investigate the pulsatile flow in a tapered tube in order to simulate blood flow in arteries. Niederer (1985) investigated the shock-like wave in human being by assuming the constitutive equation of the arterial wall and an approximation of the damping effect in the artery. Stergiopulos *et al.* (1992) have also simulated pressure and flow propagation in the human arterial system.

The middle descending thoracic aorta was modelled by Ling and Atabek (1972) with a two dimensional Navier-Stokes equations model, in which the velocity profile was calculated by assuming an axially symmetric flow profile, the nonlinear connective acceleration terms and tapering of the tube were also included. Belardinelli and Cavalcanti (1992) studied the tapering effect by applying a two dimensional model in a single tube, the nonlinear deformation and the nonlinear convection terms were taken into account. They found a large attenuation of the backward waves at the angle of 0.14°. Lou and Yang (1993) considered the effect of the non-Newtonian behaviour of blood on a pulsatile flow at the aortic bifurcation. Helal *et al.* (1994) studied the interaction between an arterial stenosis and a bypass graft.

In order to model the propagation of waves in the arterial system, the method of characteristics is the most popular method to solve the governing one-dimensional flow equations since it has the advantages that it automatically contains the nature of the wave propagation and is able to deal with the nonlinearities. The differences between various authors are mainly in the types of boundary conditions used, the constitutive law of the pressure-diameter relationship and the linear or nonlinear assumptions. The input or the

boundary conditions are normally specified by empirical data at the aortic root, either pressure or velocity versus time. However, the specification of conditions at the aortic root may introduce some confusion into the understanding of the arterial system since the waveforms measured at the aortic root are the results of the interaction between the heart and the arterial system. Furthermore, so many factors, such as viscous dissipation, convection effects and tapering of the tube, are included in most models, that even though the results from the numerical calculations are similar to the experimental findings, there is no clear evidence about which factors cause the wave shape changes. Thus a conclusion such as "*...the characteristic shape changes of pressure and flow pulses as they propagate along the different branches of the arterial tree are primarily due to the geometrical arrangement and the taper of the arteries as well as the mechanical properties of the vessel wall and the blood.*" (Stergiopulos *et al.,* 1992) must have been known before the calculation.

The wave intensity method developed by Parker and Jones (1990) is based on the method of characteristics and has been applied to analyse experimental measurements. The solutions of the one-dimensional hyperbolic equations can be written as the differences of the Riemann invariants across characteristics when dissipation is neglected. Applying this analysis to aortic waveforms shows that the waveforms are dominated by two groups of forward waves and one group of backward waves (forward is toward the periphery and backward is toward the heart). This analysis takes into account both elastic and convective effects and makes no assumption about periodicity.

1.4 Motivation

McDonald (1974) made the remark about the arterial system that one would expect a system of branching tubes with considerable internal damping to be an almost perfectly sound absorber. Nevertheless, the hypothesis that pulse wave reflections in the cardiovascular system play a significant role in determining haemodynamic parameters is today accepted by the majority of authors, as has been discussed in the review paper by Papageorgiou and Jones (1988). Furthermore, the reflected waves may carry information about the condition of organs (Milnor, 1982), such as renal failure causing hypertension and impedance changes. Modern ultrasound technology allows one to measure the flow patterns in large blood vessels non-invasively within a range of about 10 cm from the skin using appropriately designed ultrasonic instruments. Once the structure of the arterial waveform is fully understood, the diagnostic significance could be immense.

Despite decades of study of the basic physical phenomena of pressure and velocity waveforms in the systemic arteries, we still lack a clear view of how it works. The Windkessel model does not properly treat wave travel since it restricts itself to the prediction of the stroke volume and afterload. The impedance method considers the systemic arteries as a single or a T-tube and the length of the tube is predicted by the impedance, the value of pressure after the Fourier transform divided by velocity after the Fourier transform, and the "quarter wavelength" concept in which both the incident and reflected waves are in phase at the end of the tube and out of phase when the observation is shifted to a quarter wavelength from the end. However, the pattern of arteries is a complicated branching system. The oversimplified single or T-tube model with the quarter wavelength assumption may not be able to describe the arterial system properly. One of the biggest assumptions in the impedance model is that the arterial system is linear, otherwise

the Fourier transform would be invalid, but the aortic valve is a nonlinear device whose effect could never be negligible. The fluid dynamics simulations can predict local flow patterns given the presumed boundary conditions, but could never properly separate the factors influencing them (Barnard *et al.*, 1966 a, b).

Our other area of interest is in left ventricular function because the waveforms in the aorta are the result of the interaction between the heart and the arterial system. The heart is normally taken as a pressure pump, flow pump or a mixed model, which depends on the phase of the heart. The afterload is one of the important factors in describing cardiac performance but none of these factors could clearly explain left ventricle function. The knowledge of the left ventricle will surely be improved when the function of the systemic arteries is more clearly understood.

2

Theoretical Analysis

2.1 Introduction

The systemic arterial tree is a succession of branching points. A useful model of the large arteries is shown in **Fig. 3** (Westerhof *et al.*, 1969), which contains 55 large arteries and is based on a healthy subject with a height of 175 cm and a mass of 75 kg. The major geometrical structures are bifurcations with few, if any, trifurcations and no anastomoses in conduit arteries. The bifurcating tree structure extends to the very small arteries in most parts of the body, although there are exceptions such as the kidney, liver, head, hand and foot where there are interconnections. The microcirculation is a much more complex network.

As mentioned in §1, The aortic waveforms are strongly influenced by reflected waves. A wave will be reflected to some extent when it encounters a discontinuity or any impedance mismatch during its travel. Branching points of the small arteries and the arterioles have long been considered as two possible sites where the mismatching could occur (Remington, 1965; Wetterer *et al.*, 1977; Westerhof *et al.*, 1978, 1979; Murgo *et al.*, 1980; Latham *et al.*, 1987). If all of the branching points and the arterioles, which are connected to the large arteries, reflect waves, the study of wave behaviour in the arterial system becomes difficult because of the huge number of reflections and transmissions by the numerous reflection sites. This difficulty was realised by several researchers as early as the 1960's (McDonald, 1974). However, dealing with these possible repeated reflections, transmissions and reverberations is extremely difficult (McDonald, 1974;

O'Rourke and Nichols, 1990; and Berger *et al,* 1993) and the problem remained unsolved. Several simplified approaches were introduced, such as the transmission line model (Taylor, 1957 a, b) which has traditionally considered the effect of a multi-branched arterial tree with multi-reflections as a single tube with a single reflection site. The waveform is the superposition of one forward and one backward travelling wave. The former is generated by the heart and the latter is reflected by the single reflection site which was assumed to be located at the aortoiliac junction. Recently, Berger *et al.* (1993) extended this model by assuming that the waves are rebounding between the reflection site and the heart. However, there is little improvement in our understanding of the wave behaviour in the arterial system from this model.

Most of the models, including all of the impedance models, Windkessel models and some of the computational fluid dynamics models, treat the wave as a wavetrain. However, this is not true in the real arterial system. There are differences between the waveforms in different cycles caused by the variation of the system and the output of the heart. In our study, the "wave" is considered as a single waveform instead of a wavetrain. This description of the wave system allows the concept of a wavefront to be introduced whereas the wavetrain description does not (Parker and Jones, 1990).

2.2 Governing Equations

The behaviour of blood in the arterial system is simulated as one-dimensional, incompressible flow in an elastic tube (Skalak, 1972). By postulating one-dimensional flow, the pressure and velocity are assumed to be uniform over the cross-sectional area. It has been observed by Schultz *et al.* (1969) that the velocity distribution in the arteries is rather flat and uniaxial under normal conditions, and this is true even in the ascending aorta (Paulsen

(Paulsen and Hasenkam, 1983). Although there is evidence of secondary flow with radial components of velocity in the aortic arch, the axial flow is still dominant (Pedley, 1980). This can be confirmed by observations in the curved pipe: the amplitude of the averaged secondary flow, both directions perpendicular to the axial flow, are around 10% of the mean axial flow (Talbot and Gong, 1983). The similar conclusion was made by Niederer (1985) with the estimation of arterial elasticity and it was verified by Doppler measurements.

This system must fulfil the laws of conservation of mass and momentum. In order to close the calculation, the relationship between pressure and cross-sectional area of the artery also has to be specified:

(*a*) ***Continuity Equation***: Conservation of mass requires that the rate of mass increasing inside a section of vessel is equal to the net influx of mass. For an incompressible fluid and allowing for an outflow of fluid through arterial wall.

$$S_t + (US)_x = -\frac{W}{\rho} \qquad (2.1)$$

where the subscripts indicate partial derivatives.

S: the cross-sectional area of the segment (m^2).

U: the velocity of blood averaged over the cross-sectional area (m/s).

W: the rate of blood leaking out of the artery (kg/ms).

ρ: the density of blood which is 1019 kg/m^3 at 37° C.

x: the axis co-ordinate and the positive direction is toward the periphery (m).

t: time (s).

(*b*) ***Momentum Equation***: Conservation of momentum requires that the rate of momentum increasing inside a section of blood vessel is equal to the net influx of momentum minus the net momentum change which is caused by the pressure exerted on boundary surfaces and

the force exerted on both fluid and boundary surfaces.

$$U_t + UU_x = -\frac{P_x}{\rho} + F \tag{2.2}$$

P: the blood pressure which is averaged over the cross-sectional area (Pa).

F: the dissipation term (m/s^2).

F models the momentum changes caused by any forces other than pressure forces, such as the shear force between the artery wall and blood. *F* is called a dissipation function. The dissipation term is normally a function of pressure *P* and velocity *U*.

Eq. (2.1) and (2.2) constitute two equations for the three unknowns, *U, P, S*. The third equation is the relation between pressure and the cross-sectional area of the blood vessel. In this study, the area is assumed to be a function of the transmural pressure only :

$$S = A(P(x,t)) \tag{2.3}$$

The properties of blood and of the vessel wall are assumed to be uniform and constant in each segment. Using (2.3) to write (2.1) in terms of *P* rather than *S* gives:

$$P_t + UP_x + \frac{A}{(\frac{dA}{dP})}U_x = -\frac{W}{\rho(\frac{dA}{dP})} \tag{2.4}$$

If transient effects such as the influence of respiration or the transient response to a vasoactive drug are taken into account, the area is a function of time as well, $S=A(P(x,t), t)$. In this case, one more term, $A_t/(dA/dP)$, must be included on the right hand side of (2.4). If the tapering or the structural variation of the segment is also incorporated, the cross-sectional area is also a function of the distance *x*. Eq. (2.2) then becomes $S=A(P(x,t), x, t)$ and the term $(A_t+UA_x)/(dA/dP)$ must also be included on the right hand side of (2.3). We, however, will not consider these effects.

Eq. (2.2) and (2.4) are a first order hyperbolic system of nonlinear partial differential equations, which can be solved by the method of characteristics. Writing (2.2) and (2.4) in matrix form:

$$\omega_t + \Omega \omega_x = \Phi \tag{2.5}$$

where $\omega = \begin{bmatrix} P \\ U \end{bmatrix}$ $\Omega = \begin{bmatrix} U & \frac{A}{(\frac{dA}{dP})} \\ \frac{1}{\rho} & U \end{bmatrix}$ $\Phi = \begin{bmatrix} -\frac{W}{\rho(\frac{dA}{dP})} \\ F \end{bmatrix}$

The eigenvalues, λ, of the matrix Ω can be determined from the equation $|\Omega - \lambda I| = 0$

as $$\lambda_{\pm} = U \pm c$$

where the local wavespeed, c is defined as:

$$c^2 \equiv \frac{A}{\rho}(\frac{dP}{dA}) \tag{2.6}$$

or, more conveniently $$c^2 = \frac{1}{\rho D}$$

where D is the distensibility, $D \equiv \frac{1}{A}\frac{dA}{dP}$.

Along the directions $$\frac{dx}{dt} = \lambda_{\pm} \tag{2.7}$$

the partial differential equations reduce to the ordinary differential equations

$$\frac{dU}{dt} \pm \frac{1}{\rho c}\frac{dP}{dt} = F \mp \frac{cW}{\rho A} \tag{2.8}$$

Eq. (2.8) are ordinary differential equations which hold along the characteristic directions with slope λ_+ and λ_- in the (x,t) plane. The positive sign refers to the forward direction which is toward the periphery and the minus to the backward characteristic

direction. c is the local wavespeed with which the disturbances travel relative to the fluid. The physical meaning of the characteristic direction, dx/dt, is the propagation speed of disturbance.

It is noted that the distensibility of the artery, and hence the wavespeed, can be a function of the pressure. The complex structure and material properties of arteries make the area-pressure curve nonlinear, which is manifested by a strong dependence of the compliance of the arterial wall on the pressure. The definition of the compliance is different between different authors, such as compliance $\equiv dV/dP$ by McDonald (1974); compliance $\equiv dA/dP$ by Murgo and Westerhof (1981 b), Langewouters *et al.* (1984, 1985) and Tardy *et al.* (1991). Langewouters *et al.* (1984, 1985) calculated the compliance of the wall by measuring the static and dynamic mechanical properties of blood vessel wall versus the aortic pressure *in vitro* for 35 thoracic and 16 abdominal human aortae. The experiment was done by increasing the aortic pressure stepwise, from 20 mmHg to 180 mmHg. The arterial compliance, defined by them to be dA/dP, is nonlinear and exhibits a significant dependence on pressure, even in the physiological range, 80 to 120 mmHg (**Fig. 4**). They found that the value of compliance drops from 1.2×10^{-8} m^2Pa^{-1} at 70 mmHg to 0.3×10^{-8} m^2Pa^{-1} at 130 mmHg in a typical human abdominal aorta. There is an inflection point in the area curve at 40 mmHg which marks the maximal compliance. A direct consequence of the large variations in arterial compliance is that the wavespeed will also depend on pressure and vary over a pulse cycle. The influence of the pressure dependant wavespeed on the waveform will be discussed in §4.

If the wavespeed is continuous and a function of local pressure only, $c = c(P(x,t))$ then, (2.5) along the characteristics direction (2.7) can be written in terms of the Riemann functions,

---

[1] V refers to v me

$$R_{\pm} = U \pm \int_{P_0}^{P} \frac{dP}{\rho c} \tag{2.9}$$

where P_0 is an arbitrary reference pressure. If the dissipation forces are insignificant locally (F=0), no flow leaks through the wall (W=0) and the arterial properties are uniform and constant within each segment, then the right hand side of (2.8) is zero, and the Riemann functions across the wavefront can be simplified as:

$$dR_{\pm} = dU \pm \frac{dP}{\rho c} = 0 \tag{2.10}$$

The operator d in (2.10) is a difference operator defined as the change across the characteristic. At a fixed position, the difference is just the change in the Riemann function as the wavefront passes.

When (2.10) is valid, the Riemann functions are generally called Riemann invariants. The physical meaning is that any changes in pressure and velocity imposed upon the flow will cause a change in the Riemann functions which will propagate along the characteristic direction. As sketched in **Fig. 5**, at each point (x,t), there is a unique pair of characteristics, a forward R_+ and a backward R , intersecting at that point which determine the local pressure and velocity. When the pressure P is known, the velocity U can be calculated by (2.10) and vice versa.

Rewriting (2.10) along a characteristic, i.e., across a wavefront

$$dP = \pm \rho c dU \tag{2.11}$$

Where + denotes the forward and - denotes the backward direction. The relationship, between the amplitude of the pressure pulse and flow velocity across each wave, given by (2.11) is called the water hammer equation, which was first derived by Allievi (1909) and applied to the analysis of the circulation by Frank (1930) and Broemer (1930). This formula

forms a useful guide to the relationship between the amplitude of the pressure pulse and velocity of the flow generated by a rapid ejection of liquid into an elastic tube. Referring to the assumptions leading to (2.11), this relationship only holds for a nonviscous flow.

The validity of this relationship was demonstrated by the experiments using transient impulse excitation of the system, such as those by Peterson (1954) where he injected a rectangular pulse of liquid into the proximal aorta. The initial rise of pressure can be predicted quite closely by the water hammer equation. Starr and Schild (1957) measured the pressure caused by injecting a single slug of blood into the arterial system of a cadaver, and he found that the water hammer equation fits the results better than other more complicated ones which are derived from the Windkessel model.

If intersecting forward and backward wavefronts superimpose linearly, i.e.,

$$dP = dP_+ + dP_-$$

$$dU = dU_+ + dU_-$$

then we can separate the measured dP and dU into their forward and backward components

$$dP_\pm = \frac{1}{2}(dP \pm \rho c dU)$$

$$dU_\pm = \frac{1}{2}(dU \pm \frac{dP}{\rho c})$$

We conclude this section by noting that all of the above analysis is for a single segment of tube and that there is no assumption of periodicity.

2.3 Linearised Treatment

The arterial system is clearly nonlinear in the precise sense of the term. The mass and momentum equations contain the nonlinear terms, UU_x and UP_x. The relation of pressure with the cross-sectional area in an elastic tube can cause the wavespeed to be pressure dependant, as discussed above, which also leads to nonlinear behaviour. Most of the methods which consider wave reflections, such as the transmission line method, are linearised. Whether a linearised model is reliable depends upon the significance of the nonlinearity. If the predicted nonlinearities are not greater than the order of accuracy of the calculation of the model, it is not necessary to include all of the nonlinearities. Normally an "all inclusive" nonlinear model is so complicated that it would not tell us much about reality or provide as much insight into the physical processes as the simpler models do.

Many investigations have tested the linearity of the arterial system. Womersley (1955,1957) showed that the nonlinearities in the pressure-flow relationships are quite small in his theoretical work. Attinger *et al.* (1966) concluded that the nonlinear terms did not amount to more than 5 per cent. Dick *et al.* (1968) concluded that the arterial system behaved as a linear system at least in regard to pressure and flow relations.

Once it is linearised, the system can be treated by conventional analyses such as the Fourier transform and convolution methods. Linearisation may introduce excessive errors in a prediction of the detailed variations in the pressure and flow patterns with distance from the heart, but this approximation may help us understand the gross behaviour and reveal some of the intrinsic properties of the system.

Normally the assumption used in the linearisation of the wave propagation problem in the arterial system is that the wavespeed is an order of magnitude larger than the flow speed. From the data collected by McDonald (1974), a typical wavespeed in the arterial

system is of the order of 10 m/s, and the averaged peak speed of the blood flow is only 0.5 m/s, so that the magnitude of the peak flow is only about 5% of wavespeed. However, this ratio could be as high as 20% at the ascending aorta because of the greater distensibility and, hence, lower wavespeed. Using a non-dimensionalisation argument, the convection term UU_x and UP_x could be negligible when compared with the inertial terms U_t and P_t: since

$$\frac{U\,U_x}{U_t} \cong \frac{U\,\dfrac{\Delta U}{\Delta x}}{\dfrac{\Delta U}{\Delta t}} \approx \frac{U}{c}$$

and similarly,

$$\frac{U\,P_x}{P_t} \cong \frac{U\,\dfrac{\Delta P}{\Delta x}}{\dfrac{\Delta P}{\Delta t}} \approx \frac{U}{c}$$

Most of the analyses of wave behaviour in the arterial system consider that the heart beats regularly and establishes a steady-state oscillation. A different point of view is taken in our model. The value of pressure and velocity can be calculated by the infinitesimal wavefronts, or "wavelets", passing the point where we measure the waves, $dP_{\pm} = \pm\rho c dU_{\pm}$. dP and dU are the changes in the pressure and velocity when a wavefront passes.

2.4 Reflections

The previous two sections discussed how the pressure and velocity in a single segment are determined by the intersection of waves. In this section, we will discuss the generation of waves in the arterial system apart from those generated by the heart. Discontinuities of either geometry or elastic properties can produce reflections.

We will adopt the definition made by Grashey (1881) and Von Kries (1892) that a reflected wave that has the same sign with the incident wave is positive, and it is negative

when it is opposite in sign. A positive reflection will occur at a closed end and a negative reflection will occur at an open end of an elastic tube. In the arterial system, the reflection sites are neither completely closed nor open, and so we are dealing with intermediate conditions which cause partial reflections.

An incident wave travelling toward the discontinuity will be partially transmitted and partially reflected. Neglecting dissipation and nonlinearities, the reflected and transmitted waves will have the same waveform as the incident wave and each wave will travel with the speed of the characteristic of the segment in which it is propagating. The pressure at a fixed point in the blood vessel is assumed to be the superposition of the pressures associated with the incident and reflected waves. If the nonlinearities are considered in the model, the assumption of superposition may not be valid. This will be discussed in §4.1.

2.4.1 Reflections at Arterial Bifurcations

As mentioned before, wave reflections originate from any discontinuity in the arterial tree. Possible reflecting sites are branching points, areas of alteration in arterial distensibility and high resistance arterioles.

Consider the bifurcation shown in **Fig. 6**. A tube, the parent, branches into two daughter tubes. A wave travelling down the parent artery will be partially reflected at the junction and partially transmitted to the daughter vessels. The relationship between the incident, reflected and transmitted waves is determined by the conditions of one-dimensional flow at junctions: (1) the mass must be conserved and (2) the pressure is continuous across the junction. Let P_0, P_1, P_2 indicate the absolute pressure in the parent and daughter vessels, and the subscript denotes the vessel number. ΔP_0 is the incident wave and

dP_0 denotes the reflected pressure wave from the junction back to the parent vessel and dP_1, dP_2 are the changes in pressure associated with the transmitted waves in the two daughter vessels.

Pressure is uniform at the junction :

$$P_0 = P_1 = P_2 \tag{2.12}$$

$$P_0 + \Delta P_0 + dP_0 = P_1 + dP_1 = P_2 + dP_2 \tag{2.13}$$

Combining (2.12) and (2.13)

$$\Delta P_0 + dP_0 = dP_1 = dP_2 \tag{2.14}$$

Conservation of mass:

$$U_0 A_0 = U_1 A_1 + U_2 A_2 \tag{2.15}$$

$$(U_0 + \Delta U_0 + dU_0)A_0 = (U_1 + dU_1)A_1 + (U_2 + dU_2)A_2 \tag{2.16}$$

Here we have neglected higher order terms arising from changes in tube area with pressure.

Combining (2.15) and (2.16)

$$(\Delta U_0 + dU_0)\, A_0 = dU_1\, A_1 + dU_2\, A_2 \tag{2.17}$$

The left hand side of (2.17) represents the change in flow out of the parent vessel and the right hand side represents the change in flow into the daughters.

Using (2.11) for the incident wave

$$\Delta P_0 = \rho\, c_0\, \Delta U_0 \tag{2.18}$$

For the wave which is reflected back into tube 0, the change in velocity is opposite in sign to the change in pressure:

$$dP_0 = -\rho\, c_0\, dU_0 \tag{2.19}$$

For the waves transmitted into the daughter tubes

$$dP_1 = \rho c_1 dU_1 \tag{2.20}$$

$$dP_2 = \rho c_2 dU_2 \tag{2.21}$$

Substituting (2.18), (2.19), (2.20), (2.21) into (2.17).

$$(\Delta P_0 - dP_0)\frac{A_0}{\rho c_0} = \frac{A_1}{\rho c_1} dP_1 + \frac{A_2}{\rho c_2} dP_2 \tag{2.22}$$

Substituting dP_1 and dP_2 by ΔP_0 and dP_0 from (2.14)

$$\frac{A_0}{\rho c_0}(\Delta P_0 - dP_0) = \frac{A_1}{\rho c_1}(\Delta P_0 + dP_0) + \frac{A_2}{\rho c_2}(\Delta P_0 + dP_0)$$

Therefore, the reflection coefficient for the forward wave at the junction is

$$R \equiv \frac{dP_0}{\Delta P_0} = \frac{Z_0^{-1} - Z_1^{-1} - Z_2^{-1}}{Z_0^{-1} + Z_1^{-1} + Z_2^{-1}} \tag{2.23}$$

where $Z_i \equiv \rho c_i / A_i$, i=0, 1, 2 are the characteristic impedances of the different vessels.

The transmission coefficient is

$$T \equiv \frac{dP_1}{\Delta P_0} = \frac{dP_2}{\Delta P_0} = \frac{2Z_0^{-1}}{Z_0^{-1} + Z_1^{-1} + Z_2^{-1}} \tag{2.24}$$

The relation between the reflection and the transmission coefficients can be derived from (2.23) and (2.24):

$$T = 1 + R \tag{2.25}$$

Both the reflection and transmission coefficients at the junction depend on the area and wavespeed of each segment. If there is no reflection, R=0, the junction is called "well-matched". The results show that reflection coefficients at branching points are direction sensitive which was noted by Hardung in 1952.

2.4.2 The Reflection Coefficient as a Function of Geometry

Two general parameters are used to represent the relationship between the reflection coefficient and the geometry of the bifurcation, the ratio between total daughter area of the vessels and parent area, $\alpha = \frac{A_1 + A_2}{A_0}$, and the degree of asymmetry of the daughter vessels, $\gamma = \frac{A_2}{A_1}$ $(0 \leq \gamma \leq 1)$. Without loss of generality, we have taken vessel 2 to be the smaller of the two daughter vessels.

To calculate the reflection coefficient, we must also know how the wavespeeds of the vessels depend upon their geometry. There are two models which can be used to describe the relationship between the wall thickness and the diameter of the vessel:

(1) Constant wall thickness-to-radius model: In this model the wall thickness is assumed to be directly proportional to the radius in both parent and daughter vessels. The wavespeed, *c*, for thin-walled vessels is given by the Moens-Korteweg equation (Moens 1878 and Korteweg 1878):

$$c_i = \sqrt{\frac{E_i h_i}{2 \rho r_i}} \qquad (2.26)$$

Where E is the Young's modulus of the wall, h the wall thickness and r the segment radius, the subscript i denotes the segment number. Because h/r is a constant in this model, the ratio of wavespeeds in the parent and daughter vessels varies as the square root of the ratio of the Young's modulus.

If the Young's modulus in both the parent and daughter vessels are equal, the reflection coefficient R, (2.23), depends only on the ratio of the daughter to parent luminal area and is independent of the branching asymmetry

$$R = \frac{1-\alpha}{1+\alpha} \tag{2.27}$$

Measurements by Bergel (1961a, b) in the aorta, femoral and carotid arteries of dogs showed that the assumption of a constant relative wall thickness appears to be close to the structure of the large arteries. The same conclusion was also reached by McDonald (1974, p.89) who found no significant variation of the ratio, h/r, in any artery from the carotid to the saphenous. If there is not much difference in the wall thickness-to-radius ratio, and the wavespeed does change from one artery to another, then this indicates that the elastic properties of the wall are different from one segment to another.

The ratio of wall thickness to radius could be related to ageing. The ratios for different arteries are not very different in the young, but in older people, the ratio increases progressively from the thoracic aorta to the femoral arteries(Learoyd and Taylor, 1966).

(2) Constant wall thickness model: If the wall thickness and the Young's modulus are constant in all of the three segments, the ratio of the wavespeed in the daughter to parent vessels is:

$$\frac{c_1}{c_0} = \left(\frac{A_0}{A_1}\right)^{\frac{1}{4}}$$

and the reflection coefficient is a function of both α and γ,

$$R = \frac{1 - \left(\frac{\alpha}{1+\gamma}\right)^{\frac{5}{4}}\left(1+\gamma^{\frac{5}{4}}\right)}{1 + \left(\frac{\alpha}{1+\gamma}\right)^{\frac{5}{4}}\left(1+\gamma^{\frac{5}{4}}\right)}$$

The variation of the reflection coefficient calculated for these two models with respect to the area ratio, α, for different γ, is plotted in **Fig. 7**. There are three characteristics

of this figure which should be mentioned:

(1) In the constant wall thickness-to-radius model, the zero reflection coefficient for the forward going waves will occur at $\alpha = 1.0$ for both symmetric and asymmetric bifurcations.

(2) In the constant wall thickness model, the zero reflection coefficient for forward going waves is at $\alpha = 1.15$ for a symmetric bifurcation ($\gamma = 1$), and at a lower value of α for asymmetric bifurcations.

(3) If a bifurcation is well matched for forward travelling waves, there is a significant reflection when a wave is moving back from a daughter to the parent vessel.

The daughter to parent area ratio for a well matched bifurcation is approximately 1, and so a wave travelling backward in one of the daughter vessels in a symmetrical bifurcation would encounter a bifurcation with an area ratio of 3. For $\alpha = 3$, $R \cong -0.5$ (**Fig. 7**) which means that half of the backward going wave will be reflected by the junction. This effect of decreasing retrograde waves can be very significant when a wave moves backwards through several bifurcations. For example, in a symmetrically bifurcating system which is well matched for forward travelling waves, the amplitude of a reflection from an occlusion at the periphery would be only $1/2^5$ or about 3% after encountering 5 bifurcations.

This phenomenon helps clarify the results of several experiments done in the early 1960's which have been taken as evidence for the absence of reflected waves in the arterial system. The observations of Peterson and Gerst (1956) were important but their deduction was incorrect. They did experiments on living dogs, in which pulses with known volumes were injected into a distal large artery such as the iliac artery, the femoral artery or even more distal arteries. There were no waves detected at the aortic root. Starr (1957) generated a pulse wave in the aorta of a corpse with an amplitude approximately the same as the physiological value. He recorded only a small reflected wave at the site of the aortic arch,

and no sign of secondary reflection from the aortic valve. He doubted the presence of reflections in the aortic root. O'Rourke and Nichols (1990; p 251) questioned his conclusion by remarking that the peripheral blood vessels would be completely dilated in cadavers, so there would be very few reflections from the periphery.

From the architecture of the human arterial tree model, there are 10 major bifurcations from the heart to the iliac artery. If a backward wave comes from the iliac artery toward the heart, it would suffer a large loss in amplitude before returning to the aortic root. Later in §3.3, we will show that the backward waves in the ascending aorta are mainly from the trunk, upper limbs and head, with very few coming from the lower limbs.

There are several studies of the daughter to parent area ratio in arterial junctions. Papageorgiou *et al.* (1990) made extensive measurements on 444 junctions at various anatomical locations of the human arterial system including the coronary arterial tree. They found that the mean value of the area ratio for coronary bifurcations is 1.179 ± 0.041, this value is slightly higher for the higher generations. Similar values of area ratio were found in other systemic bifurcations where the overall averaged area ratio was 1.14 ± 0.027 which is close to the value for a well matched symmetrical bifurcation predicted by the constant wall thickness model, $\alpha=1.15$ (**Fig. 8 (a)**). An exception was the aortoiliac junction where the area ratio was 0.848 ± 0.073. Hess (1927) also measured the area ratio of the aortoiliac junction in humans, and found the mean area ratio of 0.83 ± 0.08. He found that there was no significant variation between young people and adults. Gosling *et al.* (1971) did a series of measurements of the area ratio of the aortoiliac junctions in different species, including cockerels, dogs and humans. The area ratio was 1.16 ± 0.06 for cockerels, and 1.23 ± 0.05 for dogs. In humans, they found that the value is strongly related to age, being about 1.10 in the first decade and 0.75 in the fifth decade (**Fig. 8 (b)**). They did not find significant

differences between females and males. Patel *et al.* (1963) measured the area ratio of the aortoiliac junction by casting the central arterial system, and found a value of 1.108. Newman *et al.* (1972) induced atheroma in cockerels and found that during early atherogenesis, the haemodynamics of the abdominal aortic junction are markedly changed, and the values of the area ratio fell to well below 1.0. Papageorgiou and Jones (1990) suggested that the low area ratio of the aortoiliac junction found in their study was due to a systematic bias in their subjects that indicates the need to find an ethically acceptable way of measuring this ratio in subjects who do not show symptoms of vascular disease in the legs. We conclude that, with the possible exceptions of the aortoiliac junction, the daughter to parent area ratios of most arterial junctions are very close to the value for which they are, theoretically, well matched for forward travelling waves.

Well matched bifurcations for the forward going waves may have important physiological functions. Womersley (1957) suggested that minimal reflections for the forward going waves are expected at the junctions of a healthy arterial system, so that most of the energy can transmit through the arterial system. Pulsatile flow is observed not only in the aorta and large arteries, but also in arterioles and capillaries (Intagbetta *et al.*, 1970; Ashikawa *et al.*, 1986). Ganong (1983) claimed that effective pulse wave transmission throughout the arterial system is necessary for effective tissue perfusion.

The data of physiological and geometrical quantities collected by Westerhof *et al.* (1969) represent a model of the arterial tree corresponding to average, healthy human adults (**Table 1**). However, the data does not satisfy the well matched condition for forward travelling waves. For example, at the junction of the thoracic aorta I and the intercostals where the daughter to parent area ratio is only 0.53, the sudden shrinkage of the cross-sectional area causes a reflection coefficient $\cong 0.25$. There are several other mismatched

bifurcations in this data. One possible reason for this could be that the anatomists normally specialise in a specific part of the body, so the dimension of each artery is an average of a specific segment collected from many corpses, not necessarily from the same subject (Williams, 1995). Our model seeks to represent the pressure and velocity waveforms in a healthy human and so each bifurcation of the arterial tree in our model is adjusted to be well matched for forward going waves so that the reflection coefficient for forward waves is equal to zero.

Table 1 contains the diameter, length, wall thickness and Young's modulus given by Westerhof *et al.* (1969). The new dimensions for our model are adjusted from **Table 1** by fixing the wall properties (elasticity, density, wall thickness) and the diameter of the parent vessel, then decreasing or increasing both of the daughter vessels by the same percentage until the zero reflection condition is fulfilled for every junction. The adjusted data are listed in **Table 2**. The properties of both legs are equal in the data of Westerhof so that both legs respond identically. In our model, we have deliberately extended the length of each segment of the right leg by 1 mm to prevent simultaneous reflections from the two legs. The problem of simultaneous reflections from the arms did not arise because they are not symmetric.

2.4.3 The Variation of the Reflection Coefficient Caused by Pressure Changes

Patel *et al.* (1963) found that the area ratios of daughter to parent vessel were remarkably stable under a wide range of distending pressure. If the wall properties are pressure independent, the reflection and transmission coefficient will be invariants within a cycle. However, Macfarlane *et al.* (1980) noted that the Young's modulus changes with increases in static distending pressure.

A simple model was made to explore the variation of the reflection coefficient with changes of pressure. The relationship between wavespeed c and the cross-sectional area is expressed by (2.6). It is assumed that the cross-sectional area A of a given segment is a function of P alone and the variation of wavespeed is linear versus the changes of pressure

$$c = c_0(1 + k(P - P_0)) \tag{2.28}$$

(which is reasonable in the physiological range, see **Fig. 48**). The values of the constants c_0 and k are chosen according to measurements. Integrating (2.6) with (2.28), the pressure dependent cross-sectional area A is

$$A(P) = A_0 \exp\left(\frac{k(P - P_0)}{kc_0^2\rho(1 + k(P - P_0))}\right) \tag{2.29}$$

Once c_0 and k are known for daughter and parent vessels, the variation of the reflection coefficient with the pressure changes can be calculated by (2.23).

We considered two bifurcation junctions, the aortoiliac junction and the brachiocephalic junction. The data from **Table 2** are assumed to be at 100 mmHg, the "0" state. At present, we do not have sufficient information to determine k for each segment. We assume that the variation of wavespeed is 2 m/s over the physiological range for both parent and daughter vessels, i.e., k=0.05 Pa^{-1}. The results show that within the physiological range, the variation of the reflection coefficient is less than 2% at both the aortoiliac junction (**Fig. 9 (a)**) and the junction of the aortic arch and the brachiocephalic artery (**Fig. 9 (b)**). Thus, it is reasonable to regard the reflection and transmission coefficients as constants during a cardiac cycle. There may be others factors causing variation of the reflection coefficient (Mayer *et al.*, 1984; Brown, 1993) but they are not included in this model.

2.4.4 Reflections at the Terminal Arteries

A large amount of research has been carried out on both large arteries and the microcirculation but very little is known about the small arteries and arterioles in between. Vascular resistance is largely determined by the arterioles because of their narrow lumens and the limited number of these vessels (Levick, 1992). There is a general agreement that friction forces in the large arteries are relatively negligible. The mean arterial pressure in the ascending aorta is about 100 mmHg and falls very little in the large arteries, as shown in **Fig. 10**. It then falls to about 70 mmHg at the proximal side of the arterioles and to 20 mmHg at the distal side. Thus, most of the pressure drop occurs in the arterioles which constitute the largest part of the total vascular resistance. The high resistance arterioles are considered to be the major sites of wave reflection in the circulation as supported by many different studies (Karreman, 1952; McDonald, 1974; O'Rourke, 1982 b; Milnor, 1989).

The peripheral resistance is defined as the ratio of the pressure difference across the arterioles and capillary bed to the volume flow rate through them. The assumption that flow rate is proportional to pressure has been widely used in the simulation of the terminals in the arterial system (Anliker *et al.*, 1971; Stettler *et al.* 1987; Stergiopulos *et al.*, 1992). If we disregard the cross-sectional area changes of the resistance vessels with pressure, the local blood velocity is directly proportional to the blood flow, and we can define a resistance based on mean velocity rather than flow, $R_T \equiv \frac{P}{U}$, where U is the mean velocity and P is the pressure upstream of the resistance. The venous pressure is assumed to be zero in this study. The value of the reflection coefficient at the terminal arterioles of the femoral bed is around *0.8* under normal conditions but can be as high as *0.95* with marked arteriolar constriction and could drop to nearly zero with maximum vasodilatation (O'Rourke and Taylor, 1966).

The simulation of the terminal arterioles in this work is by a pure resistance element R_T connected with a reservoir at zero pressure (which simulates the pressure of the veins). The value of each terminal resistance shown in **Table 3** is presented in terms of pressure over flow rate, i.e., R_T/A (Stergiopulos *et al.*, 1992).

From the definition of terminal resistance R_T, before and after the wave impinges on the resistance element (see **Fig. 11**):

$$P = R_T U \tag{2.30}$$

$$P + \Delta P + dP = R_T (U + \Delta U + dU) \tag{2.31}$$

where ΔP and ΔU are the pressure and velocity changes across the incident wave and dP and dU are the changes across the reflected wave. Combining (2.30) and (2.31),

$$\Delta P + dP = R_T (\Delta U + dU) \tag{2.32}$$

Replacing ΔU and dU in (2.32) by the water hammer relation (2.11), the reflection coefficient is

$$R_c \equiv \frac{dP}{\Delta P} = \frac{R_T/A - Z}{R_T/A + Z} \tag{2.33}$$

where $Z=\rho c/A$. The values for the terminal reflection coefficients, R_c, are listed in **Table 3**.

2.5 The Method of Calculation

The main arterial system is analogous to a bifurcating tree. The simulations of wave propagation in this system were performed to accomplish the following objectives:

(1) To explain the patterns of the pressure and velocity waveforms at different regions of the arterial system.

(2) To study the contribution of the forward and backward waves to the observed waveforms.

(3) To calculate the impact of interventions such as the occlusion of an artery on the arterial waveforms.

The reasons for the particular waveforms seen in the arterial system are largely unknown. Most of our information comes from observations at a single location and generally neither the input nor the function of the arterial system is known. The concept of the transfer function formulation is introduced to help us investigate the arterial system. This method is widely used to describe electrical networks or filters. Such a filter may be thought of as a "black box" into which an electric current or a voltage is fed as an input $I(t)$ and out of which comes a resulting output $O(t)$. If we can find a function $H(t)$ such that:

$$O(t) = H(t) \otimes I(t)$$

where $\otimes$ denotes the convolution operator, then $H(t)$ is called a transfer function. The physical meaning is that in a linear system, the output is the convolution of the input with the transfer function.

If the input is a unit pulse at t = 0,

$$I(t) = \delta(t) \quad \text{where} \quad \delta(t) = 1 \quad \text{when } t = 0$$

$$\delta(t) = 0 \quad \text{when } t \neq 0,$$

then the output is the transfer function of the arterial system since

$$O(t) = H(t) \otimes \delta(t) = H(t)$$

2.5.1 The Transfer Function of the Arterial System

From the above discussion, the transfer function of the arterial system is the response of the arterial system to a unit pulse input. In other words, the transfer function can be thought of as the history of the input pulse which has gone through multiple transmissions and reflections in the arterial system. The amplitude of each pulse is weakened by passing backwards through the bifurcations and by reflections by the terminal resistances.

Consider a pulse wave originating from the heart. At the first junction part of it is transmitted to the two daughter vessels, and in general, part of it is reflected. The transmitted waves will be partly reflected and partly transmitted at the junction of the next generation. Moreover, the reflected wave will be re-reflected and transmitted at the junction of the previous generation. These processes continue unceasingly as sketched in **Fig. 12.**

When we try to understand wave propagation in the arterial system by following each wave, three possible difficulties could occur: (1) At each bifurcation, it is not necessary for the two daughter vessels to have equal properties and so it is possible that one pulse wave has gone through several segments before the other finishes traversing one. (2) Two waves originating from the same junction, may go through the same route but in different sequence. For example, two waves will come back to the origin simultaneously for the route $1\text{-}2\text{-}2_b\text{-}3\text{-}3_b\text{-}1_b$ and $1\text{-}3\text{-}3_b\text{-}2\text{-}2_b\text{-}1_b$ (**Fig. 12**), where the subscript b denotes the backward path. These two waves must be summed together at the origin. The number of 'duplicate' paths increases combinatorially with the number of segments. (3) The reflections and transmissions in the arterial system is unlimited so that some waves may never return to the origin. Therefore, there is no end for the computation.

To solve these problems, we adopt a new concept, the "tree of waves", and introduce

a numbering method for the arterial tree suitable for the computation. Each wave will generate three waves when it encounters a bifurcation; two transmitted waves and one reflected wave. If we separate the incident wave from the newly generated three waves, we can consider each incident wave as generating a "trifurcating tree of waves" as shown in **Fig. 13**. The backward waves are denoted by a negative index. The structure of the arterial system is a bifurcating tree, so the binary system is suitable for the numbering of the branches. For example the ascending aorta is assigned as **1**, its daughter vessels, the aortic arch and brachiocephalic artery are assigned as **2** (**2×1**) and **3** (**2×1+1**) and so on. If one segment is assigned as **N** (not a terminal segment) its daughter vessels will be assigned as **2N** and **2N+1**. If **N** is in a terminal segment, it generates only the wave **-N**. A backward travelling wave **-N** will generate a backward transmitted wave **-N/2 mod 1** (the smallest integer greater than **N/2**), a forward transmitted wave **N+1** and a forward reflected wave **N**. Each backward wave can generate three waves except ones travelling back to the ascending aorta, **-1**. If the heart is an absorber, the wave will terminate. If the heart is a total reflector, it will behave like a terminal artery with a reflection coefficient of unity. This tree of waves model successfully overcomes the problem of the unlimited reflections and allows us to follow waves that traverse the same path in different sequences.

The number of waves in each level of a symmetrical bifurcating tree is derived in the Appendix by using iterative arguments. If the heart totally or partly reflects waves, the number of waves in level i is 3^i. If the heart completely absorbs waves, there is one wave in the first level of the tree of waves, three waves in the second level, 48 waves in the fifth level, and the number of waves will be more than 10^{14} in the thirtieth level. Storing this information could fill all of the hard disks in Imperial College. It is clearly impossible to record all of the waves that are generated in a bifurcating system and fortunately it is

unnecessary since many of the waves become very small in amplitude. We choose a threshold and neglect all the waves whose amplitude compared with the input is less than the threshold. We have taken the threshold as both 10^{-3} and 10^{-4} and have chosen 10^{-3} as the threshold in the calculations shown in this report, since there is no discernible difference in the waveforms generated using these two thresholds.

In the next section, we will obtain the transfer function by calculating the response of the system to a unit pulse and then use this transfer function to calculate the response of the system to more realistic input conditions.

2.6 Algorithm for Calculating the Transfer Function

The main purpose of this program is to keep track on each wave which passes through a specific point of each segment of the arterial tree. Here we adopt the middle of the segment as our reference point to observe the waveforms. In other words, the time, magnitude and direction of a wave will be recorded when it passes through the point of observation.

The flow chart of this program is shown in **Fig. 14** and the procedure is as follows:

(1) Input the data for calculations: the density of the blood, ρ, the terminal resistances R_T, and for each segment the radius r, wall thickness h, length of the blood vessel L and Young's modulus of the wall E. Calculate the travelling time in segment 0, $t(0)$, the wavespeed c, reflection coefficients R, and transmission coefficients T, by (2.23), (2.24), (2.26) and (2.33).

(2) The generation of waves starts from a unit pulse ($A=1$) coming in the ascending aorta ($N=1$) and calculates the time when the input pulse passes the middle of the ascending aorta ($t=t_1$).

(3) Check the sign of the wave. A positive sign denotes a forward going wave and a negative sign signifies backward going. If it is a positive sign, go to (4). If it is a negative sign, the backward wave generates three waves. The numbering is determined by whether it is in an odd or an even segment. When N is even, the three waves are $-N, -N+1, N/2$. When N is odd, the three waves are $-N, -N-1, (N-1)/2$. The new amplitudes are calculated by the incident amplitude times the transmission or reflection coefficient. The travelling time is the value from the incident wave plus the time taken to traverse this segment. Go to (5), cf Fig 13.

(4) Check whether it is at a terminal segment. If it is a terminal segment, the reflected wave is $-N$. The amplitude of the reflected wave is the amplitude of the incident wave times R_T. The travelling time is $t + t(-N)$. If it is not a terminal segment, the wave generates three waves, two forward ($2N$, $2N+1$) and one backward ($-N$). The amplitude of the two transmitted and one reflected waves are the amplitude of the incident wave times the transmission coefficient and reflection coefficient respectively. Go to (5).

(5) All these newly generated waves are stored for the next level (i+1) calculation and the same data are sent to the output in which the data are classified by their segment numbers

(6) Repeat for the next wave at the same level i.

(7) If this level is finished (i.e. no waves left at this level) go to (8), otherwise go to (9).

(8) The calculation goes on to the first wave of the next level, i+1. Go to (10).

(9) Check the amplitude of the wave. If it is less than the threshold, kill this wave and go to (6) for the next wave at this level. If it is greater than the threshold, go to (3).

(10) If the number of waves at this new level is zero, that means there are no more waves generated by the system, then go to (11), otherwise go to (9).

(11) Program terminated.

3

Results and Extension of the Tree of Waves Model

3.1 Introduction

The transfer function of each segment in the systemic arteries is calculated by the method discussed in §2.6. At the point of observation of each segment (the mid point of the segment), the pressure and velocity waveforms are calculated by the convolution of the input wave with the transfer function. Many investigations are concentrated on the ascending aorta, because it is relatively accessible for measurements. Our study of waveforms also begins from the ascending aorta (§3.2 and §3.3). Our method allows us to separate the waveform into forward and backward components and to discover the reflection sites which dominate the waveforms in the ascending aorta (§3.4). The importance of the aortic valve cannot be overestimated in determining the aortic waveforms. We first study the case of total reflections by the heart (§3.5), and then introduce a model to simulate the aortic valve function (§3.6).

In §3.7, the tree of waves model is applied to study pathological situations. A complete occlusion is introduced in the arterial system and the waveforms in the ascending aorta are analysed. The result may resolve the classical debate about the existence of reflections in the arterial system.

The wave intensity, *dPdU*, is the rate of work per unit area of the cross-section convected by the wave and it allows us to look at the wave reflections from another point of view (§3.8). Two cases are studied, the influence of the aortic valve and the influence in the

ascending aorta when an occlusion moves from the thoracic aorta to one of the iliac arteries.

Numerous experiments have been carried out to determine the afterload in the cardiovascular system which is one of the determinants of myocardial performance, yet there are no general conclusions. We believe that this is because the ventricular waveform is still unknown and if it was known, our understanding of myocardial performance would be improved. It is clear that the measurements of the left ventricular waveform contain both output and reflections from the system. And so, finally, we discuss how the left ventricular waveforms can be calculated from the measurements of the waveform in the ascending aorta if the transfer function is known (§3.9).

3.2 Waveforms in the Ascending Aorta

The ascending aorta is probably the site of the most intensive studies in the systemic arteries. The pressure and velocity measured in the ascending aorta are considered as important indices of the heart performance (Nichols *et al.*, 1977; Murgo *et al.*, 1980, 1981 a; Laskey *et al.*, 1985).

The pressure transfer function (**Fig. 15 (a)**) is obtained by calculating all of the pressure pulses at the point of observation resulting from a unit pressure pulse introduced at time t=0. In this section, the heart is assumed to be an absorber, none of the reflections from the periphery return to the arterial system once they reach the heart. The transfer function at the ascending aorta is considered as the response of the systemic arteries to a unit pulse input. O'Rourke (1982 b) tried to characterise the arterial system in the time domain in terms of its impulse response, which he claimed was the inverse Fourier transformation of the input impedance of the arterial system.

To model ventricular systole, the input waveform is assumed to be a half sinusoidal

wave with ∧ period of 0.3 s (the dotted line of **Fig. 15 (c)**) which is typical of the duration from the opening of the aortic valve to its closure. The pressure waveform at the point of observation in the ascending aorta can be found by the convolution of the input waveform with the pressure transfer function (**Fig. 15 (c)**). The velocity waveform (**Fig. 15 (d)**) is calculated by the same procedure but using the velocity transfer function (**Fig. 15 (b)**). It is noted that the pressure transfer function is not the same as the velocity transfer function, since the backward waves produce pulses which are opposite in sign. Since the only forward wave in this case is the input pulse, the rest of the pulses in the velocity transfer function are opposite in sign with those in the pressure transfer function. The shape of the waveform after 0.3 s is formed by the summation of the reflected waves. The separation of the waveforms into the forward and backward components can show us the interaction of heart and arterial load (Westerhof, 1996). **Fig. 15 (e)** shows that the pressure waveform at the point of observation decomposed into forward and backward pressure waveforms. In the ascending aorta, the forward wave is the input because the heart is assumed to be a perfect absorber.

Several methods have been used to separate the arterial pressure and flow waveforms into the forward and backward waveforms. The forward waveform contains information from the heart and the backward waveform contains information from the periphery of the arterial system. The first separation method was developed by Westerhof *et al.* (1972). His model is based on two assumptions: the arterial system is linear and the waveform is periodic. To separate the waveform, the model needs another parameter, the aortic characteristic impedance, which is derived from measurements. Because the calculation is easy and only needs information about the characteristic impedance at the aortic root, this method has been widely used. Recently, the wave intensity method which

was developed by Parker and Jones (1990) allows the waveform to be separated nonlinearly, both the convective acceleration and pressure dependent wavespeed were taken into account. This method is based on the Riemann invariants and no assumption of the periodicity is needed. Pythoud *et al.* (1996) extended the wave intensity model by arguing that intersecting forward and backward waves are not additive in the nonlinear system and the results should be solved numerically. They included friction in their model by combining the method of characteristics model with a linear model which accounts for friction. However, the combination does not necessarily improve the model because, although there is no periodic assumption in the nonlinear model, somehow the periodic wave is reintroduced into their linear friction model. Also, the accuracy of the results may not be improved significantly by a numerical solver instead of using the additive assumption. When forward and backward waves intersect, their nonlinear method differed only by 4-8% from their linear frictionless model, i.e., Westerhof's model. However, the load of computation was surely much heavier.

3.3 Characteristics of the Pressure and Velocity Waveforms

The transformation of the waveforms along the main aortic trunk is one of the most striking features of wave behaviour in the systemic arteries (**Fig. 2**). Several similar characteristics are noted in rabbits, sheep, dogs, wombats, kangaroo as well as children and adult humans. Similar results, produced by different simulations (fluid dynamics models and electrical analogues), have been obtained by several authors (Westerhof *et al.*, 1969; Anliker *et al.*, 1971; Stetter *et al.*, 1981; and Stergiopolus *et al.*, 1992):

(1) The amplitude of the systolic pressure increases distally even though the mean pressure is decreasing s ght y,

(2) The amplitude of the velocity wave decreases initially to a site around the abdominal aorta then increases.

(3) The magnitude of the reversed flow decreases initially and then begins to increase at a site around the abdominal aorta.

(4) The slope of the wavefront becomes steeper as it moves distally (**Fig. 2** and **Table 4**).

The variations of the transfer function and waveforms along the major arteries calculated by the tree of waves model are shown in **Figs. 15-27**. The peak values of the pressure, velocity and the reversed flow are shown in **Fig. 28**. All the four characteristics discussed above are reproduced and the reasons are clear through the study of transfer functions at the different sites of the arterial system. At distal sites, the pulses in the transfer function are more concentrated and closer to the input wave, which makes the pressure waveform steeper and the period of the pressure waveform narrower. The amplitudes of the pulses are larger distally, which makes the amplitude of the pressure wave larger distally.

Compression backward waves coming to the point of observation from downstream increase the pressure but decrease the velocity, whereas expansion waves decrease the pressure but increase the flow. However, compression reflections from upstream sites to the point of observation increase both the pressure and velocity waveforms. This fact causes the increase in pressure and the decrease of the amplitude of both the forward velocity and the reverse flow from the heart to the site of abdominal aorta, while further downstream the biggest waves are forward travelling waves produced by reflections in branches upstream.

Referring to **Fig. 15**, there are seven large reflected waves, four positive and three negative, in the ascending aorta transfer function. The location where a reflected wave originated can be found by examining its sign in both the velocity and the pressure transfer function. The sign of a backward going wave in the pressure transfer function is opposite in

sign in the velocity transfer function, but is the same sign when it is a forward going wave. The origin of these reflected waves can be identified through checking the sign of a wave in both the pressure and velocity transfer functions in different segments. For example, wave I (**Fig. 15**) is positive in the pressure and negative in the velocity transfer function in the ascending aorta (segment 1) to the thoracic aorta II (segment 27) and becomes positive in both in the abdominal aorta I (segment 28). Therefore, wave I can be identified as a reflection from the hepatic artery (segment 29). Because the arterial tree is assumed to be well matched for the forward going waves, the wave which is generated from the hepatic artery propagates downstream with a constant amplitude, but the amplitude will be diminished as it propagates upstream to the heart.

Similarly, the origins of the other 6 marked waves can also be identified. Wave II is reflected from the renal artery (segments 36, 38), wave III is from the splenic artery (segment 33) and wave IV is from superior mesenteric artery (segment 34). Wave V is also from the renal arteries (segments 36, 38), wave VI is also from the splenic artery (segment 33), and wave VII is also from the superior mesenteric artery (segment 34). Waves V, VI and VII are thus the second reflections of waves II, III and IV from the terminal resistance. When the input wave is reflected by the terminal resistances and encounters a bifurcation, part of it will transmit through the junction and propagate to the heart (wave II, III and IV), part of it reflects back to the terminal resistance as an expansion wave and is reflected by the resistance the second time which then propagates to the heart (wave V, VI and VII).

The seven largest reflections are from the four arteries, hepatic, renal, splenic and superior mesenteric which share a large portion of the cardiac output. Approximately 20% of the cardiac output goes to the renal circulation under basal conditions (Sapirstein 1981; Milnor 1989; O'Rourke and Nichols, 1990), 25% goes into splenic circulation which

supplies the gastrointestinal tract, liver, spleen and pancreas, and 5-20% flows into the superior mesenteric artery where the variation of the blood flow may be large according to the body status, being quite low during the exercise and increasing to 20% of the cardiac output just after a meal (Levick, 1992).

The rest of the smaller reflections in the ascending aorta are from the upper limbs, re-reflected from the aortic trunk and the carotid arteries. Only very few waves, all with very small amplitudes, are from the lower limbs. Their contributions are so small that they have no discernible influence on the waveforms of the ascending aorta. This has been tested by setting the reflection coefficients of the terminals of the lower limbs to zero (the terminal resistance at the end of segment 45, 47, 48, 49, 51, 52, 54 and 55). This result rebuts the arguments that the major reflected waves are from the lower body and cause an inflection point on the systolic part of the wave (Murgo *et al.*, 1981 a, b; O'Rourke, 1982 b).

The waveforms in the ascending aorta are most strongly influenced by the conditions of the abdominal organs, such as the kidney, colon, intestine and pancreas. In other words, the backward waves do carry the information from the periphery, but this information may be restricted to the upper limbs, carotid artery and aortic trunk.

3.4 The General Features of Wave Transmission in the Systemic Arteries

Since the tree of waves model is such a powerful tool, we would like to study some features about wave transmission in the systemic arteries with it:

(1) The dispersion of the backward waves which has been discussed by McDonald (1974), Milnor (1989) and O'Rourke and Nichols (1990).

(2) The inflection point in the early systolic pressure waveform which is normally found in humans age over 35 (Murgo *et al.*, 1981, a, b).

(3) The changes of waveforms when the heart reflects waves.

The general explanation by the transmission line theory for dispersion of the waveforms in the arterial system is that the initial waveform has a wide range of frequency components, and the wavespeed is frequency dependent because of the viscosity of the blood and visco-elastic properties of vessel wall. Thus, after travelling a considerable distance, the different components with different wavespeeds would be spread out and the waveform would be rounded (McDonald, 1974, pp 312-313). The shape of the waveform is somewhat altered, the amplitude is lower and the period is extended (Westerhof, 1996).

This interpretation is not that convincing: (1) Based on their own studies, the wavespeed is strongly frequency dependent only when the Womersley number, α, is less than 3. Since for most of the harmonics α is greater than 3, their wavespeeds can be considered to be frequency independent. (2) Visco-elastic properties of vessel walls are normally considered not to be very important and the frequency dependent viscosity cannot cause such a lag in the length of the human body. There must be another reason for the dispersion.

Our model allows us to look at the problem in a simple and straightforward way without any assumption of periodicity. The forward and backward waves are shown in **Fig. 15 (e)**, where the period of the backward wave is 0.6 s, twice the period of the input wave, and its amplitude is half of the forward (input) wave. The result in **Fig. 15 (a)** shows that the backward pulses are scattered widely and that is caused by the multi-reflections from various sites. When the observation point moves downstream, the waveform will contain waves reflected from other terminal elements without passing the heart (where they will be

absorbed) and so the amplitudes of both forward and the backward waves are higher.

An inflection point, which is frequently found in the early systolic pressure waveform of humans over 35 years of age, is noted as the point where the reflected wave arrives back at the point of observation. From the separation of the forward and backward waves, (**Fig. 15 (e)** to **27 (e)**) we see that the time lag between these waves is less and the amplitude greater distally. The former causes the inflection point to occur earlier while the latter causes the slope of the waveform to become much steeper distally.

As discussed above, we have assumed that each segment of the right leg is 1 mm longer than the corresponding segment of the left (**Table 2**). The waveforms of the right leg are shown in **Fig. 25-27** and those of the left are shown as the dotted line in **Fig. 29 (j)**, **(k)** and **(l)**. There was no discernible difference between two waveforms.

3.5 The Role of the Heart in Wave Reflection

The role of the heart in wave reflections is poorly understood and controversial. Frank (1899, 1905) and Hamilton (1944) were among the first to study waves reflected by the heart. They presumed that the reflection by the valve may form a standing wave in the arterial system. McDonald (1974) rejected this idea because he did not find any waves reflected by the aortic valve in his canine experiments. O'Rourke (1967) did a similar experiment on the wombat and came to a similar conclusion. However he did find the repeated reflections from the terminal arterioles of the front and hind part of the body. Recently, O'Rourke and Nichols (1990) suggested as a result of their experiments that the heart valve should make some contribution to the pressure and velocity waveform.

If there is a reflection, it is most likely to occur when the valve is closed. McDonald and Taylor (1959) simulated this circumstance by making a hydraulic model which was

built with a mechanical pump to analyse the reflection from the heart, and total reflection was found at the aortic root. Robinson (1965) studied the reflection coefficient of the isolated left ventricle by controlling the cardiac output and discovered that reflections at the aortic root could be as high as 70 percent.

In this section, the heart is considered as a total reflector in order to study the changes in the waveforms caused by the heart. The pressure and velocity waveforms for the total reflection case are shown in **Figs. 29** together with the results when the heart is a total absorber (the dotted line). Several characteristics shown in these figures deserve comment:

(1) The period of the solid line is similar to that of the dotted line which indicates that waves reflected by the heart do not change the period of the waveform.

(2) The deviation between the solid line and the dotted line of the pressure waveform starts from 0.1 s, approximately one sixth of the period. This shows that the major contribution to the waveform by reflections from the heart is about 0.1 s behind the input wave.

(3) The gap between the solid and the dotted line of the pressure waveform is approximately the same through all the segments. That is because the systemic arteries are well matched for forward going waves so the reflections by the heart will propagate without reflection to the terminal segments.

(4) The velocity waveform is approximately the same as the input and there is almost no flow after the 0.3 s in the ascending aorta (**Fig. 29 (a)**), aortic arch I segment (**Fig. 29 (b)**) or the aortic arch II segment (**Fig. 29 (c)**). When the heart is a reflector, the waves coming back from the periphery are reflected with a change in sign in the velocity which leads to a cancellation of the velocity waveform but with the same sign in the pressure which leads to an amplification of the pressure waveform. Thus, the input becomes the only component left in the velocity waveform and the pressure waveform is amplified. In the aortic arch, some

waves are transmitted through the brachiocephalic artery as forward going waves but without matched backward waves to cancel them, and so the flow is not strictly zero.

(5) A second "hump" appears in the velocity waveform at the thoracic aorta I segment, where a larger lag between the waves reflected from the heart and peripherally reflected waves is expected. Also, some waves propagate directly from the resistances in the upper limbs and the head to the observation point, and they will not have any counterpart to cancel their effects.

In **Fig. 15 (e),** the peak pressure of the backward waveform at the point of observation is at around 0.3 s. If the timing of the reflected wave is as we predict, the wave reflection might help the closure of the aortic valve. Another contribution might be increasing the pressure at the aortic root during diastole, which maintains the coronary flow (discussed later).

3.5.1 Aortic Valve Regurgitation-Pathological Waveforms Related to the Reflections of the Aortic Valve

Aortic valve regurgitation can be produced by disease processes that directly affect the valve. This in turn can affect the proximal aorta, particularly its diameter. It is often found in patients who suffer from rheumatic fever (an autoimmune or allergic disease), trauma of the aortic valves, ankylosing spondylitis and noninflammatory aortic root dilation. The common syndrome is that the heart valves are likely to be damaged or destroyed, so the blood surges back through the defective valve into the heart during diastole.

There is a distinctive feature of the heart sounds in patients who have aortic valve regurgitation. No sound is heard during systole, but blood flows backwards from the aorta into the left ventricle during diastole causing a murmur of relatively high pitch and with a

swishing sound when heard over the left ventricle. If the aortic valve is so badly destroyed that essentially all of the return of blood from the arterial tree into the heart takes place during early diastole, the sound of aortic regurgitation may not be heard at all during late diastole.

Measurement of blood flow in the femoral artery of patients who suffer from aortic valve regurgitation shows that there is a much larger reverse flow during diastole than in normal persons (Heinen, 1997, personal communication). It is difficult to comprehend the reasons for this syndrome without considering the waves. Aortic valve regurgitation can be simulated by considering the heart as an absorber while the normal heart is simulated by a total reflector. The result of this calculation is shown in **Fig. 29 (l)**. The amplitude of the reverse flow with aortic valve regurgitation (the dotted line) is almost the same in contrast to the normal case when the heart is a reflector where the magnitude of the reverse flow is much lower. This result qualitatively matches the measurements of Heinen.

3.6 The Incisura and Diastolic Wave

The mechanism of closure of the aortic valve was comprehensively studied by Henderson and Johnson (1912). They simulated the closure function of the aortic valve by a mechanical device which is a curved tube joined to the mid portion of a straight tube which is connected to a reservoir (**Fig. 30 (1)**). An excised bovine heart valve membrane was placed across the entrance to the curved section. Fluid flow was directed down the straight tube into a water-filled tank and it was observed that very little motion occurred in the curved portion. When the flow in the straight tube was stopped by an occlusion, the circulating flow in the curved tube causes the valve to close against the downward flow. Lee and Talbot (1979) explained Henderson and Johnson's experiment by a mathematical model

which is simulated by a one-dimensional uniform flow in a tube. They concluded that the reverse pressure gradient, which causes the closure of the aortic valve, is due to the deceleration of the blood flow.

Bellhouse and Bellhouse (1969, 1972) illustrated the operation of the aortic valve with the sinus of Valsalva by model experiments (**Fig. 30 (2)**). The flow, which is ejected from the ventricle at the beginning of systole, pushes open the valve and is split into two streams at each valve cusp. Part of the stream flows into the sinus of Valsalva where it forms a vortical flow before reuniting with the main stream in the ascending aorta. The deceleration of flow starts immediately after the aortic pressure reaches its peak, and an adverse pressure gradient is produced. In other words, p_2 at the valve cusp tip exceeds the pressure p_1 at the station upstream (see **Fig. 30 (2)**). The higher pressure p_2 causes a greater flow into the sinus which brings the cusp toward apposition. The peak deceleration occurs just before the valve closes. The vortical flow established earlier around the opening of the valve can keep the valve cusp from bulging outward to contact the walls of the sinuses.

Immediately after the closure of the aortic valve, normally there is a pressure jump which is accompanied by a sudden cessation of the flow in the ascending aorta. This pressure jump is called the incisura which is characterised as the reaction of the aortic pressure to the closure of the aortic valve. Normally the magnitude of the jump is between 6 to 10 mmHg in humans (**Fig. 2**), but sometimes it can be higher so that the pressure (after the closure of the aortic valve) is at the same magnitude as the systolic pressure (Sugawara, 1996, personal communication). The aortic valve function is fully nonlinear and certainly not negligible, so any linear analysis, such as the Fourier transform, of the experimental measured pressure and velocity waveforms could introduce errors.

The well accepted interpretation for the incisura is that the backflow causes the

closure of the aortic valve but the momentum of the backflow is large enough to bring more blood into the aortic root. The sudden halt of the backflow which is caused by the closure of the aortic valve raises the pressure again, thus giving the short positive pressure wave immediately after the closure of the valve (Guyton, 1981). If the 6 mmHg pressure rise is solely caused by the sudden stagnation of the reverse flow, then this backflow should be at least 1 m/s at the time of closure, which is not true in the normal physiological state. The other factor which could contribute to the pressure increase after the valve closed is the waves. The tree of waves model allows us to do the non-stationary analysis which can simulate the effect of the aortic valve on wave reflections.

Smith and Craige (1986, 1988) investigated the mechanism of the incisura through an abnormal pulse caused by weak left ventricular contraction. The contraction strength is so low that there is only one normal output every two or three left ventricular contractions (**Fig. 31**). This syndrome is called the dicrotic pulse. Peak 1 is too weak to push open the aortic valve, so there is no sign of a notch in the aortic pressure and velocity waveforms at the corresponding time. The aortic pressure decreases exponentially after the previous opening of the aortic valve. If the strength of ventricular systole is just enough to push the valve open, an incisura notch will be produced, even though no forward ejection has occurred (**Fig. 31** peak 2). The aortic pressure is higher than the ventricular pressure immediately after the valve opens. This reverse pressure gradient induces the reverse flow, and the aortic pressure decreases until the closure of the valve (the arrow). The flow is back to zero and the pressure is back to the trend of an exponential decay. Peak 3 is even stronger, it pushes open the aortic valve and generates a small amount of forward flow into the arterial system. The magnitude of the backward flow and the pressure drop is greater than peak 2. However, the pressure continues in the trend of an exponential decay. Both

pressure and velocity disturbances generated by peak 2 or 3 are in the same form. However, the pressure waveform is different from the velocity if they are generated by a normal beat.

In general, waves might be neither totally absorbed nor totally reflected by the heart, but depend on the situation of the valve during a heart cycle. In order to incorporate the aortic valve within our model, the reflection coefficient of the heart is simply classified as having two states, the aortic valve is either fully opened or completely closed. For the convenience of interpretation, a heart cycle in our definition is from the opening of the aortic valve to the dying out of the wave. It is different from the general definition, according to the ECG.

The first state is from the opening to the closure of the aortic valve, which is 0.3 s on average in normal people. During this period the blood is ejected into the arterial system (input). There is no available data about the effective reflection coefficient during the opening of the aortic valve. Some models have treated the heart as a sealed elastic chamber or an ellipsoidal shell (Rushmer, 1961; Vayo, 1966; Welkowitz, 1987) from which they predicted the reflection coefficient should vary with time when the valve is open. The complicated structures inside the ventricle such as the chordae tendineae and papillary muscles could function like a sound absorber inducing the cancellation of reflected waves inside the chamber. It is reasonable to assume that no reflections can be generated by the heart when the valve is open. The second state is after the valve closes to the dying out of the waveform. The reflection coefficient of the heart after the valve is closed is assumed to be unity. This assumption was also adopted by Bauer *et al.* (1970) and Berger *et al.* (1993), who simulated pulse wave propagation in the arterial system by repeated reflections in a single tube.

It is still possible to calculate the pressure and velocity waveforms when the aortic

valve is functioning by taking the convolution of the transfer functions with the input. The transfer function which we adopt should include the reflections from the heart, i.e. the heart is a total reflector but we modify the convolution by considering the time of arrival at the aortic root of each pulse wave. As mentioned in §2.5.1, a pulse wave which has the amplitude A and is located at time τ in the transfer function represents the input wave which travels in the arterial system and arrives at the point of observation at time τ with an amplitude A. However, when the behaviour of the aortic valve is considered, some pulse waves in the transfer function may no longer represent complete waves, half sinusoidal waves, because part of the wave is swallowed and the rest is reflected when the aortic valve closes. For example, consider a pulse wave arriving at the aortic root at time 0.2 s. One third of the wave will be swallowed by the left ventricle before the aortic valve closes at 0.3 s and the other two thirds of the wave will be reflected back into the arterial system. As long as the pulse wave comes to the aortic root before the closure of aortic valve, some part of it will be absorbed. Thus, the waveform becomes the summation of many incomplete and complete waves.

We first consider the waveform at the ascending aorta. The transfer function acquired at the point of observation can be separated into forward and backward transfer functions, $C(t) = C^+(t) + C^-(t)$ ("+" denotes the forward and "-" denotes the backward). The forward transfer function can be further separated into (1) the input and (2) those reflected by the heart, $C^+(t) = C_0^+(t) + C_R^+(t)$ ("0" denotes the input, "R" denotes the waves reflected by the heart). The backward transfer function can also be separated into those arriving for the first time, the second time and so on to the n-th time at the heart, $C^-(t) = C_1^-(t) + C_2^-(t) + \cdots + C_n^-$ (the subscript denotes the n-th time of arrival at the heart). The forward waves in the ascending aorta can be calculated by:

$$P^+(t) = C_0^+(t) \otimes r(t) + [C_R^+(t) \otimes r(t)]H(t - (T - \tau_0)) \quad (3.1)$$

where $P^+(t)$ is the forward pressure waveform.

$r(t)$ is the input waveform, which is assumed to be a half cycle of a sinusoidal wave.

$H(t\text{-}t^*)$ is the Heaviside function: $H(t\text{-}t^*) = \begin{matrix} 0 \\ 1 \end{matrix}$ when $\begin{matrix} t < t^* \\ t >= t^* \end{matrix}$

T is the duration from the valve opening to its closure which is 0.3 s in this model.

τ_0 is the travel time from the aortic root to the point of observation. It is 0.00424 s for the ascending aorta.

$\otimes$ is the convolution operator.

The waves arriving at the heart for the first time can retain their complete waveform at the point of observation but the waves arriving for the second time may not, depending upon the time when they first arrive at the aortic root. If they arrive after the valve is closed, they can retain the whole waveform. The pressure waveform caused by the backward waves can be calculated by:

$$P^-(t) = C_1^-(t) \otimes r(t) + \sum_{i=2}^{n} [C_i^-(t) \otimes r(t)]H(t - (T - \omega_i)) \quad (3.2)$$

where ω_i is the travel time of each wave from its first time arriving at the aortic valve to this point of observation. Each pulse wave has its own ω_i. The pressure waveform can be calculated by the summation of the forward and backward waveforms,

$$\begin{aligned} P(t) = P^+(t) + P^-(t) &= C_0^+(t) \otimes r(t) + [C_R^+(t) \otimes r(t)]H(t - (T - \tau_0)) \\ &+ C_1^-(t) \otimes r(t) + \sum_{i=2}^{n} [C_i^-(t) \otimes r(t)]H(t - (T - \omega_i)) \end{aligned} \quad (3.3)$$

The separation of the backward transfer function is very difficult because of the large number of pulse waves in the backward transfer function. For example, there are more than 6,000 waves when the threshold is 0.001. For this calculation, the number of waves

was decreased by raising the threshold to 0.1. With the increased threshold, there are two groups of waves left, the first and the second time arriving at the heart. The separation of these two groups is carried out by comparing the backward waves between two cases, (1) the heart is a total reflector and (2) the heart is an absorber. When ω_t is greater than T in (3.3), this wave returnsafter the closure of the aortic valve, so it can retain a full waveform.

Since the closing of the aortic valve is not instantaneous, we assume that the duration from the onset of closing to completely closed is 0.01 s. The reflection coefficient during the closing is assumed to be directly proportional to the cross-sectional area covered by the aortic valve which is presumed to be linear in time.

The results of the pressure and velocity waveforms with the aortic valve function are shown in **Fig. 32 (a)**, where the input is a half sinusoidal wave. Several distinct characteristics of the *in vivo* measured waveforms (**Fig. 2**) are reproduced by this model:

(1) The large pressure jump immediately after the closure of the aortic valve.

(2) The reverse flow halts immediately after the valve closed.

(3) During the diastolic phase, apart from a little oscillation, the flow velocity is nearly zero.

The zero flow after the closure of the aortic valve results from the cancellation of the backward waves and those reflected from the heart which, actually increase the pressure. Similar results are seen in §3.5, when the heart is a total reflector. This study shows that the aortic valve plays an important role in determining the aortic waveforms. The magnified pressure waveform after the closure of aortic valve has been found in the human ascending aorta (Sugawara, 1996, personal communication), but generally the increase of pressure after the valve closed is less than our results (discussed later). An amplified pressure after the closure of the aortic valve is frequently found in dogs and kangaroos (Avolio *et al.*, 1984; Nichols *et al.*, 1986; O'Rourke and Nichols, 1990).

The variation of the incisura as the observation point moves downstream is an interesting feature in the waveform transformation. However, the computation becomes more complicated distally. For example in the aortic arch I, the transfer function is still separated into forward and backward groups, but the forward group contains (1) the input, (2) the waves reflected from the heart and (3) the waves reflected from the carotid circulation without passing by the heart. Group (3) can retain their complete waveform as can group (1). The (3) group can be separated by comparing the waves in the forward group of both the ascending aorta and the aortic arch I segment. The analyses become still more complicated when the calculation moves distally. The backward group is still separated into those travelling towards the heart for the first time and the second time. The number of re-reflected waves increases distally and the tracing of each wave to its first time of arrival at the aortic valve becomes difficult and tedious. In principle, the variation of waveforms caused by the aortic valve can be carried out by the separation of the transfer function, segment by segment, but it is extremely complicated in practice. However, the results shown in §3.5, where the heart is a total reflector throughout the cycle, reveal the maximum possible contributions of reflections from the heart in determining the waveforms.

3.7 The Effect of a Complete Occlusion of the Aorta

This model can be extended to study waveform changes when a pathological problem, such as an occlusion in the artery, occurs in the arterial system. Van Der Bos *et al.* (1971) introduced a complete occlusion in the canine aorta with a balloon. The waveforms were recorded at the ascending aorta (**Fig. 33 upper panel**). The waveforms were analysed by Davies (1994) by the wave intensity method (**Fig. 33 lower panel**). The locations of the four occlusion sites are the upper descending aorta, the level of the diaphragm, lower

abdominal aorta and one of the iliac arteries.

When the occlusion is in the upper descending aorta (**Fig. 33 (b)**), there is a large systolic wave and a prominent inflection point. The peak pressure is about twice as high as the control waveform. When the occlusion moves to the diaphragm (**Fig. 33 (c)**), the inflection point delays and the peak pressure decreases to about 20 % higher than the peak pressure of the control case. The peak pressure decreases even more and the inflection point delays to late systole when the occlusion is in the abdominal aorta (**Fig. 33 (d)**). When the occlusion moves to one of the iliac arteries, there is no discernible difference compared with the control waveforms (**Fig. 33 (a), (e)**). It is noted that there is not much deviation of the velocity waveform when the occlusion is introduced in the system.

We did a simulation at the corresponding sites of the human model by blocking the thoracic aorta I segment, abdominal aorta I segment, abdominal aorta V segment and one of the iliac arteries. The heart is assumed as a total absorber. The results are shown in **Fig. 34** and are compared with the control case in which there is no occlusion (dotted line). There are several important features:

(1) When the occlusion is located in the thoracic aorta I segment (**Fig. 34 (a)**), the reflected waves arrive at the point of observation (middle of the ascending aorta) at 0.11 s and form a prominent inflection point. The peak pressure is about 40% higher than the control waveform. When the occlusion moves to the abdominal aorta I segment (**Fig. 33 (b)**), the reflected waves delay their arrival at the point of observation (0.13 s), and the strength is weaker. The peak pressure decreases to about 20% higher than the control waveform. When the occlusion is in the abdominal V segment, the reflected waves are even weaker and arrive even later at the point of observation. Finally, only a small deviation is found when the occlusion is in the left external iliac artery. The deviation of the velocity waveforms is

relatively small in all cases.

The weakening of the reflected wave as the occlusion moves distally, is due to the dispersion caused by the mismatching for backward waves, even though the input wave does not suffer any decrease when it was reflected by the occlusion in the iliac artery. This fact was taken as an evidence for no reflections in the systemic arteries by Peterson and Gerst (1956) who induced a pressure pulse in a dog's femoral artery and did not find any response in the ascending aorta. Similar results were seen in the canine experiments by Van Der Bos. *et al.*, (1971). Latham *et al.* (1985) did a similar experiment by occluding the bilateral femoral artery of a dog and did not find any significant difference with the control pressure waveform measurement in the ascending aorta.

(2) When the occlusion is in the thoracic aorta I segment, there is a significant pressure increase in the later portions of the waveform. This gradually dies out when the occlusion is moved distally. The second "pressure hump" is due to the group of waves reflected by the occlusion. This can be demonstrated by comparing the time of the inflection points (pressure or velocity waveforms) between **Fig. 34 (a)** and **(b)**.

Normally a sudden aortic occlusion or the increasing in the peripheral resistance would induce a decrease of the ventricular output and an accumulation of blood in the ventricle in the first several beats. The enlargement of the ventricle due to the accumulation will increase the output of blood to make the system return to normal (Starling's law of the heart). This calculation assumes that the duration of the occlusion is short enough that no physiological adjustment occurred in the cardiovascular system.

3.8 Analysis by the Wave Intensity Method

The wave intensity method which is based on the method of characteristics was developed by Parker and Jones (1990) and Jones *et al.* (1992). Neglecting dissipation, the solution for the nonlinear intersection of waves in the arterial system can be written in terms of the Riemann invariants across characteristics (§2.2). If the product of the pressure variation and velocity variation (with respect to time) is positive definite at the point of observation ($dPdU>0$, P and U are averaged over the cross-sectional area), it is a forward running wave. And it is a backward running wave when the product is negative definite ($dPdU<0$). This analysis allows us to determine the net magnitude and direction of waves from the measured waveforms. The analysis is carried out in the time domain and can be applied to the transient and non-periodic waveforms.

The analysis of the aortic waveform (with a functioning aortic valve) by the wave intensity method is shown in **Fig. 32 (b)**, and its separation into the forward ($dPdU^+$) and backward components ($dPdU^-$) , **Fig. 32 (c)**. The $dPdU^+_1$ ("1" denotes the first peak) is the forward compression wave generated by the contraction of the heart. The second peak of $dPdU^+_2$ is a forward expansion wave which is originated by the relaxation of the left ventricle. The second peak decelerates the flow and is considered as a suction function during the late systole. $dPdU^-_1$ is the reflection of $dPdU^+_1$ from the termini. $dPdU^-_2$ is originated by the expansion wave $dPdU^+_2$, although it is not necessarily an expansion wave. $dPdU^+_3$ is $dPdU^-_2$ reflected by the aortic valve, since apart from a slight time lag between $dPdU^+_3$ and $dPdU^-_2$, they are exactly the same.

We applied the wave intensity analysis to the waveforms which are shown in **Fig. 34** and the result is shown in **Fig. 35**. The aortic valve is not included in the calculation. The wave intensity, $dPdU$, in the left panel is calculated directly from the analysis of the

waveforms at the corresponding sites. $dPdU^+$ and $dPdU^-$ are separated from $dPdU$ and are shown in the right panel.

There are several important characteristics revealed in **Fig. 35**: When the occlusion is in the thoracic aorta I there are three groups of backward waves (**Fig. 35 (a)**). $dPdU^-_1$ and $dPdU^-_2$ are similar in shape to $dPdU^+_1$ and $dPdU^+_2$. The first backward wave is observed at 0.11 s. When the occlusion moves to the abdominal aorta I segment (**Fig. 35 (b)**), $dPdU^-_3$ is declining. $dPdU^-_1$ and $dPdU^-_2$ are still approximately similar in shape to $dPdU^+_1$ and $dPdU^+_2$. However, the backward waves are delayed in time. When the occlusion moves to the abdominal aorta V segment (**Fig. 35 (c)**), the third group of backward waves is greatly diminished. $dPdU^-_1$ and $dPdU^-_2$ are so dispersed that it is difficult to determine the arrival time of these backward waves. When the occlusion is in the right common iliac artery (**Fig. 35 (d)**), the amplitudesof both $dPdU^-_1$ and $dPdU^-_2$ decrease and are similar as the corresponding waves when there is no occlusion (**Fig. 32 (c)**).

It is noted that the shape of the wave intensity, $dPdU$, analysed from measurements (**Fig. 33**) is quite different from those calculated in our model (**Fig. 35**). This is primarily because of the simplistic idealised half sinusoidal waveform which has been assumed in the model. While this simple input function is useful because it allows us to differentiate between features of the arterial waveforms introduced by the complexity of the reflections from those introduced by the complexity of the ventricular input function, it is not a good model of the physiological ventricular input function. This question is discussed further in the next section where we discuss how to derive the ventricular input function from experimentally measured waveforms.

Despite the differences between the unknown ventricular input function in the experiments and the simple one assumed in our model, some of the characteristics of the

wave intensity are the same in both analyses. There is a large and early reflection when the occlusion is in the upper descending aorta (**Fig. 33 (b)**). This reflection is weaker and occurs later when the occlusion moves distally. When the occlusion moves to one of the iliac arteries, the wave intensity is the same as the control case. We conclude that despite differences in detail, the model results are useful in interpreting the experimental results.

3.9 Left Ventricular Analysis

Heart failure is the pathophysiological state in which the heart is unable to pump a supply of blood adequate for the metabolic needs of the body, provided there is adequate venous return to the heart. There are four major determinants of myocardial function: preload, afterload, contractility, and heart rate. The pumping ability of the ventricles depends on these four variables. Preload and afterload are directly related to the anatomical structure of the heart and the arterial system. Preload is the force which imparts a given stretch and length to the ventricular muscle or simply the stretching force that determines pre-contraction (end diastolic) muscle length. Afterload is the tension that must be developed by the myocardium to overcome the forces which oppose ejection of blood from the ventricle. Traditionally, the afterload is calculated by the aortic impedance, which is the Fourier transform of the pressure divided by the Fourier transform of the flow. Many measurements of pressure have been made inside the left ventricle. The purpose of the measurement is to understand the contractility of the left ventricular which can help us to understand the function of the heart muscle. It is clear that the pressure measured in the left ventricle is not solely due to the ventricular output but is the resultant of the output and the backward waves. Cardiac function can not be fully understood without clear knowledge about the real output.

Most studies about left ventricular function are based on the analysis of the hydraulic input impedance of the ascending aorta or a Windkessel model (Milnor, 1975). Westerhof *et al.* (1972) pointed out that the harmonics of the left ventricular pressure and either the aortic pressure or the aortic flow cannot be related since the aortic valve is a nonlinear device. Therefore the division of the ascending aortic pressure harmonics by the aortic flow harmonics could not give proper information about the left ventricular output.

In a sense, the problem is the inverse of the process of our simulation. We can acquire the aortic waveform easily by measurement, but do not know the left ventricular function. Then the question is asked, can we determine the left ventricular function by inverting the process of our model to calculate the left ventricular function from a measured waveform and the transfer function? To answer this question, we have to return to (3.3). Unfortunately, (3.3) is a nonlinear function in which the ventricular input, $r(t)$, can not be separated simply through the inverse Fourier transform.

Actually, only the systolic part of the waveform needs to be included in order to calculate the left ventricular function. The pressure waveform at the ascending aorta of a human was collected by Davies (1994). The data contains 372 points for a cycle and the first 189 points constitute the systolic portion (from the first point defined as the foot of the wave to the dicrotic notch).

The convolution is still applied to calculate the left ventricular waveform. Because both the aortic waveform and the transfer function are discretized functions, the convolution is converted into a series of algebraic equations. The left ventricular function is the unknown V_i. The aortic pressure is the measured data P_i, and the corresponding transfer function is H_i, where i = 1 to 189. The algebraic relation can be described in matrix form:

$$\begin{bmatrix} P_1 \\ P_2 \\ P_3 \\ \vdots \\ P_{189} \end{bmatrix} = \begin{bmatrix} H_1 & 0 & 0 & \cdots & 0 \\ H_1 & H_2 & 0 & \cdots & 0 \\ H_1 & H_2 & H_3 & \cdots & 0 \\ \vdots & \vdots & \vdots & \vdots & \vdots \\ H_1 & H_2 & H_3 & \cdots & H_{189} \end{bmatrix} \begin{bmatrix} V_1 \\ V_2 \\ V_3 \\ \vdots \\ V_{189} \end{bmatrix} \tag{3.5}$$

Because of the triangular form of H, this can be solved by forward substitution.

$$V_m = \frac{1}{H_1}(P_m - \sum_{j=1}^{m-1} P_{m-j+1} V_j) \qquad m=1..189$$

However, the transfer function is not sampled in the same time span as the aortic pressure. To solve this problem, the transfer function is converted into the frequency domain by Fourier transform and sampled with the same frequency span as the aortic pressure, then converted back to the time domain.

The left ventricular pressure function calculated by (3.5) is shown in **Fig. 36**. This result can be calculated only when the transfer function of the arterial system is known. Spikema *et al.* (1980) induced a pulse pressure in dogs and acquired the transfer function, but there are no similar experiments on humans. If it was possible to have a breakthrough in the measurement of transfer function in the human arterial system, the diagnostic significance would be immense.

3.10 The Influence of Terminal Resistances and the Coronary Circulation on Waveforms in the Ascending Aorta

We would like to discuss the variation of the waveform in the ascending aorta under the influenced of two factors: (1) the variation of terminal resistance and (2) the inclusion of the coronary circulation in the calculation. The left ventricular function calculated above is adopted as the input, which is fitted by a tenth order polynomial equation (solid line in **Fig. 37**).

To test the influence of the terminal resistances, the reflection coefficient of each terminal is decreased in 10% increments to 30% of the values shown in **Table 3**. The result is shown in **Fig. 38**. The dotted line is the experimental data. All waveforms are normalized by the peak value of the experimental data.

As expected, when the terminal resistance decreases, the amplitude of the pressure decreases, and the decrease is greatest in late systole and diastole. Concurrently, the amplitude of the velocity increases and there is less reverse flow. Stronger reflections can generate higher pressure in diastolic phase and larger reverse flow, but they do not affect the zero flow after the closure of the aortic valve.

It is well known that terminal resistance will be decreased with exercise (Murgo *et al.*, 1981 b). **Fig. 39 (a)** shows the aortic pressure and velocity of a man at rest and during exercise. The terminal resistance and characteristic impedance are listed in the table in **Fig. 39 (b)**. During exercise, there is little change of the incisura and the backflow, but the pressure in the diastolic phase decreases distinctly. The resistance falls about 35-55% during exercise, and the variation of the reflection coefficient of the terminal resistance which can be calculated by Eq. (2.33) falls about 10-20%,. As predicted by the calculation, there is not much variation of the incisura and backward flow, but a

noticeable fall in the pressure after the closure of the valve, when the terminal reflection coefficient changes 20% (compare **Fig. 38** and **Fig. 39 (a)**).

The coronary circulation, which supplies the blood to the heart, has been neglected in most of our model calculations. However it may have a prominent influence on the aortic waveforms, especially in the diastolic phase.

The right and left coronary arteries emanate from the aorta directly above the cusps of the aortic valve. The branches of the coronary artery in the myocardium are compressed during each systole, so the coronary blood flow is interrupted and even reverses in early systole. The coronary flow is restored during the ejection phase as stress in the ventricle wall eases and arterial pressure rises, but flow is only restored fully during diastole. This pattern of blood flow is different from most of the organs (Khouri and Gregg, 1963). About 80 % of the coronary flow occurs in the diastole phase at basal heart rates (Levick, 1992). About 5 % of the cardiac output goes to the coronary circulation, so that 4 % of the total cardiac output flows into the coronary circulation during the diastolic phase. This is large enough to influence the waveforms in the ascending aorta. Therefore, the reflection coefficient of the heart, which incorporates the coronary circulation, may not be unity after the valve closed.

The overall reflection coefficient of the heart in the diastolic phase is still uncertain. In this simulation, we re-modelled the overall reflection coefficient of the heart as 1.0, 0.9, 0.8, 0.7 and 0.6 when the valve is closed and no reflection when the valve is opened. The calculation of the waveforms in the ascending aorta is shown in **Fig. 40**. The dotted line is the experimental pressure in the ascending aorta, the upper solid line is the pressure and the lower line is the velocity. All the calculations are normalized by the peak value of the measurement.

There are two features of the calculation which should be noted:

(1) The incisura is not very sensitive to the changes of the reflection coefficient of the heart. The pressure in the diastolic phase is the result of the summation of the backward waves and the waves reflected by the heart, which are the only waves influenced by the heart's reflection coefficient.

(2) The inverse flow does not go to zero immediately after the valve closed. The less the heart reflects, the longer it takes for the backward flow to go to zero. This is different from the modified terminal resistance case where all the reverse flow was zero whenever the valve was closed.

4

Nonlinear Programming

4.1 Introduction

The "tree of waves" model described in the previous chapter has shown many of the features of the behavior of waves in the systemic arteries. It successfully incorporates the function of the aortic valve which is probably the greatest source of nonlinearity in the arterial system. In this chapter we will discuss the influence of the other factors which may cause the system to behave nonlinearly, such as a pressure dependent wavespeed, convection effects and the tapering of arteries.

The importance of these nonlinearities has been debated for decades (Lambert, 1958; Ling *et al.*, 1973). Those authors who apply the impedance method to the study of arterial waves generally dismiss the importance of the nonlinearities (Westerhof *et al.*, 1973; O'Rourke, 1982 b). Whereas those using nonlinear fluid dynamics to study the problem emphasise the importance of the nonlinearities (Anliker *et al.*, 1971). Anliker *et al.* (1968, 1969) made measurements in anaesthetized dogs and found that the wave velocity is strongly influenced by changing the transmural pressure and suggested that the wavespeed could vary during a cardiac cycle.

Most of the theoretical studies of nonlinear effects on waveforms in the arterial system were modelled by one-dimensional Navier-Stokes equations and solved numerically by finite difference or finite elements (Skalak and Stathis, 1966; Anliker and Rockwell, 1971; Stettler *et al.*, 1981; Stergiopulos, 1992). As mentioned in §1.4, those results can provide few physical insights into the arterial system because it is difficult to

link a single phenomenon with a single factor. Furthermore, as demonstrated in previous chapters, the dicrotic notch is generated by the aortic valve interacting with wave reflections from the arterial system. Normally in the fluid dynamics models, the pressure or velocity waveform at the ascending aorta, including the incisura, is specified as a boundary condition. Therefore, some confusion of the physical meaning of the phenomena which are observed is inevitable. The nonlinear models introduced here are capable of clarifying the effects of each nonlinear factor.

4.2 Nonlinear Factors

There are several nonlinear factors which may influence the waveforms:

(1) Arterial Tapering: Arterial segment diameters generally become smaller as the distance from the heart increases (Patel *et al.*, 1963; Iberall, 1967; Kimmel and Dimmar, 1983; Latham *et al.*, 1987). Caro *et al.* (1978) simulated the arterial cross-sectional area versus distance with an exponential decay function with the distance from the heart, $r_i=r_0e^{-kz}$. Where r_i is the inner radius, $r_i = r_0$ at the heart and z is the axial distance. For the femoral artery, Li *et al.* (1981) used a value of 0.02 for k in the above equation. Belardinelli and Cavalcanti (1992) did a numerical simulation of the influence of a continuous tapering on the pulse pressure waveforms in a 60 cm tube. Instead of the percentage of the area decrease, a tapering angle,0l 4°, was introduced. They found that the amplitude of the pulse increases about 40% at the end of the 60 cm trip.

Papageorgiou and Jones (1987) scrutinized the geometry of the arteries using several sources and concluded that the decreasing of the arterial diameter distally seems more likely to be due to the branching of the system. A similar conclusion was reached in the observation of Milnor and Nichols (1975). The diameter of arteries between

bifurcations remains essentially constant (Milnor and Bertram, 1978). From the studies of the data measured by different groups, Papageorgiou and Jones (1987) concluded that the arterial diameter is most likely a non-continuous variable and it would be more realistic to consider the changes of the arterial diameter in steps, each step corresponding to a branching point.

In the absence of accurate data about the degree of tapering in individual arterial segments, we conclude that there is no need to introduce a further tapering inside each single segment in our model.

(2) Convection effects: The presence of a forward flow, U, will increase the wavespeed for forward propagating waves to $U+c$, and will decrease it for backward propagating waves to $U-c$. The contribution of the flow velocity to the waveform was neglected in the tree of waves model by the assumption that the flow velocity is small compared with the wavespeed (§2.3). However, the convection term may not be negligible in the ascending aorta and the large arteries of the aortic trunk where the peak flow speed is about 20% of the wavespeed (see **Table 2**). The effect of convection will be studied in a nonlinear model and compared with the linear tree of waves model.

(3) Pressure dependent wavespeed: The properties of vessels in the linear model are assumed to be isotropic, i.e. the Poisson's ratio is the same in all directions, which is regarded as an acceptable approximation when the strains are small. It is well known that the blood vessel wall gets stiffer when the transmural pressure increases and that the wavespeed increases when the stiffness of the wall increases (Cox, 1971). Since the pressure changes by approximately 5330 Pa (40 mmHg) during a cycle, each portion of the wave will travel with its own wavespeed according to its absolute pressure.

The elastic modulus of the blood vessel is neither a constant nor changing linearly

as the pressure varies in the physiological range (Bergel, 1961 a, b), probably because of the contribution of the different wall components to arterial stiffness at different pressures. Resting vascular smooth muscle cells have a peak Young's modulus of 5×10^4 Pa (Dijk, 1983), which is smaller than the stress exerted by the arterial pressure. The Young's modulus of elastin, $2\text{-}5\times10^5$ Pa is of the order of magnitude of the pressures in the arteries. The Young's modulus of pure collagen, $5\text{-}50\times10^7$ Pa, is much higher than the arterial pressure. Therefore, elastin and partially stretched collagen fibers bear the stress in the wall and determine its mechanical properties rather than smooth muscle. Also, with increasing pressure and distention, more and more collagen fibers in the aortic wall become stressed. As a result of this collagen recruitment, the elasticity is determined more by collagen and less by elastin as pressure increases.

Frank (1899, 1905) first noticed that the pulse wave velocity would increase when the mean arterial pressure increases. Bramwell and Hill (1922) used excised arterial segments filled with mercury to decrease the wavespeed to make accurate measurements of the wave transit time. They found that the foot to foot wave velocity increased proportionally with the pressure in the diastolic phase. This concept was extended (Bramwell and Hill, 1923) when they postulated that the portion of the wave at the systolic peak would ultimately overtake the foot. McDonald and Taylor (1959) found that the foot to foot wavespeed correlated well with both the mean arterial pressure and the diastolic pressure, but not with the wavespeed where the pressure is maximum. Anliker *et al.* (1968) studied the velocity of a discrete wavetrain at various pressures during the cardiac cycle in anaesthetized dogs with an electromag netic impactor and found that the wavespeed changes from about 3.7 m/s at 30 mmHg to 6.0 m/s at 120 mmHg.

Theoretically, the shift of the Young's modulus of the vessel due to the variation

of pressure should change the wavespeed. Langewouters *et al.* (1985) made a model of the mechanics of the aorta by using a second order function to fit their measurements of the Young's modulus as a function of pressure, in experiments on 45 thoracic and 20 abdominal aortas from humans. When the pressure of a typical thoracic aortic segment changes from 80 to 140 mmHg, the static Young's modulus increases from 6×10^5 to 40×10^5 Pa, and the wave velocity predicted by their model increases from 5 m/s at 80 mmHg to 10 m/s at 140 mmHg. Histand and Anliker (1973) measured wavespeed in the canine aorta as a function of the instantaneous aortic pressure and frequency. The experiment was done by blocking the flow into the descending aorta or by clamping the thoracic aorta above the diaphragm to raise or decrease the pressure. A typical wavespeed of 4.2 m/s was found when the aortic pressure was 80 mmHg and 5.5 m/s at 120 mmHg. They found that wavespeeds are frequency independent.

In this study, the wavespeed predicted by Moens-Korteweg equation is assumed to be a half way value between peak and bottom of the amplitude (§2). The range of variation of the wavespeed in each segment was assumed to be 2 m/s, i.e. the fastest wavefront in this segment is 2 m/s faster than the slowest wavefront. The validity of this assumption will be discussed later.

Other potentially nonlinear effects are present in arterial flows. The principal one, viscous friction, will not be discussed in our model since the flow-dependent shear stress at the artery wall is still not adequately described *in vivo*. Most of the studies which included viscous friction assume the flow in each segment as a Poiseuille flow (Anliker *et al.*, 1971; Rumberger and Nerem, (1977); Stettler *et al.*, 1987; Stergiopulos *et al.* 1992). If friction is considered, the right hand side of Eq. (2.10) is non-zero and the characteristic lines will not be straight lines on an x-t diagram, and the equations can only be solved by

integration along the characteristic lines. In addition, blood vessels exhibit visco-elastic behavior (Langewouters *et al.*, 1985) and a more complicated equation for the elastic modulus is needed to incorporate this viscous effect. However, the order of error in neglecting the visco-elastic properties of the aorta is probably less than those arising from other assumptions, for example assuming that the wavespeed is predicted by the Moens-Korteweg equation. Through measuring strain rates on the aortas of eight dogs within the physiological range *in vivo*, Ling and Atabek (1972) could not detect any measurable visco-elastic behaviour in these arteries.

4.3 Governing Equations

In the linear model, the pressure and velocity at the point of observation are assumed to be the superposition of all the infinitesimal wavefronts without worrying about their sequence of arrival. In the nonlinear model, the amplitude is finite and since convection or pressure dependent wavespeeds are considered, the properties after the intersection of waves do not fulfill the conditions necessary for superposition. Also, because of the nonlinearity, the intersection of waves should follow the true time sequence. For example, in the nonlinear case the properties of wavefront 1 meeting with 2 first then intersecting with 3 are different from the properties of wavefront 1 meeting 3 first then intersecting with 2.

The equation for one-dimensional flow in an elastic tube without wall friction or leakage out of the wall can be written as:

$$\frac{dU}{dt} \pm \frac{1}{\rho c(P)} \frac{dP}{dt} = 0 \qquad \text{when} \quad \frac{dx}{dt} = U \pm c(P) \qquad (2.10)$$

where the wavespeed is a function of pressure. As mentioned in §2.2, $U \pm \int \frac{dP}{\rho c}$ is

constant along the characteristic direction, $\frac{dx}{dt} = U \pm c$. The properties of two finite amplitude wavefronts after an intersection are (**Fig. 41**):

$$dU_1 + \frac{dP_1}{\rho c(P_1)} = dU_3 + \frac{dP_3}{\rho c(P_3)} \tag{4.1}$$

$$dU_2 - \frac{dP_2}{\rho c(P_2)} = dU_3 - \frac{dP_3}{\rho c(P_3)} \tag{4.2}$$

where $dU_i=U_i-U_0$ and $dP_i=P_i-P_0$, $i=1,2,3$, are the amplitude of pressure and velocity disturbance change across a wave. $c(P_i)$ is the local wavespeed, which is pressure dependent.

From (4.1) and (4.2), dP_3 and dU_3 are:

$$dP_3 = \frac{1}{2}\rho c(P_3)\left[(dU_1 - dU_2) + \left(\frac{dP_1}{\rho c(P_1)} + \frac{dP_2}{\rho c(P_2)}\right)\right]$$

$$dU_3 = \frac{1}{2}\left[(dU_1 + dU_2) + \left(\frac{dP_1}{\rho c(P_1)} - \frac{dP_2}{\rho c(P_2)}\right)\right] .$$

The new changes across the waves after the intersection are:

$$\begin{aligned} dP_2' = dP_3 - dP_2 &= \frac{1}{2}\rho c(P_3)\left[(dU_1 - dU_2) + \left(\frac{dP_1}{\rho c(P_1)} + \frac{dP_2}{\rho c(P_2)}\right)\right] - dP_2 \\ &= c(P_3)\left[\frac{dP_1}{c(P_1)} + \frac{dP_2}{c(P_2)} - \frac{dP_2}{c(P_3)}\right] \end{aligned} \tag{4.3}$$

$$\begin{aligned} dU_2' = dU_3 - dU_2 &= \frac{1}{2}\left[(dU_1 + dU_2) + \left(\frac{dP_1}{\rho c(P_1)} - \frac{dP_2}{\rho c(P_2)}\right)\right] - dU_2 \\ &= dU_1 + dU_2 - dU_2 = dU_1 \end{aligned} \tag{4.4}$$

$$dP_1' = dP_3 - dP_1 = c(P_3)\left[\frac{dP_1}{c(P_1)} + \frac{dP_2}{c(P_2)} - \frac{dP_1}{c(P_3)}\right] \tag{4.5}$$

$$dU_1' = dU_3 - dU_1 = dU_2 \tag{4.6}$$

It is noted that after the intersection, the amplitudes of velocity just pass through each other without changing their values, but the amplitude of pressure may change. If the wavespeed is pressure invariant, the amplitude of the changes in pressure can be simplified:

$$dP_2' = \frac{1}{2}\rho c\left[\left(dU_1 - dU_2\right) + \left(\frac{dP_1}{\rho C} + \frac{dP_2}{\rho c}\right)\right] - dP_2 = dP_1 + dP_2 - dP_2 = dP_1 \tag{4.7}$$

$$dP_1' = \frac{1}{2}\rho c\left[\left(dU_1 - dU_2\right) + \left(\frac{dP_1}{\rho c} + \frac{dP_2}{\rho c}\right)\right] - dP_1 = dP_2 \tag{4.8}$$

When the wavespeed is pressure independent, the amplitudes of both pressure and velocity changes will not change during wave intersections.

In order to identify the different effects of convection and the pressure dependent wavespeed on the changes of the waveform, the two effects are considered separately in two nonlinear models:

(1) Convection is included but the wavespeed is not dependent on the pressure.

(2) The wavespeed is pressure dependent but convection is not included.

In the first case, the amplitudes of each intersection should be computed by (4.4), (4.6), (4.7) and (4.8), the propagation speeds of the two waves are U_1+c and U_2-c. For the second case, the amplitudes of each wavefront can be calculated by (4.3) to (4.6), the propagation speeds of two waves are $c(P_1)$ and $c(P_2)$.

4.4 Mechanism of Wave Transmission in the Arterial System

In order to compare with the result of the tree of waves model, the input is again taken to be a half sinusoidal wave but it is divided into a number of equal amplitude wavefronts. When these wavefronts come into the systemic arteries, each wavefront will

have the reflection-transmission behaviour discussed in the previous two chapters. In the nonlinear model, the amplitude of pressure and velocity of each wavefront may be changed when they intersect, as will the propagation speed, because of the changes of the absolute velocity (convection case) or absolute pressure (pressure dependent wavespeed case).

The strategy for dealing with the nonlinear model is totally different to the linear one. The waveform is no longer the input waveform convoluted with the transfer function. There are four main difficulties of the nonlinear programming which must be overcome:

(1) The intersections between wavefronts and the information transmitted between segments are strongly time dependent, i.e. an intersection of waves somewhere in the body cannot be predicted until the properties of all the previous intersections are calculated. Thus, an intersection in the renal artery may effect a later intersection in the iliac artery or the ascending aorta.

(2) The number of waves which we are dealing with in the model is at least forty times larger than in the tree of waves model. Moreover, each intersection between wavefronts has to considered whenever the intersection happens, so the number of calculations can be be more than three orders of magnitude greater than the tree of waves model. The number of waves which are generated by a single wave passing through several levels of bifurcations in the linear model was discussed in the §2.5.1. In the nonlinear model, we must consider the finite waveform as the summation of numerous small wavefronts, each of which will generate its own tree of waves.

(3) There are huge amounts of data which have to be saved in the computation, including (a) the pressure, velocity, speed of propagation, location and travel time of each

wavefront, (b) the data of each intersection point, which are necessary for updating the properties of waves when a new wave enters, and (c) the data when waves pass the point of observation. The memory of the workstation is not adequate, and so swapping between the hard drive and memory is needed for the computation.

(4) The complicated mechanisms of the intersections between waves, such as a face to face intersection, shock-like catching up and the spreading out of expansion waves must be considered. The intersections in the model will be a mixture of these three types, which makes the programming more difficult.

The nonlinear programming inevitably entails an enormous computation and a large amount of data book-keeping. To save computation time, we improved the efficiency of the program by analysing the different ways that waves can intersect. Also the threshold for killing off waves was increased to 4% of the input wavefront. In this study, the half sinusoidal wave was separated into 40 equal amplitude wavefronts.

4.4.1 Program Structure

The program essentially provides a "snap shot" of all of the waves in all of the arterial segments at a specific time. If a wave in one of the segments arrives at any of the bifurcations (defined as a 'boundary arrival'), each of the other two segments connected to the same junction will receive a transmitted wave. The segment can be considered as independent when there is neither an internal boundary arrival nor the reception of a wave from a contiguous segment.

Within a segment, each wave must meet the wave adjacent to it, either left or right, before it can intersect any other waves. Therefore, examining the intersection of waves can be done pair by pair according to their locations. In order to calculate the

boundary arrivals, the two boundaries are considered as two "motionless waves" without amplitudes.

The structure of the program is composed of two main stages, (I) consider the intersection of waves within each segment and (II) update the information among segments in the arterial system by examining the time of arrival at the boundary of each of the waves in each segment.

Stage I:

(a) Calculate the wave intersections pairwise from the proximal to the distal boundary. The properties of each pair will be updated only when their intersection time is the shortest amongst all of the wave pairs. (The two boundaries are considered as two motionless waves with no amplitude, and the magnitudes of the resultant waves are given by (4.3)-(4.6) if the problem is a pressure dependent wavespeed case or (4.3), (4.6), (4.7) and (4.8) if it is a convection case).

(b) Store the intersection properties and check whether the waves pass the point of observation.

(c) Continue steps (a) and (b) until a boundary arrival is found.

Stage II:

(a) Find the segment which has the shortest boundary arrival time.

(b) Update the properties of the waves in this segment and the two contiguous segments, which each receives a transmitted wave, to the time of the boundary arrival. The properties of reflected and transmitted waves are calculated from the reflection and transmission coefficients at the junction which are given in §2.4.1 and 2.4.2.

(c) Go through the calculations of stage I again for each of these three segments.

4.5 The Effect of Convection

A half sinusoidal wave with a period of 300 ms is evenly divided into forty equal amplitude wavefronts. There is no special reason for choosing 40, it is a compromise between precision and computation time. The first 20 wavefronts are compression wavefronts, and the final 20 are expansion wavefronts.

The properties of each input wavefront:

(1) The time each wavefront enters the arterial system is:

$$t_i = \frac{0.3}{\pi}\sin^{-1}\left(\frac{i}{20}\right) \qquad i = 0, 1, 2, 3....., 19$$

$$t_i = 0.3 - \frac{0.3}{\pi}\sin^{-1}\left(\frac{40 - i - 1}{20}\right) \qquad i = 20, 21, 22....., 39$$

For convenience in the computation, each input wavefront is treated as a wavefront starting at t=0 at a negative distance from the aortic root. For example, the 2nd wavefront enters into the system at t = $0.3/\pi$ $\sin^{-1}(0.1)$ s which is the same as a wavefront travelling from the distance

$$d = -\frac{0.3}{\pi}\sin^{-1}(0.1) \times C_p \qquad (4.9)$$

with the propagation speed, C_p=c+U_2, where c is the wavespeed, and U_2 is the flow speed of the second wavefront.

(2) The pressure amplitude of each wavefront is $\frac{P}{20}$ and the velocity amplitude is $\frac{U}{20}$, where the amplitude of the sinusoidal pressure input is P and the velocity is U. The amplitude of pressure and the amplitude of velocity of a wave must fulfil the relation U = $P/\rho c$. P in this calculation is assumed to be 5330 Pa, which is 40 mmHg (from 80 to 120 mmHg). The wavespeed c may be different in different segments.

(3) The absolute pressure is the diastolic pressure plus the pressure of each wavefront, $\frac{(i+1)}{20}P$ $(0 \le i < 20)$, and $\frac{40-i-1}{20}P$ $(20 \le i < 40)$. The absolute velocity is $\frac{(i+1)}{20}U$ $(0 \le i < 20)$ and $\frac{40-i-1}{20}U$ $(20 \le i < 40)$.

4.5.1 Intersections of Waves

There are two types of intersections between waves in a single segment: face to face intersections which were discussed in §4.3 and a shock-like intersection where a fast wave catches up with a slower one. In the shock-like intersection, the propagation speed is the wavespeed plus the flow speed in the convection case and the wavespeed depends only on the segment, since the properties of the faster wave are the same as the combined wave after the catch-up (because its pressure and velocity do not change during the intersection). The slower wavefront can be considered as being simply swallowed by the faster one (**Fig. 42**).

Since each wave can only intersect with the waves adjacent to it, to improve the efficiency of the computation the data should be stored in the sequence representing their location inside the segment. Whether two adjacent waves can intersect is decided solely by the difference in their propagation speeds, $I = V_1 - V_2$, where $V=C \pm U$ is the wave velocity, with the positive direction defined toward the periphery and the numbering of waves is from the proximal end of the segment to the distal end ($x_1 < x_2$). Two waves can intersect only when I is positive. The location, x', and time, t', of the intersection are given by:

$$x' = \frac{V_1 V_2 (t_2 - t_1) + V_2 x_1 - V_1 x_2}{V_2 - V_1} \qquad (4.10)$$

$$t' = \frac{x_1 - x_2 + V_2 t_2 - V_1 t_1}{V_2 - V_1} \tag{4.11}$$

When the segment is chosen, the computation focuses on the waves intersecting within the segment. The intersection is examined pair by pair from the first pair, which includes the first wave and the proximal boundary, to the last pair, which includes the last wave and the distal boundary. The pair of waves with the shortest intersection time are selected and their data are updated to the intersection time. Then the next shortest intersection is found, updating their properties at the intersection point to the new intersection time. This calculation continues until one of the wavefronts reaches the boundary, i.e. the shortest time of intersection is either on the proximal or the distal boundary.

4.5.2 Algorithm

The flowchart of the program is shown in **Fig. 43**, all the symbols have the same meaning as in the tree of waves model. In order to improve the computational efficiency, the longer segments were separated into several smaller ones with the same properties. Also, only one leg is included in this model, since the main intention is to estimate the nonlinear effects and both legs have the same properties. The complete data for the segments are listed in **Table 5,** and the numbering of the segments of the arterial tree is shown in **Fig. 44** (the calculation includes segments 0 to 135). The pressure amplitude of each input wavefront is 266.5 Pa, and the threshold for killing off waves is 10.66 Pa, which is 4% of the input amplitude. In a typical calculation, the total number of waves in the whole system during late systolic phase is of the order of 30,000.

The program steps are (**Fig. 43**):

(1) Input the radius, r, length, L, elastic constant E for each segment and the discr tised wa l th ckness, h, half sinusoidal input wave.

(2) Calculate when the first wavefront reaches the proximal boundary of the ascending aorta. Save (a) the time of the boundary arrival, as Ta[0] (Ta[i] is the time from the very first wavefront coming into the arterial system to the latest boundary arrival of the segment i), (b) the time St[0] (St[i] is the time duration between the previous boundary arrival or a wave entering the segment and the boundary arrival of this time in the segment i), where 0 is the segment number for the ascending aorta, and (c) all the properties when a wave passes the middle of a segment, which is taken as the point of observation.

(3) Search for the shortest Ta[i] among all the segments. The segments without waves are excluded from the search.

(4) When the segment with the shortest Ta[i] is found, update all the properties of the waves to the time of its boundary arrival, including the location, absolute pressure and velocity, pressure amplitude and velocity amplitude and wavespeed. The data of the two adjacent segments, $w1$ and $w2$, are also updated to the time, Ta[i]. The updating of the properties of waves is carried out by examining the intersecting time of waves with the time Ta[i]-(Ta[$w1$]-St[$w1$]), where Ta[$w1$]-St[$w1$] is the time of the previous boundary arrival or an entrance of a wave into the segment $w1$, and Ta[i]-(Ta[$w1$]-St[$w1$]) is the duration between the previous boundary arrival or an entrance of a wave and a wave entering the segment $w1$ from the segment i. Therefore, if any pair of waves intersects after the time Ta[i]-(Ta[$w1$]-St[$w1$]), this intersection is not valid. A diagrammatic representation of a wave transmitting to the two contiguous segments is shown in **Fig. 45**. The saved data at the point of observation become the output after examining their

validity to the time Ta[*i*]-(Ta[*w1*]-St[*w1*]).

(5) Check the amplitude of wavefronts and kill those less than the threshold. Calculate the next boundary arrival of these three segments. Save Ta[n], St[n] (n=*i*, *w1* and *w2*) and the properties of waves when they (a) pass the mid point of the segment, and (b) intersect one another.

(6) If there are any waves in the arterial system, go back to step (4)

The mechanism for calculating the transmission of pressure and velocity across the junction is the same as in the tree of waves model which was discussed in §2.4.1 and 2.4.2. The amplitude of pressure reflected by the bifurcation is RdP and the transmission is $(1+R)dP$, where R is the reflection coefficient. The amplitude of velocity is calculated by the water hammer equation, $dU=\pm R/(\rho C)dP$.

There are several mechanisms to deal with special situations which can arise, such as when two waves come to the same bifurcation junction simultaneously. Three waves, one for each segment, will be generated by these two incident waves. However, the computation will generate six waves by two incident waves. Thus, we have to establish a mechanism to combine these six waves into three. The procedure is incorporated in step (4) and the detail is shown below:

(a) Assume that two segments have the same boundary arrival times Ta[*a*]=Ta[*b*]. If "*a*" has the smaller segment number, it will be chosen first because of the sequence of computation and the wave in "a" will generate one reflected wave and two transmitted waves.

(b) In the segment "*b*", this new transmitted wave has same location, either the proximal or distal boundary, but is travelling in the opposite direction of the wave arriving at the boundary. These two waves are not in the same direction and should not be added

together.

(c) Segment "*b*" now has the shortest Ta[*b*] in the system and is chosen next. Its boundary arrival wave also generates one reflected wave and two transmitted waves. In segment "*b*", the reflected wave will be travelling in the same direction and at the same location as the transmitted wave generated in the previous step. These two waves coincide and can be added together. We assume that the properties of these coincident waves are additive.

4.5.3 Results and Discussion for the Convection Case

The results of the nonlinear calculation including convection are shown in **Figs. 46** (the saw-shaped line), compared with the results from the linear model (the smooth line) with the same threshold , 4% of the input, and including only one leg. The nonlinear pressure waveform is normalised by the input pressure pulse, 5330 Pa, and the velocity is normalised by the input velocity which is $5330/\rho c_i$, where i is the segment number and c_i is the wavespeed of the i segment.

Figs. 46 reveal that the effect of convection has a relatively minor influence on the waveforms particularly in the proximal arteries. Previously, our understanding about the effect of convection on the waveforms is based on the discussion in §2.3 and 4.2, which suggested that the effect should occur in the segments where the velocity is not negligible compared to the wavespeed. This would be in the segments nearest to the heart such as the ascending aorta where the peak flow is about 20% of the wavespeed (McDonald, 1974). The results show a different pattern. In the ascending aorta, the waveforms with the convection effect are almost identical to the linear ones, which ignores the convection (**Fig. 46 (a)**). In fact the deviations between the linear and nonlinear calculation get larger distally.

One of the features of the calculations is that the systolic waveforms with convection

lead the linear ones as the wave propagates downstream but the lead time does not increase significantly as the wave moves distally. In the ascending aorta, the peak input flow speed is about 1 m/s and the wavespeed is 5 m/s. This fastest wavefront reaches the point of observation, the middle of the ascending aorta, only 0.67 ms earlier than the linear one. The other input wavefronts with lower flow speeds, have shorter time lags. Such a small differences cannot be seen in the graphs. In segments further downstream, the time gap gets wider. For instance, the fastest input wavefront arrives at the point of observation in the abdominal aorta I segment (67), 9.5 ms earlier than the linear one (**Fig. 46 (f)**) which is discernible in the figure. The earlier arriving wavefronts will also be reflected earlier, which make the contrast between two waveforms more obvious. The wavespeed increases gradually downstream (**Table 2**), and it is more than 10 m/s in the lower limbs, where the convection effect is about 10% of the wavespeed in the proximal segments. The influence of the convection effect is not as strong as in the proximal segments, so the time lag between the two models decreases again until it is no longer apparent in the most distal segments.

The threshold, the mechanism of killing waves, between the nonlinear and the linear models is very similar but not exactly the same because of the structure of the program. In the tree of waves model, once the amplitude of a pulse wave is lower than the threshold, the whole wave i.e. the half sinusoidal wave is cut off. This procedure can only occur at a boundary because the pulse waves do not change at all during their travel inside the segments. In the nonlinear model, each wavefront is treated independently. From the algorithm described in §4.5, the killing mechanism happens when any one of the inter-segment wavefronts reaches the boundary, and the threshold is applied through the whole segment. Thus, wavefronts can be killed inside the segment, not just at the boundary, when the amplitude is smaller than the threshold. The reflection-transmission processes occur

much more frequently, especially near the periphery. Therefore, the segments near the periphery will encounter more checking, which may make the nonlinear waveforms not return to the zero level (**Fig. 46 (i), (j), (k)**).

We define the deviation of the waveform between the nonlinear and linear models as

$$D = \frac{1}{t_n - t_0}\frac{1}{P}\int_{t_0}^{t_n} \left| P_{linear}(t) - P_{nonlinear}(t) \right| dt \qquad (4.12)$$

which is the deviation of pressures averaged over a whole cycle of a nonlinear waveform and compared with the input pressure pulse (the half sinusoidal wave), where t_0 is the first wavefront arriving the point of observation and t_n is the last wavefront. The result is shown in **Fig. 47**. The deviations in most of the segments are smaller than 10% of P.

4.6 Pressure Dependent Wavespeed

The second nonlinear factor which we study is the pressure dependent wavespeed. In this case the convection effect is not included. The input is the same half sinusoidal wave with an amplitude of 5330 Pa (40 mmHg) divided into 40 equal amplitude wavefronts. Unlike the case of convection considered in §4.5, the amplitude of the pressure and velocity of the wavefronts may change during intersections. These changes can be calculated by (4.3)-(4.6). The propagation speed of the waves changes only when the absolute pressure changes. The amplitude of the pressure and velocity changes still have to fulfill $U=P/\rho c_i$, everywhere.

In considering the influence of the pressure dependent wavespeed on the waveforms, three assumptions, discussed further in the next section, are made:

(1) The reference wavespeed in each segment is calculated by the Moens-Korteweg

equation and the value is assumed to be the wavespeed at the pressure half way between the systolic and diastolic pressures. For example, if the input varies from 80-120 mmHg, the wavespeed at 100 mmHg is that calculated by the Moens-Korteweg equation.

(2) The range of the variation of the wavespeed in the systolic phase is assumed to be 2 m/s.

(3) The wavespeed of the different portions of the waveform is calculated by linear interpolation with respect to the pressure.

As discussed above, the pressure dependent wavespeed is assumed to be $c(P_a) = C_d + \xi P_a$, where P_a is the amplitude of pressure wavefront, C_d is the wavespeed at the diastolic pressure, which from the assumptions above is 1 m/s less than the Moens-Korteweg wavespeed calculated from the segment. The linear coefficient ξ is calculated from the pulse pressure for the corresponding segment calculated by the linear model (**Table 6**).

4.6.1 Validity of the Assumptions

The static elastic properties of aortic wall in **Table 2** are those estimated by Westerhof *et al.*. The other dimensions of segments collected by him were measured at physiological pressures and normally were measured at 100 mmHg (Bergel, 1961 a, b), which is approximately the mean aortic pressure (**Fig. 11**).

The Moens-Korteweg equation could be used to calculate the variation of wavespeed with respect to the changes of pressure if we know the variation of the elastic constant $E(P)$, thickness $h(P)$ and radius $r(P)$ of the wall versus the aortic pressure. However, we are short of these data and also this discussion has to refer to other studies. Langewouters *et al.* (1984) developed an empirical equation, an arctangent model, to describe the variation of the cross-sectional area with pressure:

$$A(p) = A_m \left(\frac{1}{2} + \frac{1}{\pi} \tan^{-1} \frac{P - P_0}{P_1}\right)$$

where A_m, P_0 and P_1 are three independent parameters to be fitted by experiments. A_m is the maximum cross-sectional area at high pressure, P_0 is the transmural pressure at the inflection point, and P_1 represents the half-width pressure where at pressure $P_0 \pm P_1$ the aortic compliance is half of the maximum. The compliance $c(P)=dA/dP$, is derived from the fitted curve. Langewouters *et al.* (1984) claimed that this empirical equation can fit the data with 99% precision. The discussion of the wavespeed versus the pressure will be based on this equation with their measurements of the human aorta.

For this discussion of the pressure dependent wavespeed, two samples of human arteries, one thoracic aorta and one abdominal aorta, are considered. These two segments were from the same male at age 30 (Langewouters *et al.*, 1984. No. 78067 in Table 2 of their paper). From the data, the cross-sectional area and the aortic compliance of the thoracic aorta versus the aortic pressure are reconstructed in **Fig. 48 (a)** and **(b)**. The wavespeeds versus the aortic pressure are calculated by Eq.(2.6)and shown in **Fig. 48 (c)**. The variation of wavespeed over the physiological range 80-120 mmHg is about 3 m/s for both the thoracic aorta and the abdominal aorta. The variation of wavespeed for both aortas against the aortic pressure is nearly linear in the physiological range as can be seen in **Fig. 48 (c)**. Since the wavespeed, which is calculated by the Moens-Korteweg equation, is about 4.3 m/s for the thoracic aorta and 4.7 m/s for the abdominal aorta (**Table 2**), both are about 1 m/s slower than the value calculated by the arctangent model. We simply assume the variation of the wavespeed in the physiological range is proportional to the wavespeed at half way between the systolic and diastolic pressure (it is assumed to be 100 mmHg for both segments of the aorta) and thus the variation of the wavespeed is 2 m/s

over the diastolic to systolic pressure range.

4.6.2 Program of the Pressure Dependent Wavespeed Case

The pressure dependent wavespeed case has the same input waveform as the convection case. The input wavefronts of both have the same entrance time, pressure amplitude and absolute pressure. Because the amplitude of pressure and the amplitude of velocity must fulfil the relation $U=P/\rho c_i$, the amplitude of velocity in the pressure dependent wavespeed case is not necessarily equal to the value in the convection case. The "negative" initial location of each waveform is still calculated by (4.9) but where $c_p=c(P_s)$, P_s is the absolute pressure of the s-th wavefront. (4.10) and (4.11) are valid for calculating the intersection location and time.

The major structure of the program for the pressure dependent wavespeed case is the same as in the convection case but with some differences. The pressure amplitudes after an intersection are calculated from either (4.3) or (4.5). The amplitudes after the intersection are a function of wavespeed of the two pre-intersection wavefronts and the wavespeed after intersection (**Fig. 41**) and their relationship with pressure can be calculated by the pressure constant ξ.

4.6.3 The Results for the Pressure Dependent Wavespeed Case

Fig. 49 shows the results for the pressure dependent wavespeed cases (the saw-shaped line) compared with the results from the linear model (the smooth line). As in the convection case, the nonlinear waveforms are close to the linear model in the proximal segments, and the deviations are larger as the wave moves distally. Two characteristics are noted:

(1) The nonlinear waveforms (saw-shaped) gradually lag behind the linear waveforms. This is the opposite of the effect of convection.

(2) The nonlinear waveforms steepen in the early systolic phase. For example, in **Fig. 49 (e)**, **(f)** and **(g)**, during the early systolic phase the nonlinear wave lags behind the linear wave, but by mid systole it is nearly coincident with the linear wave.

The deviations between the pressure dependent waveform and the waveform of the linear model calculated by (4.12) are shown in **Fig. 50 (a)**. From **Figs. 49**, it can be seen that much of the deviation results from the time lag due to the later arrival of the pressure dependent wave. In order to compare waveform shapes, the deviations were calculated by subtracting the time lag between the nonlinear and linear waveforms as is shown in **Fig. 50 (b)**. The deviations of most of the segments in **Fig. 50 (b)** are smaller than 10%, which is the same order as the deviations caused by the convection effect.

The possibility of shock formation in a long cylindrical tapered tube was discussed by Niederer (1985). He concluded that once viscous dissipation is considered, a shock is unlikely to occur in the tube. Here we have considered waves in a multi-branched system, with neither taper nor viscous dissipation. Face to face wave intersections were explained by (4.3) and (4.5). When both are compression wavefronts, their amplitudes, as well as the wavespeeds, will increase after the intersection. If one is an expansion and the other is a compression wavefront, the amplitude and wavespeed of the expansion wave will rise but those of the compression wave will decrease. If both of them are expansion wavefronts, both of the amplitudes and wavespeeds will decrease after the intersection. Thus, when the first wavefront (compression) which is reflected by the peripheral resistance intersects with the second wavefront (compression), the speed of the second wavefront will increase which makes it more difficult for the third wavefront to catch it. We therefore conclude that shocks

will not be formed in the arterial system under normal physiological conditions.

4.7 Conclusions

The effects of a pressure dependent wavespeed and of convection have been studied by several authors with different fluid dynamics models (Anliker *et al.*, 1971; Ling and Atabek, 1972; Stergiopulos *et al.*, 1992). Because of their complicated structure and the restriction of the methods in studying the mechanism of wave propagation, these studies cannot separate the nonlinear factors such as convection or a pressure dependent wavespeed from each other or from other linear factors. The limited discussions about the nonlinear effects were for the simple case of a single, semi-infinite tube. (Pressure dependent wavespeed by Anliker *et al.* (1971) and shock formation by Niederer (1985)). It is, therefore, difficult to relate their conclusions to the arterial system.

In most of the segments, the deviations between the nonlinear and the linear waveforms are confined to within 10% of P over a whole period. We may conclude that both nonlinear effects are not significant in the aorta. The effect of convection makes the nonlinear waveforms lead the linear waveform slightly. On the contrary, the effect of a pressure dependent wavespeed makes the nonlinear waveform lag the linear waveform slightly. Neither effect changes the shape of the waveforms significantly. When both of these effects are considered simultaneously, we expect that the total deviations from the linear model will tend to be smaller because the convection effects will cancel the pressure dependent wavespeed effects.

5

Conclusions

The models used in this study of the behaviour of waves in the human arterial system are based on a realistic arterial tree, which includes the 55 largest arteries. The structure of the arterial system is known to be that of a bifurcating tree and it seems to be well-matched for the forward going waves. That is, the properties of the bifurcations are such that a forward travelling pressure and velocity wave does not undergo any reflection as it passes through a bifurcation.

Wave propagation in a human arterial segment is simulated by one-dimensional, incompressible flow in an elastic tube. The governing equations are hyperbolic in nature which means that they can be solved by the method of characteristics. With the assumptions of no leakage though the vessel wall and that viscous dissipation is negligible, the equations can be simplified by using the Riemann invariant, which is a constant along the characteristic lines. Instead of solving the equations directly, we take advantage of the Riemann invariants which allow us to analyse the simultaneously observed pressure and velocity in the aorta as the sum of the elemental wavelets coincident at the point of observation.

In the approach of traditional models, the experimental waveforms are specified at the aortic root, i.e. the waveforms at the aortic root are structure independent. However, the aortic waveforms should be the response of the arterial system to the input generated by the heart. Thus, the physical meanings of wave behaviour may be confused by these models. By introducing an input to the model system, our novel approach is able to calculate the

response of the system and, therefore, allows us to separate the effect of a single factor from another.

The model cardiovasulcar system is studied with both linear and nonlinear methods. If the effect of convection and the pressure dependent wavespeed are assumed not to be important, the arterial system can be treated linearly and the output can be calculated by the convolution of the input waveform with the transfer function of the system. The transfer function is calculated from the response of the system to a delta function input which, in this case, corresponds to a wave of unit amplitude. The transfer function is calculated by the "tree of waves" concept: each wave will generate three waves as it encounters a bifurcation; two transmitted waves and one reflected wave. As the incident wave is separated from these three newly generated waves, it can be considered as generating a trifurcating tree of waves. The waveform generated by the left ventricle is assumed to be an idealised case of a half sinusoidal wave. The linear model which simulates the waveforms in the arterial system using this method is referred to as the "tree of waves" model.

The tree of waves model successfully reproduces many important features of the arterial waveform, such as the variation of the pressure amplitudes, velocity amplitudes and of the reverse flow with distance from the heart. It allows us to separate the forward and backward waves at the point of observation, thereby allowing study of the origin of reflections or the contribution of a specific organ to the wave behaviour. Therefore, it enables the diagnoses of pathological conditions, such as the occlusion of one of the iliac arteries.

An extension of the tree of waves model allowed us to study the contribution of the aortic valve and the coronary circulation to the waveform in the ascending aorta. Most of the previous models did not consider the aortic valve, which may be the most important

nonlinear effect in determining the aortic waveforms. It is assumed that the waves are absorbed by the heart when the valve is open and fully reflected when the valve is closed. The waveforms are still calculated by the input from the heart with the transfer function. However, there are several adjustments in the convolution: The aortic transfer function is separated into the forward and backward parts. Each pulse of the backward transfer function can retain its full waveform, but the forward waveforms will be decided by the time when they first arrive at the aortic root. Again, it successfully demonstrated the influence of the reflected waves in determining the aortic waveforms by reproducing two important features: a pressure increase and the halting of the reverse flow immediately after the valve is closed.

Approximately 4% of the cardiac output goes to the coronary circulation during the diastolic phase, which probably makes the reflection coefficient of the heart less than unity after the closure of the valve. To test the effect of the coronary arteries, a simulation was done by adjusting the reflection coefficient of the heart in decrements down to 60%, which showed that the incisura is not very sensitive to the changes of the reflection coefficient of the heart.

When people are doing exercise, their terminal reflection coefficients decrease by as much as 20% while their terminal resistances decrease by 50%. The simulation shows that the diastolic waveform is more sensitive to these variations of the terminal resistances than the systolic waveform.

Afterload is one of the important indices of myocardial performance and although it is poorly defined, it has been intensively studied for decades. However, myocardial performance cannot be fully understood without the knowledge of left ventricular function, because measured aortic waveforms or even left ventricular waveforms are a combination of the left ventricular function with the effect of the backward waves. The left ventricular

function can be determined from the waveforms measured in the aortic root if we know the transfer function by an inverse convolution. Current technology enables one to measure the flow pattern and aortic waveforms precisely. If it were possible to know the transfer function of the arterial system, the diagnoses of the heart would be significantly improved. Sipkema *et al.* (1980) have succeeded in the technically difficult task of determining the impulse response of the whole arterial system in dogs.

In §4, the model was extended to investigate two important nonlinear factors, convection and the pressure dependant wavespeed. In the nonlinear model, the waveforms are no longer the convolution of the input with the transfer function. The propagation speed and the properties at the intersecting points must be determined by Eqs. (4.3)-(4.8) instead of the superposition of their values. The sequence of their intersections must be followed in real time because the properties of a wave may be different when it intersects wave 1 first and then wave 2 rather than wave 2 first and then wave 1. The new algorithm was built by linking two stages: searching for the shortest boundary arrival time within each segment and then searching for the segment with the shortest boundary arrival among all segments.

Neither convection nor a pressure dependent wavespeed significantly affected the calculated waveforms. What influence they did have was more obvious in peripheral vessels than in the segments near the heart. The pressure dependant wavespeed caused a slight delay of the waveforms when compared with the linear waveforms. On the contrary, the effect of convection made the waveform lead the linear waveforms slightly. These two effects will tend to cancel each other when they are considered simultaneously. Thus, the linear model could explain the arterial system better than might be expected.

Wave propagation in the arterial system is an extremely complicated phenomenon. There are many factors which could influence wave behaviour, such as the structure of the

wall, the geometry of the blood vessels, the condition of the organs and uniformity of the properties of the vessels. Both the tree of waves and the nonlinear models are simplified compared to the real arterial system. However, they are much closer to the real system than previous models: there is no assumption of periodicity and the realistic dimensions of arteries are considered. Because there is no fixed boundary pressure or velocity, these two models allow us to study the reaction of the waveforms to changes in the physiological situation. They also allow us to separate the effect of each factor on the features of waveforms.

All the results shown in this thesis are for the idealised case of no friction dissipation, which is probably the next most important nonlinear factor after the convection and the pressure dependent wavespeed. When viscosity is considered, the right hand side of Eq. (2.10) will no longer be zero. The concept of §4 can still be applied to the analysis of the viscous effect in the arterial system. However, the computation is much more complicated than the studies in §4 since the properties of the pressure and velocity must be integrated along the route of each wave. Another improvement would be the use of a more realistic model for the terminal segments than the single, simple resistance which is used in this work. One possibility is the use of a transfer function derived for an idealised network of vessels which models the smaller arteries. This network could be constructed using self-similar or fractal descriptions of the smaller vessels.

Although the tree of waves model and the nonlinear model consider only the multiple wave reflections and transmissions, most of the important features of the waveforms in the arterial system are represented. The predictions on the reaction of the waveforms when some changes occur in the system and identifying the contribution of a specific organ to the waveforms are qualitatively well compared with experiments.

Therefore, we may conclude that multiple wave reflections are not merely a factor in forming the waveforms but are, in fact, a dominating factor in determining the waveforms of the arterial system.

References

Allievi L (1909)
Allgenmeine Theorie uber die verandliche Bewegung des Wassers in-Leitungen.
Springer, Berlin.

Anliker M, Histand MB and Ogden E (1968)
Dispersion and attenuation of small artificial pressure waves in the canine aorta.
Circ. Res. 23: 539-551.

Anliker M, Wells MK and Ogden E (1969)
The transmission characteristics of large and small pressure waves in the abdominal vena cava.
IEEE Trans. Biomed. Eng. 16: 262-273

Anliker M and Rockwell RL (1971)
Nonlinear analysis of flow pulses and shock waves in arteries.
Part I: ZAMP 22: 217-245.
Part II: ZAMP 22: 563-581.

Ashikawa K, Kanatsuaka H, Suzuki T and Takishima T (1986)
Phasic blood flow velocity pattern in epimyocardial microvessels in the beating canine left ventricle.
Circ. Res. 59: 704-711.

Avolio AP (1980)
A multibranched model of the human arterial system.
Med. Biol. Eng. Comput. 18:709-718.

Avolio AP, Nichols WW and O'Rourke MF (1984)
Exaggerated wave reflection in the kangaroo simulates arterial counter-pulsation.
Am. J. Physiol. 264 (Regulatory Integrative Comp. Physiol. 15): R264-R270.

Attinger EO, Anne A and McDonald DA (1966)
Use of Fourier series for the analysis of biological systems.
Biophys. J., 6: 291-304.

Barnard ACL, Hunt WA, Timlake WP and Varley E (1966)
(a) A theory of fluid flow in compliant tubes.
Biophys. J. 6: 717-724.
(b) Peaking of the pressure pulse in fluid-filled tubes of spatially varying compliance.
Biophys. J. 6: 735-746.

Bauer RD, Pasch Th and Wetterer E (1970)
Neuere Untersuchungen zur Entstehung der Pulsformen in groben Arterien des Menschen.
Verhand. Deutsch. Ges. Kreislff. 36: 330-336.

Belardinelli and Cavalcanti (1992)
Theoretical analysis of pressure pulsepropagation in arterial vessels.
J. Biomech. 25: 1337-1349.

Bellhouse BJ and Bellhouse FH (1969)
Fluid mechanics of model normal and stenotic aortic valves.
Circ. Res. 25: 693-704.

Bellhouse BJ and Bellhouse FH (1972)
Fluid mechanics of the mitral valve and left ventricle.
Cardiovasc. Res. 6: 199-210.

Bergel DH (1961)
(a) The static elastic properties of the arterial wall.
J. Physiol., 156: 445-457.
(b) The dynamic elastic properties of the arterial wall.
J. Physiol., 156: 458-469.

Bergel DH and Milnor WR (1965)
Pulmonary vascular impedance in the dog.
Circ. Res. 26: 401-415

Berger DS, Li JKJ, Laskey Wk and Noordergraaf A (1993)
Repeated reflection of waves in the systemic arterial system.
Am. J. Physiol. 264: H226-H281.

Bramwell JC and Hill AV (1922)
The velocity of the pulse wave in man.
Proc. Roy. Soc. B., 93: 298-306.

Bramwell JC and Hill AV (1923)
The formation of 'breakers' in the transmission of the pulse wave.
J. Physiol., 57: lxxiii-lxxiv.

Brin KP and Yin FC (1984)
Effect of nitroprusside on wave reflections in patients with heart failure.
Ann. Biomed. Eng. 12: 135-150.

Broemer P (1930)
Anwendung mathematischer Methoden auf dem Gebiet der physiologischen Mechanik. In Abderhalden's Handbuch der biologischen Arbeitsmethoden, Abt. V, Teil 1, p.81.

Brown N (1993)
Impedance matching at arterial bifurcations.
J. Biomech. 26: 59-61.

Burattini R and Di Carlo S (1988)
Effective length of the arterial circulation determined in the dog by aid of a model of the systemic input impedance.
IEEE Trans. Biomed. Eng. 35: 53-61.

Burattini R and Campbell KB (1989)
Modified asymmetric T-tube model to infer arterial wave reflection at the aortic root.
IEEE Trans. Biomed. Eng. 36: 805-814.

Burattini R, Knowlen GG and Campbell KB (1991)
Two arterial effective reflecting sites may appear as one to the heart.
Circ. Res. 68: 85-99.

Burkhoff D, Alexander J Jr. and Schipke J (1988)
Assessment of Windkessel as a model of aortic input impedance.
Am. J. Physiol. 255: H742-H753.

Campbell KB, Lee LC, Frasch HF and Noordergraaf A (1989)
Pulse reflection sites and the effective length of the arterial system.
Am. J. Physiol. 256: H1684-H1689.

Campbell KB, Burattini R, Bell DL, Kirkpatrick RD and Knowlen GG (1990)
Time-domain formulation of asymmetric T-tube model of arterial system.
Am. J. Physiol. 258: H1761-H1774.

Caro CG, Pedley TJ, Schroter RC and Seed WA (1978).
The Mechanics of the Circulation.
Oxford University Press, Oxford.

Cox RH (1971)
Determination of true phase velocity of arterial pressure waves in vivo.
Circ. Res. 24: 407-418

Cournand AF and Ranges HA (1941).
Catheterization of right auricle in man.
Proc. Soc. Biol. Med. 46: 106-116.

Davies RH (1994)
The analysis of human cardiovascular system using the method of characteristics.
PhD Thesis, University of London, UK.

Dick DE, Kendrick JE, Matson GL and Rideout VC (1968)
Measurement of nonlinearity in the arterial system of the dog by a new method.
Circ. Res. 22: 101-111.

Dijk AM van (1983)
Vascular single smooth muscle cells and whole tissue. Mechanical properties and response to stimuli.
Ph.D. Thesis, University of Leiden, The Netherlands.

Deshpande MD, Giddens DP and Mabon RF (1976)
Steady laminar flow through modelled vascular stenoses.
J Biomech. 9:165-174

Euler L (1862)
Principia pro motu sanguinis per arterias determinado: opera posthuma mathematica et physica anno 1884 detecta, ediderunt Fuss PH et Fuss N
Pertropoli Apud Eggers et Socios.

Everett J (1973)
A mathematical model for nonlinear analysis of flow pulses utilising an integral technique.
ZAMP 24: 565-579.

Frank O (1899)
Die Grundform des arteriellen Pulses. Erste Abhandlung. Mathematische Analyse.
Z. Biol. 37: 483-526.

Frank O (1905)
Der Puls in den Arterien.
Z. Biol. 46: 441-533.

Frank O (1930)
Schatzung des Schlagvolumens des menschlichen Herzens auf Grund der Wellen-und Windkesseltheorie.
Z. Biol. 90: 405-409.

Fukushima T, Homma T, Harakawa K, Sakata N and Azuma T (1988)
Vortex generation in pulsatile flow through arterial bifurcation models including the human carotid artery.
J. Biomech Eng 110:116-171.

Ganong WF (1983)
Review of Medical Physiology, 11th ed.
Lange, Los Altos, California.

Gerrard JH (1982)
Numerical analysis and linear theory of pulsatile flow in cylindrical deformable tube: The testing of a numerical model for blood flow calculation.
Med. Biol. Eng. Comp. 20: 49-57.

Goldwyn RM and Watt TB (1967)
Arterial pressure pulse contour analysis via a mathematical model for the clinical quantification of human vascular properties.
IEEE Trans. Biomed. Eng. 14:11-17

Gosling RG, Newman DL, Bowden NLR and Twinn KW (1971)
The area ratio of normal aortic junctions-aortic configuration and pulse wave reflection.
Brit. J. Radiol. 44: 850-853.

Grashey H (1881).
Die Wellenbewegung elasticher Rohren und der Arterienpuls des Menschen. Leipzig.

Greenwald SE and Newman DL (1982)
Impulse propagation through junctions.
Med. Biol. Eng. Comp. 20: 343-350.

Gundel W, Cherry G, Rajagopalan B, Tan LB, Lee G and Schultz D (1981)
Aortic input impedance in man: acute response to vasodilator drugs.
Circ. 6: 1305-1314.

Guyton AC (1981)
Textbook of Medical Physiology.
W. B. Saunders. Philadelphia.

Hales S (1733)
Statical essays: containing haemastaticks. History of medicine series, library of New York Academy of Medicine, 1964, No. 22 Hafner Publishing, New York.

Harvey W (1628)
De Motu Cordis.
William Fitzer, Frankfurt. Translated as Movement of the Heart and Blood in Animals by Franklin KJ.

Hardung V (1952)
Zur mathematischen Behandlung der Dampfung und reflection der pulswellen.
Arch. Kreislaufforsch. 18:167-172.

Hamilton WF (1944)
The patterns of the arterial pressure pulse.
Am. J. Physiol. 141: 235-241.

Hamilton WF and Dow P (1939)
An experimental study of the standing waves in the pulse propagation through the aorta.
Am. J. Physiol. 125: 48-59.

Helal MA, Watts KC and Marble AE (1994)
Hydrodynamic simulation of arterial networks which include compliant and rigid bypass grafts.
J. Biomech. 3: 277-287.

Henderson Y and Johnson FE (1912)
Two modes of closure of the heart valves.
Heart 4: 69-82.

Hess WR (1927)
Die Verteilung von Querschnitt, Widerstand, Druckgefalle und Stromungsgeschchwindigkeit im Blutkreislauf. Handb. d. normale u. path. physiol (Bethe), Bd. VII Teil 2: 904-933. Springer. Berlin.

Histand MB and Anliker M (1973)
Influence of flow pressure on wave propagation in the canine aorta.
Circ. Res. 32: 524-529.

Hunter W and Noordergraaf A (1976)
Can impedance characterise the heart?
J. Appl. Physiol. 40: 250-252.

Iberall AS (1967)
Anatomy and steady flow characteristics.
Math. Biosci. 1: 375-395.

Intagbetta M, Tompkins WR and Richardson DR (1970)
Velocity measurements in the microvasculature of the cat omentum by on-line method.
Microvasc. Res. 2: 462-473.

Jones CJH, Parker KH, Hughes R and Sheridan DJ (1992)
Nonlinearity of human arterial pulse wave transmission.
J. Biomech. Eng., 114: 10-14.

Karreman G (1952)
Some contributions to the mathematical biology of blood circulation: Reflections of pressure waves in the arterial system.
Bull. Math. Biophys. 14: 327-350.

Khouri EM and Gregg DE (1963)
Miniature electromagnetic flowmeter applicable to coronary arteries.
J. Appl. Physiol. 18: 224-227

Kimmel E and Dimmar U (1983)
Pulsatile flow in tapered tubes: A model of blood flow with large disturbances.
J. Biomech. Eng. 105: 112-119.

Korteweg DJ (1878)
Uber die Fortpflanz ungsgeschwindigkeit des schalles in elastischen Rohren.
Ann. Phs. Chem (NS) 5: 525.

Kouchoukos TN, Sheppard LC and McDonald DA (1970)
Estimation of stroke volume in the dog by a pulse contour method.
Circ. Res. 26:611-623.

Landes G (1943)
Einige Untersuchungen an electrischen Analogie-Schaltungen zun Kreislaufsystem.
Z. Biol. 101: 418

Lambert JW (1958)
Nonlinearities of fluid flow in nonrigid tubes.
J. of Franklin Institute 266:83-102.

Langewouters GJ, Wesseling KH and Goedhard WJA (1984)
The static elastic properties of 45 human thoracic and 20 abdominal aortas in vitro and the parameters of a new model.
J. Biomech. 17: 425-435.

Langewouters GJ, Wesseling KH and Goedhard WJA (1985)
The pressure dependent dynamic elasticity of 35 thoracic and 16 abdominal human aortas *in vitro* described by a five component model.
J. Biomech. 18: 613-620.

Laskey WK, Kussmaul WG, Martin JL, Kleaveland JP, Hirshfeld JW and Shroff S (1985). Characteristics of vascular hydraulic load in patients with heart failure.
Circ. 72: 61-67.

Latham RD, Westerhof N, Sipkema P, Rubal B and Reuderink D (1985)
Regional wave travel and reflections along the human aorta : a study with six simultaneous micromanometric pressure.
Circ. 72: 1257-1269.

Latham RD, Rubal BJ, Westerhof N, Spikema P and Walsh RA (1987)
Nonhuman primate model for regional wave travel and reflections along aortas.
Am. J. Physiol. 253: H299-306.

Learoyd BM and Taylor MG (1966)
Alterations with age in the visco-elastic properties of human arterial walls.
Circ. Res. 18: 278-292.

Lee CSF and Talbot L (1979)
A fluid mechanical study on the closure of heart valves.
J. Fluid. Mech. 91 (1): 41-63.

Levick JR (1992)
An Introduction to Cardiovascular Physiology.
Butterworth-Heinemann.

Li JK-J, Melbin J, Riffle RA, Noordergraaf A (1981)
A pulse wave propagation.
Circ. Res. 49: 442-452.

Ling SC and Atabek HB (1972)
A nonlinear analysis of pulsatile flow in arteries.
J. Fluid Mech. 55: 493-511

Ling SC, Atabek HB, Letzing WG and Patel DJ (1973)
Nonlinear analysis of aortic flow in living dogs.
Circ. Res., 33: 198-212.

Lou Z and Yang WJ (1993)
A computer simulation of the non-Newtonian blood flow at the aortic bifurcation.
J. Biomech. 1: 37-49.

Macfarlane TWR, Roach MR and Chan K (1980)
The geometry of human cerebral bifurcations: effect of static distending pressure.
J. Biomech. 13: 265-277.

Mayer RA, Mandell J and Friedman MH (1984)
Changes in aortic bifurcation geometry during a cardiac cycle.
J. Biomech. 17: 637-638.

McDonald DA (1974)
Blood Flow in Arteries.
Camelot Press, Southampton.

McDonald DA and Taylor MG (1959)
The hydrodynamics of the arterial circulation.
Prog. Biophys. 9: 107-173.

Milnor RW (1975)
Arterial impedance as ventricular afterload.
Circ. Res. 36: 565-570.

Milnor RW and Nichols WW (1975)
A new method of measuring propagation coefficients and characteristic impedance in blood vessels.
Circ. Res. 36: 631-639.

Milnor RW and Bertram CD (1978)
The relation between arterial viscoelasticity and wave propagation in the canine femoral artery in vivo.
Circ. Res. 43: 870-879.

Milnor WR (1982)
Medical Physiology.
Mountcastle VB ed.
C. V. Mosby, St. Louis, Chap. 3.

Milnor WR (1989)
Hemodynamics.
Williams and Wilkins, Baltimore, MD.

Moens AI (1878)
Die Pulskurve, Leiden.

Murgo JP, Westerhof N, Giolma JP and Altobelli SA (1980)
Aortic input impedance in normal man: relationship to pressure and flow wave forms.
Circ. Res. 2: 105-116.

Murgo JP, Westerhof N, Giolma JP and Altobelli SA (1981 a)
Manipulation of ascending aortic pressure and flow wave reflections with the Valsalva manoeuvre: relationship to input impedance.
Circ. 1: 122-131.

Murgo JP, Westerhof N, Giolma JP and Altobelli SA (1981 b)
Effects of exercise on aortic input impedance and pressure wave forms in normal humans.
Circ. Res. 3: 334-343.

Newman DL, King D, Gosling R and Wille S (1972)
Reflections at aortic-iliac junctions. In : Blood Flow Measurement. Robers VC ed., Sector, London.

Nichols WW, Conti CR, Walker WE and Milnor WR (1977)
Input impedance of the systemic circulation in man.
Circ. Res. 40: 451-458.

Nichols WW, Avolio AP and O'Rrourke MF (1986)
Ascending aortic impedance patterns in the kangaroo: their explanation and relation to pressure waveforms.
Circ. Res. 59: 217-255.

Niederer PF (1985)
Damping mechanisms and shock-like transitions in the human arterial tree.
ZAMP 36: 204-220.

O'Rourke MF and Taylor MG (1966)
Vascular impedance of vascular bed.
Circ. Res. 20: 365-380.

O'Rourke MF (1967)
Pressure and velocity waves in systemic arteries and the anatomical design of the arterial system.
J. Appl. Physiol. 23: 139-149.

O'Rourke MF (1982 a)
Arterial Function in Health and Disease.
Churchill Livingstone, London.

O'Rourke MF (1982 b)
Vascular impedance in studies of arterial and cardiac function.
Physiol. Rev 62: 570-623.

O'Rourke MF and Avolio AP (1980)
Pulsatile flow and pressure in human systemic arteries: studies in man and in a multi-branched model of the human systemic arterial tree.
Circ. Res. 46: 363-372.

O'Rourke MF and Nichols WW (1990)
McDonald's Blood Flow in Arteries.
Edward Arnold, London.

Patel DJ, De Fresras FM, Greenfield JC, Fry DL. (1963)
Relationship of radius to pressure along the aorta in living dogs.
J. Appl. Physiol. 18: 1111-1117.

Parker KH and Jones CJH (1990)
Forward and backward running waves in the arteries: analysis using the method of characteristics.
J. Biomech. Eng. 112: 322-326.

Papageorgiou GL and Jones NB (1987)
Arterial system configuration and wave reflections.
J. Biomed. Eng. 9: 299-301.

Papageorgiou GL and Jones NB (1988)
Wave reflection and hydraulic impedance in the healthy arterial system: a controversial subject.
Med. Biol. Eng. Comp. 26: 237-242.

Papageorgiou GL, Jones NB, Redding VJ and Hudson N (1990).
The area ratio of normal arterial junctions and its implications in pulse wave reflections.
Cardiovasc. Res. 6:478-484.

Paulsen PK and Hasenkam JM (1983)
Three-dimensional visualisation of velocity profiles in the ascending aorta in dogs, measured with a hot film anemometer.
J. Biomech. 16, 201-210

Patel DJ, Defreitas F, Greenfield JC, Fry DL (1963)
Relationship of radius to pressure along the aorta in living dogs.
J. Appl. Physiol. 25:533-541.

Pedley TJ (1980)
The Fluid Mechanics of Large Blood Vessels.
Cambridge Univ. Press, Cambridge.

Peterson LH (1954)
The dynamics of pulsatile blood flow.
Circ. Res. 2: 127-139.

Peterson LH and Gerst PH (1956)
Significance of reflected waves within the arterial system.
Fed. Proc. 15, (496) 145.

Pollack GH, Reddy RV and Noordergraaf A (1968)
Input impedance, wave and reflection in the human pulmonary arterial tree: studies using an electrical analog.
IEEE Trans. Biomed. Eng. 15: 151-164.

Pythoud F, Stergiopulos N and Meister J-J (1996)
Separation of arterial pressure wave into their forward and backward running components.
J. Biomech. Eng. 118: 295-301.

Raines J, Jaffrin M and Shapiro AH (1974)
A computer simulation of arterial dynamics in the human leg.
J. Biomech. 7: 77-91.

Remington JW (1965)
Quantitative synthesis of head and foreleg arterial pulses in the dog.
Am. J. Physiol. 208: 968-983.

Remington JW and O'Brien LJ (1970)
Construction of aortic flow pulse from pressure pulse.
Am. J. Physiol. 218: 437-447.

Rumberger JA and Nerem RM (1977)
A method of characteristics calculation of coronary.
J. Fluid Mech. 82: 429-448.

Robinson DA (1965)
Quantitative analysis of the control of cardiac output in the isolated left ventricle.
Circ. Res., 17: 207-221.

Rushmer RF (1961)
Cardiovascular Dynamics, 2d ed.,
Saunders WB, Philadelphia.

Sapirstein LA (1981)
Textbook of Medical Physiology, 6th ed., Guyton AC ed..
W.B. Saunders Company. p 232. (Table 20-1).

Schaaf BW and Abbrecht PH (1972)
Digital computer simulation of human systemic arterial pulse wave transmission. A nonlinear model.
J. Biomech. 5: 345-364.

Schultz DJ, Tunstall-Pedoe DS, Lee G de J, Gunning AJ, Belhouse BJ (1969)
Velocity distributions and transition in the arterial system.
In Ciba Symposium on Circulatory and Respiratory and Mass Transport,
Wolstenholme GEW and Knight J eds.,
Churchill, London.

Singer A (1969)
Systems engineering analysis of aortic root blood pressure.
Bull. Math. Biophys. 31: 453-471.

Skalak R and Stathis T (1966)
A porous tapered elastic tube model of a vascular bed.
Symposium of Biomechanics, American Society of Mechanical Engineers,
New York.

Skalak R (1972)
Synthesis of a complete circulation.
In Cardiovascular Fluid Dynamics, (vol 2) Bergel DH ed.,
Academic Press, London, Chapter 19.

Smith FT (1979)
The separation flow through a severely constricted symmetric tube.
J. Fluid Mech. 90:725-754

Smith D and Craige E (1986)
Mechanism of the dicrotic pulse.
Br. Heart J. 56: 531-534.

Smith D and Craige E (1988)
Mechanism of the dicrotic pulse.
Acta Cardiologica 3: 251-252.

Spencer MP and Denison AB (1963)
Pulsatile blood flow in the vascular system.
In Handbook of Physiology, Circulation, (vol. 2). Hamilton WF and Dow P eds.,
American Physiological Society, Washington DC, USA, Chap. 25, pp 839-864.

Spikema P, Westerhof N and Randall OS (1980)
The arterial system characterised in the time domain.
Cardiovasc. Res. 14: 270-279.

Starr I and Schild A (1957)
Studies made by simulating systole at necropsy. IX. A test of the aortic compression chamber hypothesis and of two stroke volume methods based upon it.
J. Appl. Physiol. 11: 169-173.

Stettler JC, Niederer P and Anliker M (1981)
Theoretical analysis of arterial hemodynamics including the influence of bifurcations.
Part I: Mathematical model and prediction of normal pulse pattern.
Part II: Critical evaluation of theoretical model and comparison with noninvasive measurements of flow patterns in normal and pathological cases.
Ann. Biomed. Eng. 9:145-164, 165-175.

Stettler JC, Niederer P and Anliker M (1987)
Nonlinear mathmatical models of the arterial system: effects of bifurcations, wall viscoelasticity, stenoses, and counterpulsation on pressure and flow pulses.
In Handbook of Bioengineering. Skalak R and Chieng S eds.,
McGraw-Hill, New York, Chap. 17, 17.1-17.26.

Stergiopulos N, Young DF, Rogge TR (1992)
Computer simulation of arterial flow with applications to arterial and aortic stenoses.
J. Biomech. 25: 1477-1488.

Stergiopulos N, Spiridon M, Pythoud F and Meister J-J (1996)
On the wave transmission and reflection properties of stenoses.
J. Biomech. 29: 31-38.

Sunagawa K, Burkhoff D, Lim KO and Sagawa K (1982)
Impedance loading servo pump system for excised canine ventricle.
Am. J. Physiol. 243: H346-H350.

Taylor MG (1957)
An approach to the analysis of the arterial pulse wave.
(a) Oscillations in an attenuating line. Phys. Med. Biol. 1: 258-269.
(b) Fluid Oscillations in an elastic tube. Phys. Med. Biol. 2: 321-329.

Tardy Y, Meister J-J, Perret F, Brunner HR and Arditi M (1991)
Non-invasive estimate of the mechanical properties of peripheral arteries from ultrasonic and photo-plethysmographic measurements.
Clin. Phys. Physiol. Meas 12: 39-54.

Van der Bos GC, Westerhof N, Elzinga G and Sipkema P (1971)
Reflection in the systemic arterial system: effects of aortic and carotid occlusion.
Cardiovasc. Res. 10: 565-573.

Vayo HW (1966)
The motion of the left ventricle.
Bull. Math. Biophys. 28: 355.

Von Kries, J. (1892).
Studien zur Pulslehre.
Freiburg.

Warner HR (1956)
A study of the mechanism of pressure wave distortion by arterial walls using an electrical analogue.
Circ. Res. 79-84.

Welkowitz W (1987)
Engineering Hemodynamics: Application to Cardiac Assist Devices: Second Edition.
New York University Press, New York, pp 17-19.

Westerhof N, Bosman F, De Vries CJ and Noordergraaf A (1969)
Analogue studies of the human systemic arterial tree.
J. Biomech. 2: 121-143.

Westerhof N, Sipkema P, van den Bos GC and Elzinga G (1972)
Forward and backward waves in the arterial system.
Cardiovasc. Res. 6:648-656.

Westerhof N, Elzinga G and Van der Bos GC (1973)
Influence of central and peripheral changes on the hydraulic input impedance of the systemic arterial tree.
Med. Biol. Eng. 710-722.

Westerhof N, Vanden Bos CG and Laxminarayan S (1978)
Arterial reflection.
In: The Arterial System, Bauer RD and Busse R eds.,
Springer, Berlin, pp 48-62.

Westerhof N, Murgo JP, Sipkenma P, Giolma JP and Elzinga G (1979)
Arterial impedance.
In: Quantitative Cardiovascular Studies, Hwang, NHC, Gross DR and Patel DJ eds.,
University Park Press, Baltimore, pp 111-150.

Westerhof N (1996)
Cardio-vascular intersection determines pressure and flow.
In Biological Flow. Jaffrin MY and Caro CG eds.,
Plenum Press, New York, Chap. 12.

Wetterer E, Bauer RD and Busse R (1977)
Arterial dynamics. INSERM Euromech 92.
Cardiovascular and Pulmonary Dynamics. 71: 17-42.

Wezler K and Boger A (1939)
Die Dynamik des arteriellen Systems. Der arterielle Blutdruck und seine Komponenten.
Ergeb. Physiol. 41: 292-606.

Williams PL (1995)
Gray's Anatomy.
Churchill Livingstone. London.

Witzig K (1914)
Uner erzwungene Wellenbewegungen zaher, inkompressibler Flussigkeiten in elastischen Rohren.
Wyss, Inaug. Diss. Bern, Bern.

Womersley JR (1955)
Method for calculation of velocity, rate of flow and velocity drag in arteries when pressure gradient is known.
J. Physiol. 127: 553-563.

Womersley JR (1957)
An elastic tube theory of pulse transmission and oscillatory flow in mammalian arteries.
Wright Air Developement Center Tech. Rep. 56-614.

	Name of Segment	Length cm	Radius cm	Wall Thickness cm	Young's Modules $10^5 kg/m\,s^2$	Wave Speed m/s
1	Ascending aorta	4.0	1.470	0.163	4	4.67
2	Aortic arch I	2.0	1.120	0.126	4	4.70
3	Brachiocephalic	3.4	0.620	0.080	4	5.03
4	R. subclavian I	3.4	0.423	0.067	4	5.58
5	R. carotid	17.7	0.370	0.063	4	5.78
6	R. vertebral	14.8	0.188	0.045	8	9.69
7	R. subclavian II	42.2	0.404	0.067	4	5.71
8	R.radius	23.5	0.174	0.043	8	9.85
9	R. ulnar I	6.7	0.215	0.046	8	9.16
10	R. interosseous	7.9	0.091	0.028	16	15.54
11	R. ulnar II	17.1	0.203	0.046	8	9.43
12	R. internal corotid	17.6	0.177	0.045	8	9.99
13	R. external carotid	17.7	0.177	0.042	8	9.65
14	Aortic arch II	3.9	1.070	0.115	4	4.59
15	L. carotid	20.8	0.370	0.063	4	5.78
16	L. internal carotid	17.6	0.177	0.045	8	9.99
17	L. external carotid	17.7	0.177	0.042	8	9.65
18	Thoracic aorta I	5.2	1.000	0.110	4	4.65
19	L. subclavian II	3.4	0.423	0.066	4	5.53
20	Vertebral	14.8	0.180	0.045	8	9.91
21	L. subclavian II	42.2	0.403	0.067	4	5.71
22	L. radius I	23.5	0.174	0.043	8	9.85
23	L. ulnar I	6.7	0.215	0.046	8	9.16
24	L. interosseous	7.9	0.091	0.028	16	15.54
25	L. ulnar II	17.1	0.203	0.046	8	9.43
26	Intercoastals	8.0	0.200	0.049	4	6.93
27	Thoracic aorta II	10.4	0.675	0.100	4	5.39
28	Abdominal I	5.3	0.610	0.090	4	5.38
29	Celiac I	2.0	0.390	0.064	4	5.68
30	Celiac II	1.0	0.200	0.064	4	7.93
31	Hepatic	6.6	0.220	0.049	4	6.61
32	Gastric	7.1	0.180	0.045	4	7.00
33	Splenic	6.3	0.275	0.054	4	6.21
34	Sup. mensenteric	5.9	0.435	0.069	4	5.58
35	Abdominal II	1.0	0.600	0.080	4	5.12
36	L. renal	3.2	0.260	0.053	4	6.33
37	Abdominal III	1.0	0.590	0.080	4	5.16
38	R. renal	3.2	0.260	0.053	4	6.33
39	Abdominal IV	10.6	0.580	0.075	4	5.04
40	Inf. mesenteric	5.0	0.160	0.043	4	7.26
41	Abdominal V	1.0	0.520	0.065	4	4.95
4	R. common iliac	5.8	0.368	0.060	4	5.66
42	L. common iliac	5.8	0.368	0.060	4	5.66
44	L. external iliac	14.4	0.320	0.053	8	8.06
45	L. internal iliac	5.0	0.200	0.040	16	12.53
46	L. femoral	44.3	0.259	0.050	8	8.71
47	L. deep femoral	12.6	0.255	0.047	8	8.51
48	L. post tibial	32.1	0.247	0.045	16	11.96
49	L. ant. tibial	34.3	0.130	0.039	16	15.35
50	R. external iliac	14.4	0.320	0.053	8	8.06
51	R. internal iliac	5.0	0.200	0.040	16	12.53
52	R. femoral	44.3	0.259	0.050	8	8.71
53	R. deep femoral	12.6	0.255	0.047	8	8.51
54	R. post. tibial	32.1	0.247	0.045	16	11.96
55	R ant. tibial	34.3	0.130	0.039	16	15.35

Table 1: Physiological data for the arterial model (from Westerhof *et al.*, 1968).

	Name of Segment	Length cm	Radius cm	Wall Thickness cm	Young's Modules $10^5 kg/ms^2$	Wave Speed m/s
1	Ascending aorta	4.0	1.470	0.163	4	4.67
2	Aortic arch I	2.0	1.263	0.126	4	4.43
3	Brachiocephalic	3.4	0.699	0.080	4	4.74
4	R. subclavian I	3.4	0.541	0.067	4	4.93
5	R. carotid	17.7	0.473	0.063	4	5.11
6	R. vertebral	14.8	0.240	0.045	8	8.58
7	R. subclavian II	42.2	0.515	0.067	4	5.05
8	R.radius	23.5	0.367	0.043	8	6.78
9	R. ulnar I	6.7	0.454	0.046	8	6.31
10	R. interosseous	7.9	0.194	0.028	16	10.64
11	R. ulnar II	17.1	0.433	0.046	8	6.45
12	R. internal corotid	17.6	0.382	0.045	8	6.80
13	R. external carotid	17.7	0.382	0.042	8	6.57
14	Aortic arch II	3.9	1.195	0.115	4	4.35
15	L. carotid	20.8	0.413	0.063	4	5.47
16	L. internal carotid	17.6	0.334	0.045	8	7.27
17	L. external carotid	17.7	0.334	0.042	8	7.02
18	Thoracic aorta I	5.2	1.120	0.110	4	4.39
19	L. subclavian II	3.4	0.474	0.066	4	5.23
20	Vertebral	14.8	0.203	0.045	8	9.32
21	L. subclavian II	42.2	0.455	0.067	4	5.38
22	L. radius I	23.5	0.324	0.043	8	7.21
23	L. ulnar I	6.7	0.401	0.046	8	6.71
24	L. interosseous	7.9	0.172	0.028	16	11.32
25	L. ulnar II	17.1	0.383	0.046	8	6.87
26	Intercoastals	8.0	0.317	0.049	4	5.51
27	Thoracic aorta II	10.4	1.071	0.100	4	4.28
28	Abdominal I	5.3	0.920	0.090	4	4.38
29	Celiac I	2.0	0.588	0.064	4	4.62
30	Celiac II	1.0	0.200	0.064	4	7.93
31	Hepatic	6.6	0.458	0.049	4	4.58
32	Gastric	7.1	0.375	0.045	4	4.85
33	Splenic	6.3	0.386	0.054	4	5.24
34	Sup. mensenteric	5.9	0.499	0.069	4	5.21
35	Abdominal II	1.0	0.843	0.080	4	4.32
36	L. renal	3.2	0.350	0.053	4	5.45
37	Abdominal III	1.0	0.794	0.080	4	4.45
38	R. renal	3.2	0.350	0.053	4	5.45
39	Abdominal IV	10.6	0.665	0.075	4	4.70
40	Inf. mesenteric	5.0	0.194	0.043	4	6.60
41	Abdominal V	1.0	0.631	0.065	4	4.50
4	R. common iliac	5.9	0.470	0.060	4	5.00
42	L. common iliac	5.8	0.470	0.060	4	5.00
44	L. external iliac	14.4	0.482	0.053	8	6.57
45	L. internal iliac	5.0	0.301	0.040	16	10.21
46	L. femoral	44.3	0.361	0.050	8	7.37
47	L. deep femoral	12.6	0.356	0.047	8	7.20
48	L. post femoral	32.1	0.376	0.045	16	9.69
49	L. ant. femoral	34.3	0.198	0.039	16	12.44
50	R. external iliac	14.5	0.482	0.053	8	6.57
51	R. internal iliac	5.1	0.301	0.040	16	10.21
52	R. femoral	44.4	0.361	0.050	8	7.37
53	R. deep femoral	12.7	0.356	0.047	8	7.20
54	R. post. tibial	32.2	0.375	0.045	16	9.71
55	R ant. tibial	34.4	0.197	0.039	16	12.46

Table 2: Adjusted data for the zero reflection of the forward running waves.

Segment	Total Resistance (10^9 Ns/m^5)	Reflection Coefficient
6	6.01	0.906
8	5.28	0.82
10	84.3	0.956
11	5.28	0.893
12	13.9	0.784
13	13.9	0.79
16	13.9	0.784
17	13.9	0.791
20	6.01	0.906
22	5.28	0.821
24	84.3	0.956
25	5.28	0.893
26	1.39	0.627
31	3.63	0.925
32	5.41	0.921
33	2.32	0.93
34	0.93	0.934
36	1.13	0.861
40	6.88	0.918
45	7.94	0.925
47	4.77	0.885
48	4.77	0.724
49	5.59	0.716
51	7.94	0.925
53	4.77	0.888
54	4.77	0.724
55	5.59	0.716

Table 3: Terminal resistance and its reflection coefficient (from Stergiopulos *et al.* 1992)

Artery	Circumference (cm)	Mean Flow (ml/min)	Peak Velocity (cm/s)
Ascending Aorta	6.28	11870	63.0
Descending Thoracic Aorta	5.00	3243	27.0
Abdominal Aorta (proximal)	3.40	1108	21.0
Abdominal Aorta (distal)		1260	23.0
Iliac Artery	1.80	750	54.6

Table 4: Properties of arterial flow pulse at different sites of a dog (Spencer and Dension, 1963)

Branch number	Length (cm)	Diameter (cm)	Wall Thickness (cm)	Wave Speed (m/s)	Branch number	Length (cm)	Diameter (cm)	Wall Thickness (cm)	Wave Speed (m/s)
0	4.00	1.470	0.163	4.672	43	4.93	0.203	0.045	9.320
1	2.00	1.263	0.126	4.435	44	4.93	0.203	0.045	9.320
2	3.40	0.699	0.080	4.741	45	4.93	0.203	0.045	9.320
3	3.40	0.543	0.067	4.932	46	8.44	0.455	0.067	5.383
4	5.80	0.473	0.063	5.112	47	8.44	0.455	0.067	5.383
5	5.80	0.473	0.063	5.112	48	8.44	0.455	0.067	5.383
6	5.80	0.473	0.063	5.112	49	8.44	0.455	0.067	5.383
7	4.90	0.240	0.045	8.583	50	8.44	0.455	0.067	5.383
8	4.90	0.240	0.045	8.583	51	7.83	0.324	0.043	7.210
9	4.90	0.240	0.045	8.583	52	7.83	0.324	0.043	7.210
10	8.44	0.515	0.067	5.051	53	7.83	0.324	0.043	7.210
11	8.44	0.515	0.067	5.051	54	6.70	0.401	0.046	6.714
12	8.44	0.515	0.067	5.051	55	2.70	0.172	0.028	11.320
13	8.44	0.515	0.067	5.051	56	2.70	0.172	0.028	11.320
14	8.44	0.515	0.067	5.051	57	2.70	0.172	0.028	11.320
15	7.83	0.367	0.043	6.785	58	5.70	0.383	0.028	6.780
16	7.83	0.367	0.043	6.785	59	5.70	0.383	0.028	6.780
17	7.83	0.367	0.043	6.785	60	5.70	0.383	0.028	6.780
18	6.70	0.454	0.046	6.310	61	2.70	0.317	0.049	5.512
19	2.63	0.194	0.028	10.640	62	2.70	0.317	0.049	5.512
20	2.63	0.194	0.028	10.640	63	2.70	0.317	0.049	5.512
21	2.63	0.194	0.028	10.640	64	3.46	1.071	0.100	4.280
22	5.70	0.433	0.046	6.450	65	3.46	1.071	0.100	4.280
23	5.70	0.433	0.046	6.450	66	3.46	1.071	0.100	4.280
24	5.70	0.433	0.046	6.450	67	5.30	0.920	0.900	4.380
25	5.86	0.382	0.045	6.801	68	0.66	0.588	0.064	4.620
26	5.86	0.382	0.045	6.801	69	0.66	0.588	0.064	4.620
27	5.86	0.382	0.045	6.801	70	0.66	0.588	0.064	4.620
28	5.90	0.382	0.045	6.575	71	0.94	0.200	0.049	7.937
29	5.90	0.382	0.045	6.575	72	0.94	0.200	0.049	7.937
30	5.90	0.382	0.045	6.575	73	0.94	0.200	0.049	7.937
31	3.90	1.195	0.115	4.350	74	0.94	0.200	0.049	7.937
32	6.90	0.413	0.063	5.471	75	0.94	0.200	0.049	7.937
33	6.90	0.413	0.063	5.471	76	0.94	0.200	0.049	7.937
34	6.90	0.413	0.063	5.471	77	0.94	0.200	0.049	7.937
35	5.86	0.334	0.045	7.270	78	1.01	0.458	0.045	4.587
36	5.86	0.334	0.045	7.270	79	1.01	0.458	0.045	4.587
37	5.86	0.334	0.045	7.270	80	1.01	0.458	0.045	4.587
38	5.90	0.334	0.045	7.020	81	1.01	0.458	0.045	4.587
39	5.90	0.334	0.045	7.020	82	1.01	0.458	0.045	4.587
40	5.90	0.334	0.045	7.020	83	1.01	0.458	0.045	4.587
41	5.20	1.120	0.110	4.390	84	1.01	0.458	0.045	4.587
42	3.40	0.474	0.066	5.230					

Table 5: The data for the nonlinear program.

Branch number	Length (cm)	Diameter (cm)	Wall Thickness (cm)	Wave Speed (m/s)	Branch number	Length (cm)	Diameter (cm)	Wall Thickness (cm)	Wave Speed (m/s)
85	2.10	0.375	0.054	4.852	127	6.00	0.375	0.045	9.710
86	2.10	0.375	0.054	4.852	128	6.00	0.375	0.045	9.710
87	2.10	0.375	0.054	4.852	129	6.00	0.375	0.045	9.710
88	1.96	0.386	0.069	5.244	130	6.00	0.375	0.045	9.710
89	1.96	0.386	0.069	5.244	131	4.86	0.197	0.039	12.460
90	1.96	0.386	0.069	5.244	132	4.86	0.197	0.039	12.460
91	1.00	0.843	0.069	4.323	133	4.86	0.197	0.039	12.460
92	1.06	0.350	0.053	5.454	134	4.86	0.197	0.039	12.460
93	1.06	0.350	0.053	5.454	135	4.86	0.197	0.039	12.460
94	1.06	0.350	0.053	5.454	136	1.93	0.470	0.060	5.000
95	1.00	0.749	0.080	4.450	137	1.93	0.470	0.060	5.000
96	3.53	0.350	0.075	5.450	138	1.93	0.470	0.060	5.000
97	3.53	0.350	0.075	5.450	139	2.89	0.482	0.053	6.574
98	3.53	0.350	0.075	5.450	140	2.89	0.482	0.053	6.574
99	1.67	0.194	0.043	6.600	141	2.89	0.482	0.053	6.574
100	1.67	0.194	0.043	6.600	142	2.89	0.482	0.053	6.574
101	1.67	0.194	0.043	6.600	143	2.89	0.482	0.053	6.574
102	1.00	0.631	0.065	4.500	144	1.67	0.301	0.040	10.211
103	1.93	0.470	0.060	5.000	145	1.67	0.301	0.040	10.211
104	1.93	0.470	0.060	5.000	146	1.67	0.301	0.040	10.211
105	1.93	0.470	0.060	5.000	147	6.31	0.361	0.050	7.375
106	2.88	0.482	0.053	6.574	148	6.31	0.361	0.050	7.375
107	2.88	0.482	0.053	6.574	149	6.31	0.361	0.050	7.375
108	2.88	0.482	0.053	6.574	150	6.31	0.361	0.050	7.375
109	2.88	0.482	0.053	6.574	151	6.31	0.361	0.050	7.375
110	2.88	0.482	0.053	6.574	152	6.31	0.361	0.050	7.375
111	1.67	0.301	0.040	10.210	153	6.31	0.361	0.050	7.375
112	1.67	0.301	0.040	10.210	154	4.20	0.356	0.047	7.200
113	1.67	0 301	0.040	10.210	155	4.20	0.356	0.047	7.200
114	6.32	0.361	0.050	7.370	156	4.20	0.356	0.047	7.200
115	6.32	0.361	0.050	7.370	157	6.01	0.375	0.045	9.710
116	6.32	0.361	0.050	7.370	158	6.01	0.375	0.045	9.710
117	6.32	0.361	0.050	7.370	159	6.01	0.375	0.045	9.710
118	6.32	0.361	0.050	7.370	160	6.01	0.375	0.045	9.710
119	6.32	0.361	0.050	7.370	161	6.01	0.375	0.045	9.710
120	6.32	0.361	0.050	7.370	162	6.01	0.197	0.045	12.460
121	4.20	0.356	0.047	7.200	163	6.01	0.197	0.045	12.460
122	4.20	0.356	0.047	7.200	164	4.85	0.197	0.039	12.460
123	4.20	0.356	0.047	7.200	165	4.85	0.197	0.039	12.460
124	6.00	0.376	0.045	9.690	166	4.85	0.197	0.039	12.460
125	6.00	0.376	0.045	9.690	167	4.85	0.197	0.039	12.460
126	6.00	0.376	0.045	9.690	168	4.85	0.197	0.039	12.460

Table 5 (cont.)

Branch No.	Coeff. ξ	Branch No.	Coeff. ξ	Branch No.	Coeff. ξ	Branch No.	Coeff. ξ
0	0.0003127	43	0.000268	86	0.0002085	129	0.0001631
1	0.0003002	44	0.000268	87	0.0002085	130	0.0001631
2	0.0003026	45	0.000268	88	0.0002085	131	0.0001631
3	0.0002886	46	0.0002207	89	0.0002085	132	0.0001631
4	0.000268	47	0.0002207	90	0.0002085	133	0.0001631
5	0.000268	48	0.0002207	91	0.0002207	134	0.0001631
6	0.000268	49	0.0002207	92	0.0002207	135	0.0001631
7	0.000268	50	0.0002207	93	0.0002207	136	0.0002028
8	0.000268	51	0.0001876	94	0.0002207	137	0.0002028
9	0.000268	52	0.0001876	95	0.0002144	138	0.0002028
10	0.0002207	53	0.0001876	96	0.0002085	139	0.0001876
11	0.0002207	54	0.0001876	97	0.0002085	140	0.0001876
12	0.0002207	55	0.0001876	98	0.0002085	141	0.0001876
13	0.0002207	56	0.0001876	99	0.0002028	142	0.0001876
14	0.0002207	57	0.0001876	100	0.0002028	143	0.0001876
15	0.0001876	58	0.0001501	101	0.0002028	144	0.0001876
16	0.0001876	59	0.0001501	102	0.0002028	145	0.0001876
17	0.0001876	60	0.0001501	103	0.0002028	146	0.0001876
18	0.0001876	61	0.0002502	104	0.0002028	147	0.0001706
19	0.0001501	62	0.0002502	105	0.0002028	148	0.0001706
20	0.0001501	63	0.0002502	106	0.0001876	149	0.0001706
21	0.0001501	64	0.0002502	107	0.0001876	150	0.0001706
22	0.0001876	65	0.0002502	108	0.0001876	151	0.0001706
23	0.0001876	66	0.0002502	109	0.0001876	152	0.0001706
24	0.0001876	67	0.0002345	110	0.0001876	153	0.0001706
25	0.0002085	68	0.0002274	111	0.0001876	154	0.0001706
26	0.0002085	69	0.0002274	112	0.0001876	155	0.0001706
27	0.0002085	70	0.0002274	113	0.0001876	156	0.0001706
28	0.0002207	71	0.0002085	114	0.0001706	157	0.0001631
29	0.0002207	72	0.0002085	115	0.0001706	158	0.0001631
30	0.0002207	73	0.0002085	116	0.0001706	159	0.0001631
31	0.000268	74	0.0002085	117	0.0001706	160	0.0001631
32	0.0002588	75	0.0002085	118	0.0001706	161	0.0001631
33	0.0002588	76	0.0002085	119	0.0001706	162	0.0001631
34	0.0002588	77	0.0002085	120	0.0001706	163	0.0001631
35	0.000268	78	0.0002085	121	0.0001706	164	0.0001631
36	0.000268	79	0.0002085	122	0.0001706	165	0.0001631
37	0.000268	80	0.0002085	123	0.0001706	166	0.0001631
38	0.0002588	81	0.0002085	124	0.0001631	167	0.0001631
39	0.0002588	82	0.0002085	125	0.0001631	168	0.0001631
40	0.0002588	83	0.0002085	126	0.0001631		
41	0.0002588	84	0.0002085	127	0.0001631		
42	0.0002588	85	0.0002085	128	0.0001631		

Table 6: The coefficient for the variation of the wavespeed versus pressure.

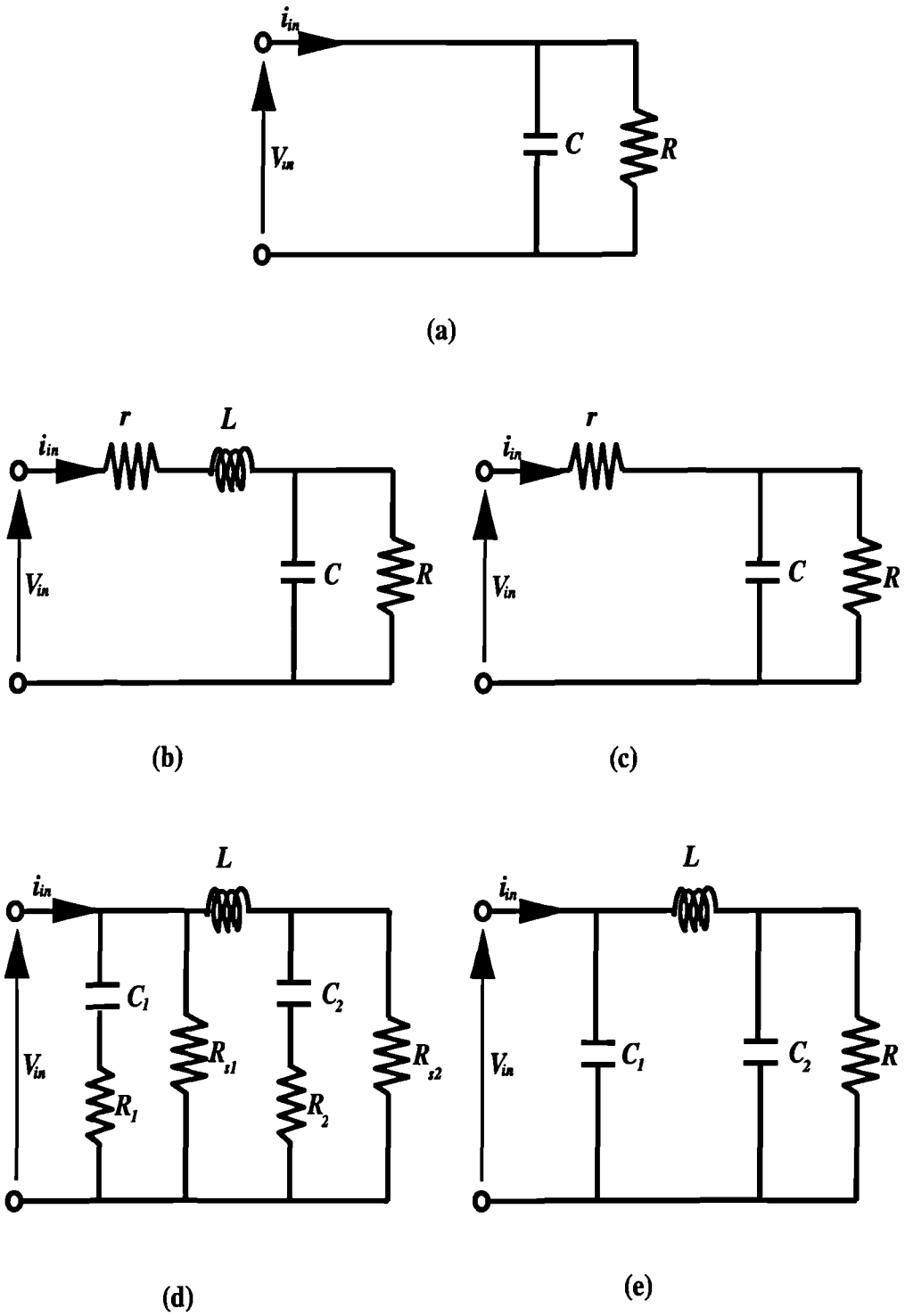


Figure 1: Lumped parameter linear models of the Windkessel type. (a) Windkessel model (b) Model proposed by Landes (1943), (c) Westerhof (1968), (d) Spencer and Denison, (e) Goldwyn and Watt (1967)

(963)

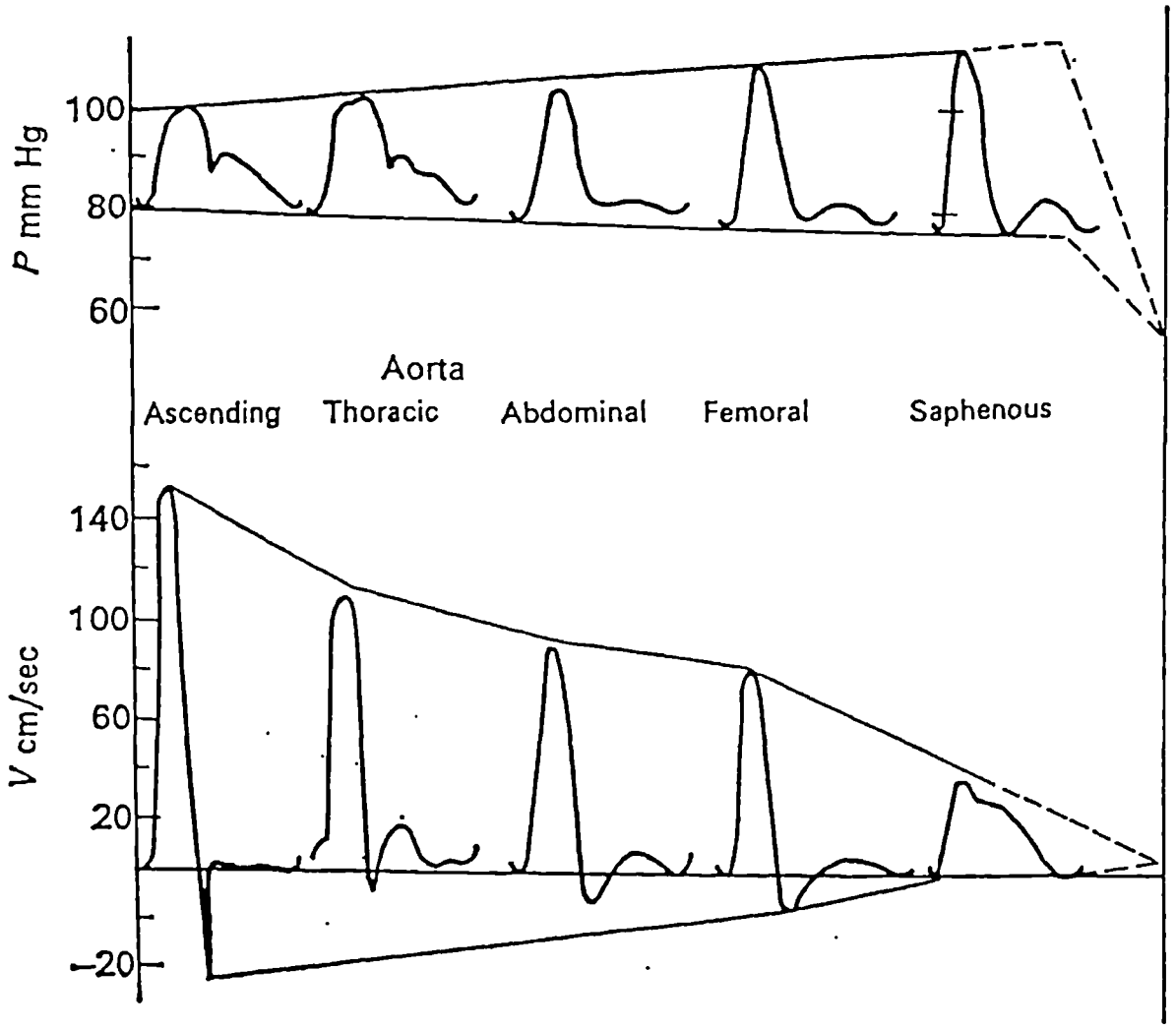


Figure 2: A diagrammatic comparison of the pressure and velocity waveforms from the ascending aorta to the saphenous artery. (from McDonald, 1974)

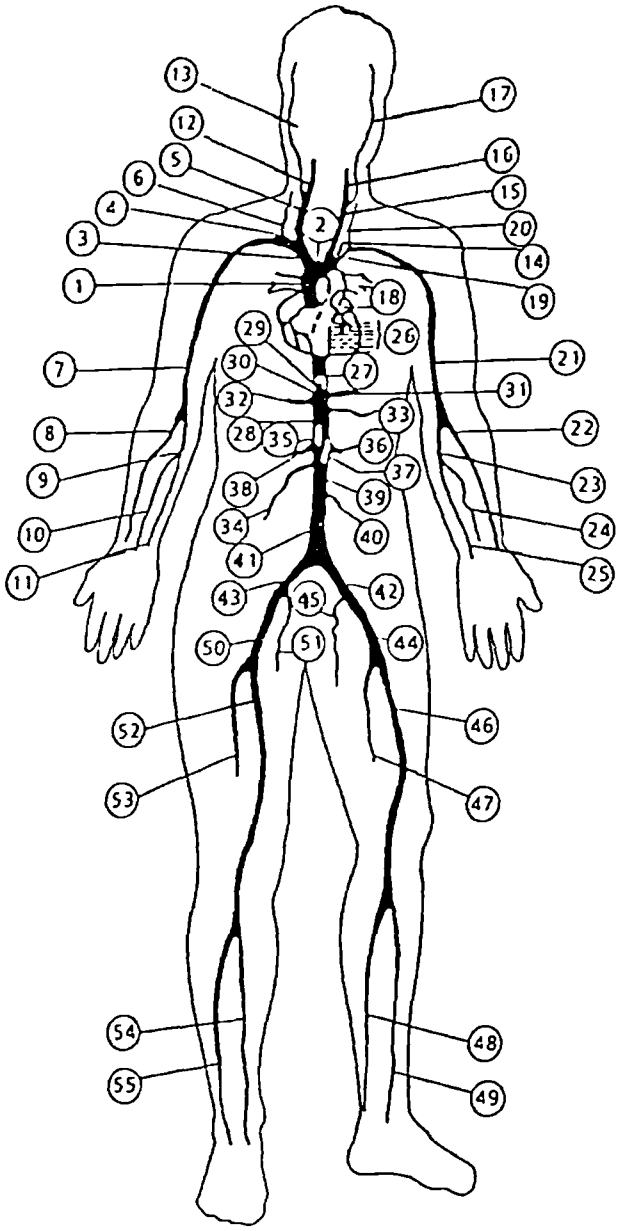


Figure 3: The arterial system model used in the calculation. This model was introduced by Westerhof *et al.* (1969) and contains data for diameter, length, wall thickness and Young's modulus of the 55 largest arteries (from Stergiopulos *et al.*, 1992)

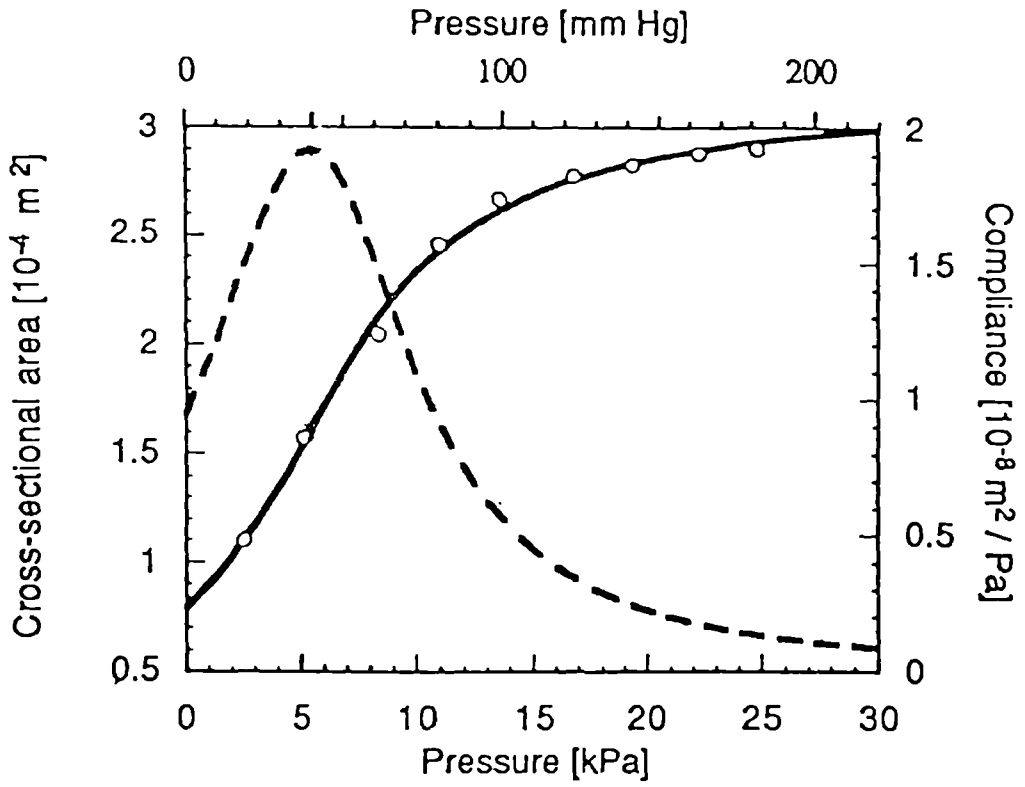


Figure 4: The cross-sectional area and compliance as a function of pressure for the human abdominal aorta *in vitro*. The experimental data (open circles) are fitted with an arctangent model (solid line). The dotted line represents the aortic compliance (Pythoud *et al.*, 1994).

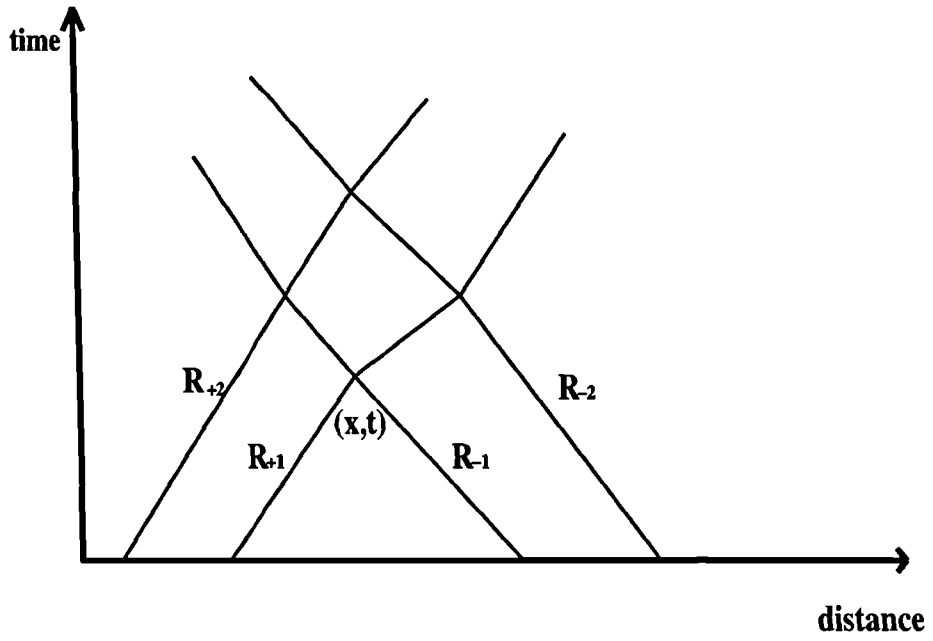


Figure 5: The forward (R_+) and backward (R_-) running characteristics intersect in the distance–time plane. The properties at each point (x,t) are determined by a unique pair of characteristics intersecting at that point. Characteristics are not necessarily straight, since they depend upon the local P and U.

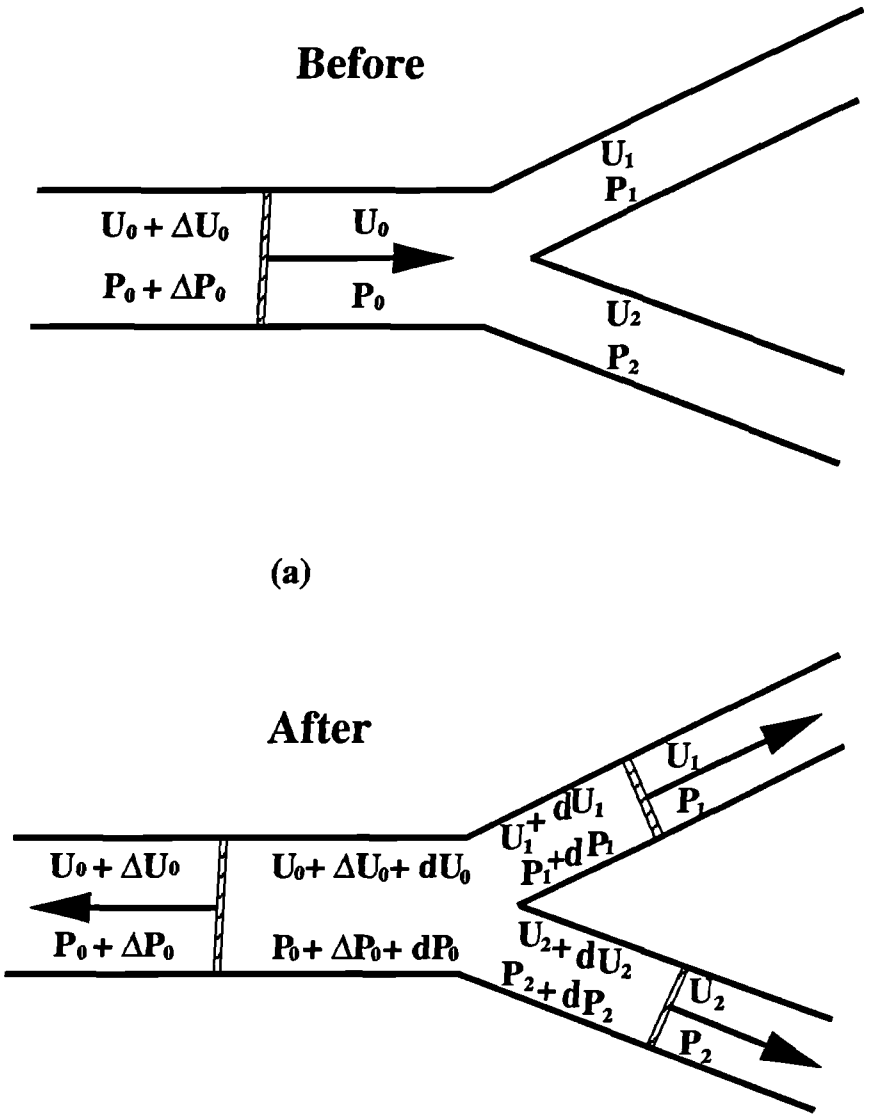


Figure 6: **(a)** A wave with amplitude ΔP_0 and ΔU_0 travels down the parent vessel. **(b)** Some time later, the wave is reflected by the junction and transmitted to the daughter vessels.

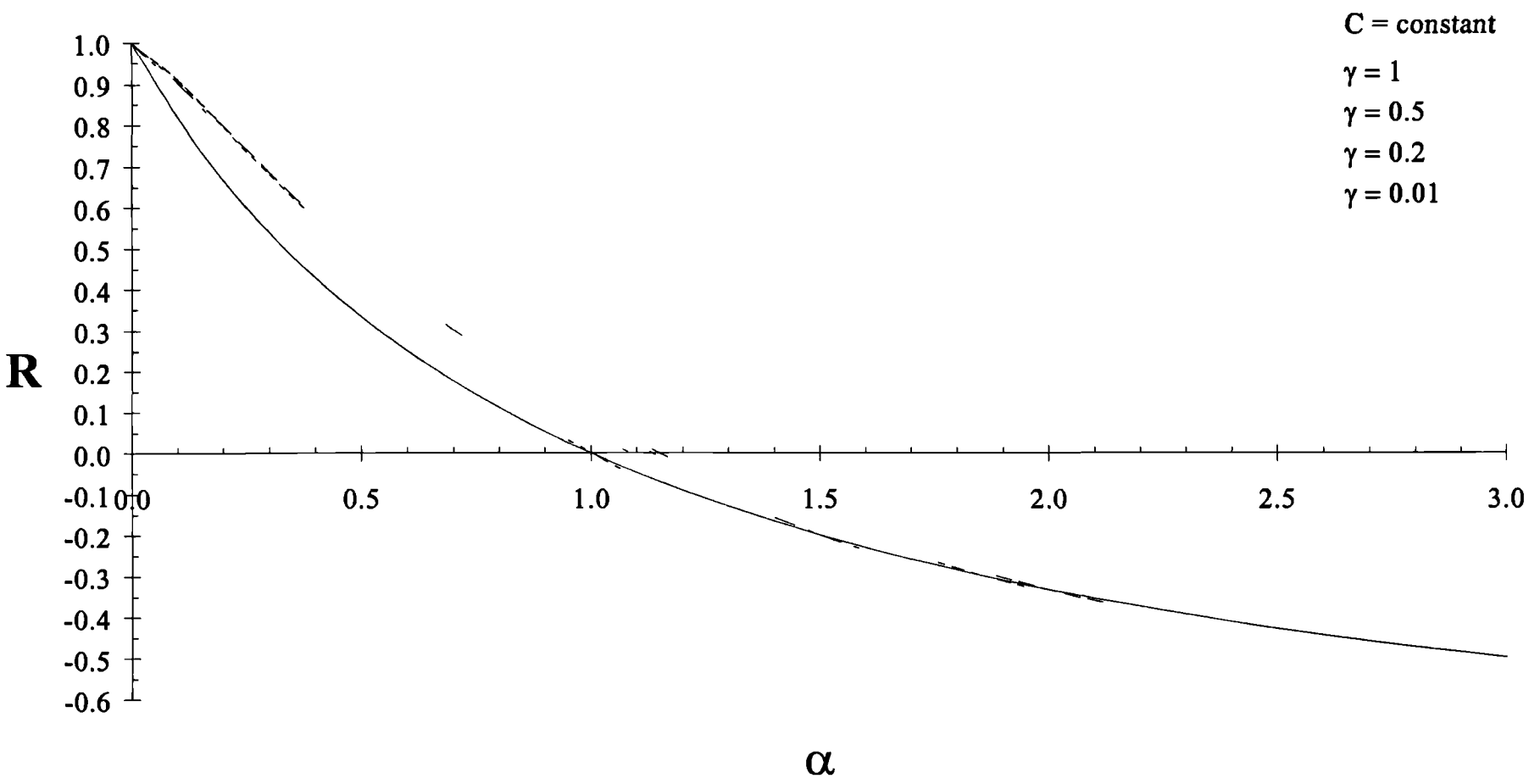
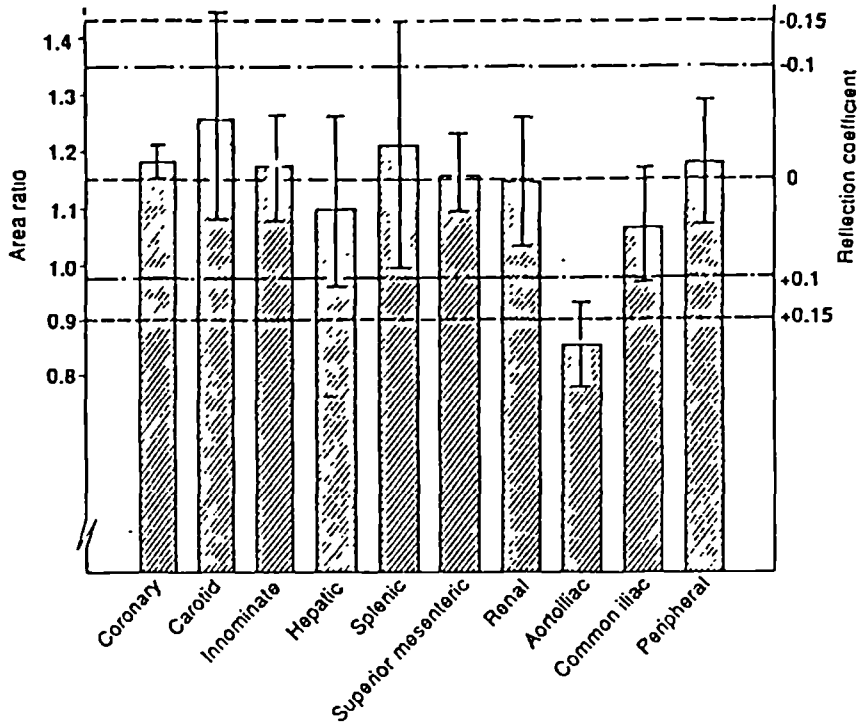
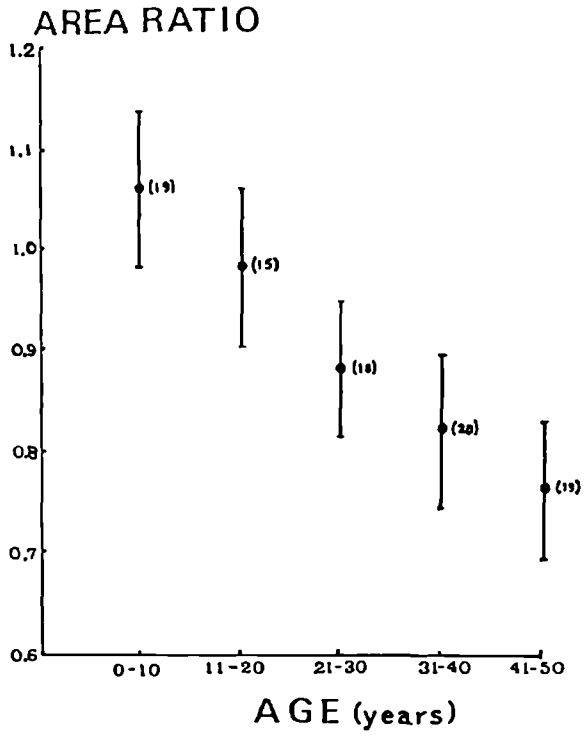


Figure 7: The variation of the reflection coefficient calculated for the two models, constant wall thickness and constant radius to wall thickness ratio. α is the area ratio of the daughter to parent vessels. γ is the area ratio between the two daughters.

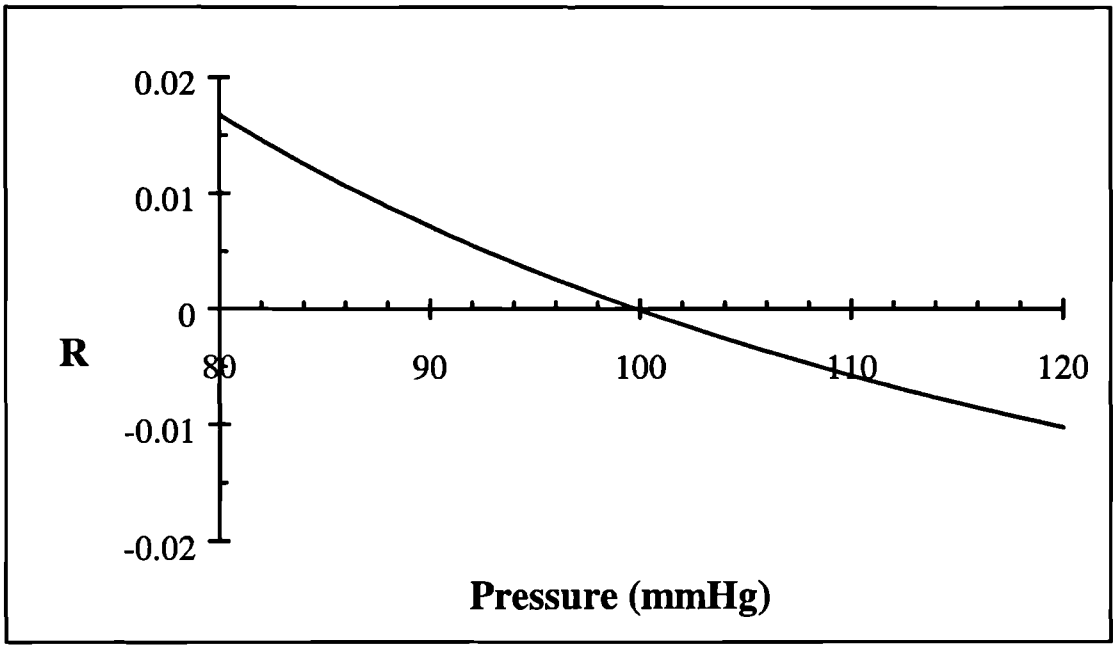


(a)

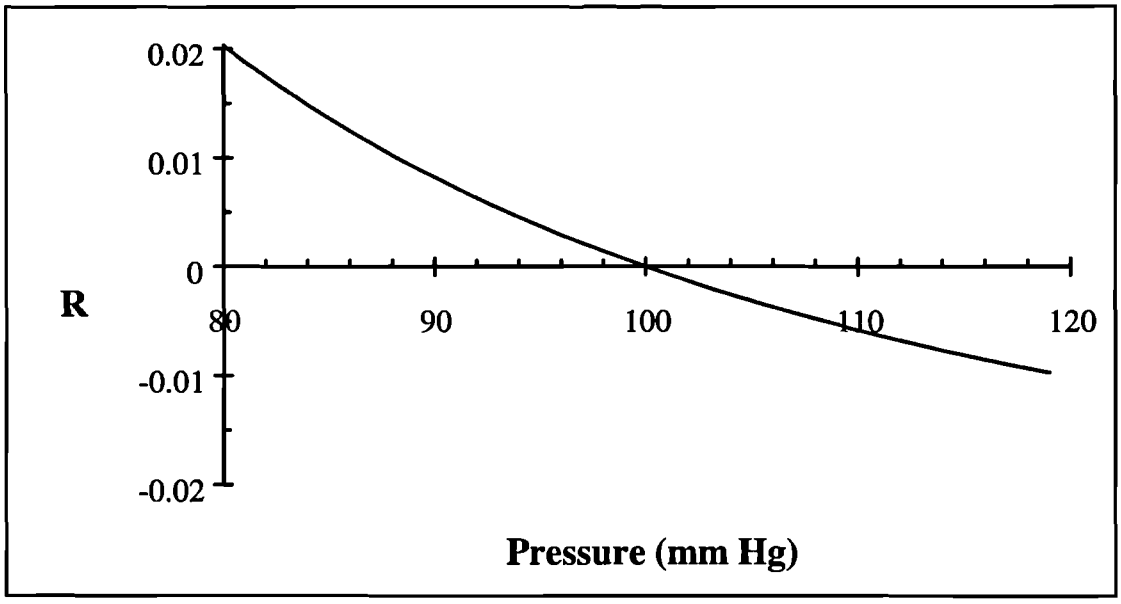


(b)

Figure 8: (a) Area ratios of bifurcations together with the corresponding reflection coefficients (Parpageorgiou and Jones, 1990). (b) The variation of the area ratio of the aortoiliac junction in man with age. The number in the brackets is the number of subjects in each age group (Gosling et al., 1971).



(a)



(b)

Figure 9 The variation of the reflection coefficient for forward going waves versus the changes of pressure within the physiological range calculated by assuming that the bifurcation is well matched for forward waves at 100 mmHg. (a) aortoiliac bifurcation, (b) brachiocephalic bifurcation.

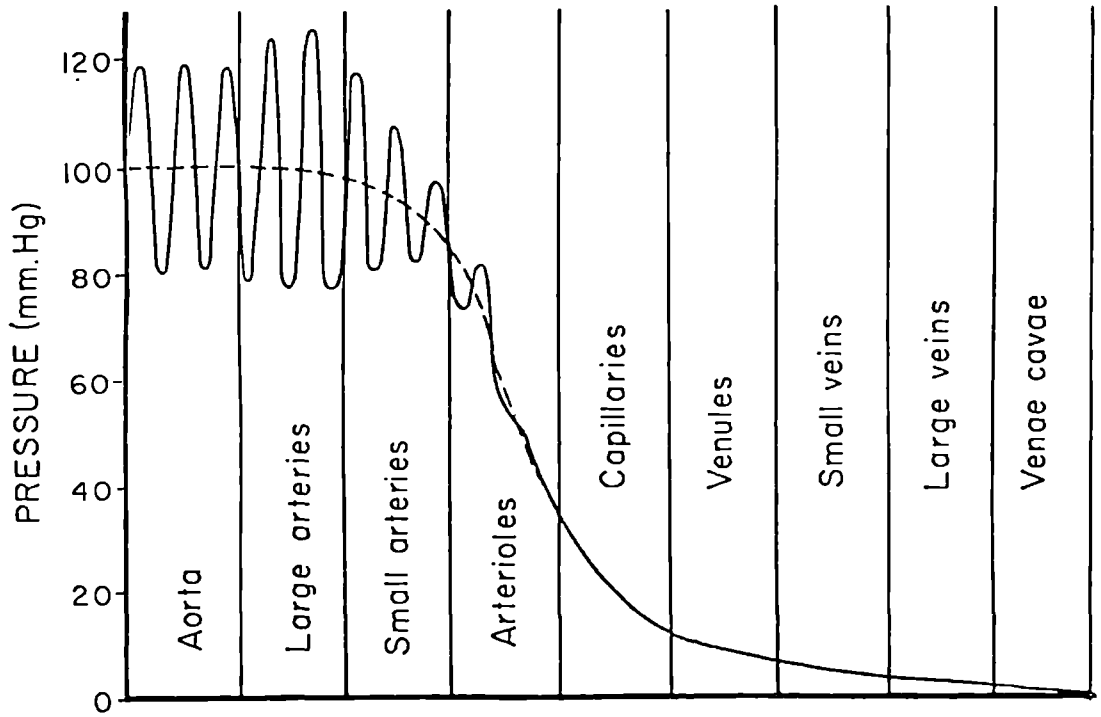


Figure 10: Blood pressure measured at different locations in the systemic circulation. The mean aortic pressure (dotted line) is nearly constant in the aorta and large arteries. There is a large pressure drop in the arterioles and it is believed that the resistance of the arterioles is the greatest of any part of the systemic circulation (from Guyton, 1982).

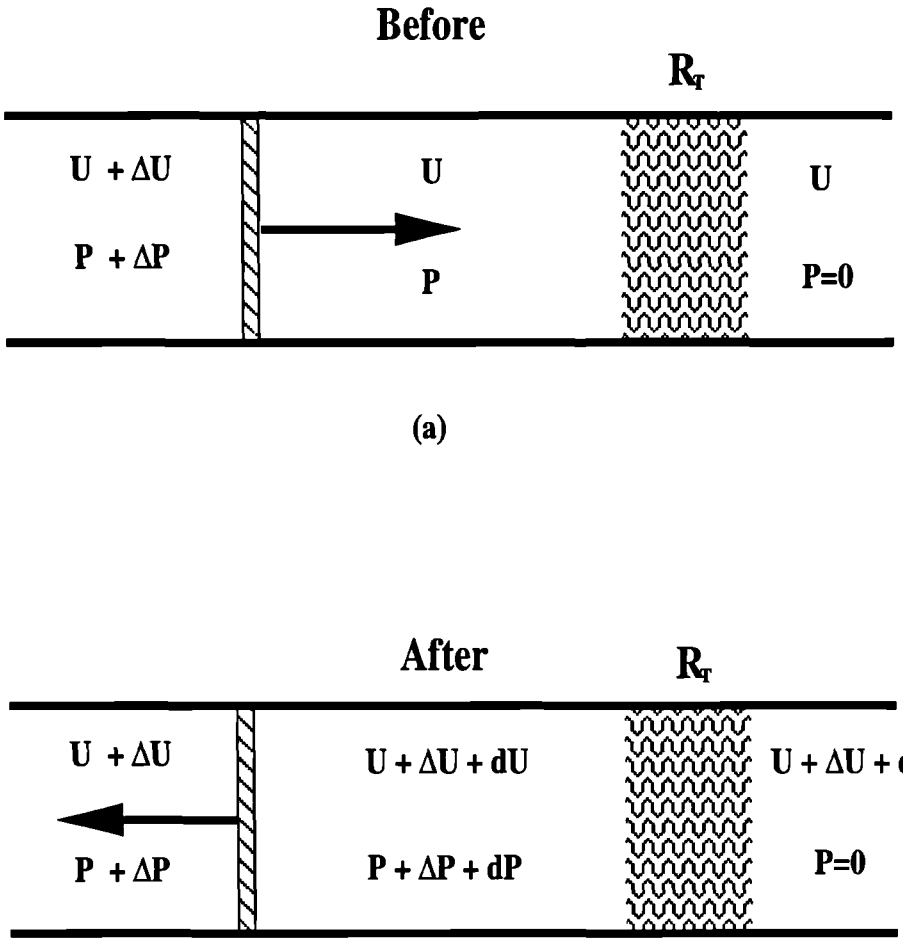


Figure 11: The termination of each terminal artery is simulated by a pure resistance connected to a zero pressure reservoir. The upper figure shows the wave before it reaches the resistance and the lower shows the conditions after the reflection.

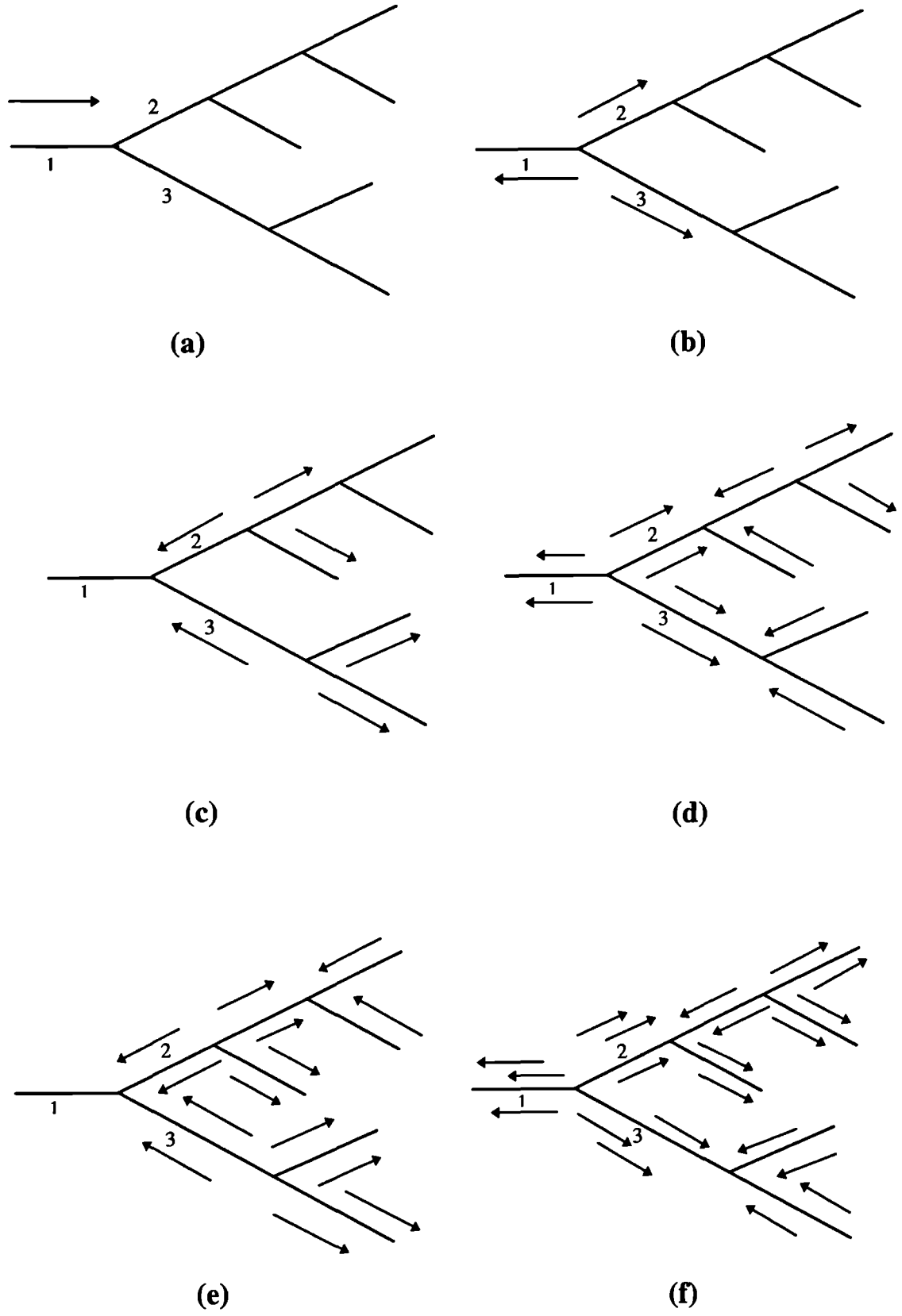


Figure 12: Diagrammatic representation showing wave transmission in an arterial tree. (a) The first wave starts from the aortic root, part of the wave is transmitted to its daughter segments and part of the wave is reflected when it reaches a junction where the impedance is not matched. Waves after passing through (b) one, (c) two, (d) three, (e) four and (f) five junctions. The segments are not necessarily equal in length.

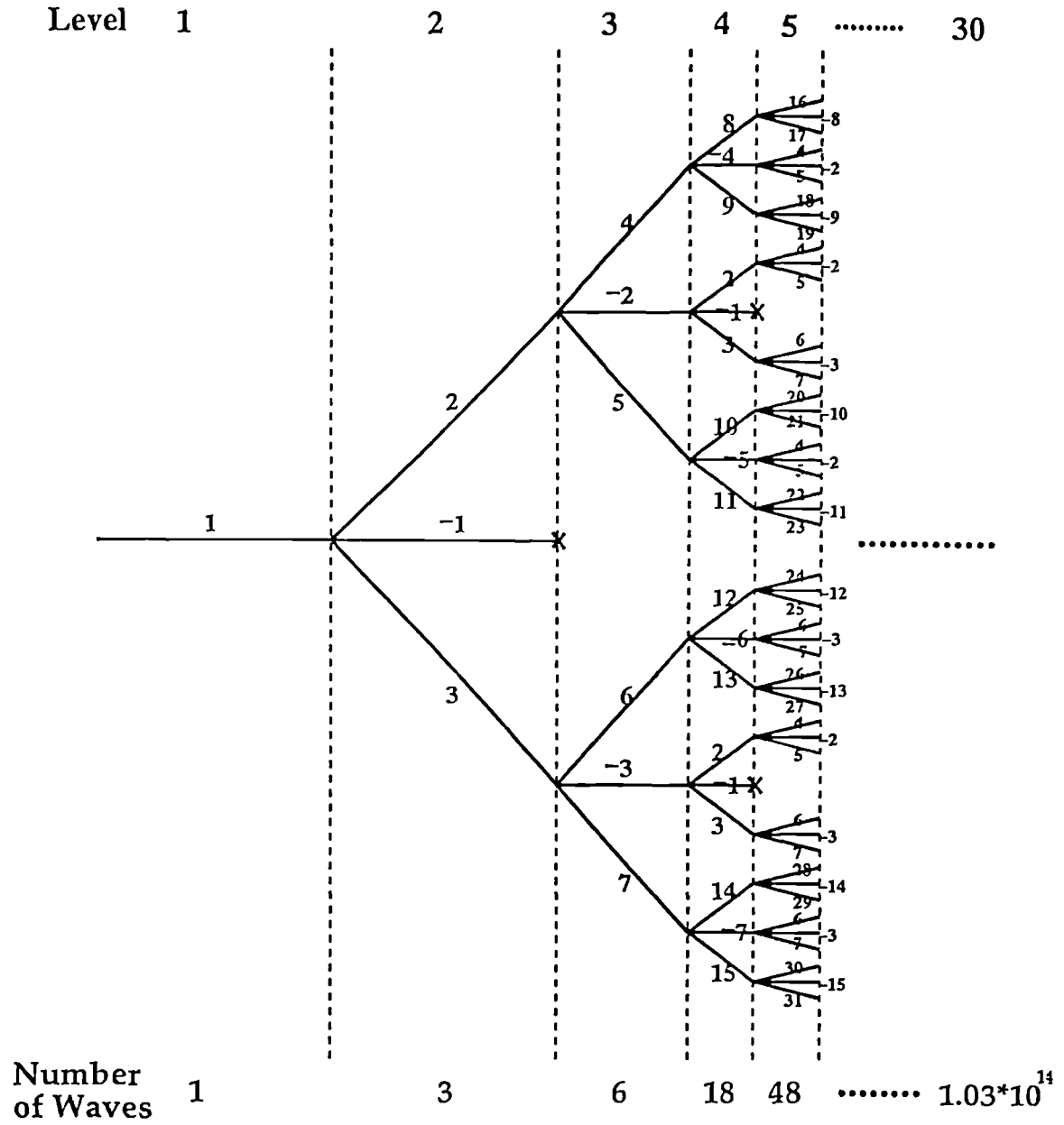


Figure 13: Diagrammatic representation of the tree of waves showing the various levels. '-' denotes a backward travelling wave. 'x' indicates the termination of a wave when it reaches the heart which is assumed to be an absorber. When the heart is assumed to be a reflector, these waves will be reflected back into the system.

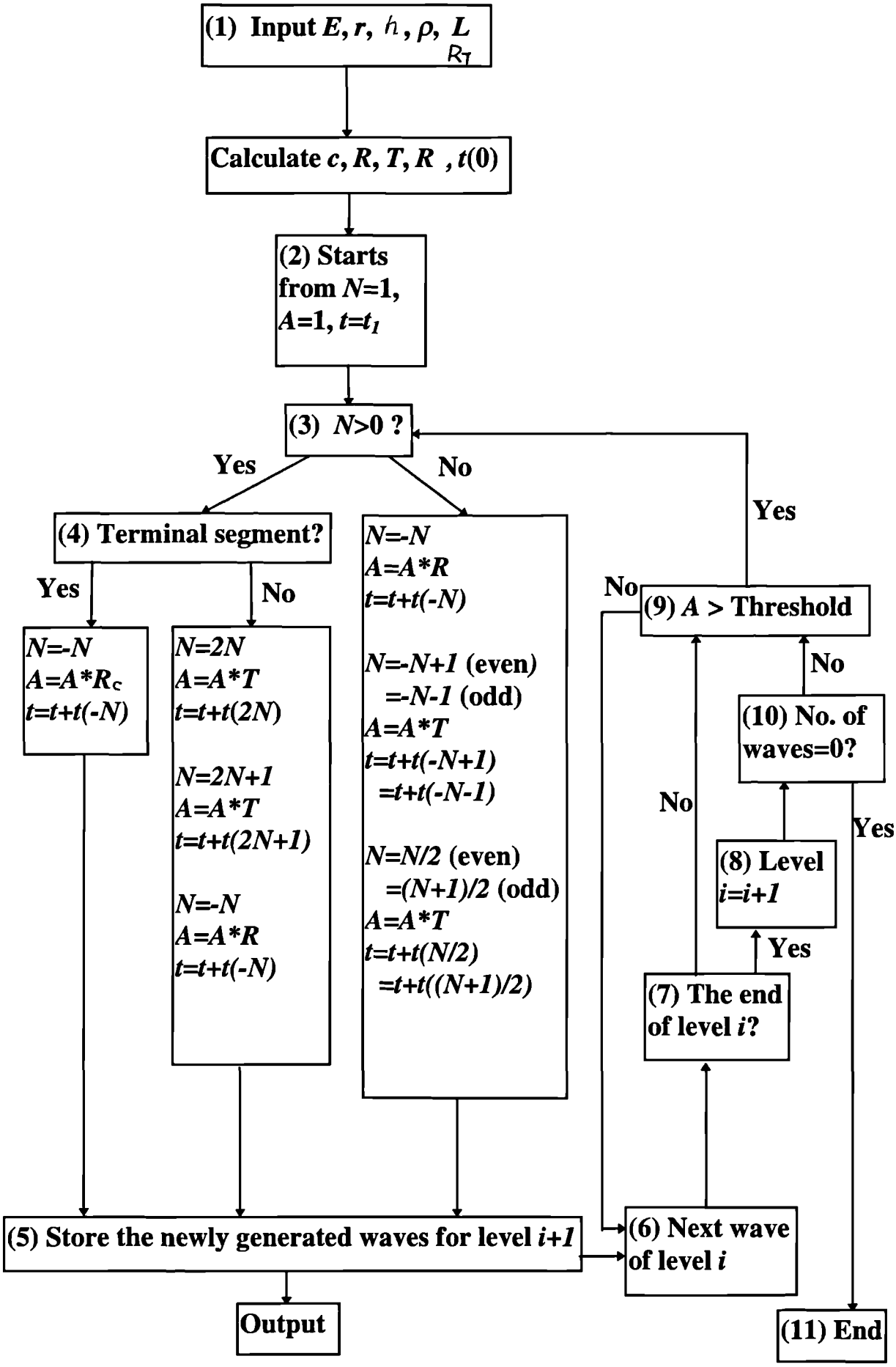


Figure 14: The flow chart for calculating the transfer function.

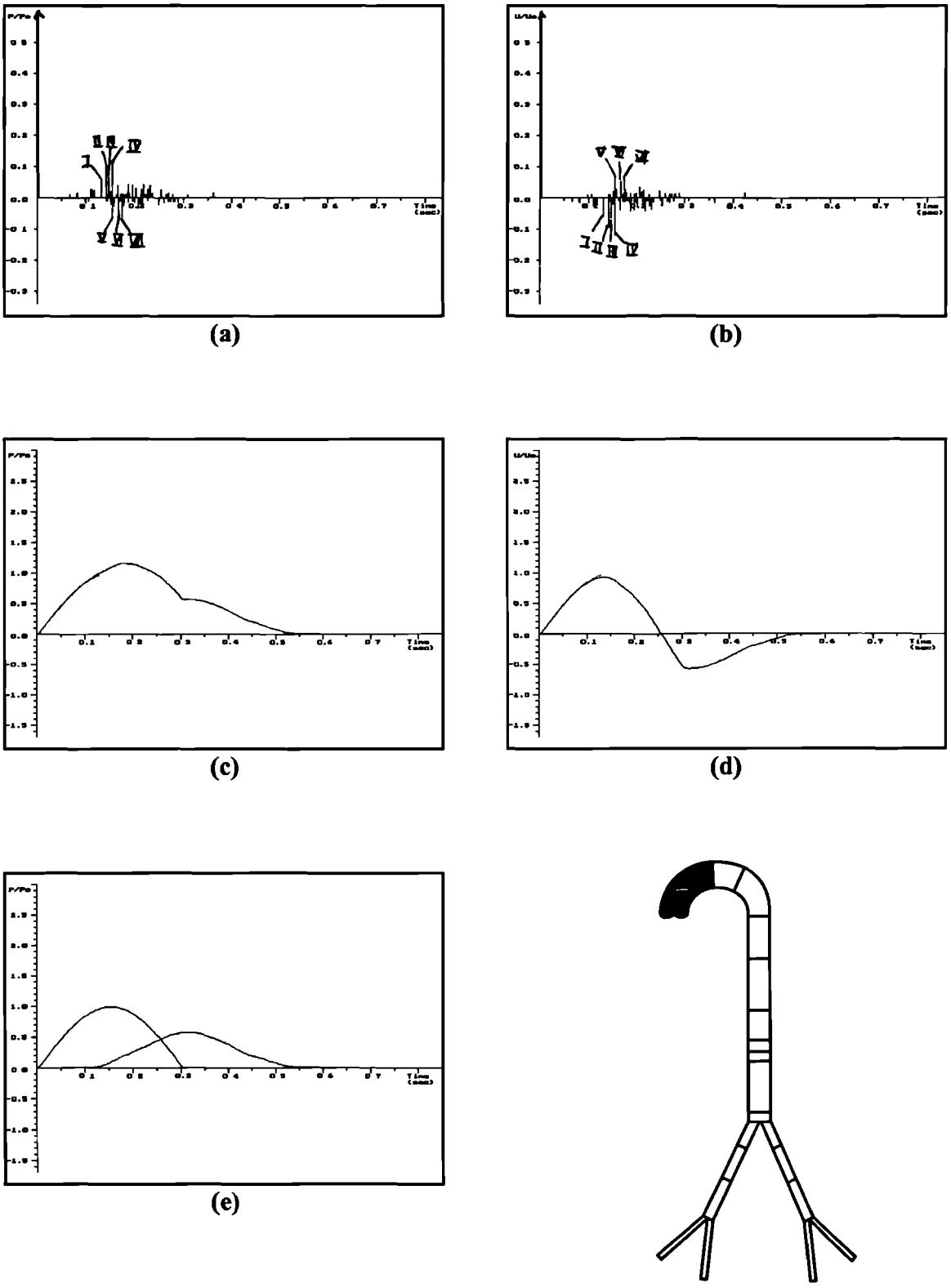


Figure 15: The ascending aorta. (a) The transfer function for the pressure, where the 7 largest reflections are marked, the arrow signifies the signal is off the scale. (b) The transfer function for the velocity. (c) The pressure waveform which is the convolution of the input (the dotted line) with the pressure transfer function. (d) The velocity waveform. (e) The forward (left hand side) and backward (right hand side) pressure waves separated according the direction of wavelets in the pressure transfer function.

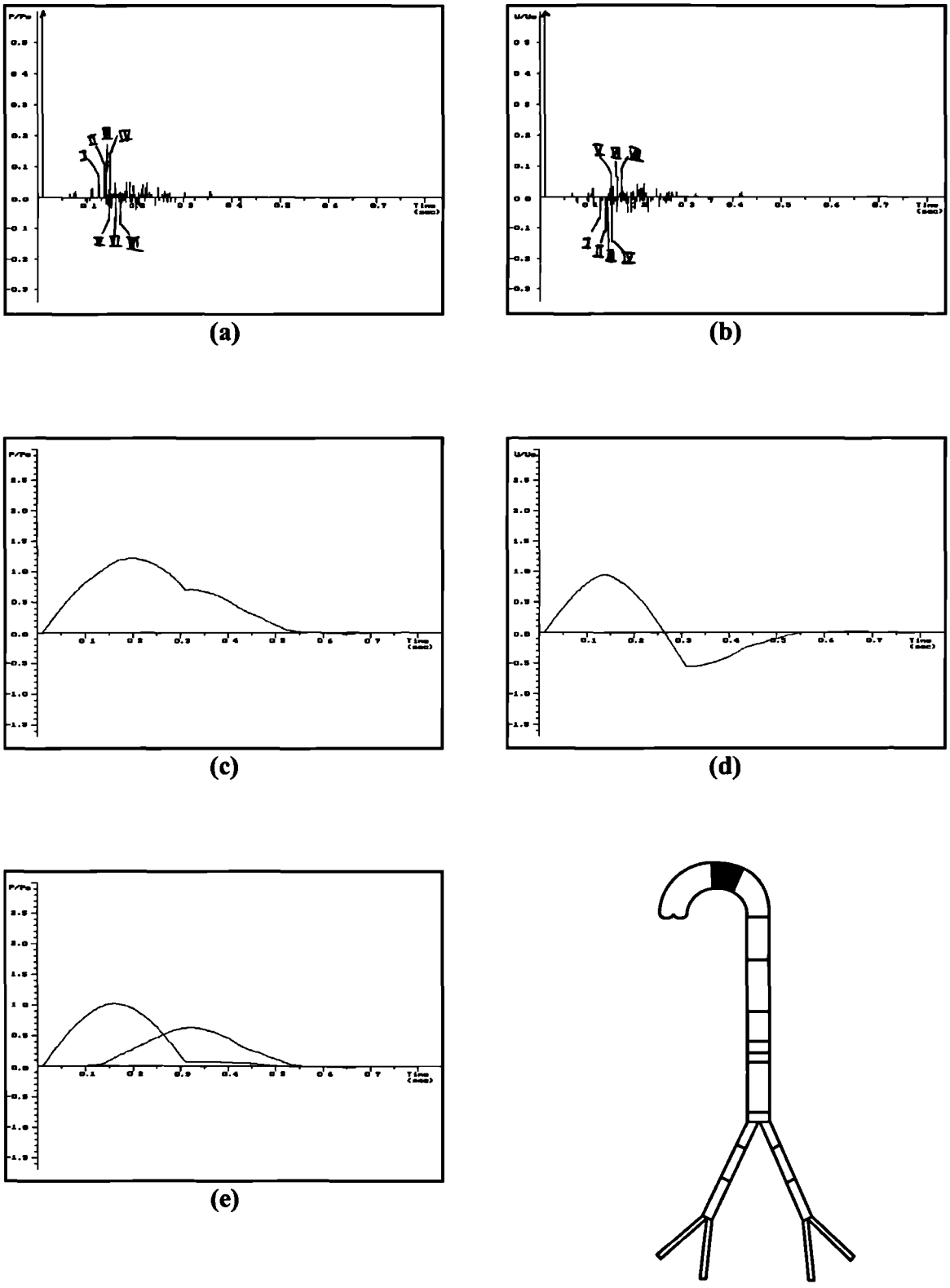


Figure 16: The aortic arch I segment. (a) The transfer function for the pressure, where the 7 largest waves are marked. (b) The transfer function for the velocity. (c) The pressure waveform. (d) The velocity waveform. (e) The forward (left hand side) and backward (right hand side) pressure waves.

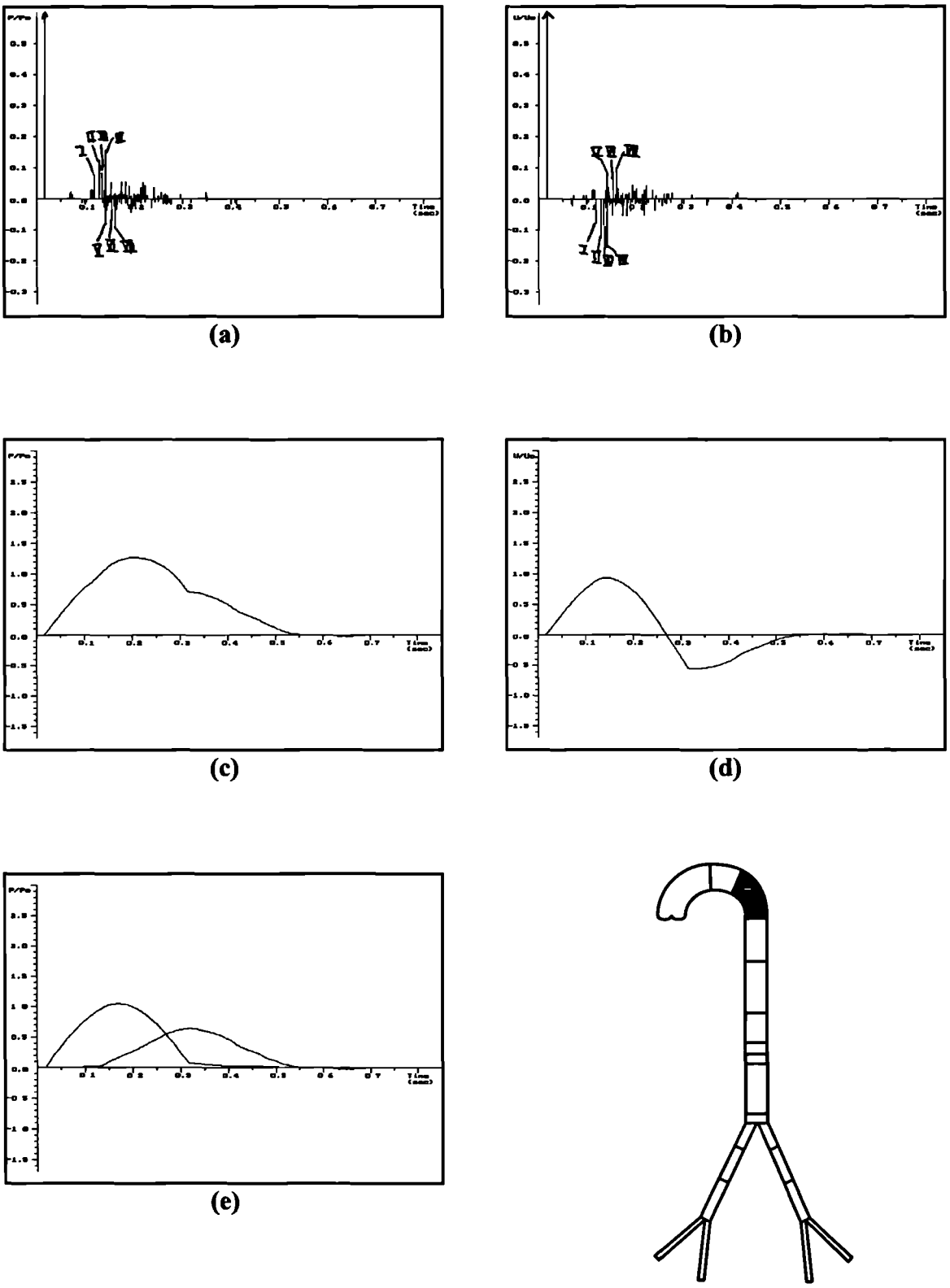


Figure 17: The aortic arch II segment. (a) The transfer function for the pressure. (b) The transfer function for the velocity. (c) The pressure waveform, where the inflection point in early systole can be seen. (d) The velocity waveform. (e) The forward (left hand side) and backward (right hand side) pressure waves separated according to the direction of the wave of the pressure transfer function.

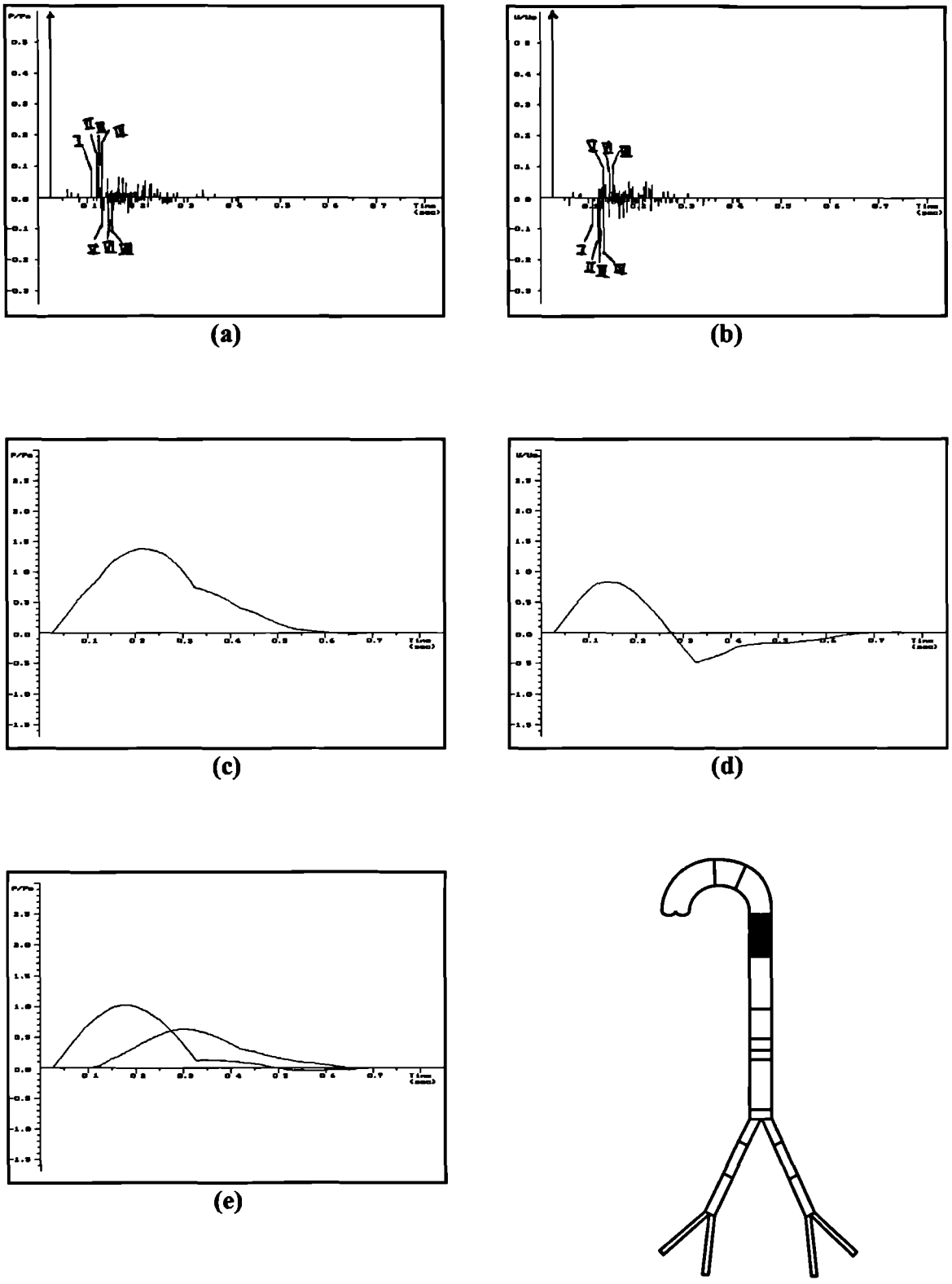


Figure 18: The thoracic aorta I segment: (a) The transfer function for the pressure. (b) The transfer function for the velocity. (c) The pressure waveform. (d) The velocity waveform. (e) The forward (left hand side) and backward (right hand side) pressure waves.

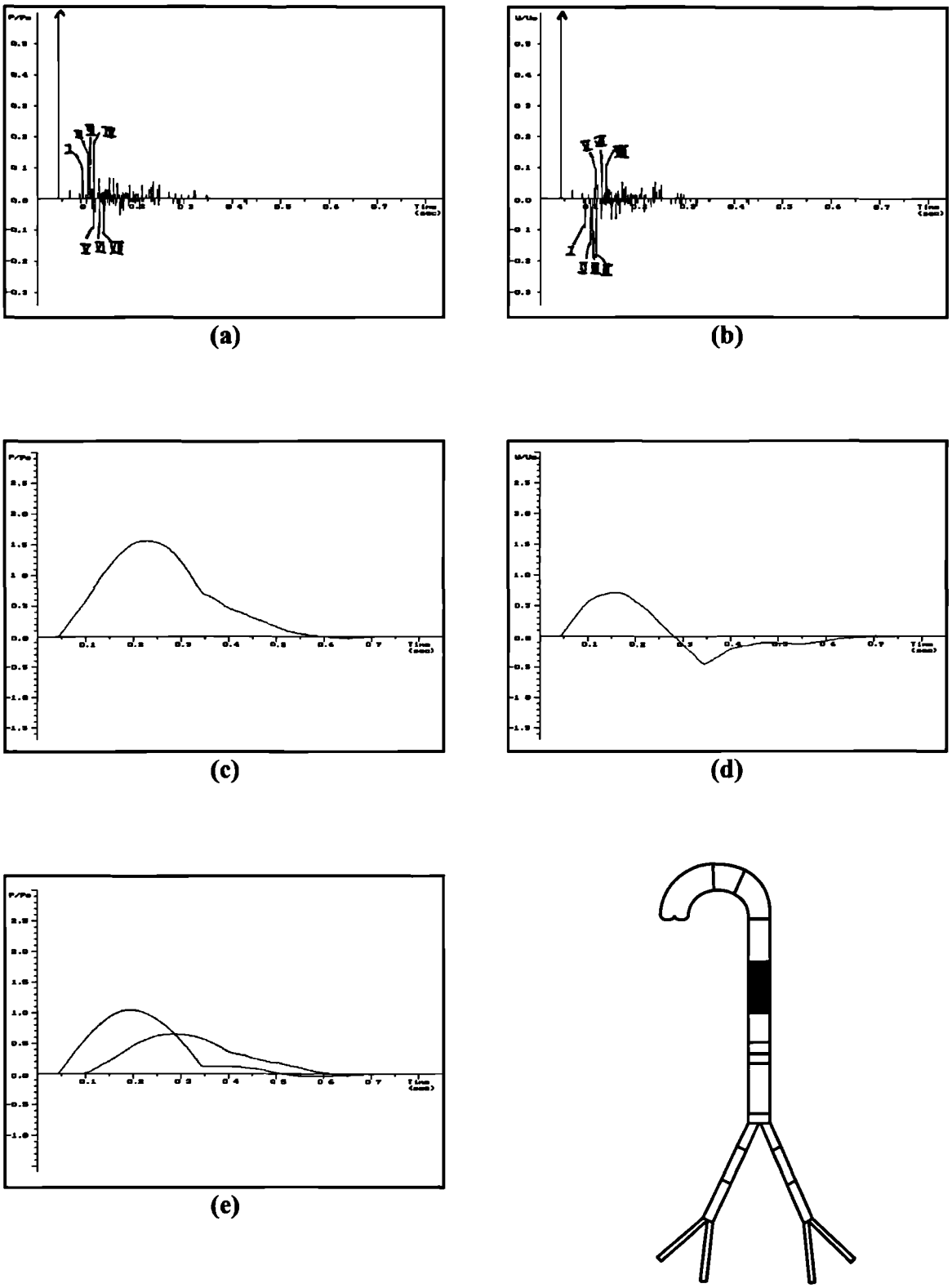


Figure 19: The thoracic aorta II segment. (a) The transfer function for the pressure. (b) The transfer function for the velocity. (c) The pressure waveform. (d) The velocity waveform. (e) The forward (left hand side) and backward (right hand side) pressure waves.

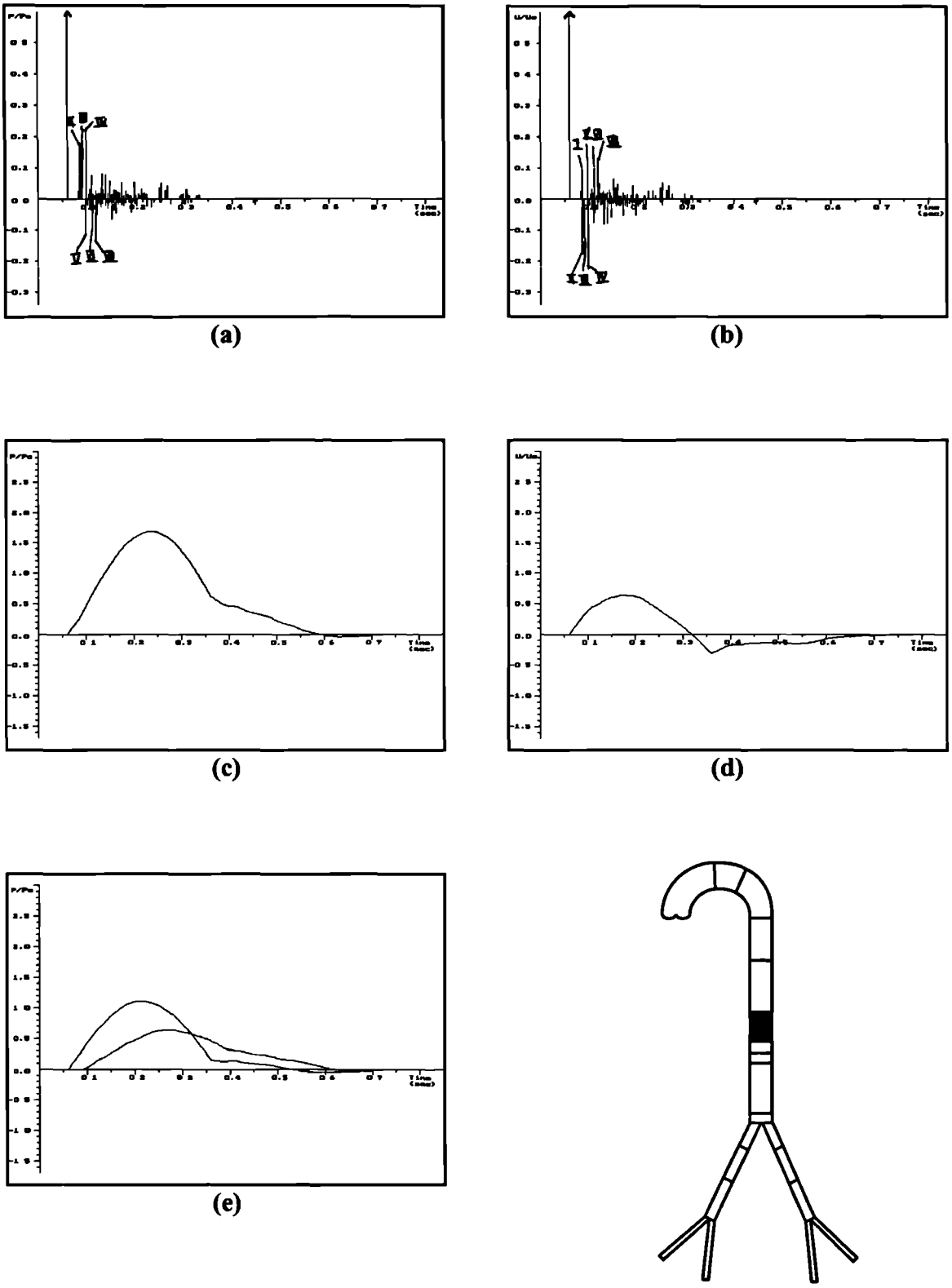


Figure 20: The abdominal aorta I segment. (a) The transfer function for the pressure. (b) The transfer functions for the velocity. Wave I is in phase in both pressure and velocity transfer function but out of phase in Figure 19. This indicates that wave I comes from the celiac artery I segment, 29. (c) The pressure waveform. (d) The velocity waveform. (e) The forward (left hand side) and backward (right hand side) pressure waves.

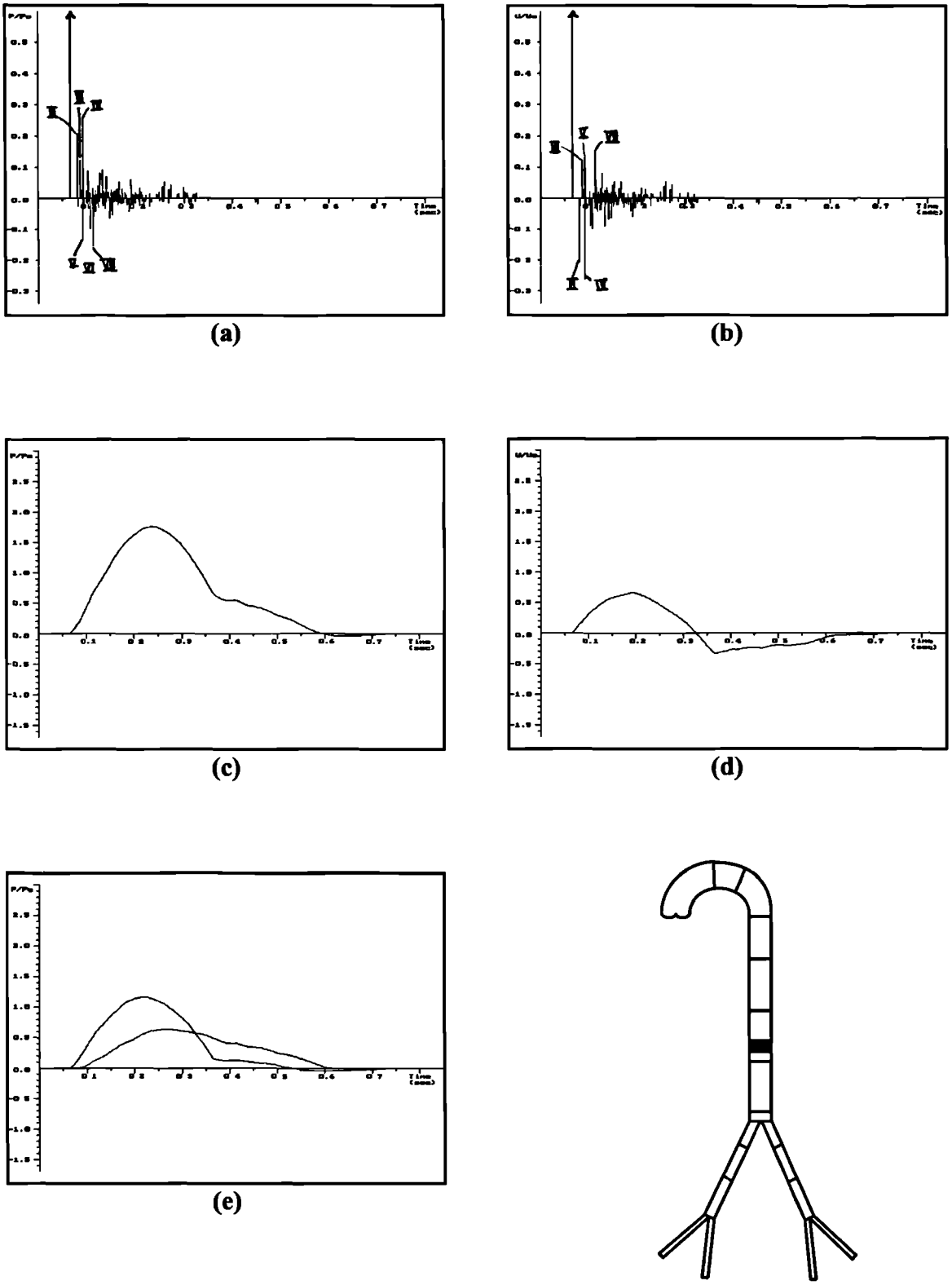


Figure 21: The abdominal aorta II segment. (a) The transfer function for the pressure. (b) The transfer function for the velocity. Waves III and VI are the same sign in both pressure and velocity transfer functions, but out of phase in Figure 20. This indicates that both waves are from the splenic artery segment, 33. (c) The pressure waveform. (d) The velocity waveform. (e) The forward (left hand side) and backward (right hand side) pressure waves.

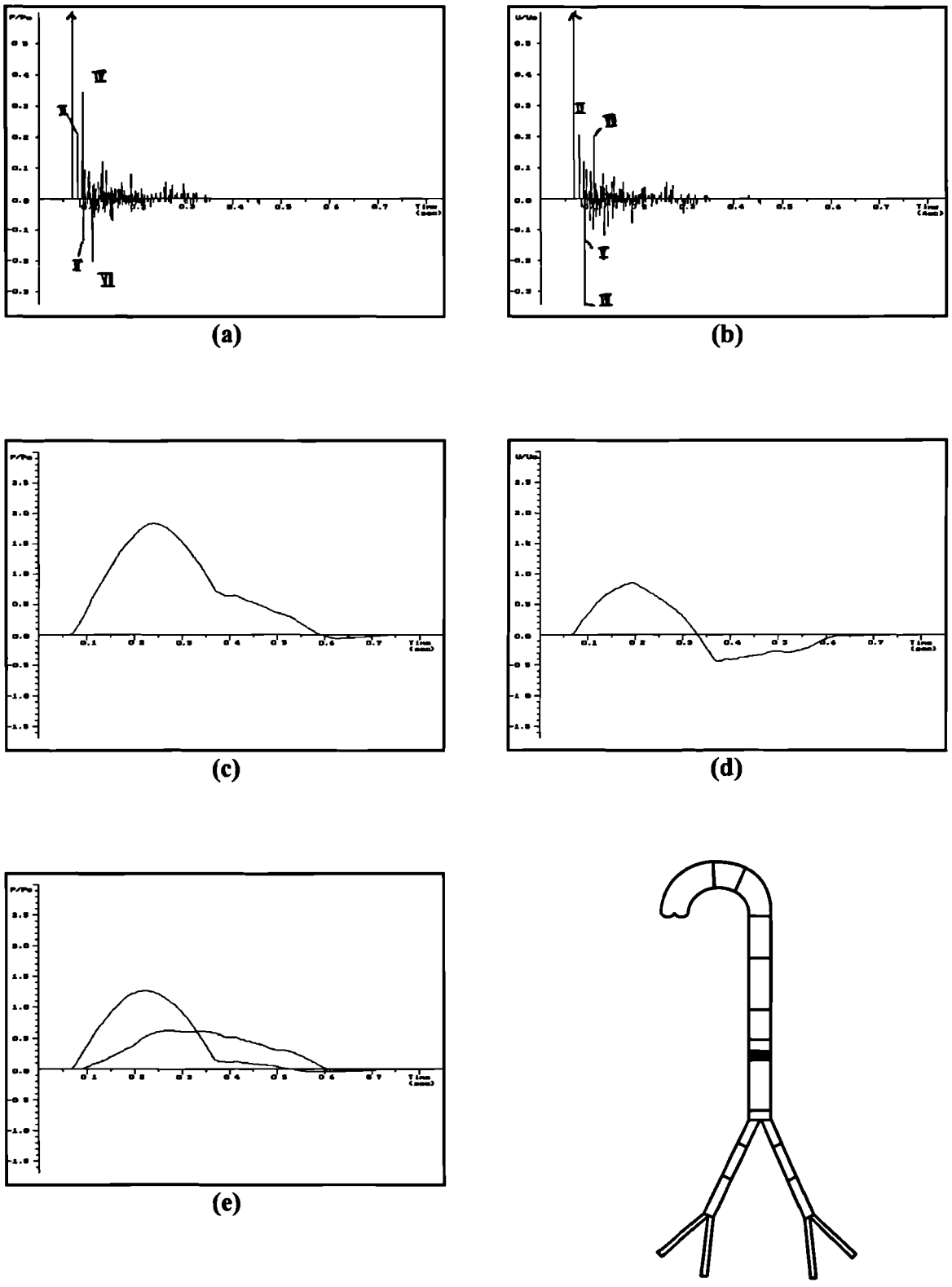


Figure 22: The abdominal aorta III segment. (a) The transfer function for the pressure. (b) The transfer function for the velocity. Waves II and V are the same sign in both pressure and velocity transfer function, but opposite sign in Figure 21. This indicates that both waves are from the renal arteries, segment 36 and 38. (c) The pressure waveform. (d) The velocity waveform. (e) The forward (left hand side) and backward pressure waves (right hand side).

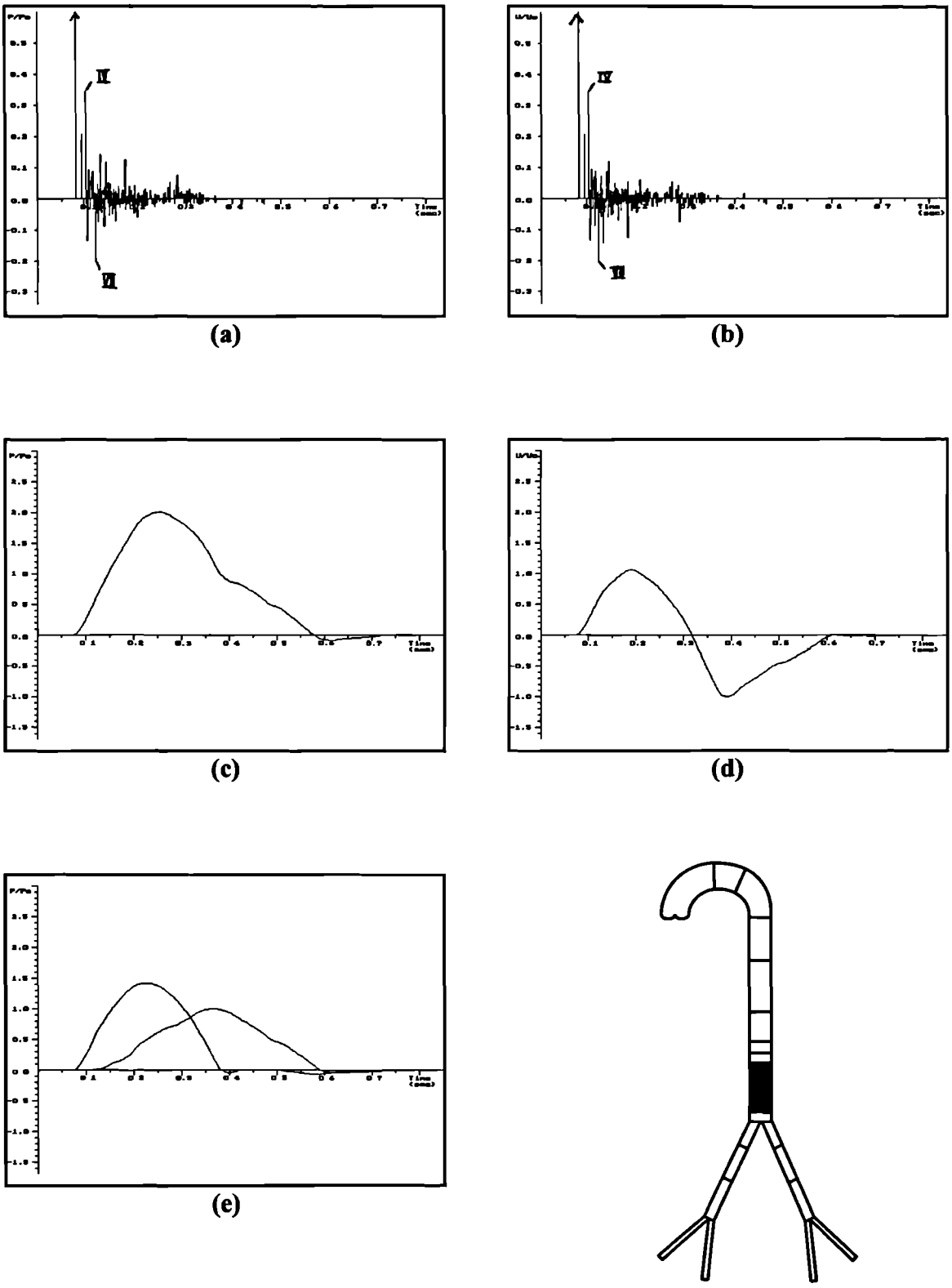


Figure 23: In the abdominal aorta IV segment. (a) The transfer function for the pressure. (b) The transfer function for the velocity. Waves IV and VII are the same sign in both pressure and velocity transfer functions, but opposite sign in Figure 22. This indicates that both waves are from segment 34. (c) The pressure waveform. (d) The velocity waveform. (e) The forward (left hand side) and backward (right hand side) pressure waves.

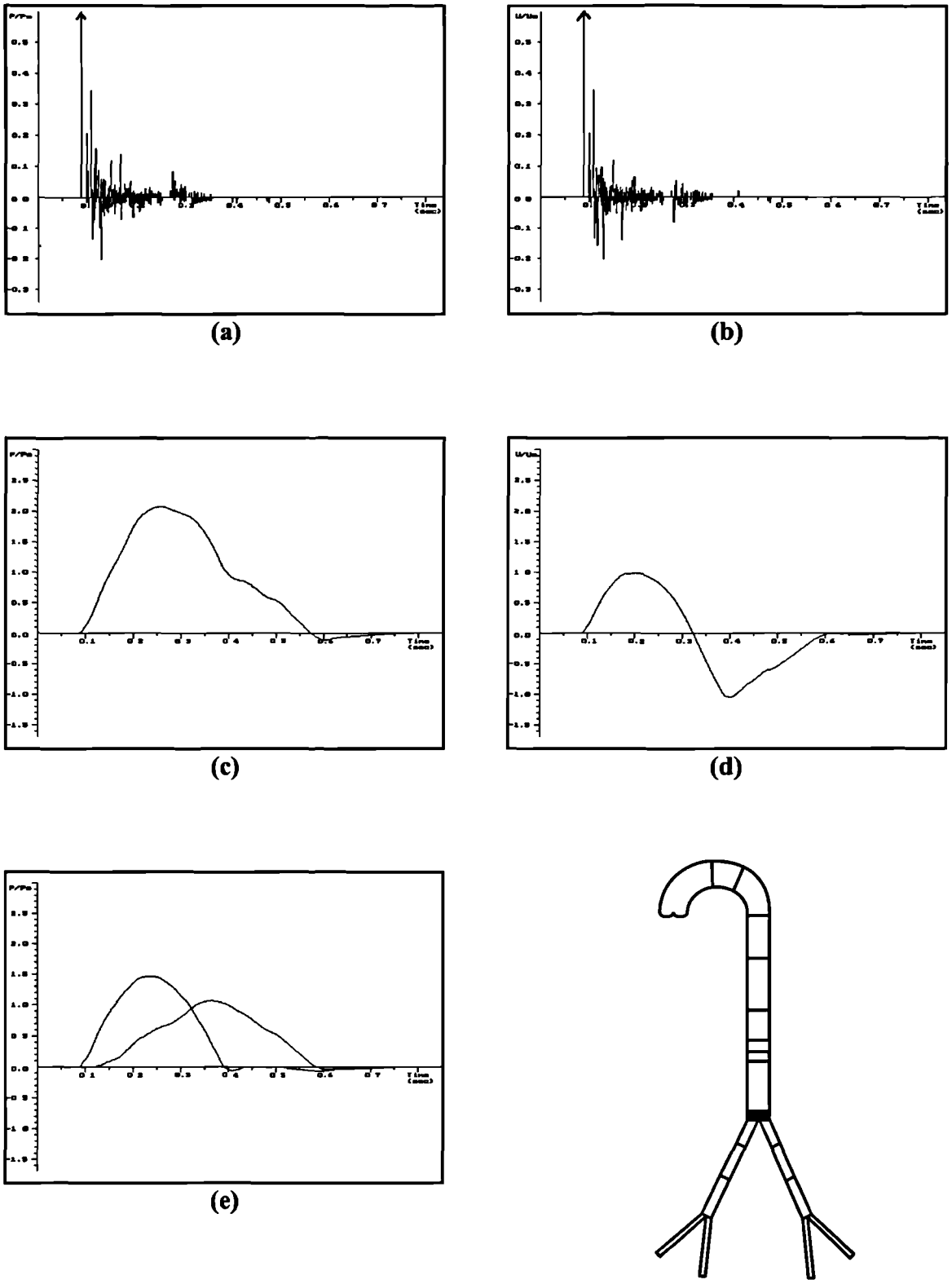


Figure 24: The abdominal aorta V segment. (a) The transfer function for the pressure. (b) The transfer function for the velocity. (c) The pressure waveform. (d) The velocity waveform. (e) The forward (left hand side) and backward (right hand side) pressure waves.

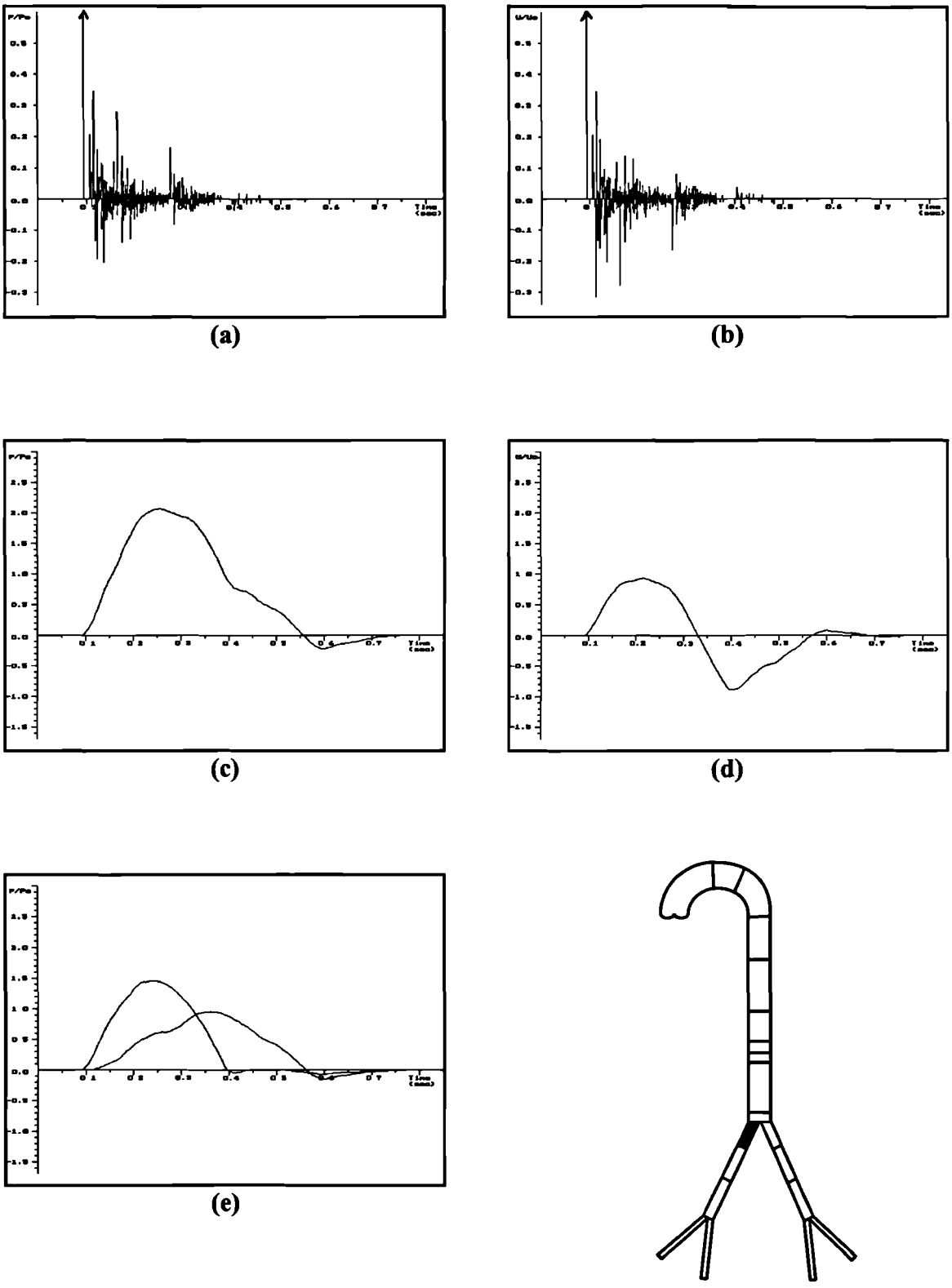


Figure 25: The right common iliac artery segment. (a) The transfer function for the pressure. (b) The transfer function for the velocity. (c) The pressure waveform. (d) The velocity waveform. (e) The forward (left hand side) and backward (right hand side) pressure waves.

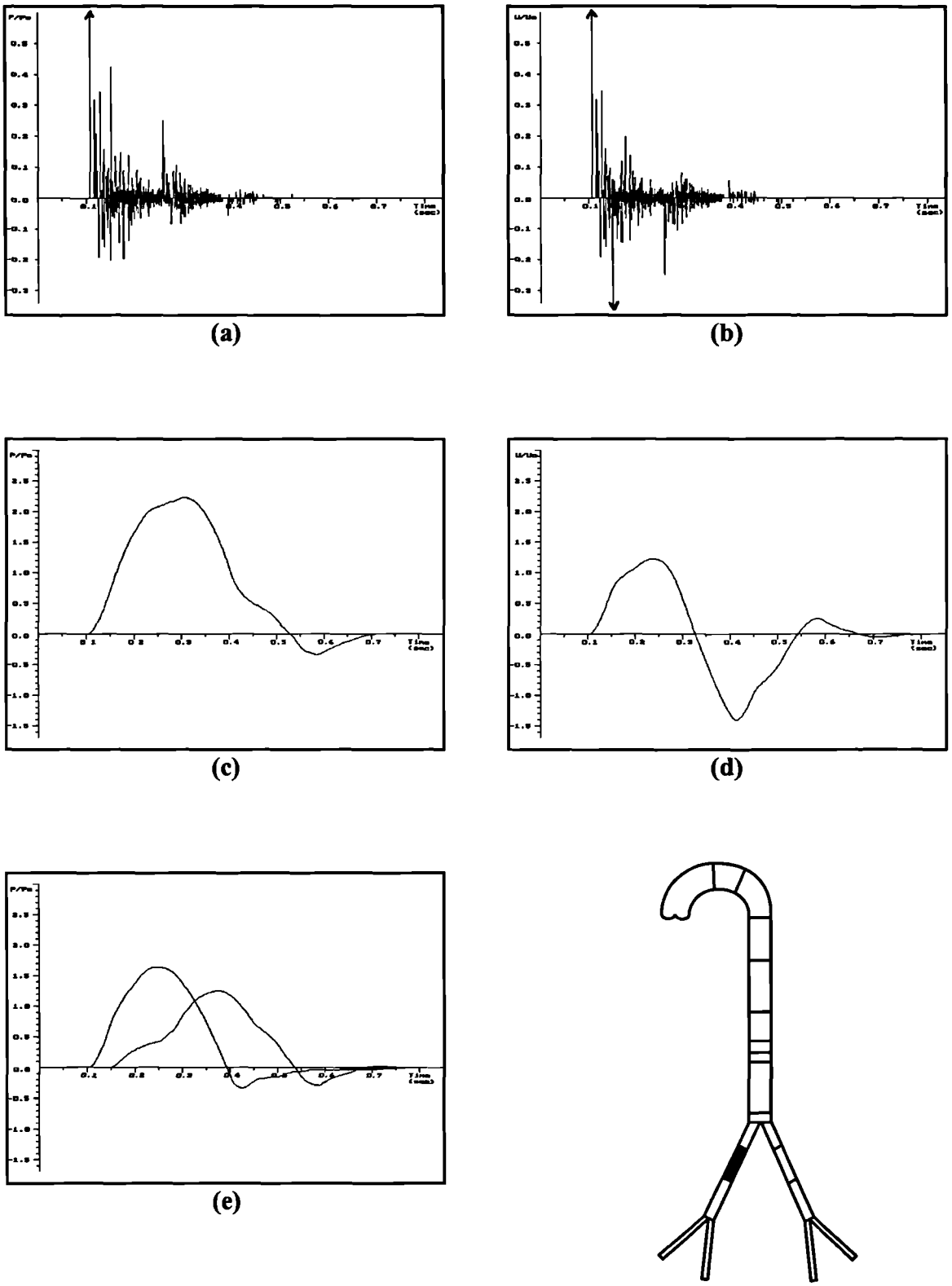


Figure 26: The right external iliac artery segment. (a) The transfer function for the pressure. (b) The transfer function for the velocity. (c) The pressure waveform. (d) The velocity waveform. (e) The forward (left hand side) and backward (right hand side) pressure waves.

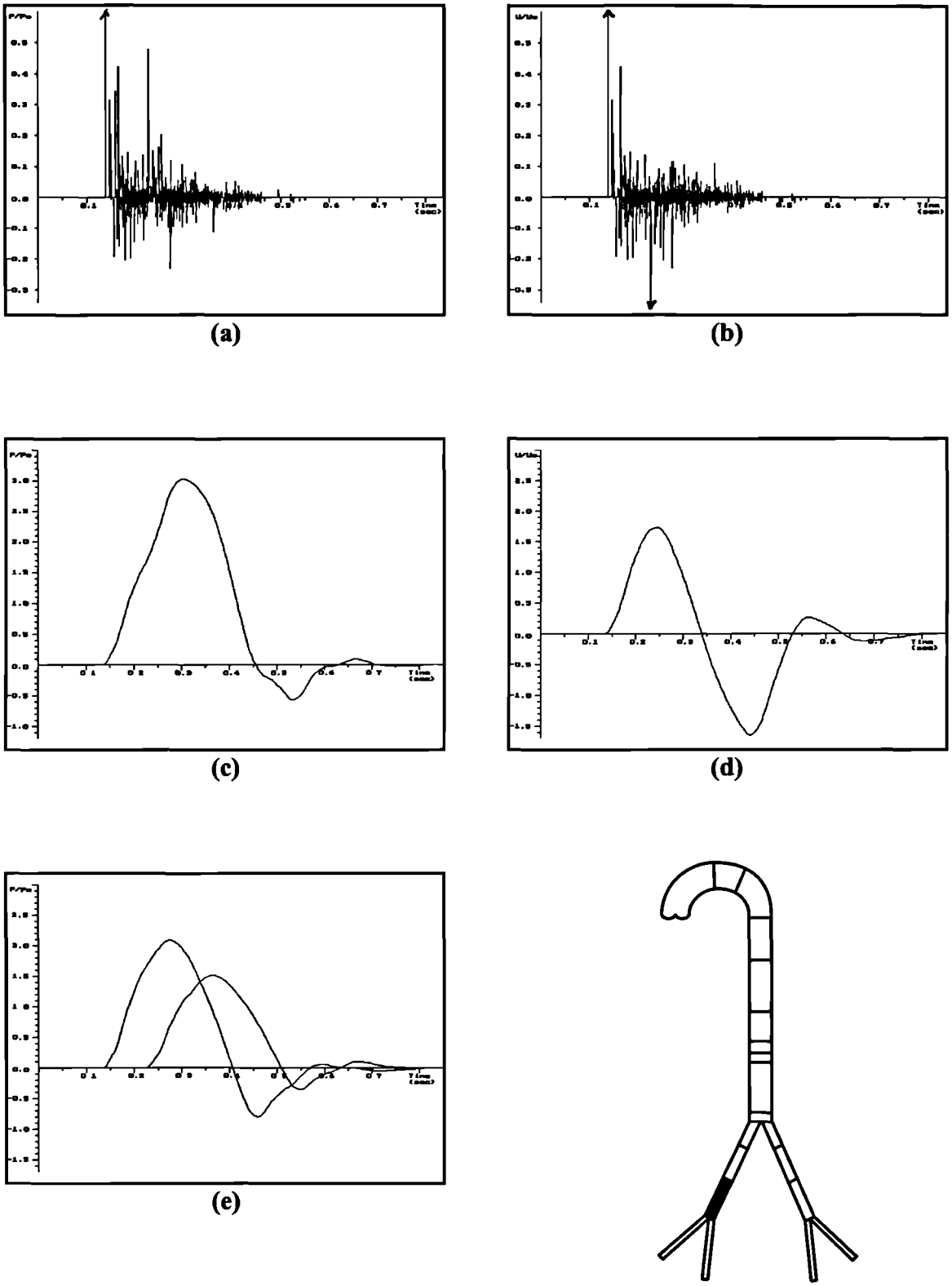
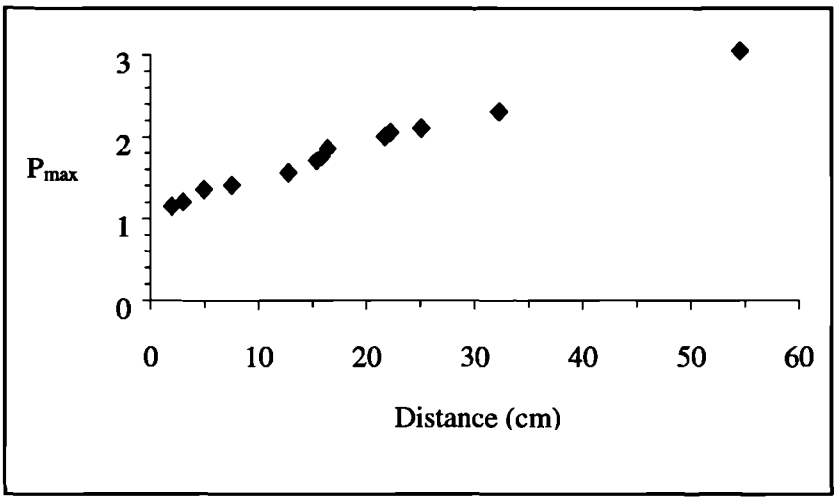
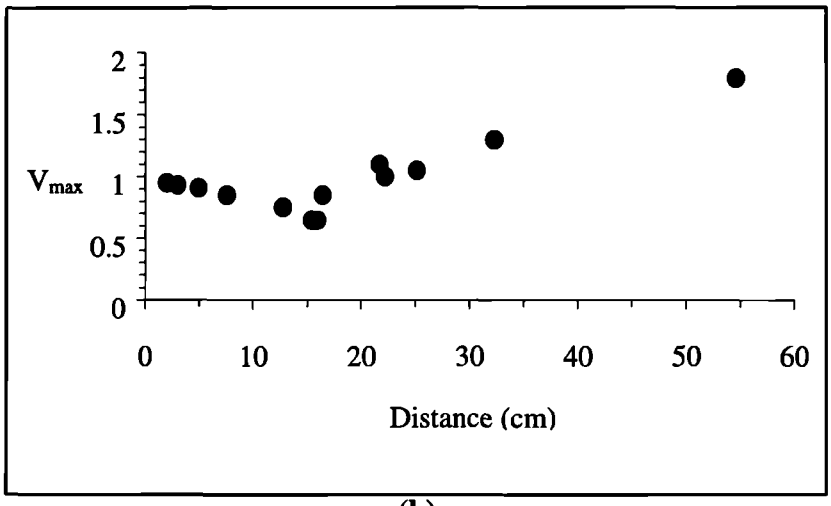


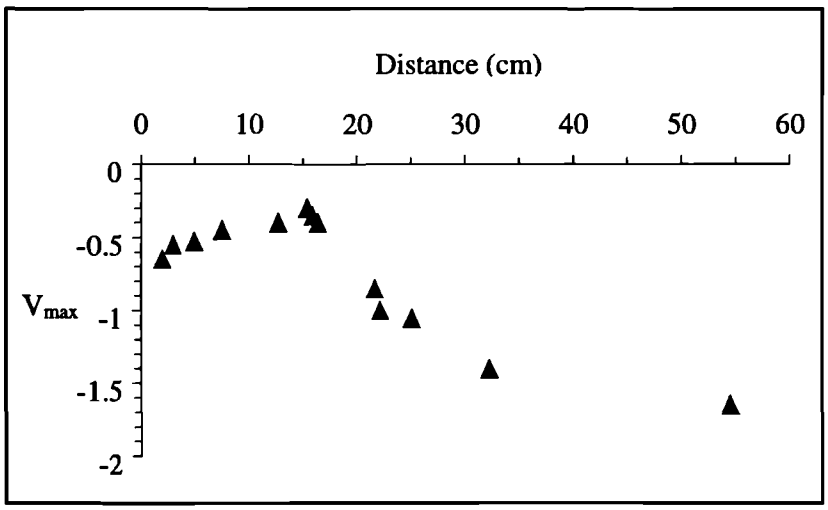
Figure 27: The right femoral artery segment. (a) The transfer function for the pressure. (b) The transfer function for the velocity. (c) The pressure waveform. (d) The velocity waveform. (e) The forward (left hand side) and backward (right hand side) pressure waves.



(a)



(b)



(c)

Figure 28: (a) The peak value of pressure, (b) the peak velocity, (c) and the peak reverse flow at the mid point of different arterial segments from the ascending aorta to the right femoral artery plotted against distance from the heart.

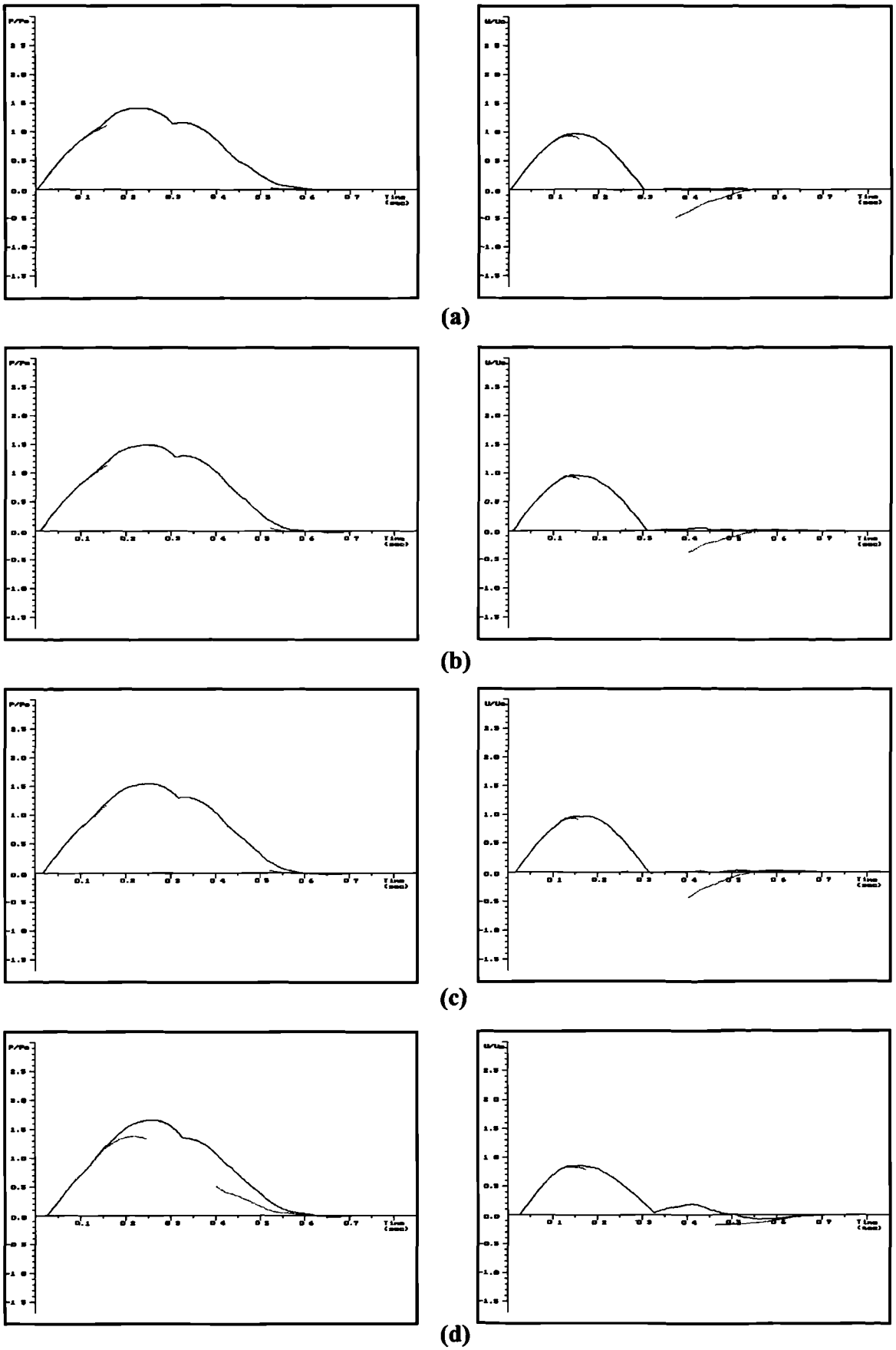
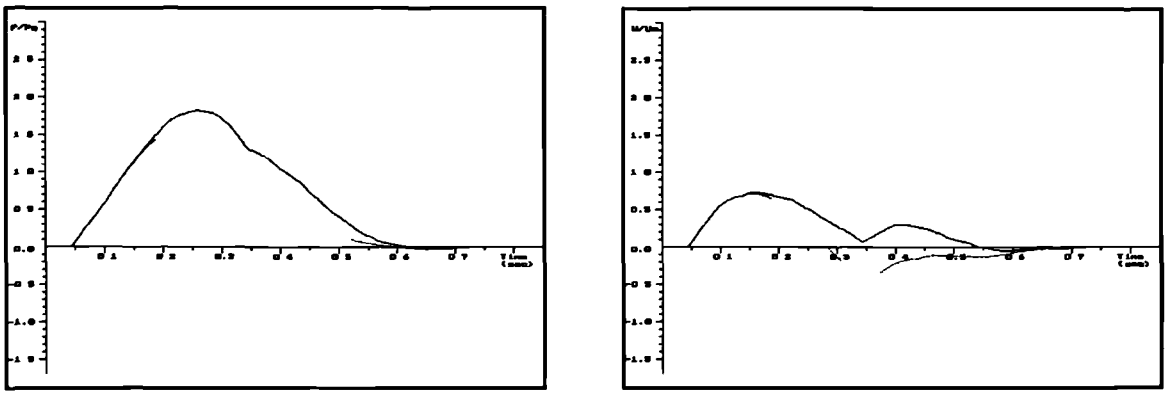
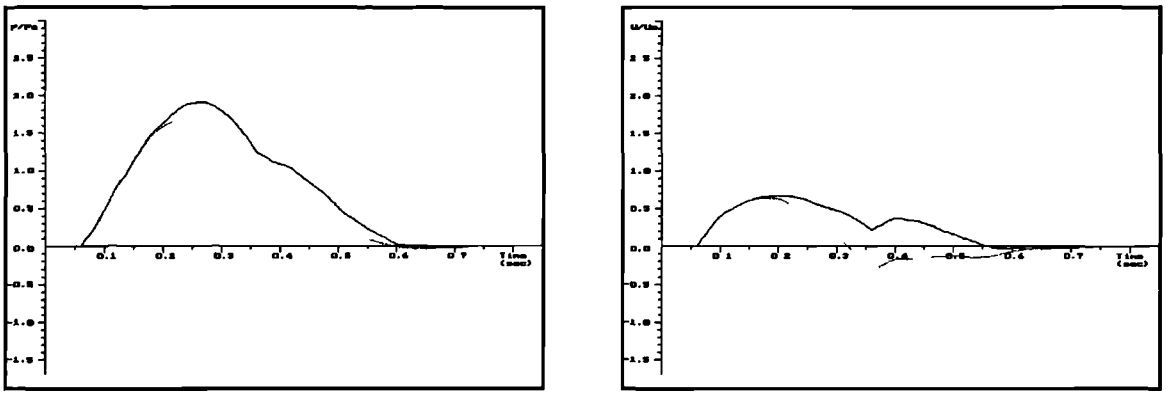


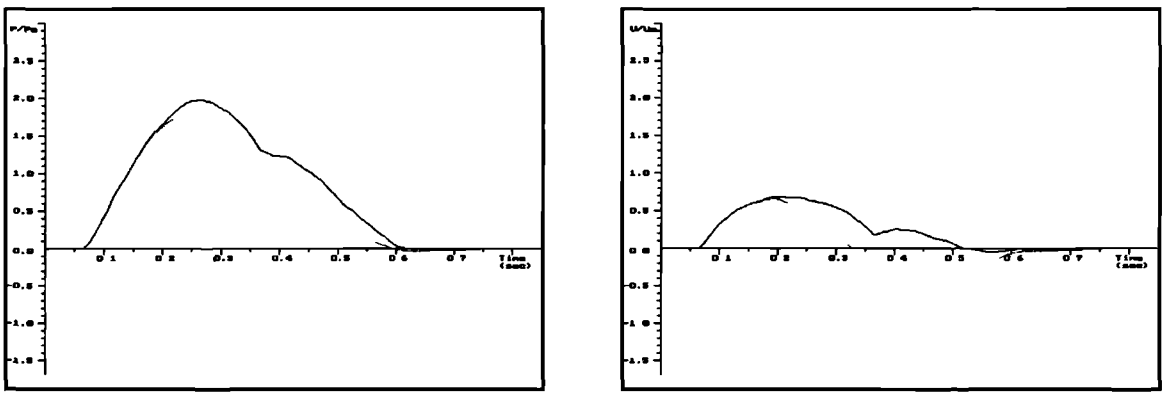
Figure 29: Results assuming the heart is a total reflector. (a) Pressure and velocity waveforms in the ascending aorta segment, 1. (b) The aortic arch I segment, 2. (c) The aortic arch II segment, 14. (d) The thoracic aorta I segment, 18. The graphs are compared with the control cases (the dotted line), where the heart is an absorber.



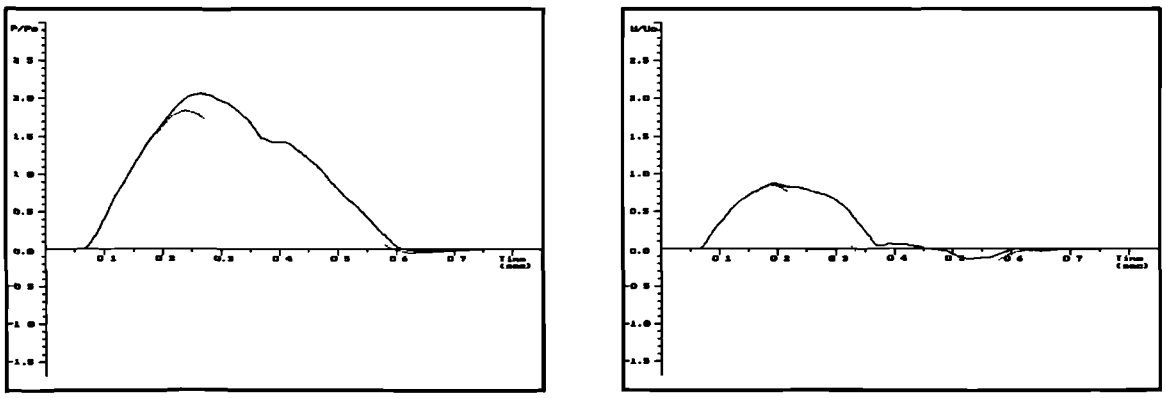
(e)



(f)

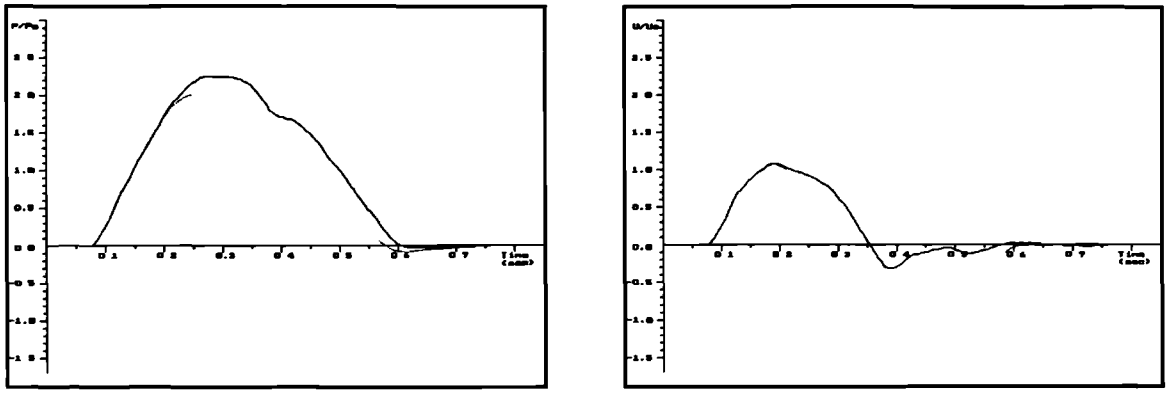


(g)

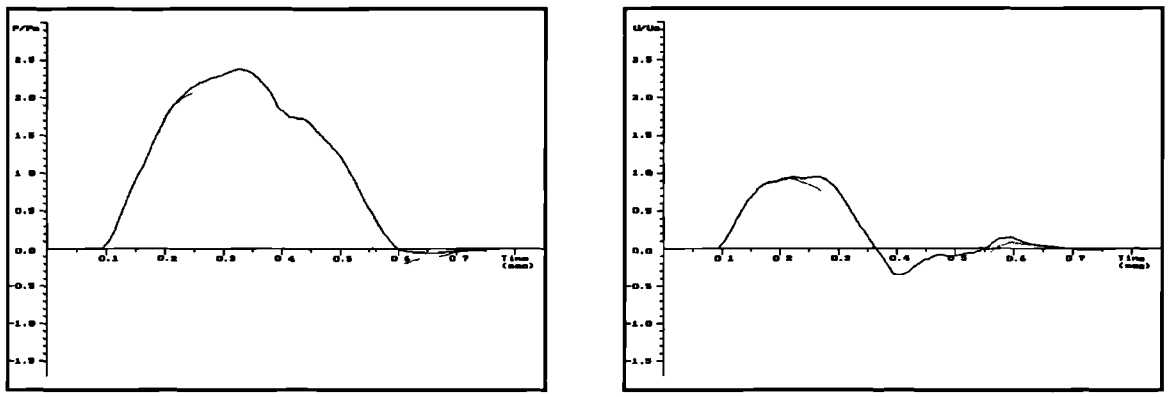


(h)

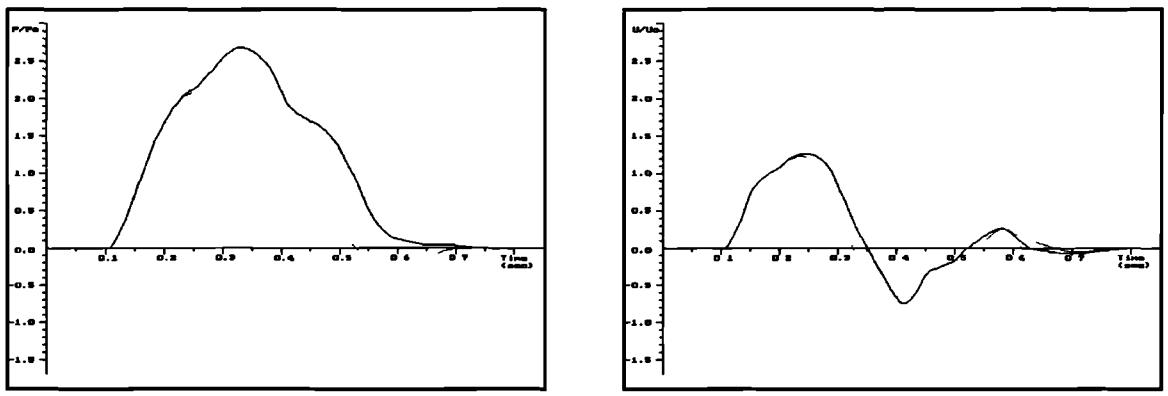
Figure 29 (cont.): (e) The thoracic aorta II segment, 27. (f) The abdominal aorta I segment, 28. (g) The abdominal II segment, 35. (h) The abdominal aorta III segment, 37.



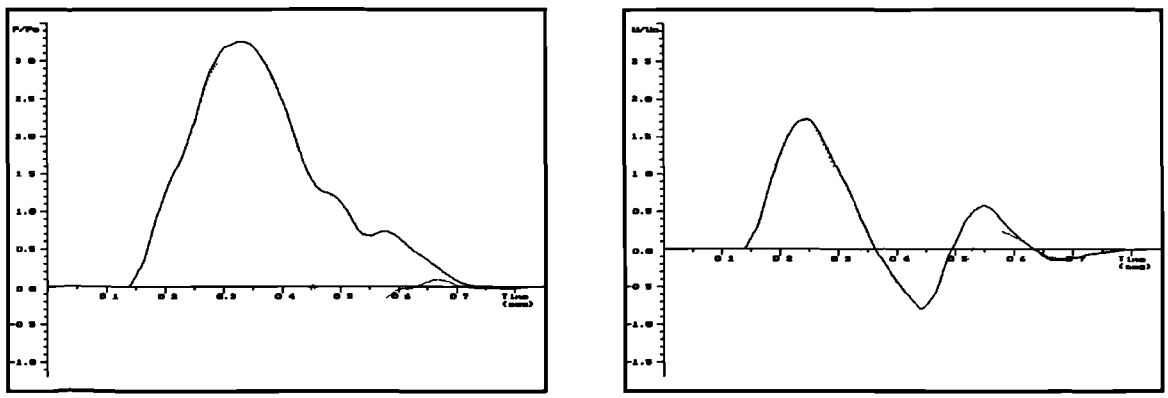
(i)



(j)

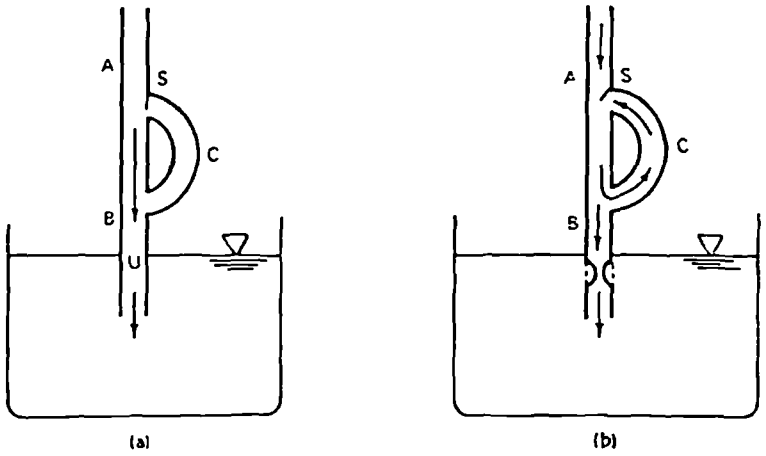


(k)

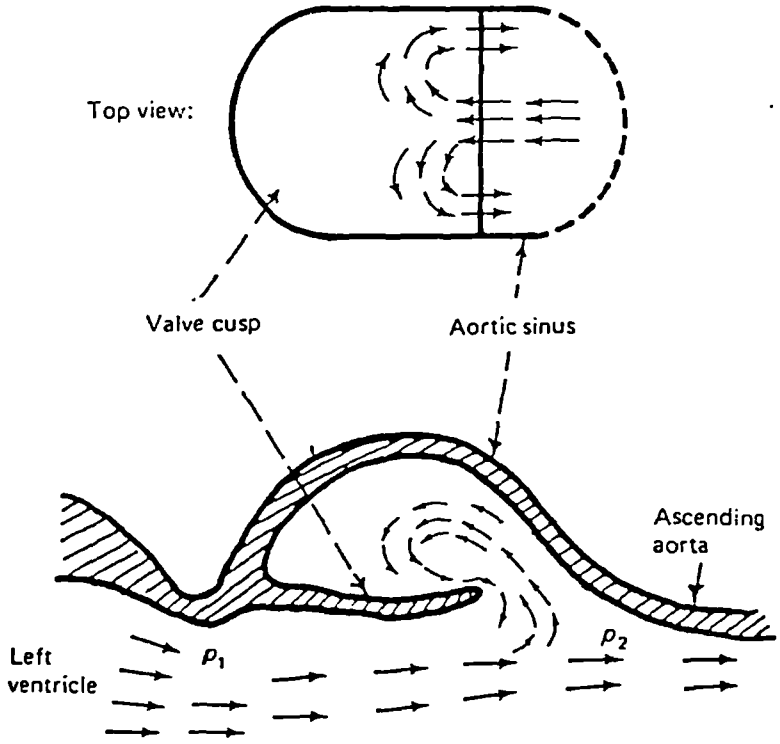


(l)

Figure 29 (cont.): (i) The abdominal aorta IV segment, 39. (j) The left common iliac artery, 42. (k) The left external iliac artery, 44. (l) The left femoral artery, 46.



(1)



(2)

Figure 30: Classic experiments on valve mechanics (1) Henderson and Johnson, (1912) studied flow in a tube containing a curved section with a valve at position S (a) When there was flow through the straight tube into the tank, there was little, if any, flow in the curved tube. (b) When flow was occluded at B, circulating fluid in the curved tube caused the valve to close against flow from A. (2) The flow field around the sinus of Valsalva. Part of the flow issuing out of the left ventricle will flow into the sinus of Valsalva. After peak systole, the flow starts decelerating which makes more flow goes in the sinus and helps the closure of the aortic valve. (Adopted from Fung, 1984)

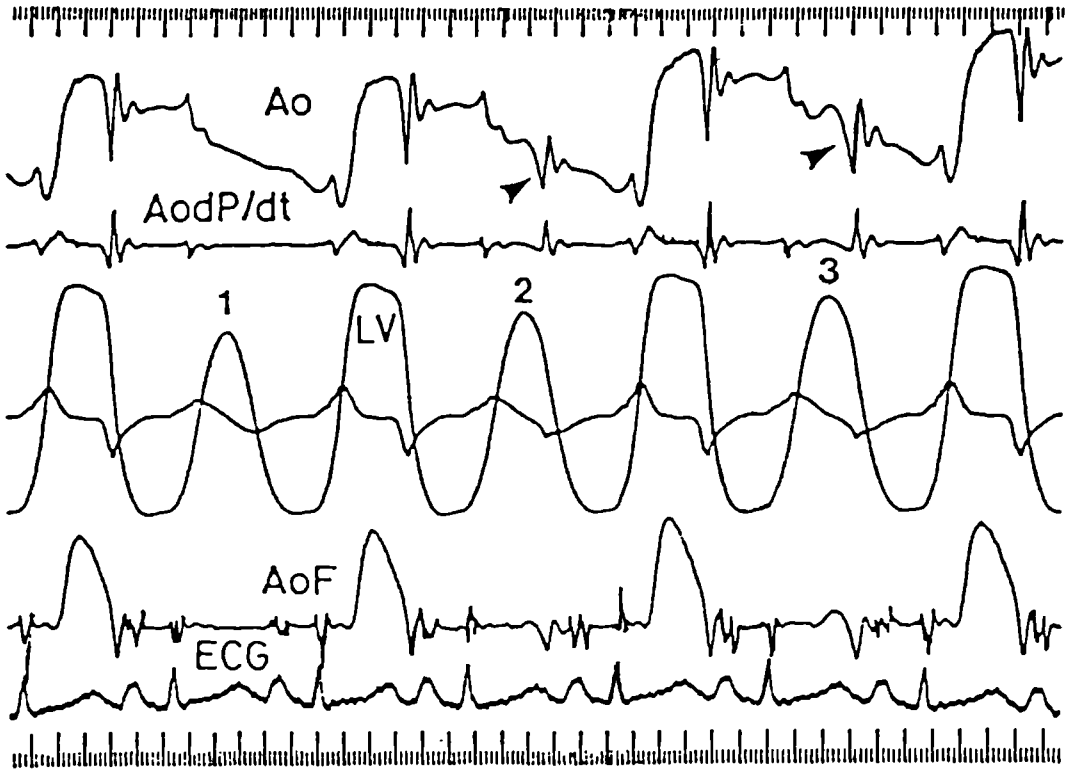
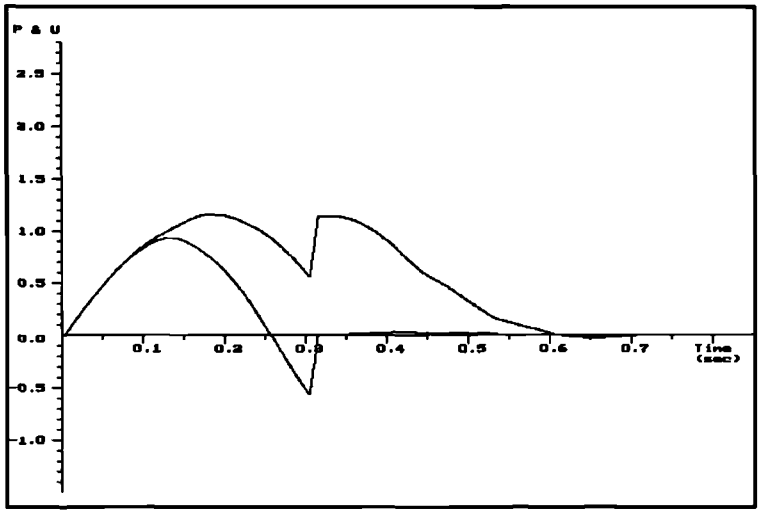
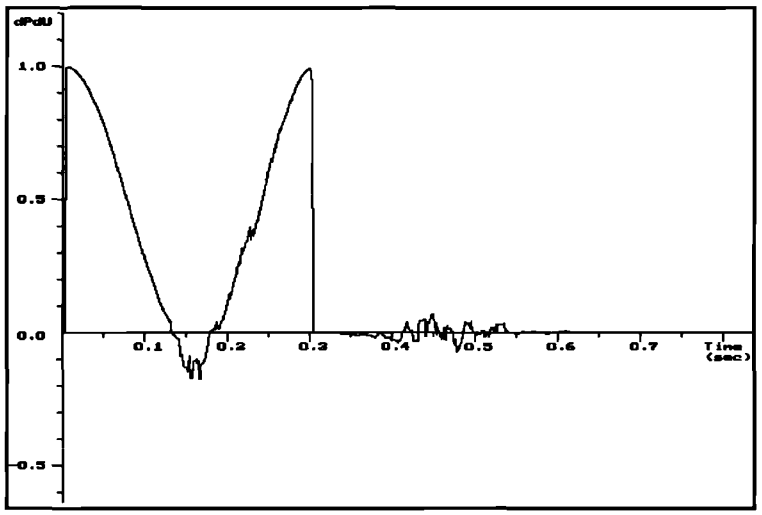


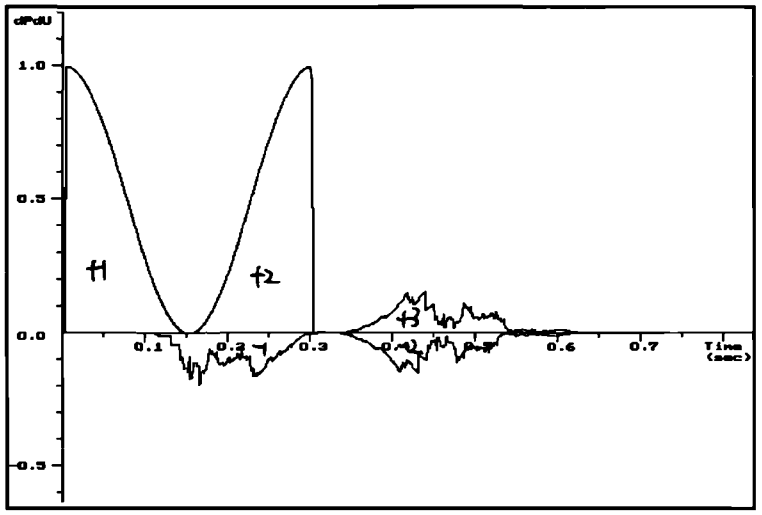
Figure 31: Pressure, flow and ECG from the experiments on dogs during the pulsus alternans. The weak beats 1, 2 and 3 are progressively larger in peak systolic pressure. Weak beats 2 and 3 result in incisura notches of the aortic pressure signal (arrows). Ao is the high fidelity aortic pressure signal; Ao dP/dt is the time derivative of aortic pressure; LV is the left ventricular pressure; AoF is the proximal aortic blood flow; ECG, electrocardiogram. (from Smith and Craige (1986)).



(a)



(b)



(c)

Figure 32: Results of calculation assuming the heart is an absorber when the valve is open (before 0.3 seconds) and a total reflector when the valve is closed. (a) Pressure (upper) and velocity (lower) waveforms in the ascending aorta. The waveform is normalized by the input. (b) The wave intensity analysis of the waveform. (c) Separated wave intensity, $dPdU^+$ (>0) and $dPdU^-$ (<0).

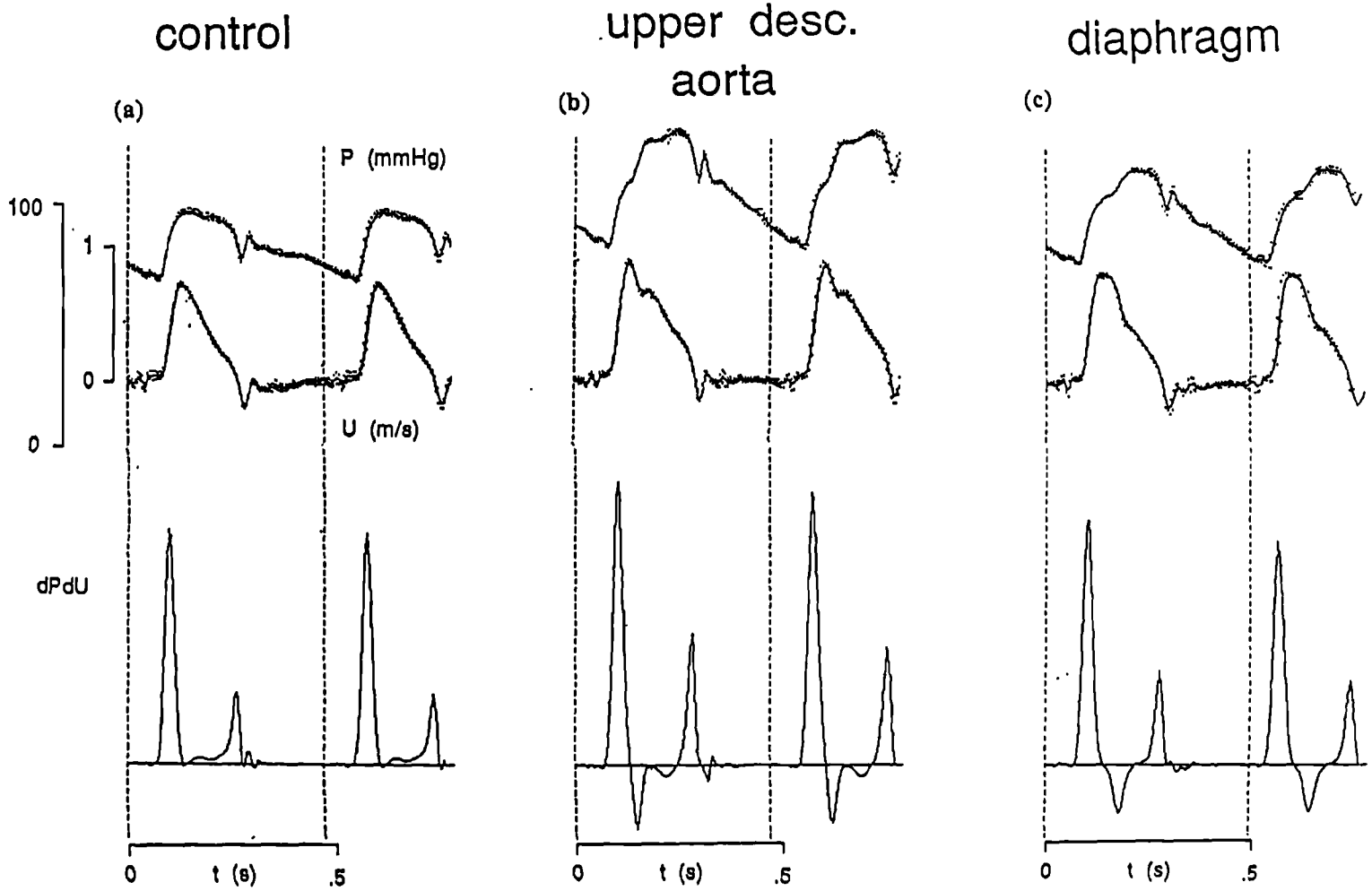


Figure 33 : (Upper) The pressure and velocity waveforms measured in the ascending aorta of the dog when the aorta is totally occluded by a balloon catheter at different sites from (b) the upper descending aorta, (c) diaphragm, (d) the end of the abdominal aorta (the next page) to (e) one of the iliac arteries. The dots on the measured pressure and velocity waveforms are one standard deviation of the ensemble averaged data. The vertical dotted line denotes the averaged interval between QRS complexes of ECG (from Ven der Bos et al., 1974). **(Lower)** The wave intensity analysed from the measurement (from Davies 1994).

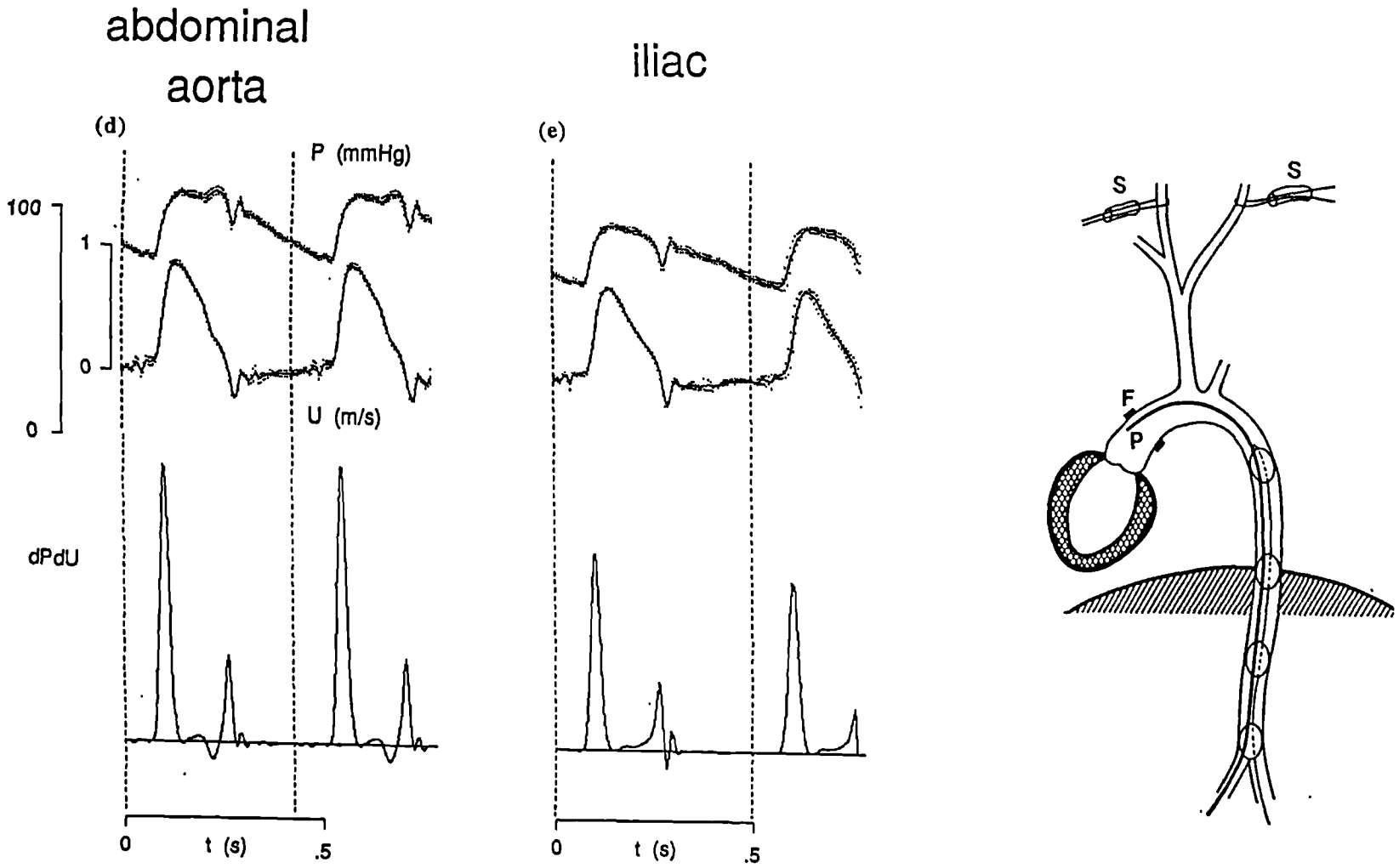


Figure 33 (cont.): The right hand side graph is a diagrammatic representation of the sites of occlusion in the dog aorta (Westerhof *et al.*, 1972). F: the position of cuff-type flow transducer. P: catheter-mounted pressure transducer. S: snares around carotid arteries.

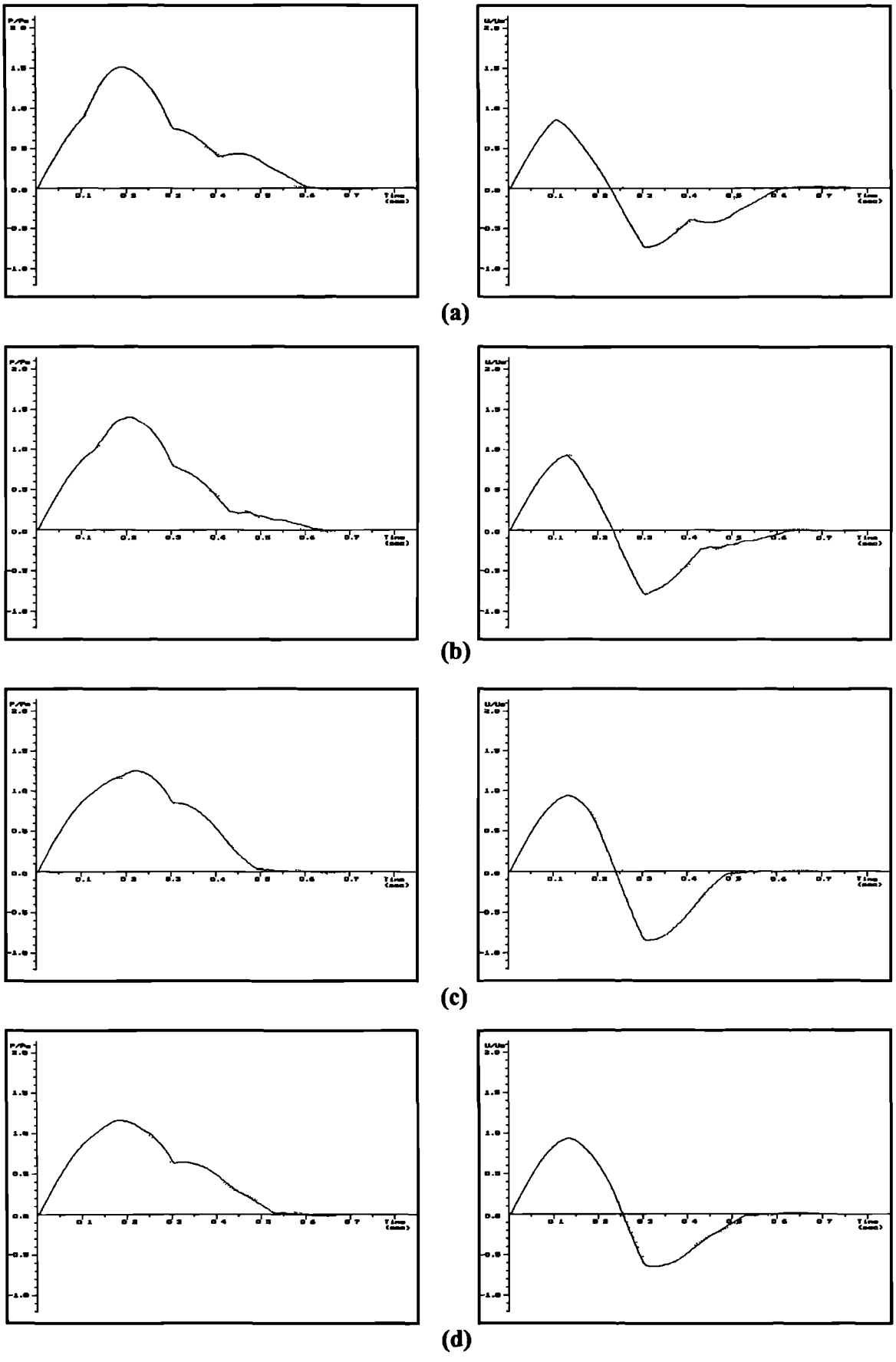


Figure 34: The waveforms in the ascending aorta when the occlusion is at: (a) the thoracic aorta I segment, 18, (b) the abdominal aorta I segment, 28, (c) the abdominal aorta V segment, 41, and (d) the right common iliac artery, 43. All the waveforms are compared with the control case (the dotted line), where there is no occlusion.

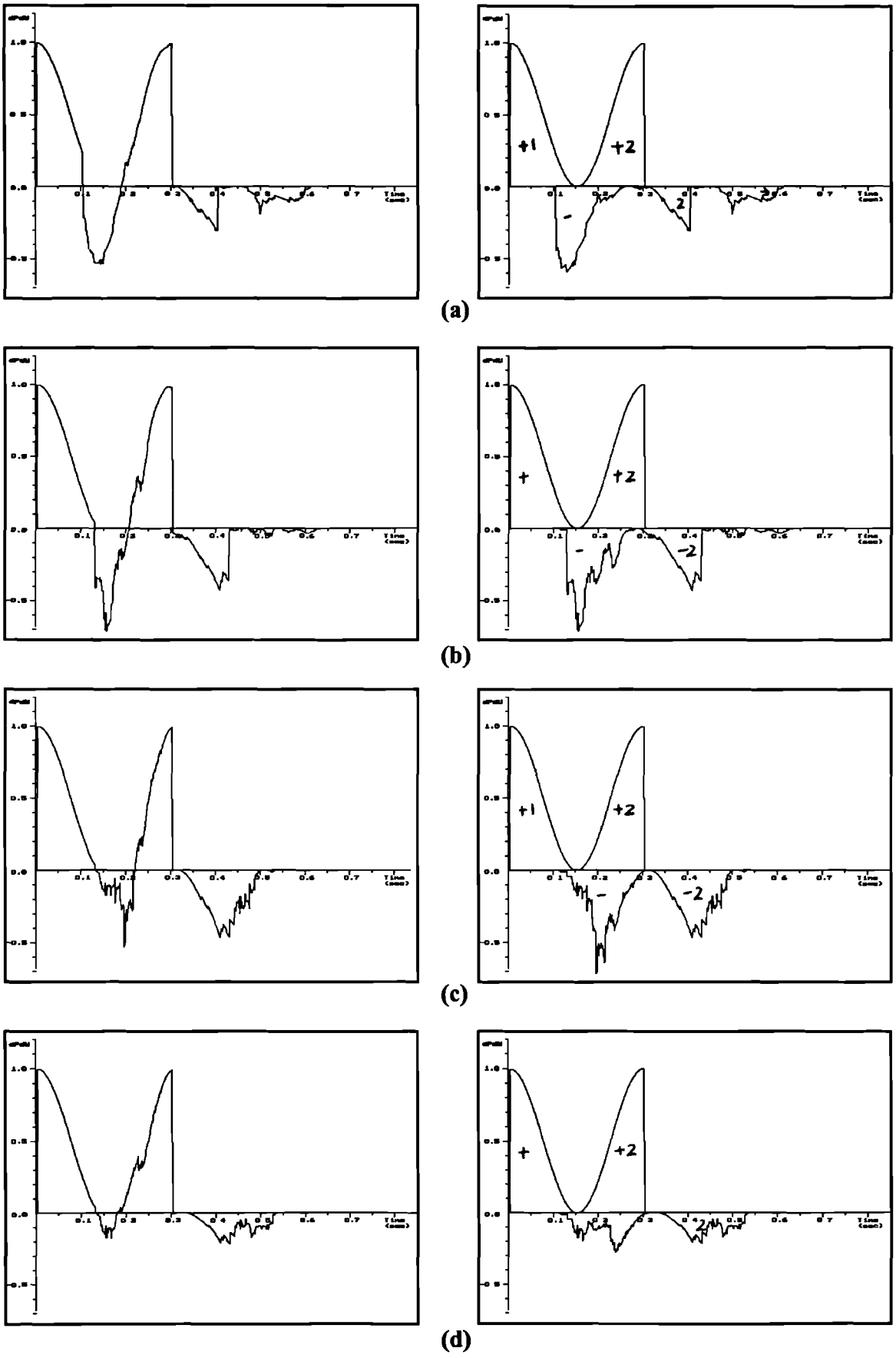


Figure 35: The wave intensity analysis of the waveforms in Figure 34. The left panel is the net wave intensity *dPdU* and the right panel is the separated wave intensity $dPdU^+$ (>0) and $dPdU^-$ (<0). The occlusion is in: (a) the thoracic aorta I segment, 18, (b) the abdominal aorta I segment, 28, (c) the abdominal aorta V segment, 41, and (d) the right common iliac artery, 43.

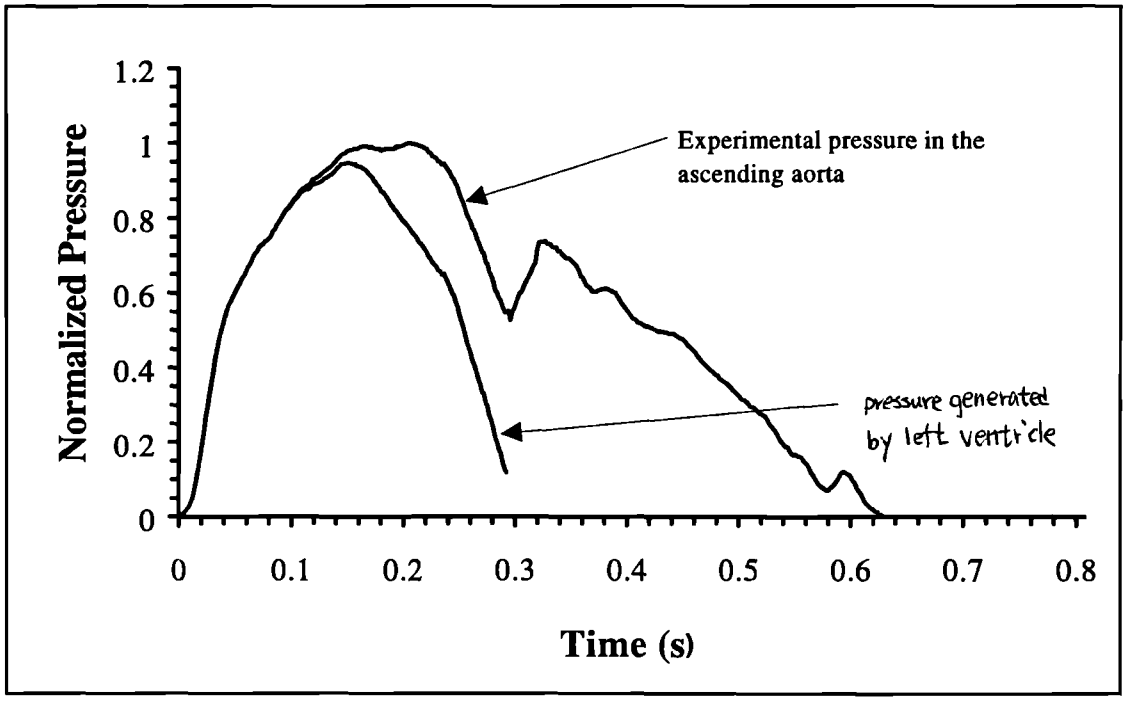


Figure 36: The left ventricular pressure as calculated from the transfer function and the experimentally measured pressure in the ascending aorta.

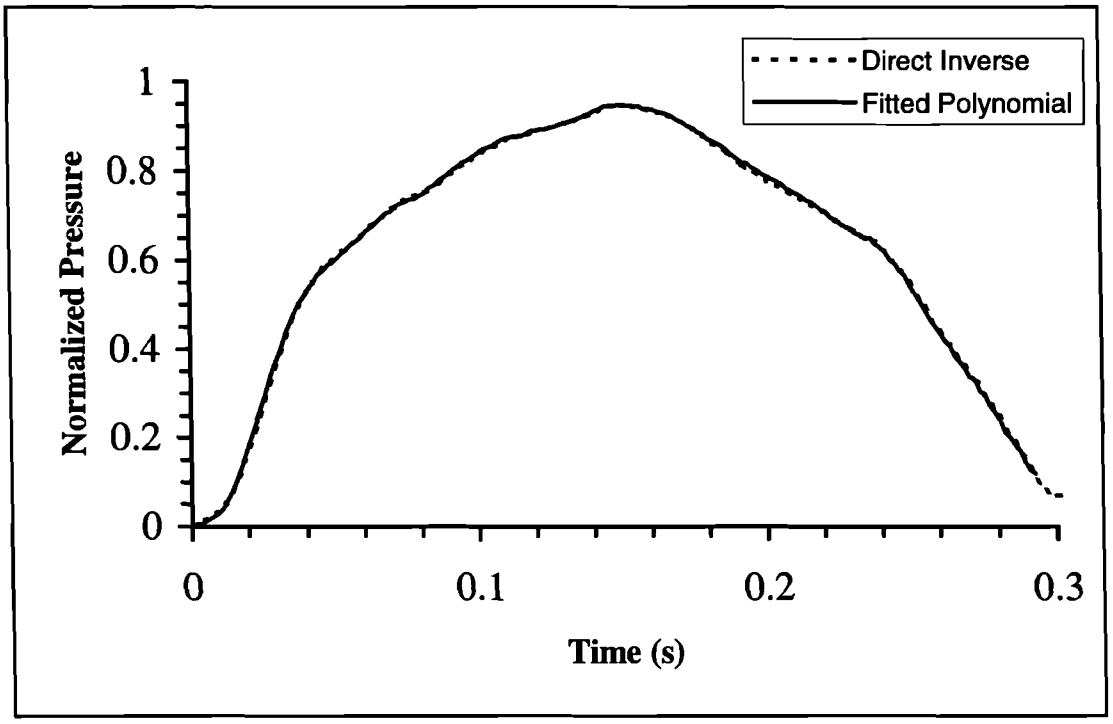
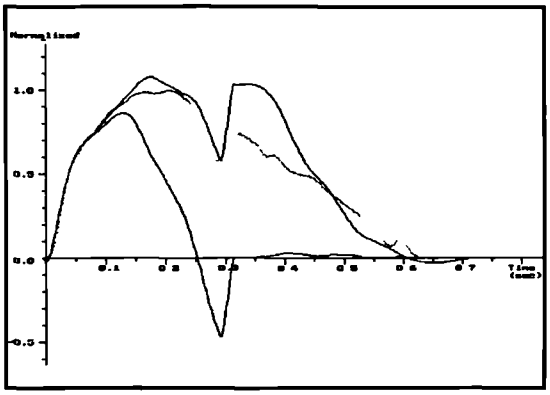
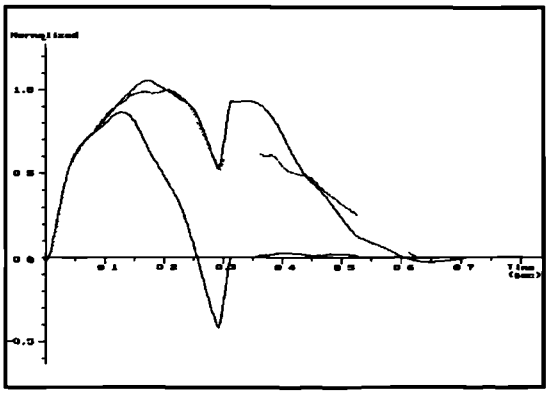


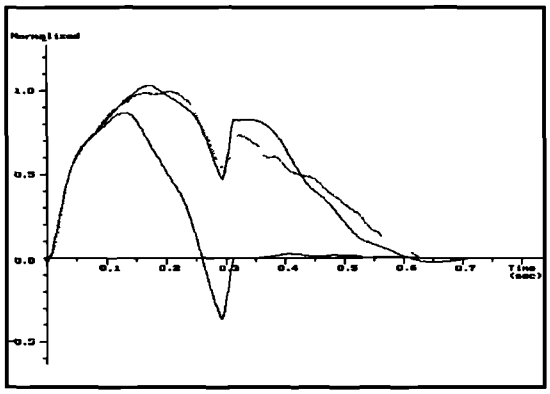
Figure 37: The left ventricular pressure predicted by the direct inverse method and the tenth order polynomial fitted to the curve which was used in calculations.



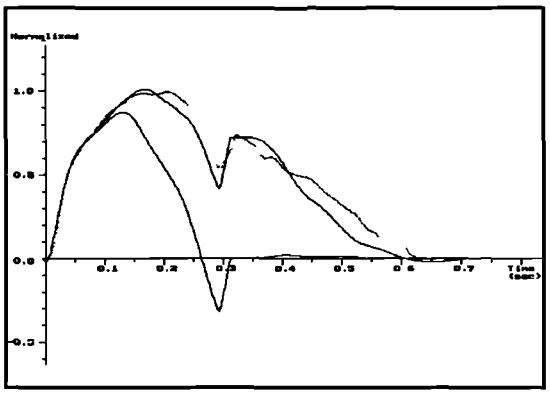
(a) 100%



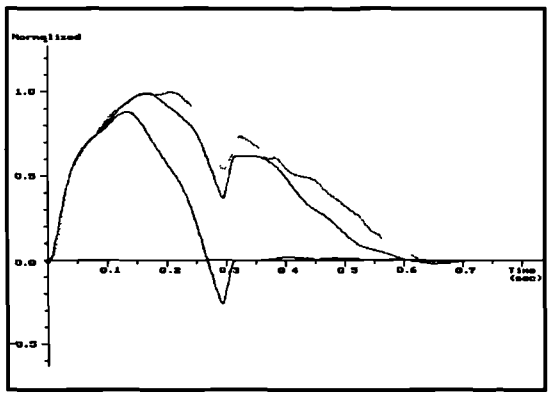
(b) 90%



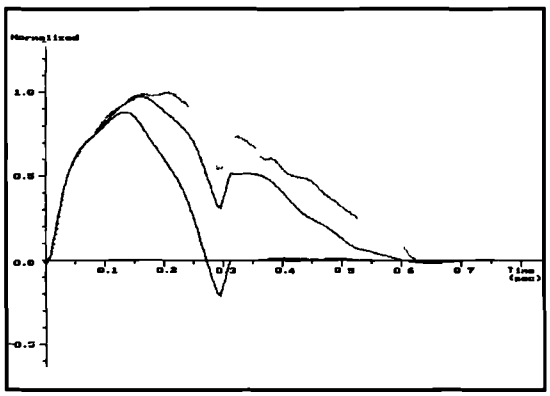
(c) 80%



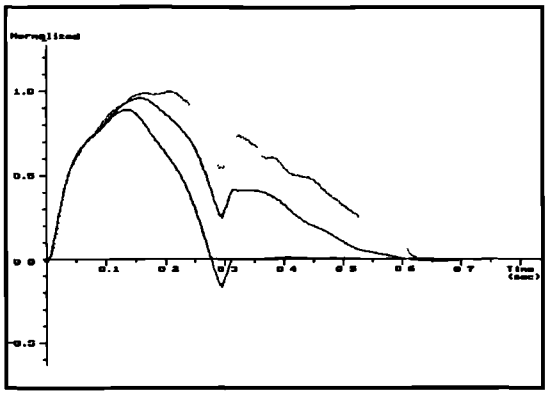
(d) 70%



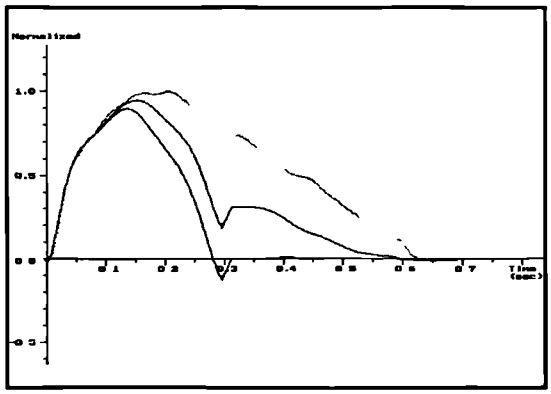
(e) 60%



(f) 50%

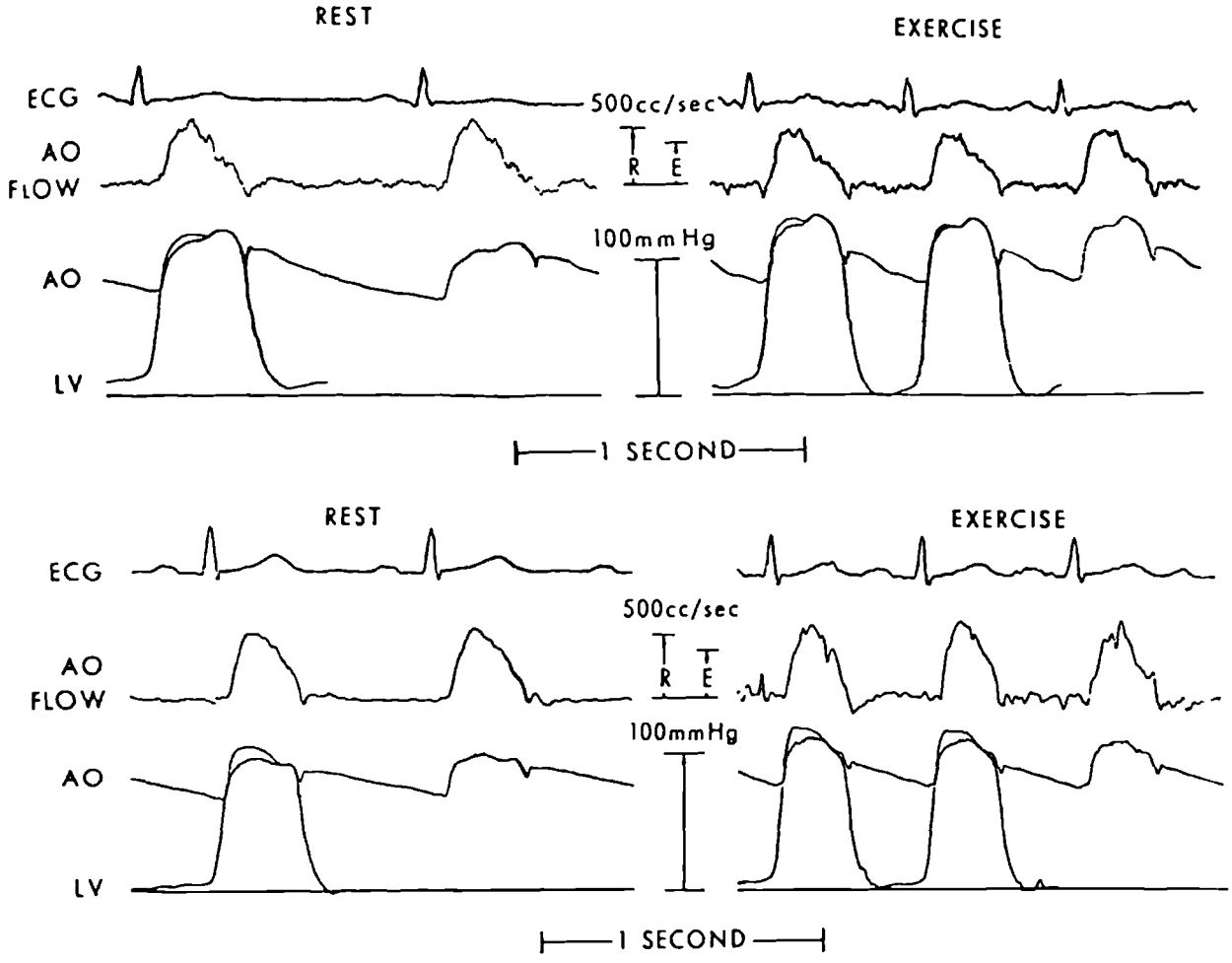


(g) 40%



(h) 30%

Figure 38: The calculated pressure (upper solid line) and velocity (lower solid line) waveform in the ascending aorta when the terminal reflection coefficients are reduced from (a) 100% (b) 90% (c) 80% (d) 70% (e) 60% (f) 50% (e) 40% and (f) 30%. The dotted line represents the experimental pressure.



(a)

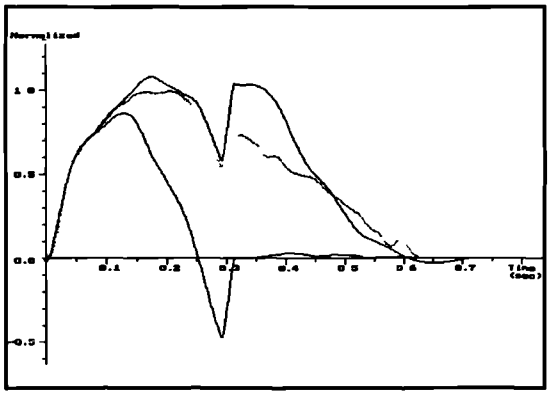
Subject	R_p* Rest	R_p* Ex	Z_c* Rest	Z_c* Ex
A3	1025	571	47	45
A5	1059	695	53	61
A6	1182	89[illegible]	39	43
A7	1333	632	3[illegible]	26
Mean ± SE $n = 4$	1150 ± 70	699 ± 71†	44 ± 4	44 ± 7
B1	1616	1051	71	68
B3	1036	579	31	31
B4	1075	710	31	36
B6	1104	740	65	52
B7	1150	676	52	43
Mean ± SE $n = 5$	1196 ± 107	751 ± 80†	50 ± 8	46 ± 7
C1	1093	622	30	29
C2	849	600	58	45
C3	1263	633	39	42
C4	1059	843	62	60
Mean ± SE $n = 4$	1066 ± 85	674 ± 56†	47 ± 8	44 ± 6
Total mean ± SE $n = 13$	1142 ± 51	712 ± 39†	47 ± 4	45 ± 4

* All impedance values in dyne sec/cm^5

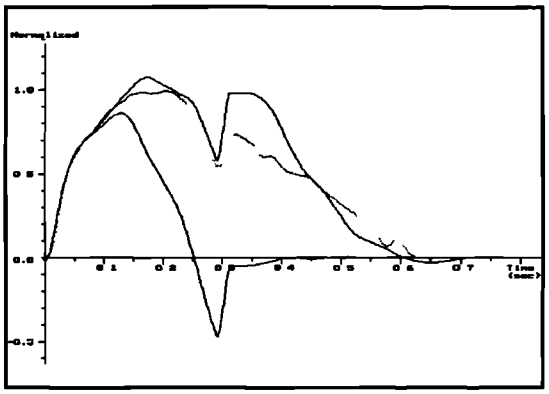
† $P < 0.05$ Analysis of variance between rest and exercise with Scheffe's test (Scheffe, 1953)

(b)

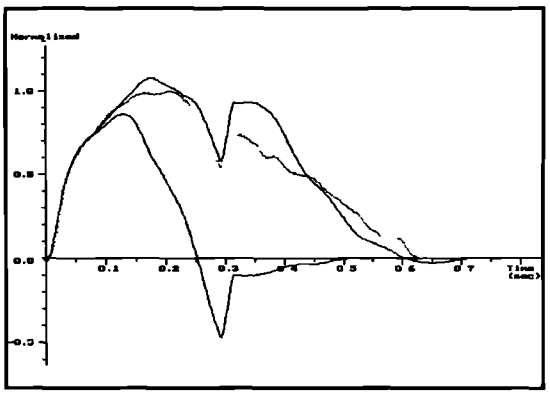
Figure 39: (a) The aortic pressure (Ao) and flow waveform (Ao flow) measured in the ascending aorta of man at rest and during exercise. (b) The data for the terminal resistance (Rp) and characteristic impedance (Zc) at rest and during exercise (from Murgo et al., 1981). The changes of the reflection coefficient of the periphery can be calculated from Eq. (2.31).



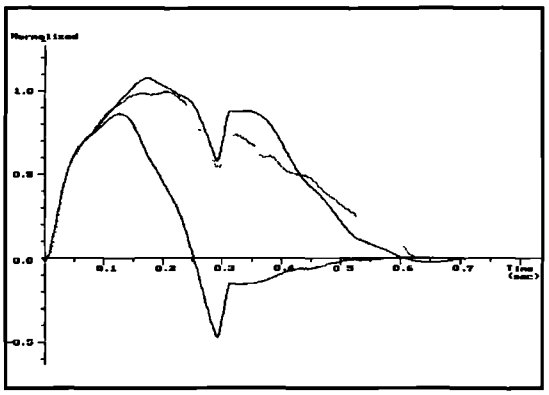
(a) R=1.0



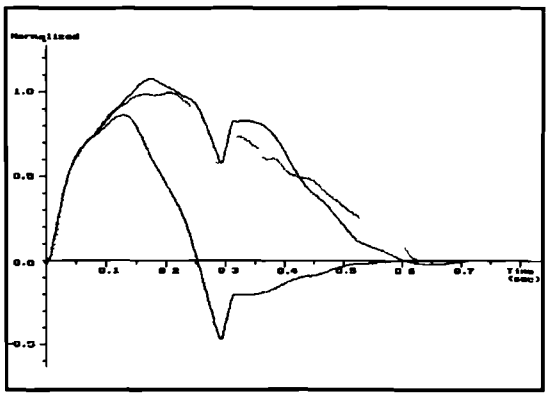
(b) R=0.9



(c) R=0.8



(d) R=0.7



(e) R=0.6

Figure 40: Results of calculation for the ascending aorta when the coronary circulation is considered, so that the reflection coefficient of the heart may not be that of a total reflector, R=1, after the valve closed. The calculated pressure (upper solid line) and velocity (lower solid line) waveforms are shown when the reflection of the heart is (a) R=1.0 (b) R=0.9 (c) R=0.8 (d) R=0.7 (e) R=0.6. The dotted line represents the experimental pressure.

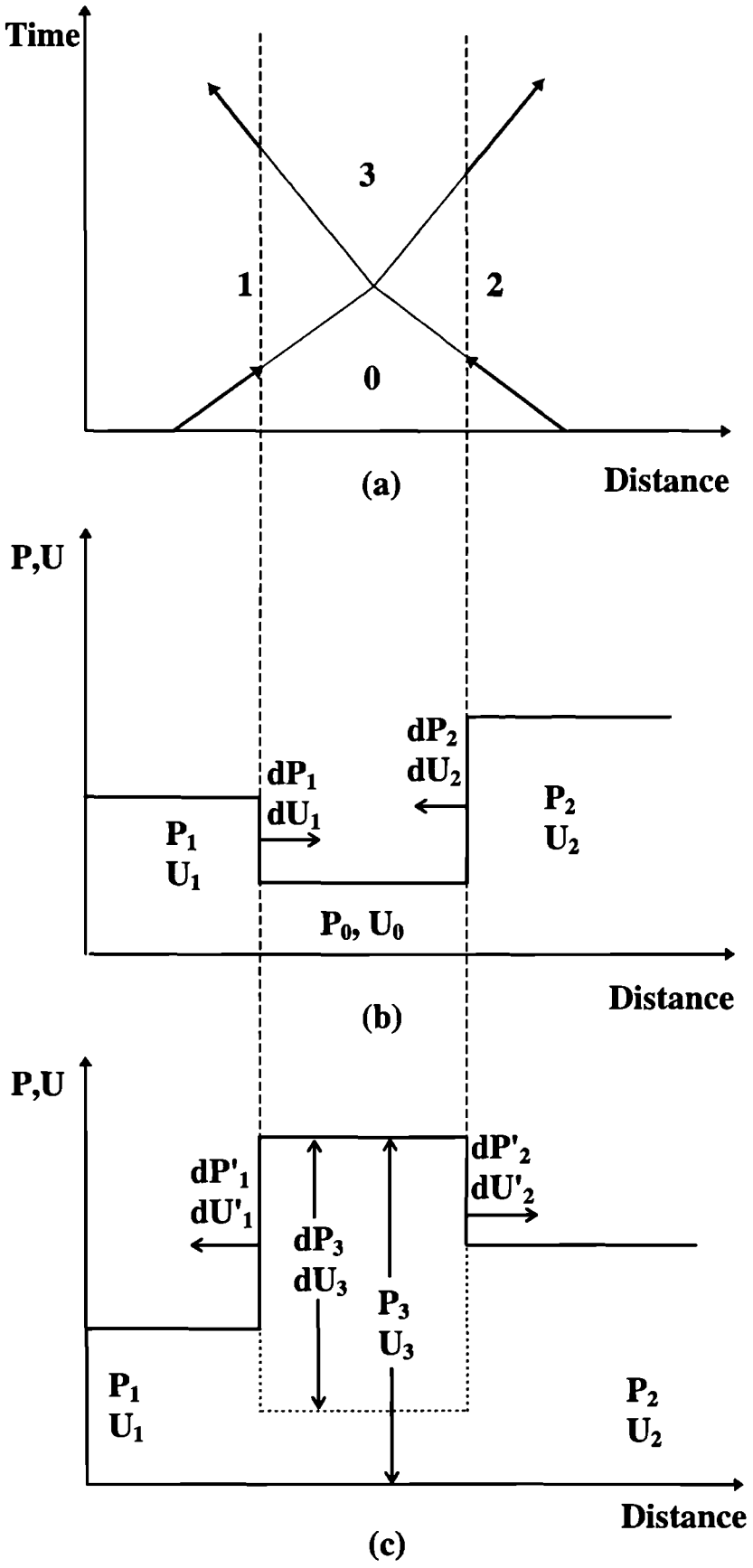


Figure 41: A diagrammatic representation of two wavefronts intersecting. (a) distance and time of two wavefronts (b) the properties of the two wavefronts before intersection (c) the properties of the two wavefronts after the intersection.

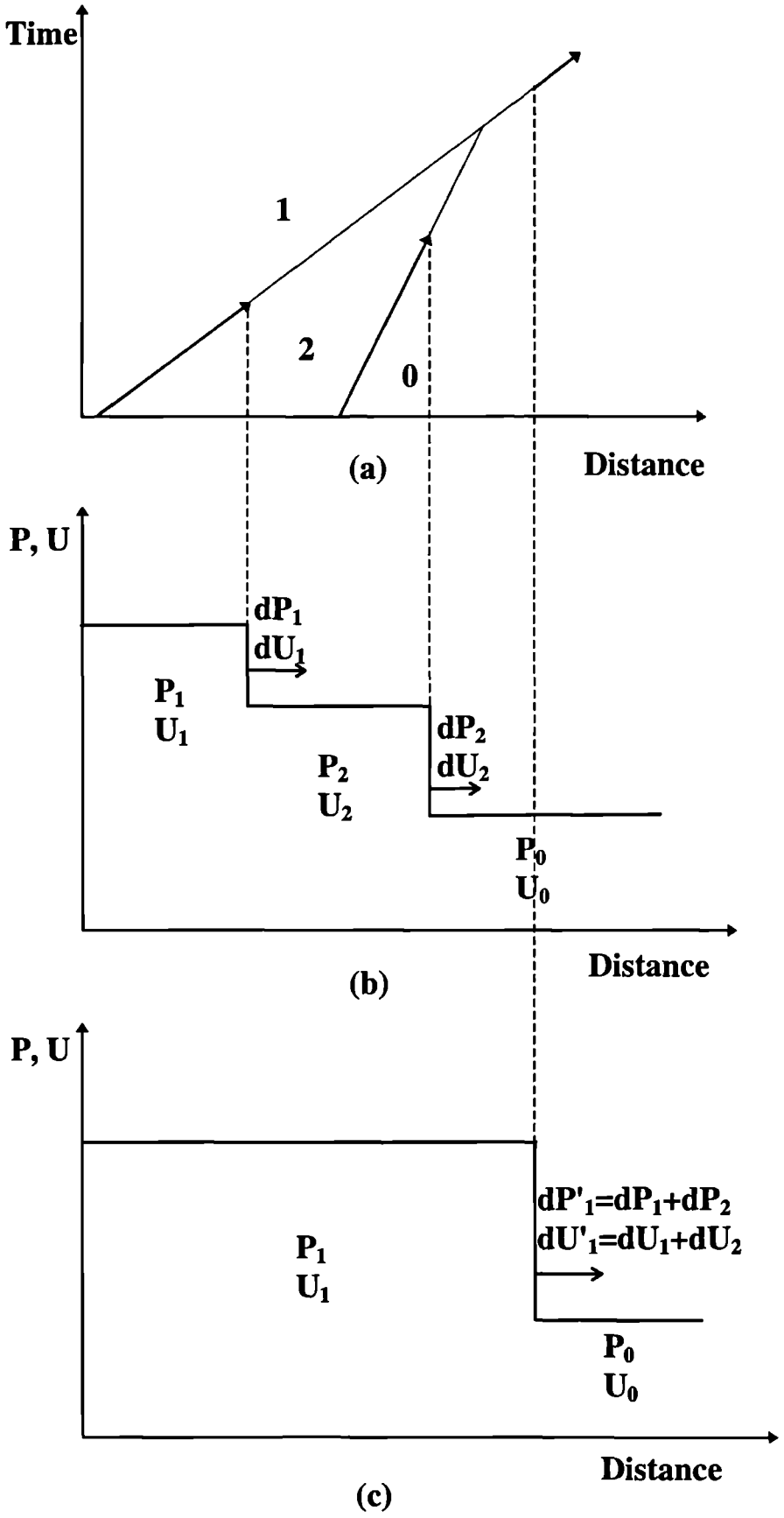


Figure 42: A diagramatic representation of one wavefront catching another. (a) distance and time of the two wavefronts (b) the properties of the two wavefronts before catching up (c) the properties of the wavefront after the intersection.

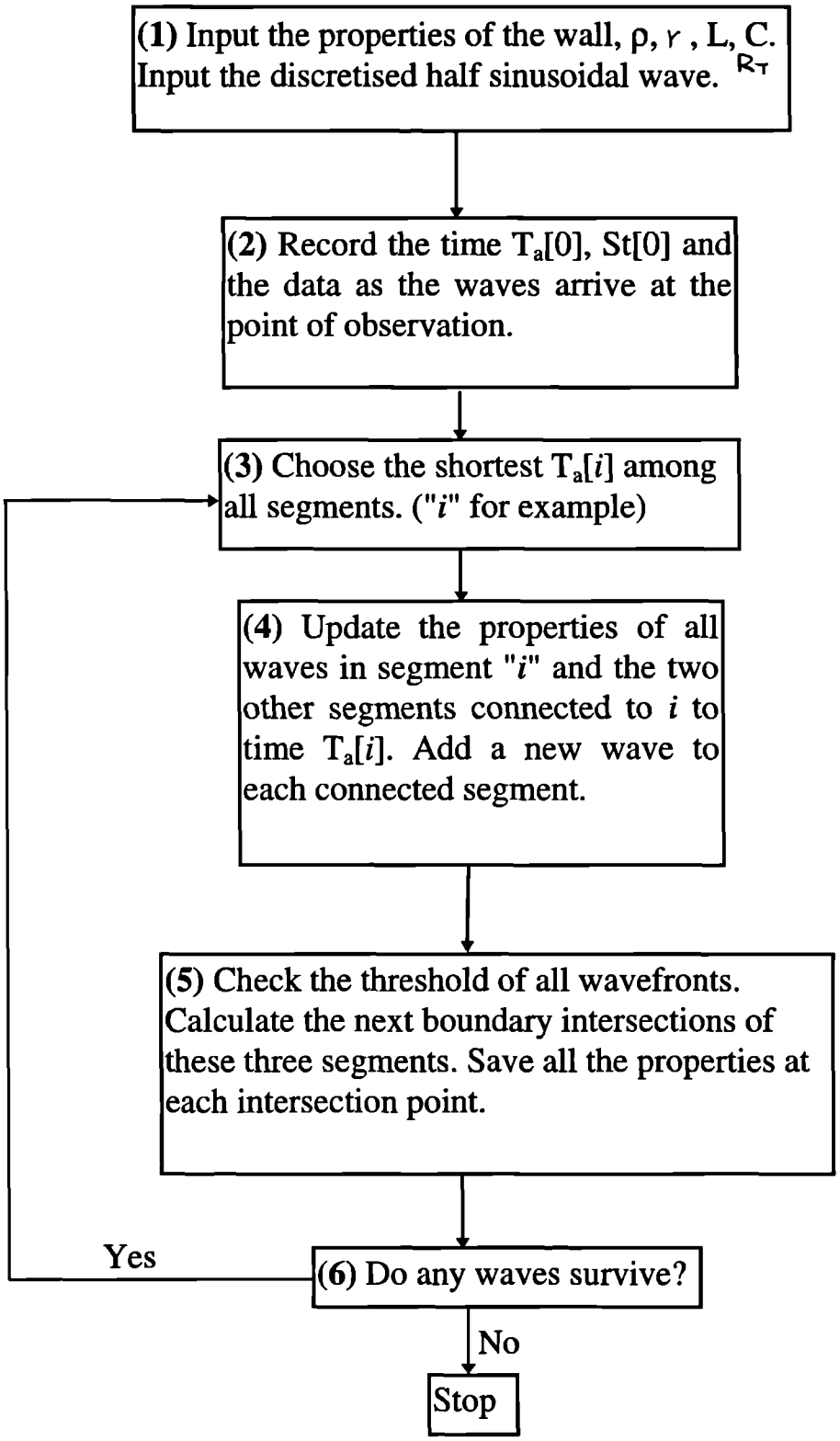


Figure 43 (a) : The flowchart of the nonlinear program.

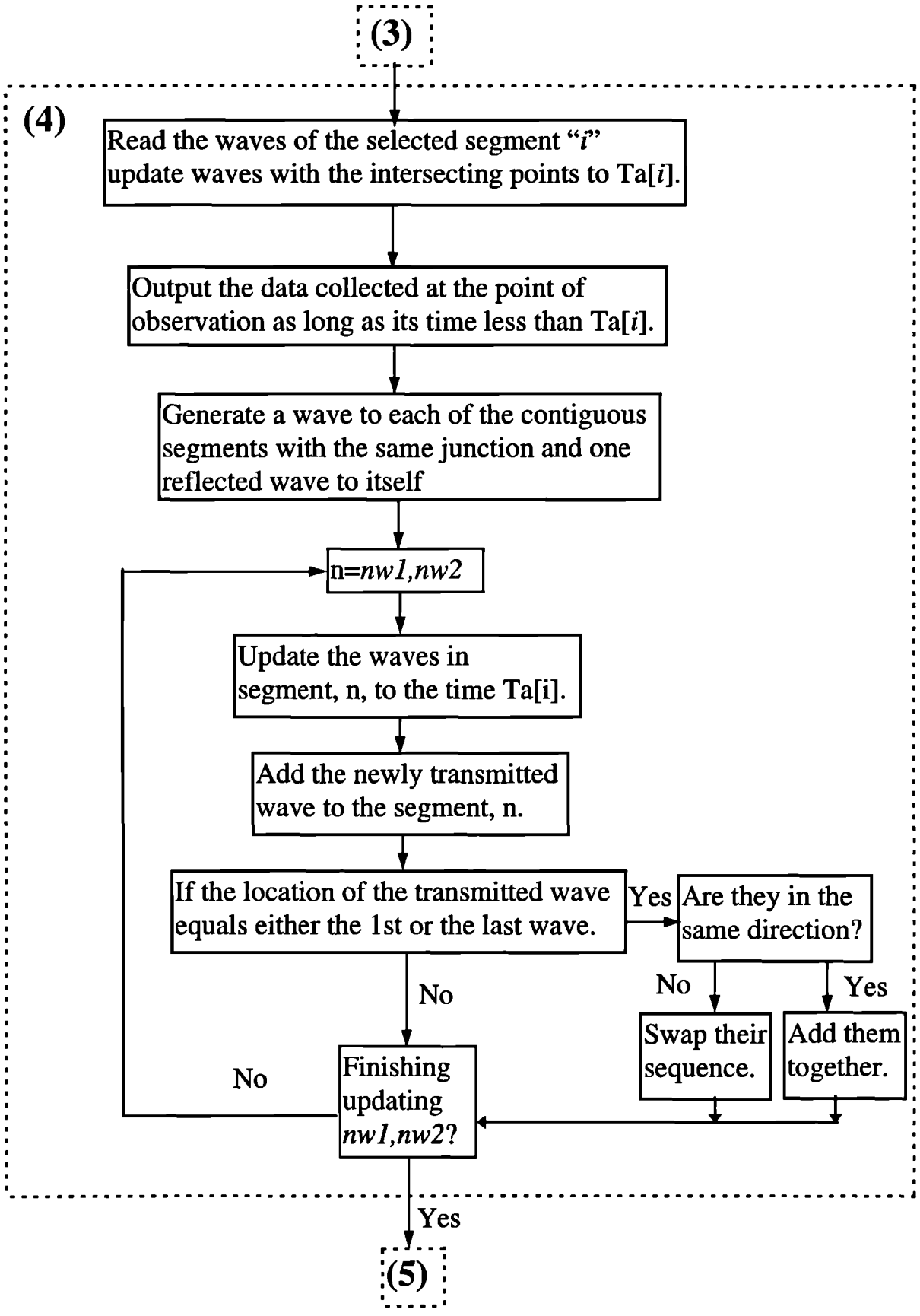


Figure 43 (b): The structure of the step (4) in (a).

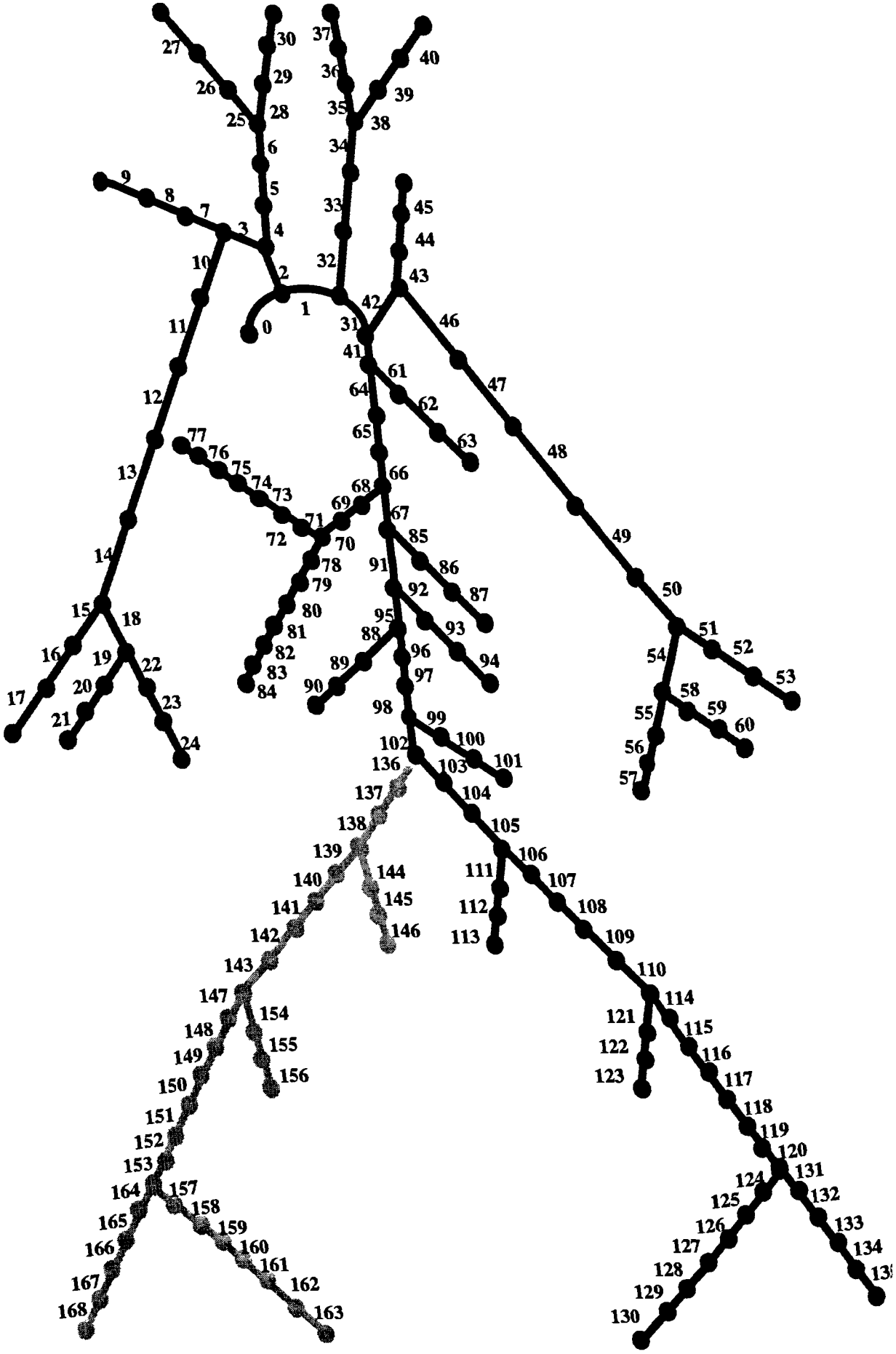


Figure 44: The arterial tree for the nonlinear model.

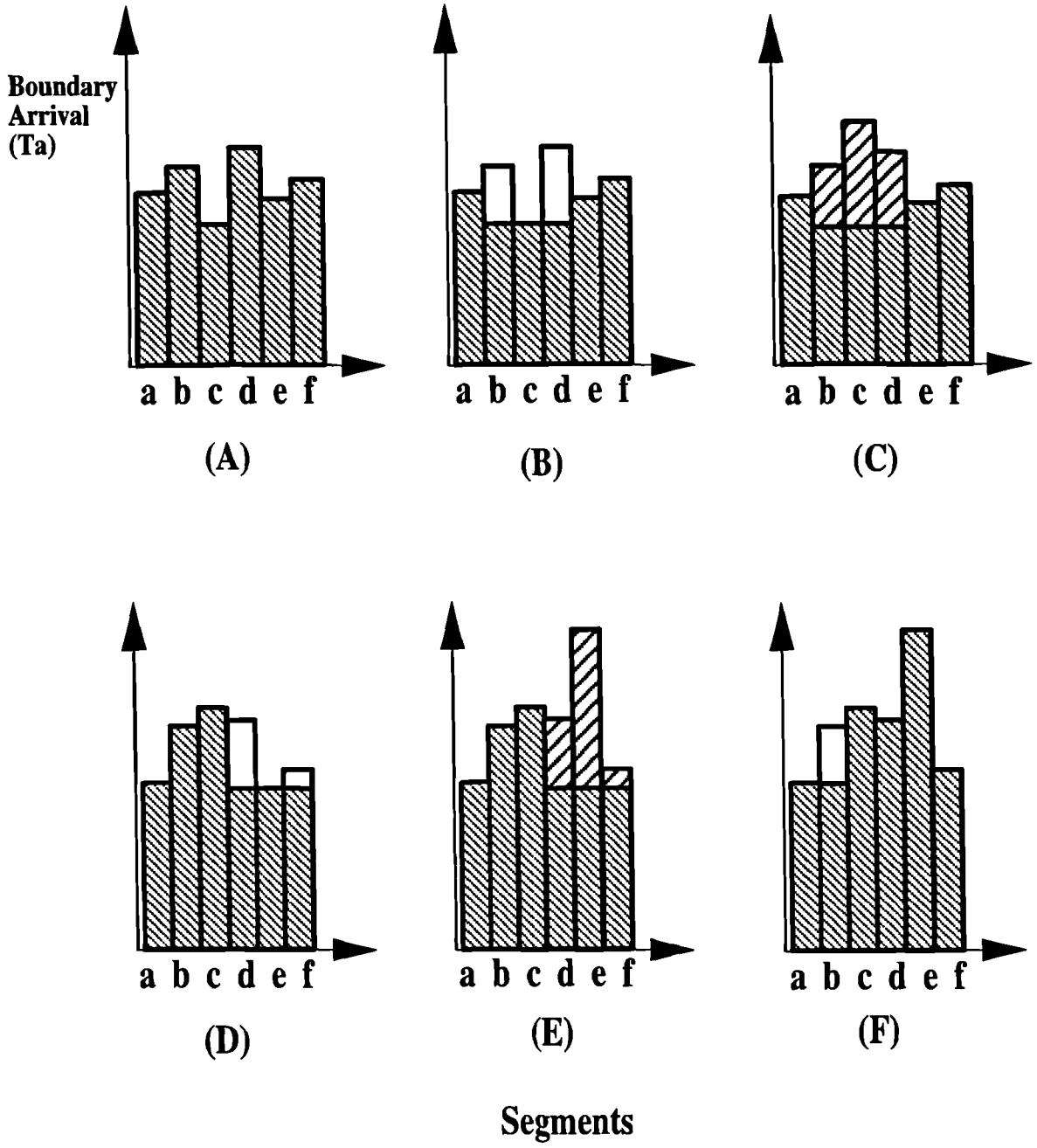


Figure 45: A diagramatic representation showing the method of chosing the segment with the earliest boundary arrival time and the updating of wave properties. Each segment can only influence the segments next to it. (A) Given the boundary arrival times of the segments, "a" to "f". The segment "c" has the shortest boundary arrival time, Ta[c]. (B) A wave transmits to both segment "b" and "d", and so the properties in segments "b" and "d" are not valid after Ta[c]. (C) Calculating the next boundary arrival of those three segments and the new Ta[b], Ta[c], Ta[d]. The segment "e" now has the shortest boundary arrival time Ta[e]. (D) The segment "e" transmits waves to segments "d" and "f". The calculation in the segments "d" and "f" are invalid after the time Ta[e], and their properties are updated to the time Ta[e]. (E) Calculate the next boundary arrival in segments "d", "e" and "f" and alsoTa[d], Ta[e], Ta[f]. The segment "a" now has the shortest boundary arrival time Ta[a]. (F) The segment "a" is chosen and it transmits a wave to segment "b". This process continues until the calculation is complete.

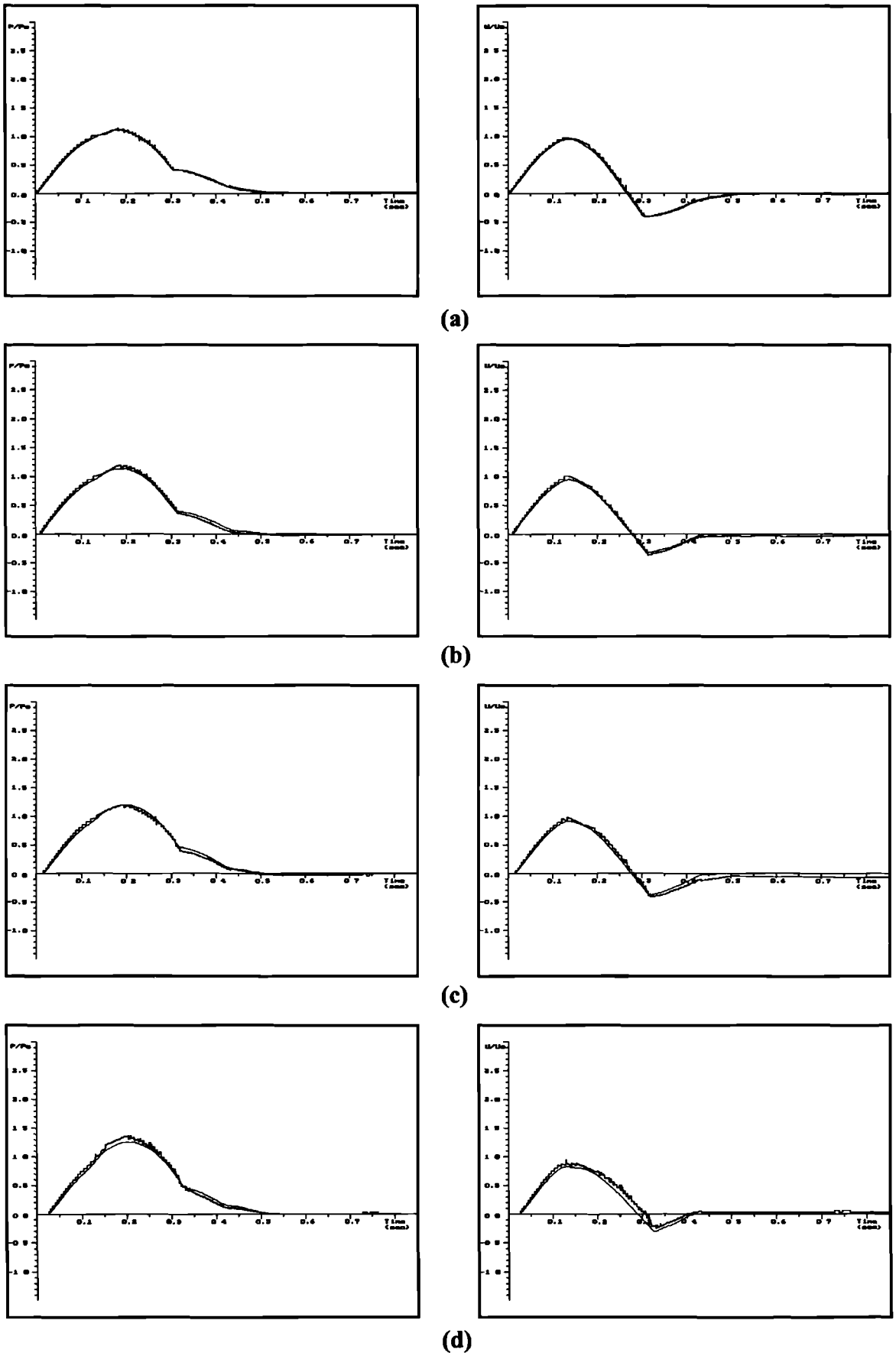
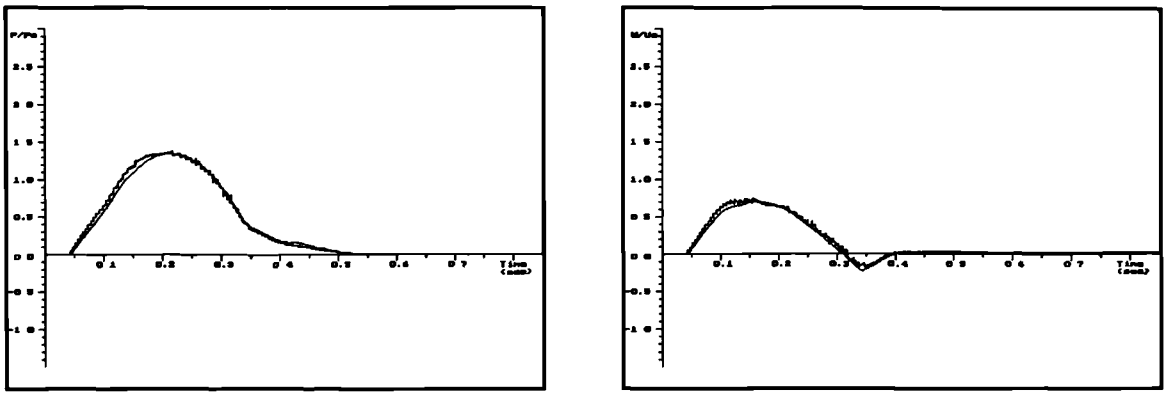
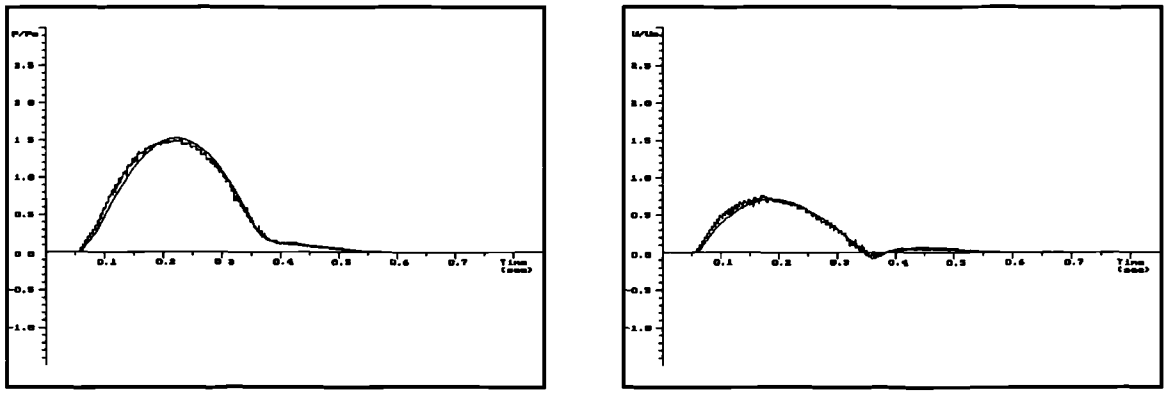


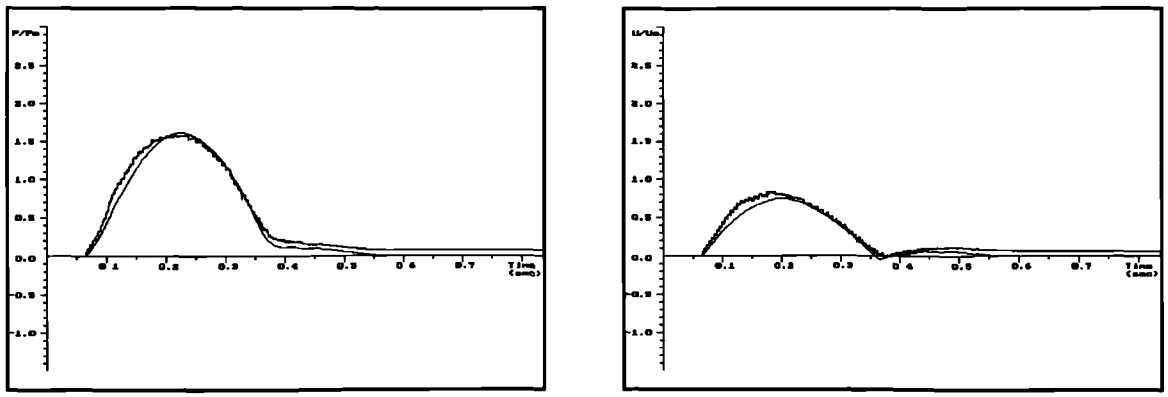
Figure 46: Nonlinear pressure and velocity waveforms when convection is considered (saw-shaped) compared with the linear waveform (smooth) of (a) the ascending aorta segment, 0, (b) the aortic arch I segment, 1, (c) the aortic arch II segment, 31, (d) the thoracic aorta I segment, 41.



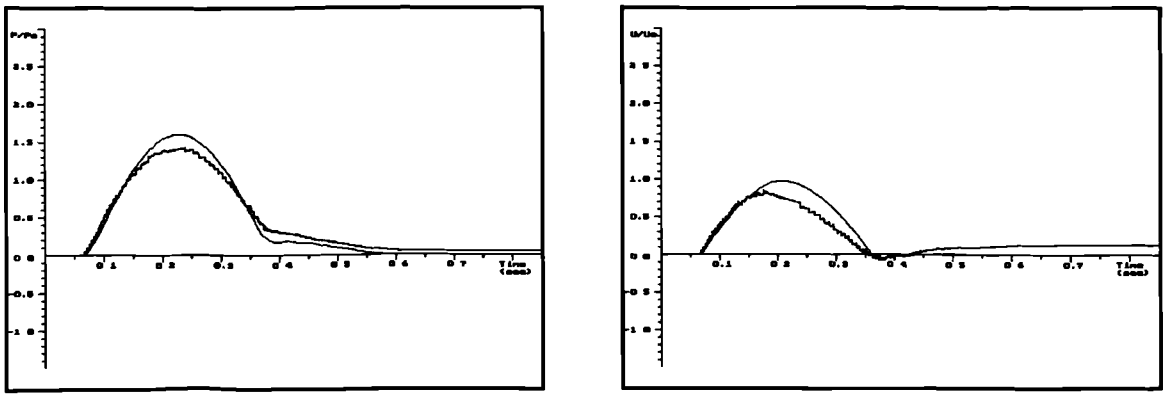
(e)



(f)

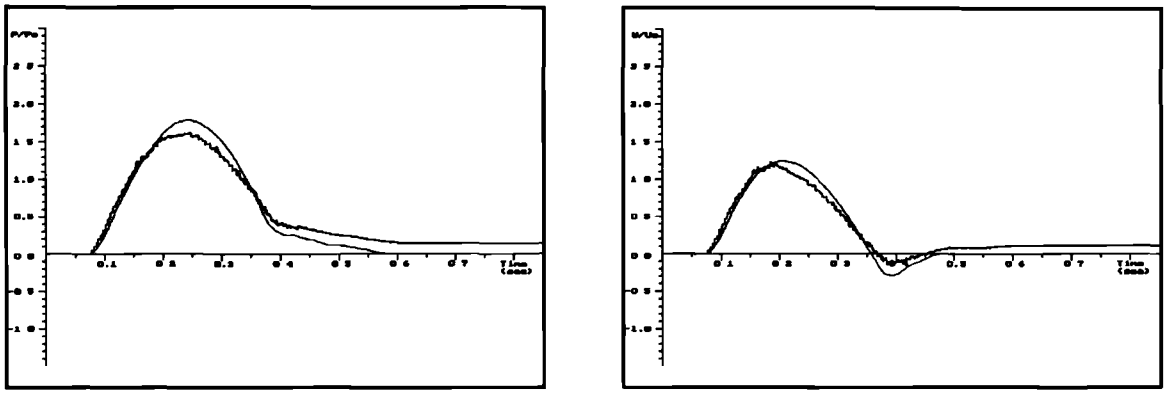


(g)

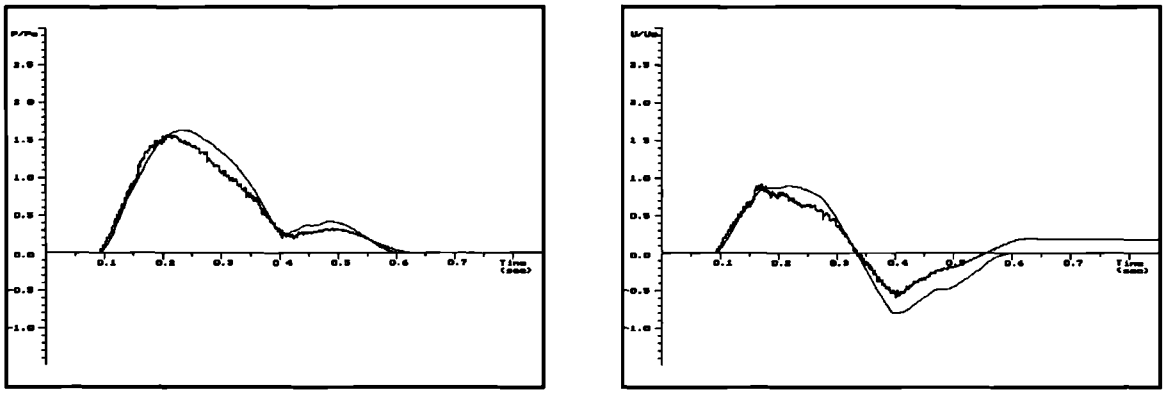


(h)

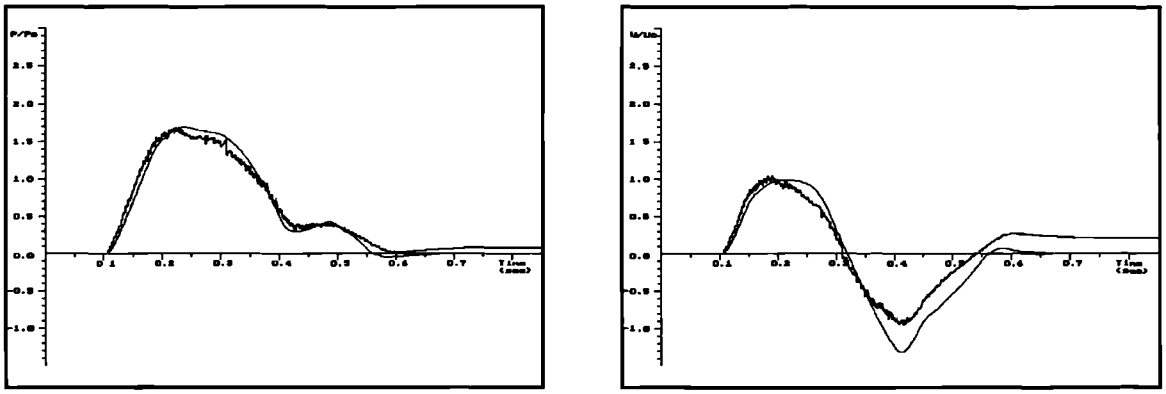
Figure 46 (cont.): (e) the thoracic aorta II segment, 65, (f) the abdominal aorta I segment, 67, (g) the abdominal aorta II segment, 91, (h) the abdominal aorta III segment, 95.



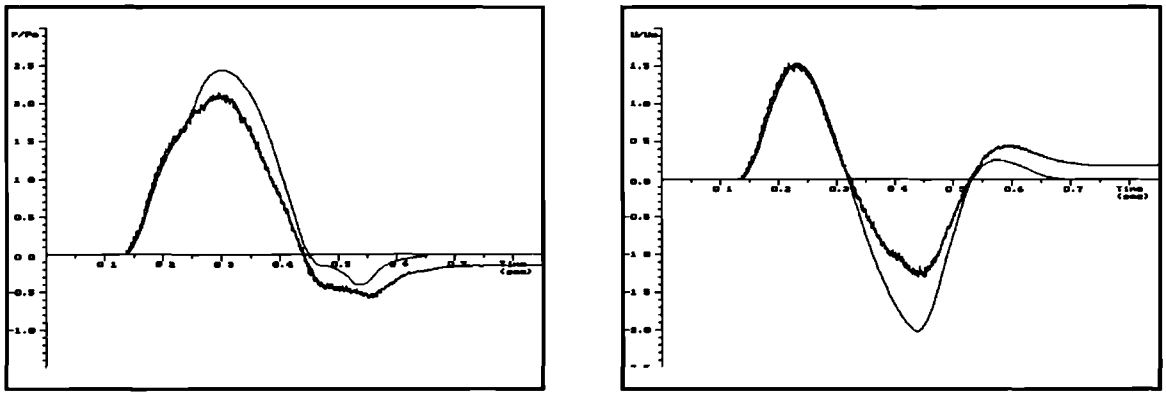
(i)



(j)



(k)



(l)

Figure 46 (cont.): (i) the abdominal aorta IV segment, 97, (j) the common iliac artery, 104, (k) the external iliac artery, 108, (l) the femoral artery, 117.

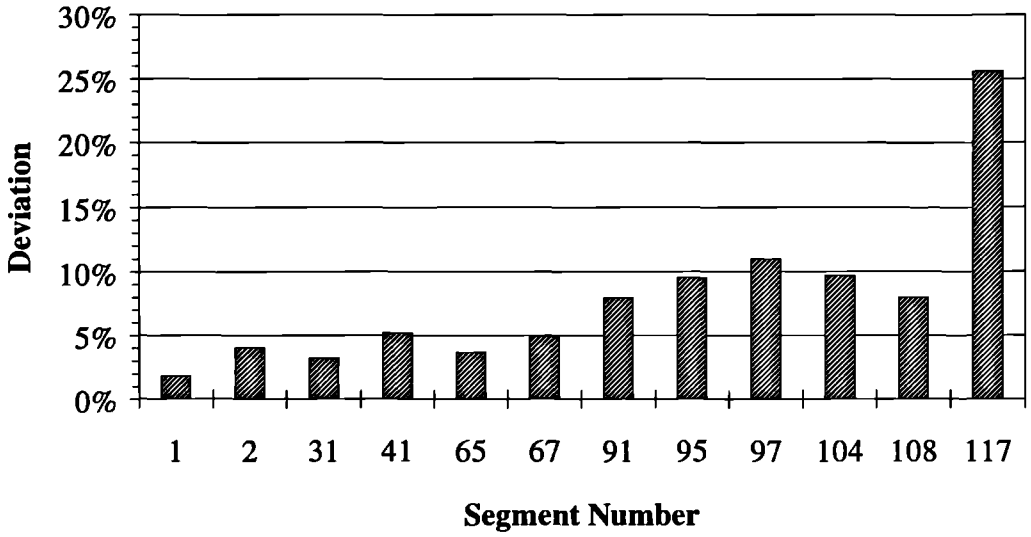
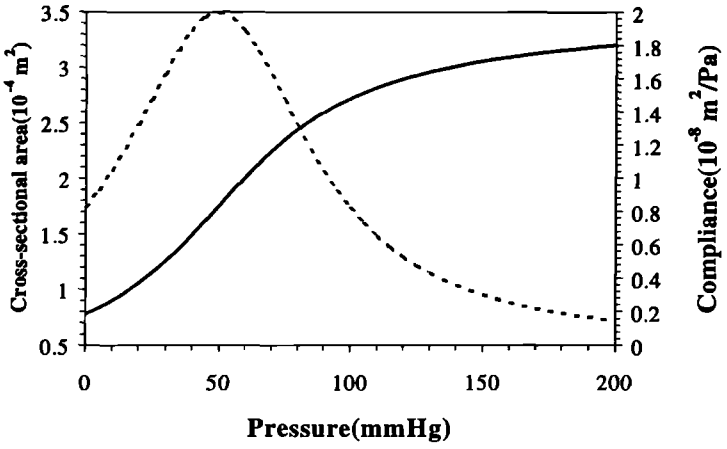
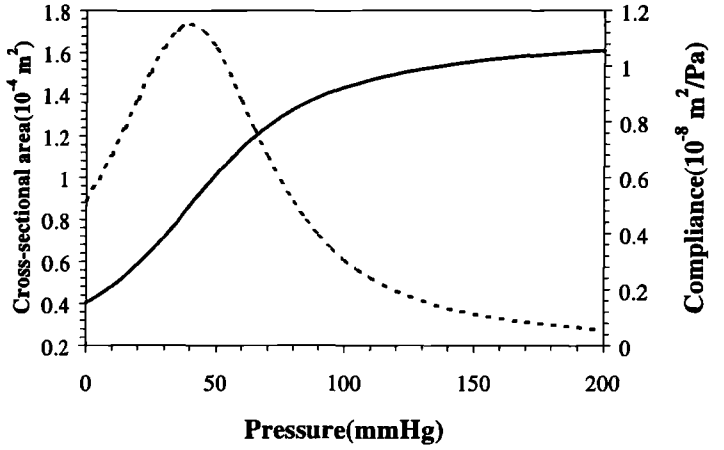


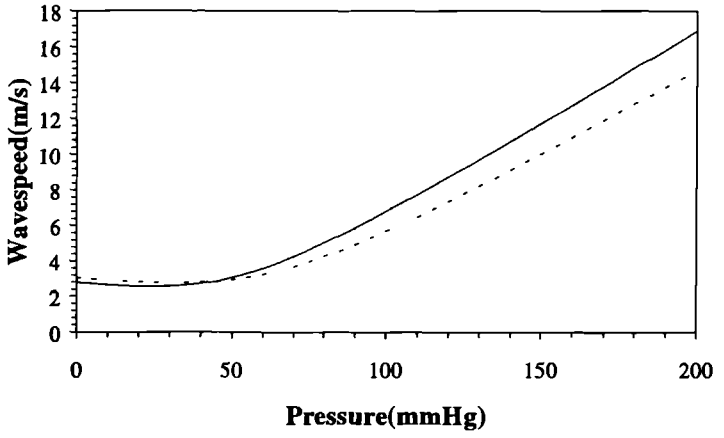
Figure 47: The deviation between the nonlinear (convection effect) and linear model of each segment. The deviation is averaged over a whole cycle of the waveform and compared with the input (the half sinusoidal wave).



(a)

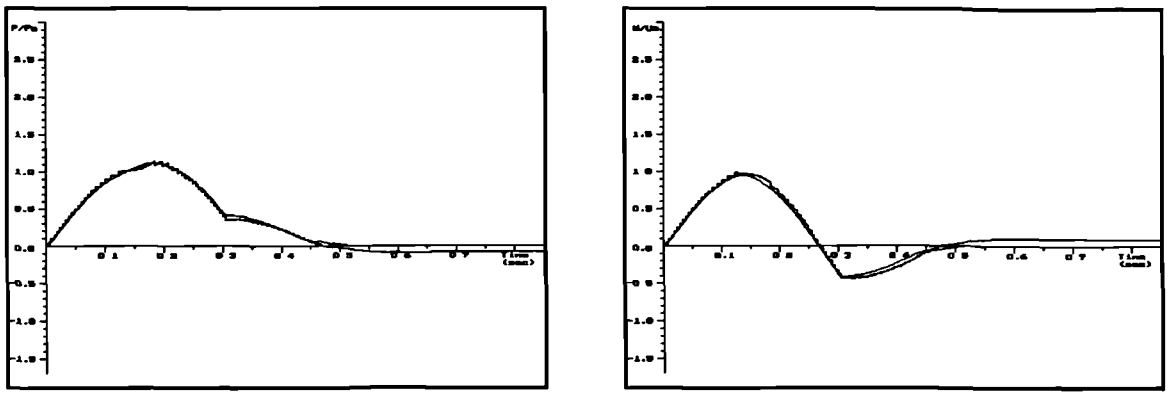


(b)

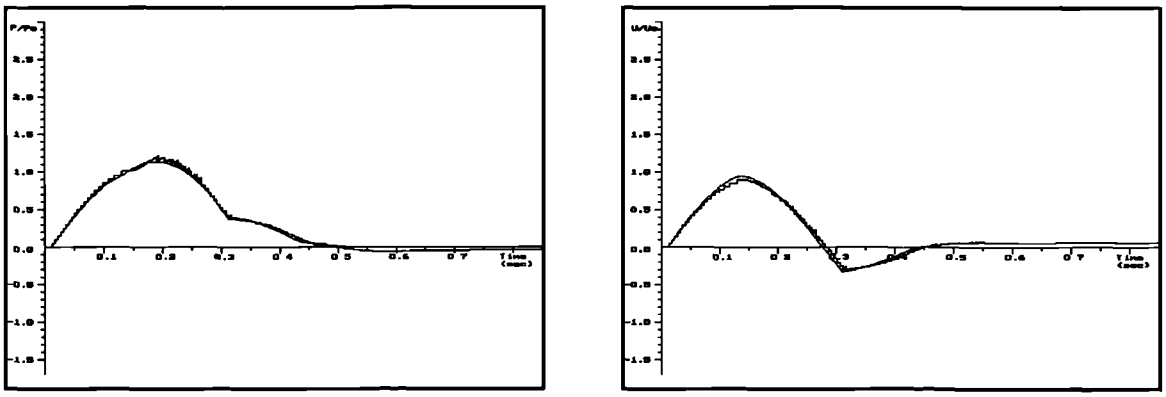


(c)

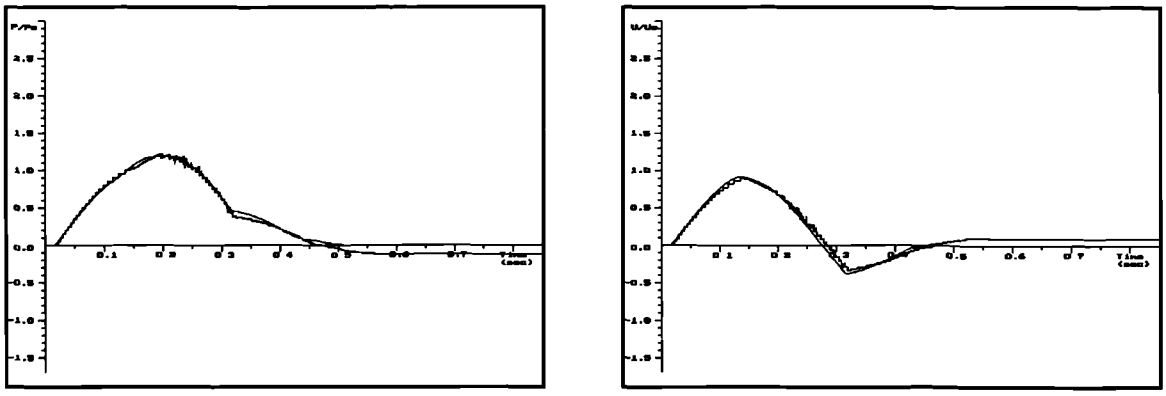
Figure 48: The aortic cross-sectional area (solid line) and aortic compliance (dotted line) of a human (a) thoracic aorta and (b) abdominal aorta over the pressure range 0 – 200 mmHg. The solid line is presented by the arctangent model fitted to human aortic measurements (Langewouters *et al.*, 1984. The patient number is 78067 of Table 2 in their paper). (b) The wavespeeds of the thoracic aorta (dotted line) and the abdominal aorta (solid line) calculated by $(AdP / \rho dA)^{1/2}$, where A is the cross-sectional area, P is the aortic pressure and ρ is the density of blood.



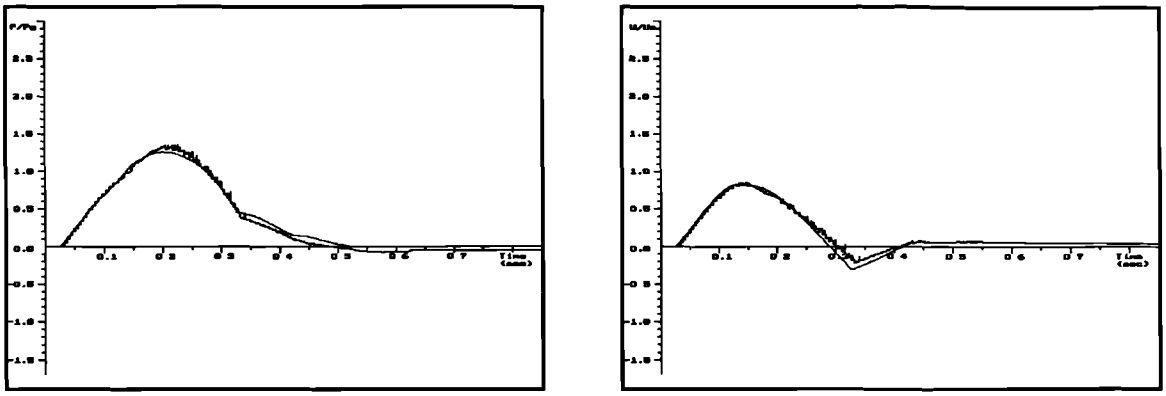
(a)



(b)

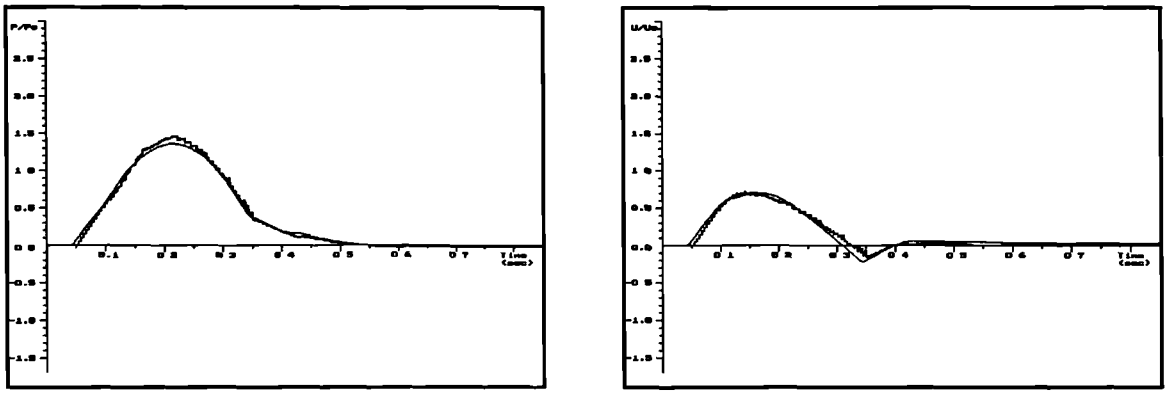


(c)

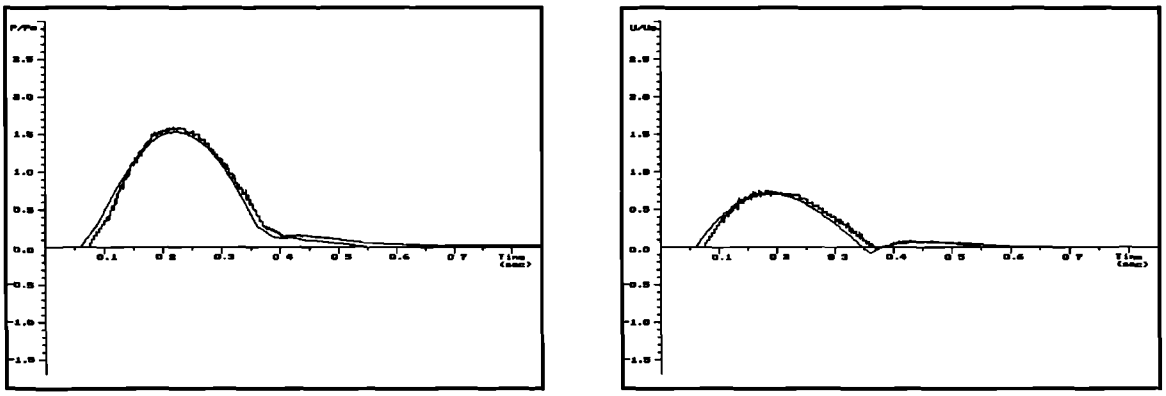


(d)

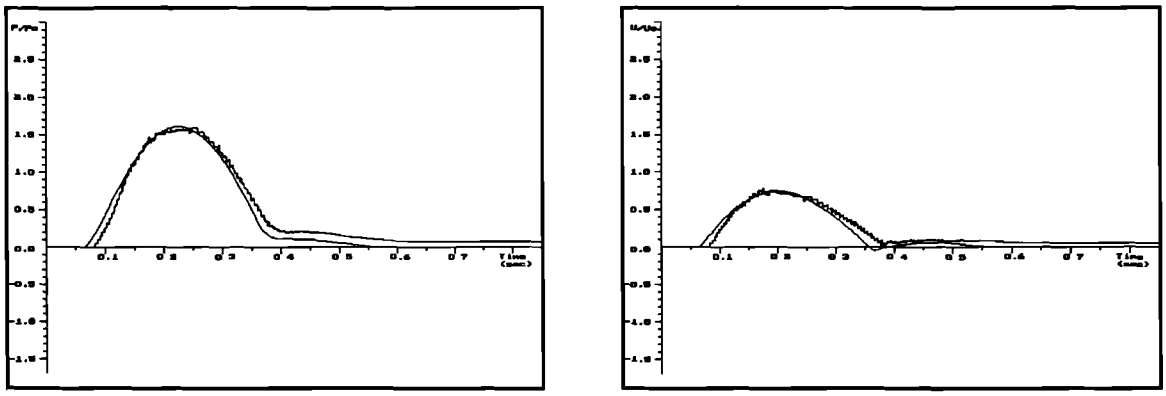
Figure 49: The nonlinear pressure and velocity waveforms when the wavespeed is pressure dependant (saw-shaped) compared with the linear case (smooth line) of (a) the ascending aorta segment, 0, (b) the aortic arch I segment, 1, (c) the aortic arch II segment, 31, (d) the thoracic aorta I segment, 41.



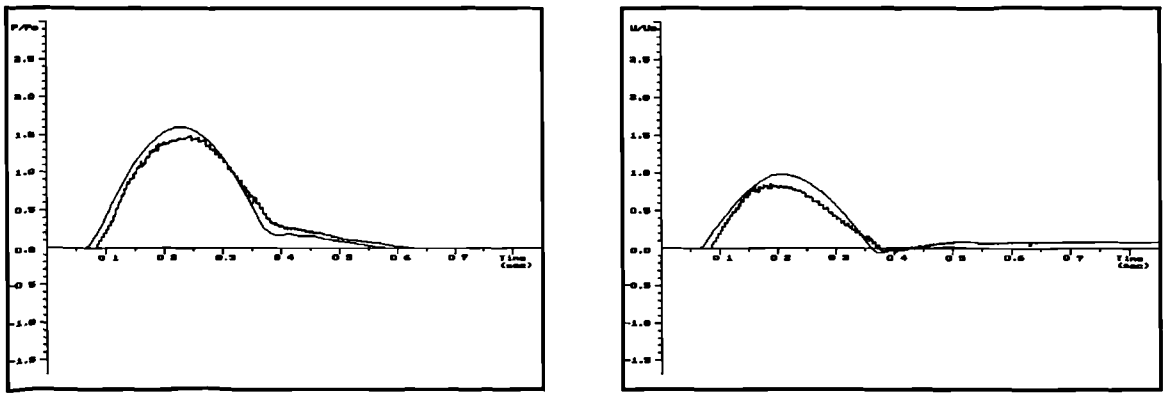
(e)



(f)

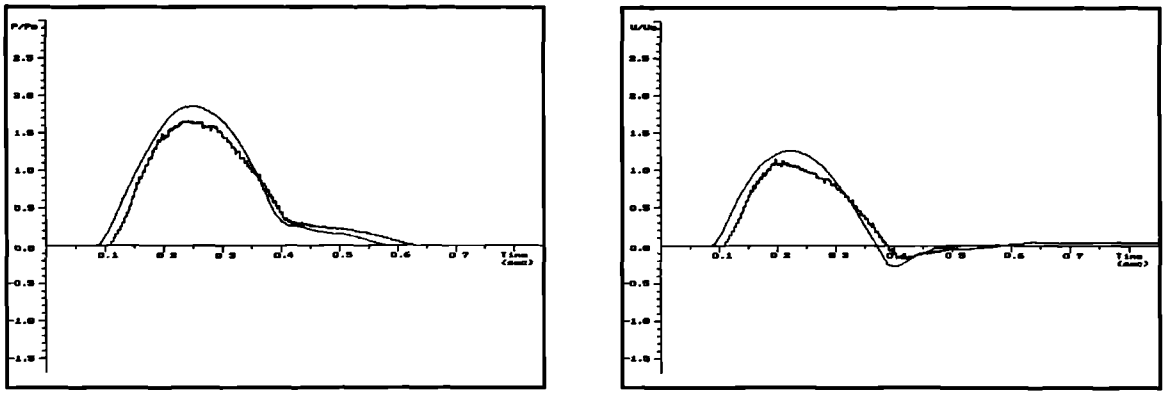


(g)

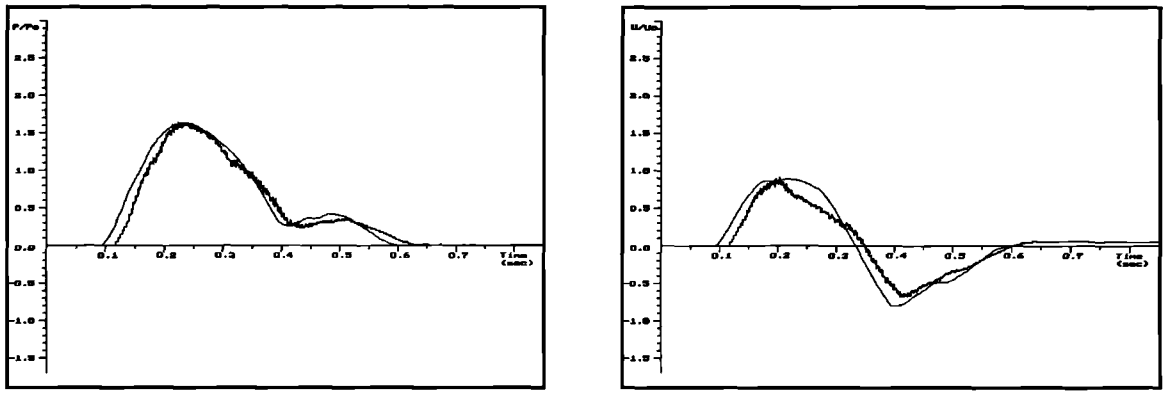


(h)

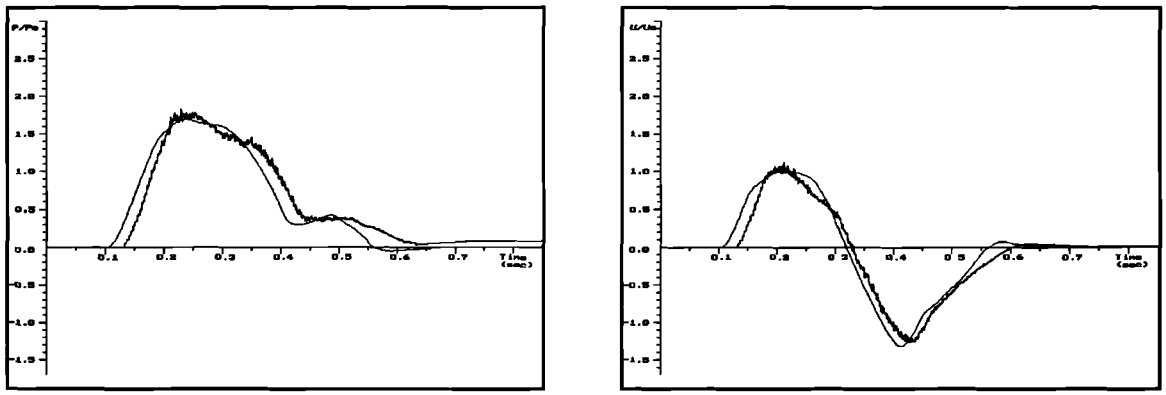
Figure 49 (cont.): (e) the thoracic aorta II segment, 65, (f) the abdominal aorta I segment, 67, (g) the abdominal aorta II segment, 91, (h) the abdominal aorta III segment, 95.



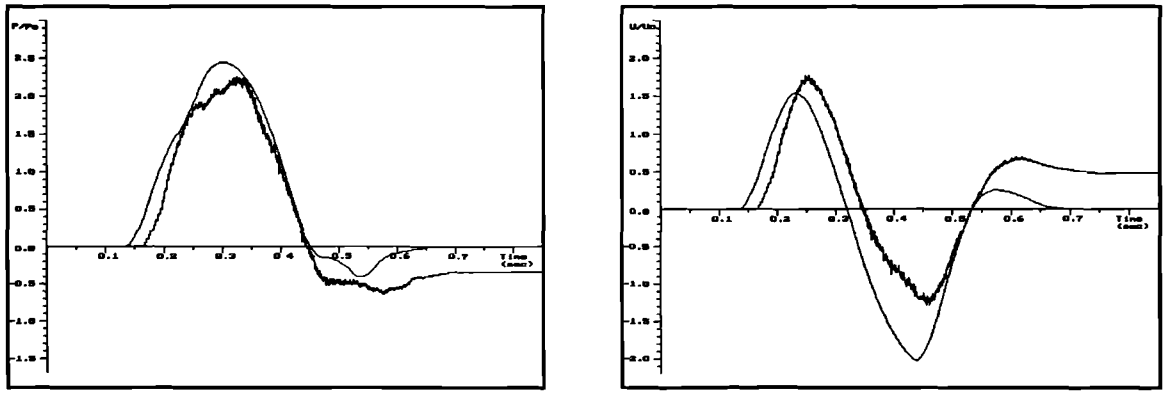
(i)



(j)

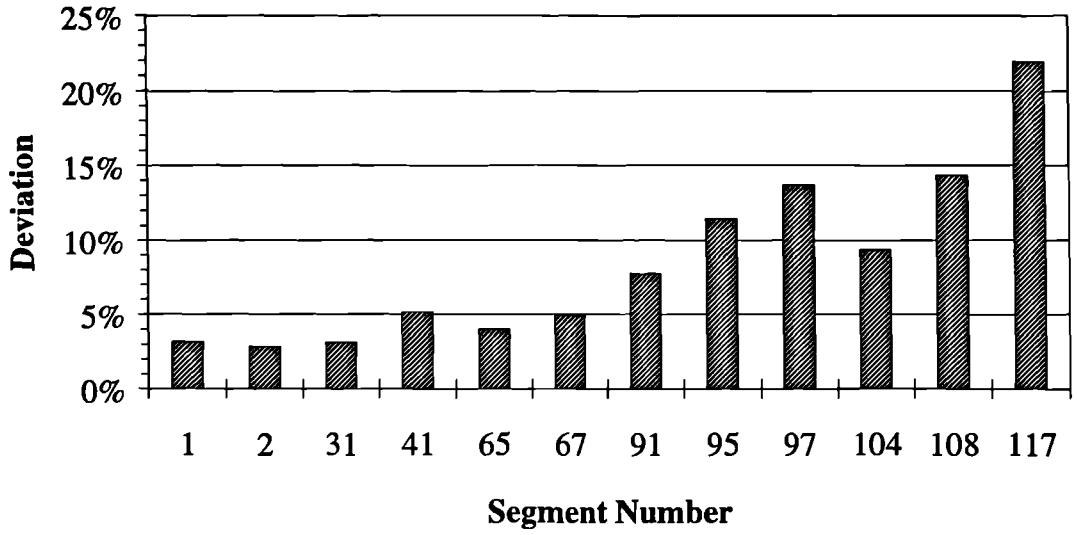


(k)

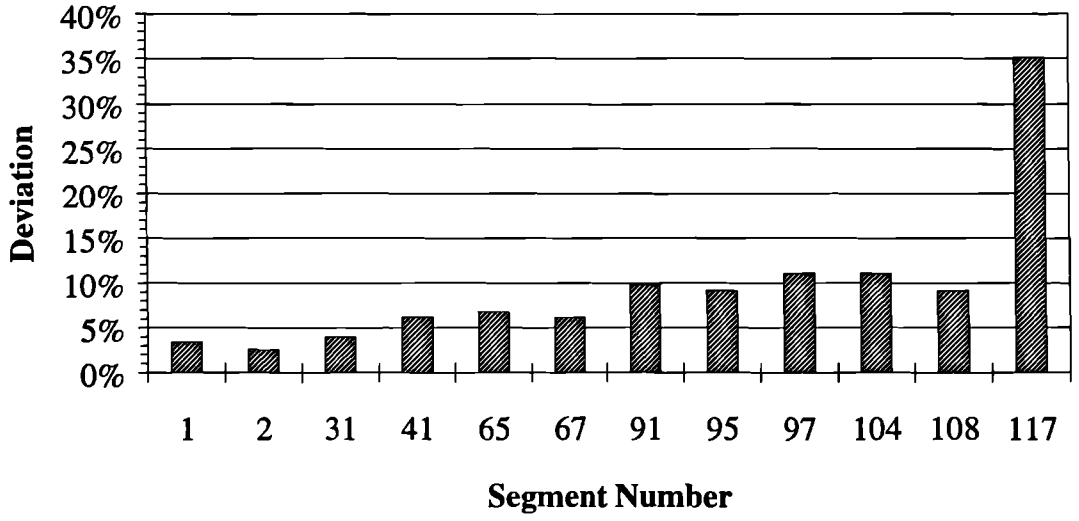


(l)

Figure 49 (cont.): (i) the abdominal aorta IV segment, 97, (j) the common iliac artery, 104, (k) the external iliac artery, 108, (l) the femoral artery, 117.



(a)



(b)

Figure 50: The mean deviation of the pressure dependent wavespeed model and the linear model at different locations. (a) The mean deviation without subtracting the delay between the nonlinear waveform and the linear waveform. (b) The mean deviation after subtracting the delay between the nonlinear and the linear waveforms.

Appendix

The number of waves

A wave arriving at a bifurcation generates 3 waves, 2 transmitted waves and 1 reflected wave (Figure A). If none of the waves are absorbed on a symmetrical bifurcating tree of vessels, there will be 3^m waves in the system after m reflections. If the heart absorbs waves, the total number of waves is less straight forward to calculate. Generations are labelled as shown below (after Phillips CG, private communication).

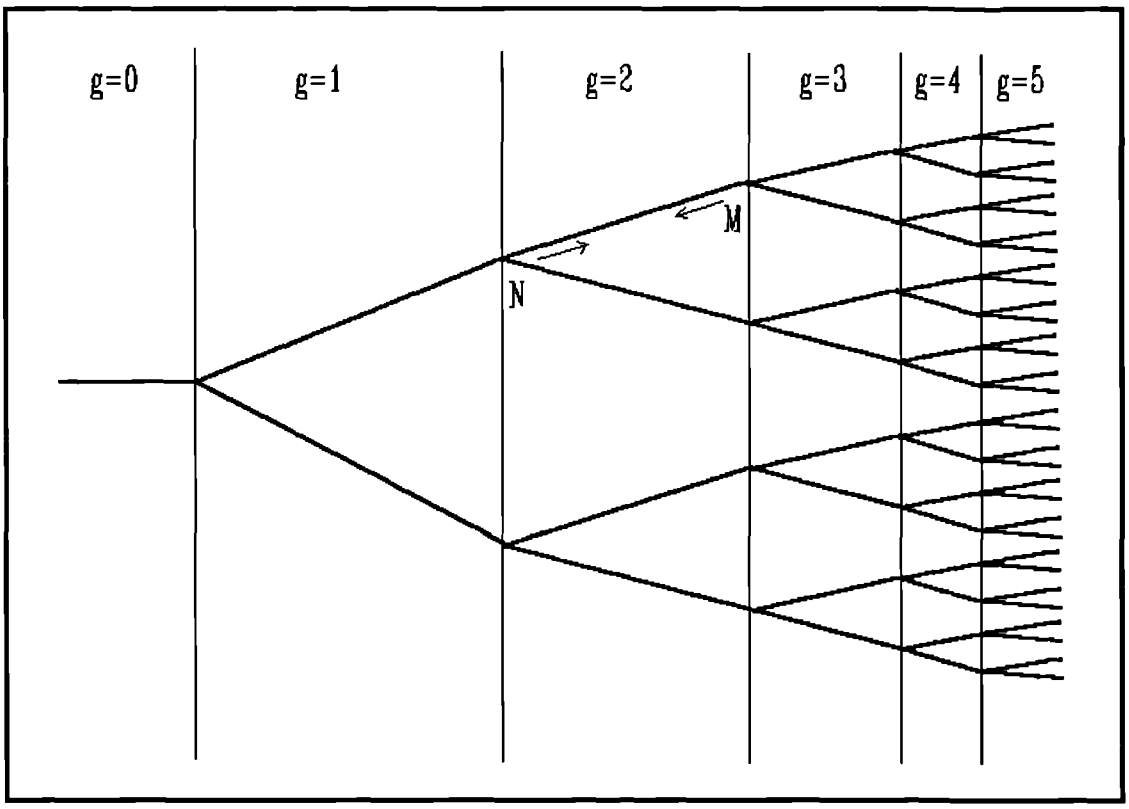


Figure A: Label generation. g is the label for generation. N denotes the forward waves. M denotes the backward waves.

Define $N_{m,g}$, as the number of waves surviving after passing m junctions and, caused by a forward-going wave which starts at the proximal end of a generation g tube and $M_{m,g}$ as the same, caused by a backward-going wave starting at the distal end of a generation g tube. The idea is shown in Figures B, C and D.

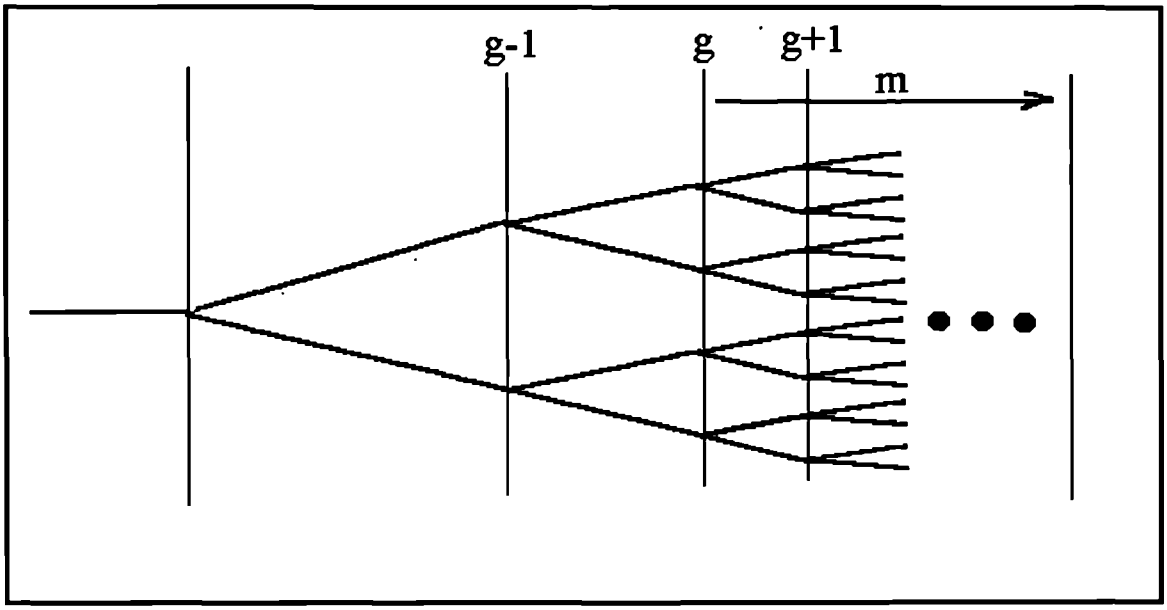


Figure B: The wave starts from g and passes m junctions.

For m = 1, N and M are equal to

$$N_{1,g} = 3 \qquad \forall\, g \geq 0 \qquad (1)$$

$$M_{1,g} = 3 \qquad \forall\, g \geq 1 \qquad (2)$$

$$M_{1,g} = 0 \qquad g = 0$$

Since the heart absorbs all backward travelling waves in segment 0 (g=0)

$$M_{m,0} = 0 \qquad \text{for all m}$$

For m > 1,

$$N_{m,g} = 2N_{m-1,g+1} + M_{m-1,g} \qquad (3)$$

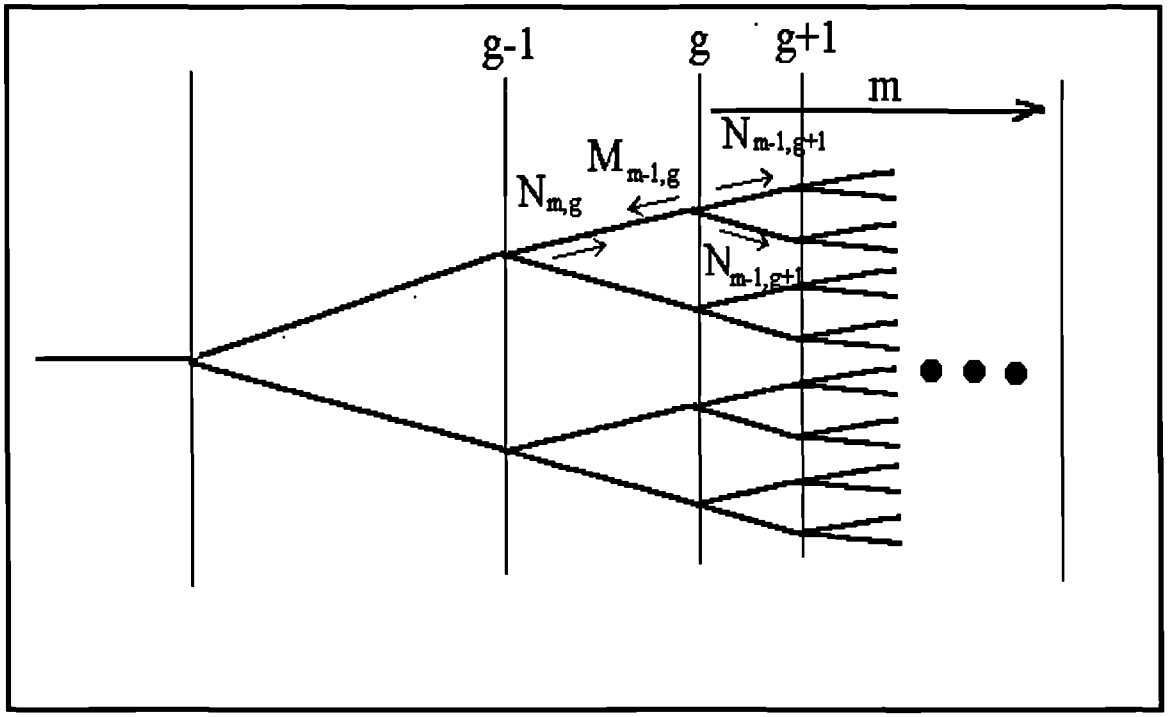


Figure C: The first wave starts at g and the direction is forward going.

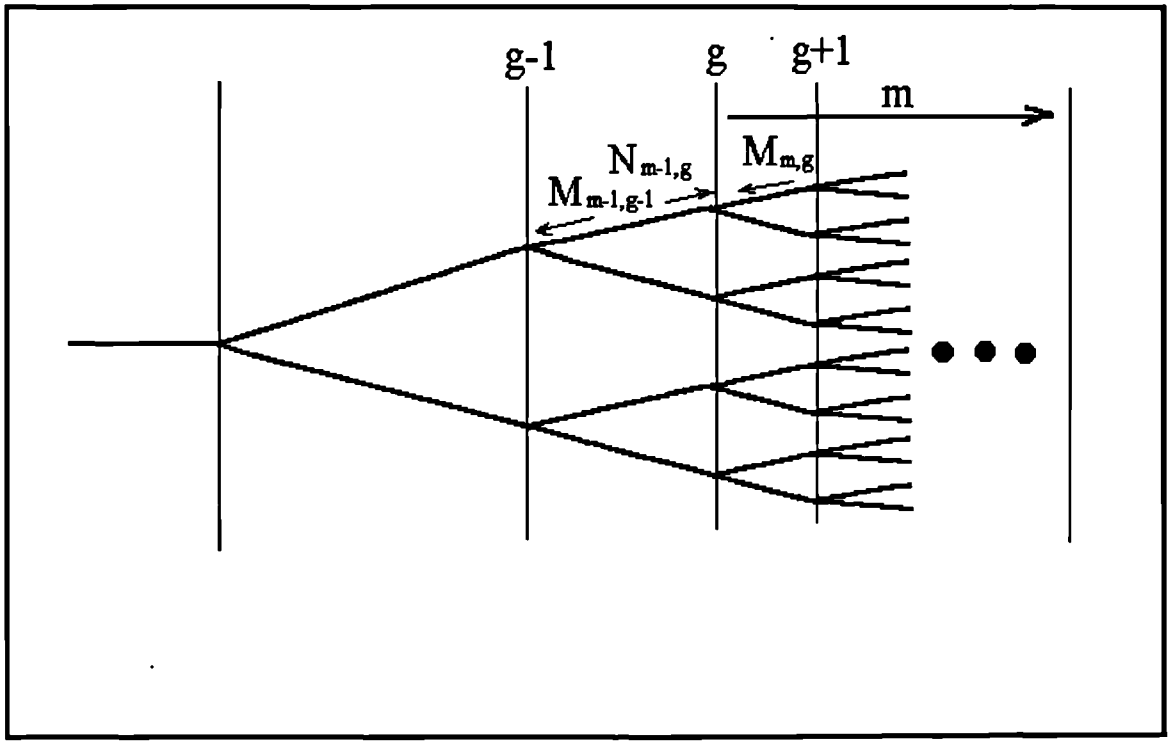


Figure D: The wave starts at g and the direction is backward going.

$$M_{m,g} = 2N_{m-1,g} + M_{m-1,g-1} \qquad \text{for } g > 0 \qquad (4)$$

Comparing (3) and (4), we find for $g \geq 0$,

$$M_{m,g+1} = N_{m,g} \qquad (5)$$

Substituting (5) into (3)

$$N_{m,g} = 2N_{m-1,g+1} + N_{m-1,g-1} \qquad \text{for } g > 0 \qquad (6)$$

We want to solve this equation in the region $m \geq 2$ and $g > 0$, with $N_{1,g} = 3\ \forall\ g \geq 0$. The equation can also be applied to $g = 0$, if we define $N_{m,-1} = 0$. Suppose for a moment that we can define 'fictional' values for $N_{1,g}$ with $g < -1$ so that if (6) applies for all (m,g) with $m \geq 2$, all the $N_{m,-1}$ are zero. Then, the problem can be expressed by using (6) to write each $N_{m,g}$ ($m>1$) in terms of the $N_{1,g}$, see Figure E. Starting from (m,g) in pathways through the lattice shown back to m=1, there are m-1 steps. If there are i forward (i.e. g→g+i) steps, the value reached by the pathway is $N_{1,g+2i-m+1}$ (there are m-i-1 backward steps) and the factor produced by the 2 in (6) is 2^i. Since there are $\begin{bmatrix} m-1 \\ i \end{bmatrix}$ such pathways, we find

$$N_{m,g} = \sum_{i=0}^{m-1} \begin{bmatrix} m-1 \\ i \end{bmatrix} 2^i N_{1,g+2i-m+1} \qquad (7)$$

The problem can be solved after defining the fictitious values for g<0. The idea is shown below (Figure E).

$$N_{1,g} = 3 \qquad \text{for } g \geq 0$$

$$N_{1,-1} = 0$$

$$N_{1,g} = -3 \times 2^{-g-1} \qquad \text{for } g < 0$$

Substituting into (7) when g = -1, we find $N_{m,-1} = 3\sum_{i>\frac{m}{2}} \begin{bmatrix} m-1 \\ i \end{bmatrix} 2^i - 3\sum_{i<\frac{m}{2}} \begin{bmatrix} m-1 \\ i \end{bmatrix} 2^{-i+m-1} = 0$

by symmetry.

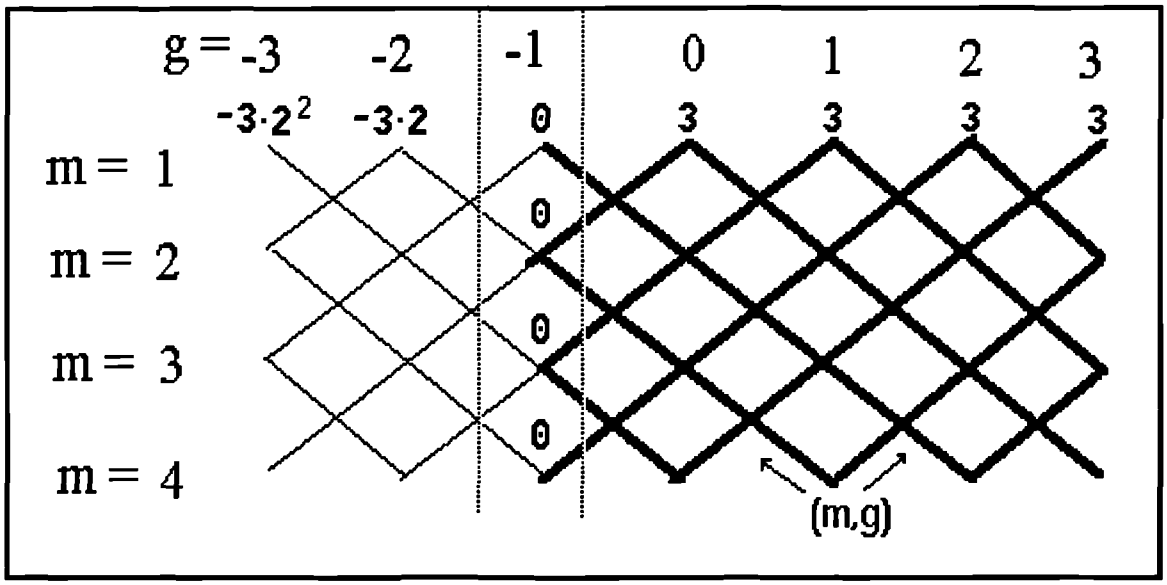


Figure E: A wave starting at (m,g) going to m=1 is like a random walk from (m,g) which can choose one of the two possible routes.

Substituting the boundary condition into (7), we get

$$N_{m,0} = 3\sum_{i=\frac{m-1}{2}}^{m-1} \begin{bmatrix} m-1 \\ i \end{bmatrix} 2^i - 3\sum_{i=0}^{\frac{m-3}{2}} \begin{bmatrix} m-1 \\ i \end{bmatrix} 2^{m-i-2} \qquad \text{for m odd} \qquad (8)$$

$$N_{m,0} = 3\sum_{i=\frac{m}{2}}^{m-1} \begin{bmatrix} m-1 \\ i \end{bmatrix} 2^i - 3\sum_{i=0}^{\frac{m-4}{2}} \begin{bmatrix} m-1 \\ i \end{bmatrix} 2^{m-i-2} \qquad \text{for m even} \qquad (9)$$

The following table is the list of the number of waves calculated by (8) and (9).

Level	Number of Waves with Absorption	No Absorption
1	3	3
2	6	9
3	18	27
4	48	81
5	144	243
6	408	729
7	1,224	2,187
8	3,552	6,561
9	10,656	19,683
10	31,296	59,049
11	93,888	177,147
12	277,632	531,441
13	832,896	1,594,323
14	2,473,344	4,782,969
15	7,420,032	14,348,907
16	22,095,360	43,046,721
17	66,286,080	129,140,163
18	197,760,000	387,420,489
19	593,280,000	1,162,261,467
20	1,772,371,968	3,486,784,401
21	5,317,115,904	10,460,353,203
22	15,899,750,400	31,381,059,609
23	47,699,251,200	94,143,178,827
24	142,736,572,416	282,429,536,481
25	428,209,717,248	847,288,609,443
26	1,282,073,100,288	2,541,865,828,329
27	3,846,219,300,864	7,625,597,484,987
28	11,520,400,392,192	22,876,792,454,961
29	34,561,201,176,576	68,630,377,364,883
30	103,552,149,454,848	205,891,132,094,649

Table A1. The number of waves, after passing through the number of levels.